INTERACTION OF PIER, CONTRACTION, AND ABUTMENT SCOUR IN CLEAR WATER SCOUR CONDITIONS

A PhD Thesis
Presented to
The Academic Faculty

by

Irfan Abid

In Partial Fulfillment
Of the Requirements for the Degree
Doctor of Philosophy in the
School of Civil and Environmental Engineering

Georgia Institute of Technology
August 2017

INTERACTION OF PIER, CONTRACTION, AND ABUTMENT SCOUR IN CLEAR WATER SCOUR CONDITIONS

Approved by:

Dr. Terry W. Sturm, Advisor
School of Civil and Environmental Engineering
Georgia Institute of Technology

Dr. Phillip J. Roberts
School of Civil and Environmental Engineering
Georgia Institute of Technology

Dr. Donald R. Webster
School of Civil and Environmental Engineering
Georgia Institute of Technology

Dr. Hermann M. Fritz
School of Civil and Environmental Engineering
Georgia Institute of Technology

Dr. James Wray
School of Earth and Atmospheric Sciences
Georgia Institute of Technology

Date Approved: April 24th, 2017

DEDICATION

Dedicated to my parents, Chaudhry Abid Elahi (Father) and Parveen Abid (mother) and my country, Pakistan.

ACKNOWLEDGEMENTS

This research was accomplished under the inimitable guidance of Dr. Terry W. Sturm, as my thesis advisor, whose unsurpassed experience in the field of hydraulics and sediment transport, not only helped in formulating the research problem but also reinforced the endeavor to crystalize the research outcome. I would also like to thank my committee members, Dr. Philip J. Roberts, Dr. Donald R. Webster, Dr. Hermann M. Fritz, and Dr. James Wray, for their time to review my thesis and give valuable input to my research work. I also appreciate the valued guidance of Dr. Thorsten Stoesser from Cardiff University UK and Dr. Bruce W. Melville from University of Auckland, New Zealand. A special thanks to Andrew Udell and his team, whose indispensable laboratory support always facilitated the experimental work and its timely completion. A constant moral and academic support from my siblings, Dr. Kamran Abid, Dr. Adnan Abid, and Dr. Imrana Imran helped me to remain consistent throughout the research work. Mere words would not convey the gratitude for my parents whose guidance and prayers have always been the source of success in my life. Last but not the least, is a very special thanks to my wife Mona Iftikhar and my daughter Daaniyah Irfan, whose unmatchable company and support helped me to traverse through this long journey.

TABLE OF CONTENTS

LIST OF TABLES

LIST OF FIGURES

LIST OF ABBREVIATIONS & SYMBOLS

ABBREVIATIONS

BLA	Bankline abutments
cfs	Cubic feet per second
C.S.	Cross Section
CSU	Colorado State University
CWS	Clear water scour
D/S	Downstream
F	Free flow
HEC	Hydraulic engineering circular
LBS	Live-bed scour
LSA	Long setback abutment
OT	Over-toping flow
SO	Submerged orifice flow
SSA	Short setback abutment
S & M	Shepard and Melville
TKE	Turbulent kinetic energy
TW	Tail water
U/S	Upstream

SYMBOLS

a	Pier diameter/ Pier width;
*a**	Projected pier width;

B	Channel width (for simple channel);
B_m	Main channel width;
B_f	Floodplain width;
d_s	Scour depth;
d_{se}	Equilibrium Scour depth;
d_{50}	Particle median diameter;
F	Approach flow Froude number;
F_c	Critical Froude number for $V=V_c$;
FS	Factor of safety;
F_d	Deterministic particle Froude number;
g	Gravitational acceleration;
g'	Buoyant gravitational acceleration;
h_b	Depth from undisturbed bed level to lower chord of bridge;
h_{br}	Bridge height (facing flow);
$\overline{K}_b$	Average bottom TKE at D/S abutment toe;
K_s	Abutment shape factor;
K_θ	Flow alignment factor;
K_{yl}	Ratio of abutment length to flow depth;
K_I	Approach flow intensity factor;
K_d	Sediment size factor;
K_g	channel geometry factor;
K_1	Pier shape factor;
K_2	Pier alignment factor;

K_3	Bed form factor
K_4	Bed armoring factor;
K_f	Roughness height of floodplain;
K_m	Roughness height of main channel;
k_s	Equivalent sand grain roughness;
L_a	Length of abutment;
L_b	Length of bridge (flow direction);
L_m	Distance of deepest scour point from toe of the abutment in transverse direction;
L_p	Distance of pier from abutment face (transverse direction);
L_s	Distance of deepest scour point from edge of floodplain in transverse direction;
L_x	Distance of deepest scour point from upstream edge of the bridge in flow direction;
M	Discharge contraction ratio;
n	Manning's flow resistance factor;
q_1	Flow rate per unit width in the approach flow section;
q_{f1}	Flow rate per unit width in the approach section floodplain;
q_{m1}	Flow rate per unit width in the approach section main channel;
q_2	Flow rate per unit width in the contracted section;
q_{f2}	Flow rate per unit width in the bridge section floodplain;
q_{m2}	Flow rate per unit width in the bridge section main channel;
q_{max}	Unit discharge coinciding with location of deepest scour;

Q	Total discharge;
Q_o	Proportion of the flow discharge in the approach flow section equal to the contracted opening;
Q_{ot}	Bridge overtopping discharge;
r_T	Scour amplification factor;
SG	Specific gravity of sediment;
u_*	Shear velocity;
u_{*c}	Critical shear velocity;
u,v,w	Flow direction, Transverse, and vertical velocity components;
u',v',w'	Flow direction, Transverse, and vertical velocity fluctuation components;
V_1	Approach flow velocity;
V_{f1}	Approach flow velocity in the floodplain;
V_{m1}	Approach flow velocity in the main channel;
V_b	Velocity through bridge before scour;
V_{fc}	Critical velocity for initiation of sediment motion in floodplain;
V_{mc}	Critical velocity for initiation of sediment motion in main channel;
V_c	Critical velocity for initiation of sediment motion;
W	Width of contracted floodplain;
w	Depth of flow above the bridge deck;
Y_{2o}	Flow depth at bridge before scour;
Y_1	Approach flow water depth;

Y_2	Contracted section equilibrium depth (contraction scour);
Y_{f1}	Approach flow water depth in the floodplain;
Y_{fo}	Flow depth in the floodplain for unconstructed flow;
Y_{m1}	Approach flow water depth in the main channel;
Y_{mo}	Flow depth in the main channel for unconstructed flow;
Y_c	Mean flow depth corresponding to contraction scour;
Y_{2max}	Maximum flow depth at location of maximum scour depth;
Y_{f2max}	Flow depth at location of maximum scour depth in floodplain;
Y_{m2max}	Flow depth at location of maximum scour depth in main channel;
Y_{bs}	Flow depth under bridge after scour;
Y_t	Water separation height below bridge (pressure flow);
Δd_s	Change in Scour depth;
ρ	Density;
μ	Viscosity;
σ	Bulk shear stress;
τ_1	Bed shear stress in approach flow;
τ_2	Bed shear stress in bridge section;
τ_f	Shear stress of approach flow in floodplain;
τ_c	Critical shear stress for initiation of sediment motion;
τ_{*c}	Shields' parameter;
σ_g	Geometric standard deviation of sediment particles;
Subscript "*m*"	Variable for main channel;

Subscript "*f*"	Variable for floodplain;
Subscript "*o*"	Variable for unconstructed flow;
Subscript "*1*"	Variable for approach section;
Subscript "*2*"	Variable for test section/ contracted section

SUMMARY

The main objective of this dissertation is to investigate the interactive scour development for all the components of bridge scour (abutment, lateral contraction, vertical contraction, and pier scour) under clear-water scour conditions for erodible, spill-through abutments and rectangular piers. Because safety and economy are important considerations for bridge design, predicting the extent and depth of scour is critical to bridge foundation design to ensure structural stability . However, bridges on waterways are vulnerable to damage due to extreme hydrologic events that cause severe floods. In the USA, more than 60% of bridge damages are due to hydraulic parameters that cause scour of the river bed. Current design practice recommends calculating the sum of all the interacting components of scour to predict the total maximum scour depth. However, the interaction and simultaneous development of scour components results in considerably less scour than predicted. A physical model-based study, which covered all individual and interactive scour conditions, was conducted on a typical compound channel river cross-section with a main channel having floodplains on both sides. The model bridge was a typical two-lane bridge design used by Georgia DOT for rural regions. The experiments comprised of all three types of flow to include free, submerged orifice, and overtopping flows. The variable parameters included approach flow intensity, unit discharge contraction ratio, backwater depth ratio, pier placement, and location of the pier for a given type and alignment of the abutment (in addition to the flow types). Experiments consisted of two phases as fixed bed and movable bed experiments. Fixed bed experiments were conducted to measure initial flow and turbulence parameters in the approach and test

section. In movable bed experiments, time development of the location and magnitude of the scour was tracked along with detailed bed elevation contours of the equilibrium scour condition. A detailed collection of data for time development of scour, hydraulic parameters, and turbulence resulted in qualitative and quantitative observations, which assisted in the formulation of a realistic model for prediction of abutment and contraction scour, pier and vertical contraction scour, and interaction of all four components. The formulated multi-part methodology for total scour prediction to account for scour interactions captures the results within 10% of measured results. The application of the suggested model to field examples validated the findings. The results will not only improve economical bridge design but will also result in reliable hydraulic variables input to the model methodology. Another important finding of this research is the prediction of the location of the scour hole which will help improve the design safety, not only for the bridge structure itself, but also the design of downstream structures. In summary, this study provides a comprehensive picture of the interactive bridge scour process and suggests a practical methodology to predict its magnitude to produce more economical design of safe bridges.

CHAPTER I

INTRODUCTION

1.1. Background

River engineers have long been studying issues related to river morphology, a complex phenomenon that includes various types of hydrologic, hydraulic, environmental, and geotechnical parameters. Because of these complex interactive parameters, a river system in totality is not stable with respect to sediment transport. More specifically, a river experiences a combination of aggradation and degradation processes. However, a part of a river can be called a “stable reach”, although a river takes time on the order of hundreds of years to become stable. An ever-increasing use of rivers for navigation, irrigation, and water supply purposes, have resulted in the construction of river training works that affect the sediment transport behavior. Various structures control river flows that include dikes, guide banks, and spurs. Structures built across rivers include dams, head-works, and bridges, which affect sediment flux. Bridges are one of the most important types of structures that affect and get affected by sediment flux, particularly during heavy floods.

Important considerations for bridge design are safety and economy. From an engineering perspective, bridges are designed for a minimum possible opening through which water can pass during floods. This minimum opening causes a great degree of flow contraction, resulting in a considerable increase in flow intensity. Flow in the contracted

section may be free (F), submerged orifice (SO), or overtopping (OT) flow as shown in Figure 1-1. An OT or SO flow at a bridge section can result from unprecedented heavy flows because of intense rainfalls of shorter duration owing to climate change, generating more frequent flash floods (Booij 2005). Bridge design can be economized by designing bridges for an overtopping flow for a 100-year flood, but the foundation design, which is more critical for stability, still requires a 500-year flood event design (Umbrell et al. 1998). Ground limitations and technical constraints may also result in an overtopping flow bridge design. Severe flooding in the Atlanta metro area in the state of Georgia in 2009 resulted in 18 stream gages recording flood volumes in excess of the 500-year flood magnitude that caused widespread damage to bridges (Gotvald and McCallum 2010).

(a) Free Flow (F)

(b) Submerged Orifice Flow (SO)

(c) Overtopping Flow (OT)

Figure 1-1 Classes of bridge flow

The contraction at a bridge section may be gradual or sudden. A contracted opening is constructed through an embankment that terminates at the abutment. The bridge structure that includes an embankment, an abutment, a bridge deck, girders, piers, and bridge foundations is vulnerable to damage from scouring. The damage may result in partial failure or even collapse of a bridge. Bridge scour is a phenomenon of removal of sediment, because of high floods, within the vicinity of obstructions that include abutments or piers. Bridge scour includes removal of sediment from the riverbed within the bridge cross section and downstream of the bridge. Examples of bridge scour are shown in Figure 1-2.

(a) Outflanking of Wing-wall Abutment

(b) Undermining of Abutment (USGS)

(c) Pier Scour

(d) Contraction Scour (USGS)

Figure 1-2 Types of bridge scour

Scour analysis holds a pivotal importance for designing a safe and economical bridge foundation. Hence, in the hydraulic design of bridges, accurate scour depth

estimation is critical, as an overestimation results in an uneconomical foundation design and an underestimation may result in exposure of the foundation to flow, which threatens the structural stability of a bridge (Kothyari and Kumar 2012). Bridge failure in most cases is because of scouring around bridge foundations (Rossell and Ting 2013). About 84% of bridges in the United States are over waterways (Landers 1992). In the United States, more than one thousand bridges collapsed in a span of 30 years and 60% of these bridges were associated with hydraulic failure, including pier and abutment scour (Shirole and Holt 1991). In 1994, in the state of Georgia alone, more than 500 bridges (locally and state owned) were damaged by scour (Arneson et al. 2012).

1.2. Research Motivation

Significant work devoted to the field of bridge scour has examined the cause and effect relationship between contraction phenomena and sediment transport. However, formulation of a model with accurate estimates of the depth of scour is difficult. The main reasons for this inaccuracy include complexity of the flow mechanism, less availability of accurate field scour data at the time of extreme flood events, and laboratory experiments' reliance on simple rectangular channels rather than more realistic compound channel experiments.

An analysis of existing models indicates that most methods overestimate local scour depth. Deficiency of field data availability is one of the most important factors which force researchers to adopt a conservative approach either by opting for an envelope scour prediction model or adding a "factor of safety" to ensure safe structural

design at the cost of economy. A safe and cost-effective design requires the collection of data from both laboratory experiments and field events (Lu et al. 2008).

Over the years, the researchers have been proposing models for different type of bridge scour to include abutment, lateral contraction, vertical contraction, and pier scour. To this end, a significant advancement in pier scour prediction has been observed since 1990 (Ettema et al. 2010). However, abutment and contraction scour and their interaction still need further investigation as they arise from complex but simultaneous physical processes arising from turbulence and flow contraction (Sturm et al. 2011). Recent climate change phenomenon may force submergence of bridges resulting in an orifice flow or overtopping of the bridge deck in weir flow. Submergence adds the contribution of vertical contraction scour, which makes the interactive scour even more complex. Concurrent processes of abutment, lateral contraction, vertical contraction, and pier scour and their interaction makes it difficult to predict maximum scour depth. A very few studies are available for the interaction of types of scour (Sturm and Janjua 1994, Sturm 2006, Oben-Nyarko and Ettema 2011, Sturm et al. 2011, Hong 2013, Hong et al. 2015).

Hydraulic Engineering Circular-18 (HEC-18) developed by the Federal Highway Administration (FHWA) recommends a sum of all four components of scour (abutment scour, lateral contraction scour, vertical contraction scour, and pier scour) for the estimation of total scour at one point (Arneson et al. 2012). Use of the HEC-18 value yields an overestimate of the scour depth, resulting in an uneconomical bridge design while the non-availability of field measurements at the peak of a flood event may result in under estimation of scour depth that threatens the stability of the structure (Lee and Sturm 2009, Sturm et al. 2011). In addition, scour depth predicted by mathematical

models may exceed the one measured in the field (Ettema et al. 2006). This discrepancy is a source of motivation for this research, which seeks to develop a more realistic and accurate scour depth estimation model by analyzing the interaction of all four components of scour under various flow conditions.

1.3. Research Objectives

Hong studied interaction of contraction and abutment scour for spill-through abutments, under all three flow conditions (Free, Submerged Orifice, and Over-toping flow), for long setback abutments (LSA), bankline abutments (BLA), and short setback abutments (SSA) and presented a set of scour prediction equations for LSA and BLA (Hong 2013). The experiments were conducted in the 14-ft wide flume at the Georgia Institute of Technology. An extension of this research has been conducted in this study, with the main objective to further explore the interaction of pier scour with the already established interaction of lateral contraction and abutment scour in the floodplain. Contribution of vertical contraction scour interacting with pier, abutment, and lateral contraction scour has also been analyzed. Figure 1-3 explains the schematic layout of interaction of bridge scour components.

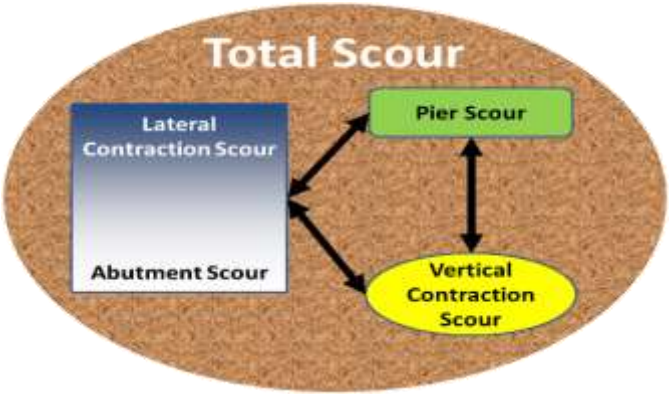

Figure 1-3 Schematic layout of interaction of bridge scour components

The objectives of the study are:

a. Study the interaction of pier scour with vertical contraction and abutment/ lateral contraction scour in the floodplain.
b. Quantify the vertical contraction scour contribution to other components of scour.
c. Develop a method of predicting the total interactive scour.
d. Plug the gaps in experiments conducted by Hong (2013) for verification of results and to help improve the data set and its range of applicability.
e. Refine criterion for long and short setback abutments.
f. Study the time development of an interactive scour and prediction of equilibrium scour location.

CHAPTER II

LITERATURE REVIEW

2.1. General

In economical bridge design, choosing the minimum possible opening through which the flow is constricted is one of the foremost design criteria. This constriction causes a considerable rise in flow intensity, resulting in scour within and near the bridge section. The causes of bridge scour are flow dynamics in the bridge section, the formation of vortices and flow structures, and excess turbulence near the bed. Bridge scour is the source of partial failure and collapse of bridges in extreme floods. In the United States, 60% of bridge damages are due to hydraulic failure, including pier and abutment scour (Jau-Yau et al. 2008). In this section, a brief review of the literature is presented regarding different components of scour associated with a bridge section.

2.2. Initiation of Particle Motion

A balance between lift and drag forces, with the gravitational force resisting the particle motion and lift force trying to move the particle, is the criterion for establishing the threshold of sediment motion in terms of a critical shear stress. For sediment motion in cohesive sediments, additional inter-particle forces also affect the force balance (Wang and Sturm 2013). As shown in Figure 2-1, critical shear stress can be determined from Shields' parameter, $\tau_{*c} = \tau_c / (\gamma_s - \gamma) d_{50}$, which depends on a dimensionless sediment

diameter, $d_* = \left((SG-1)gd_{50}{}^3/\nu^2\right)^{1/3}$, in which τ_c is critical shear stress, γ is specific weight of water, γ_s is specific weight of sediment, d_{50} is the median sediment grain size, SG is specific gravity of the sediment and ν is kinematic viscosity of water.

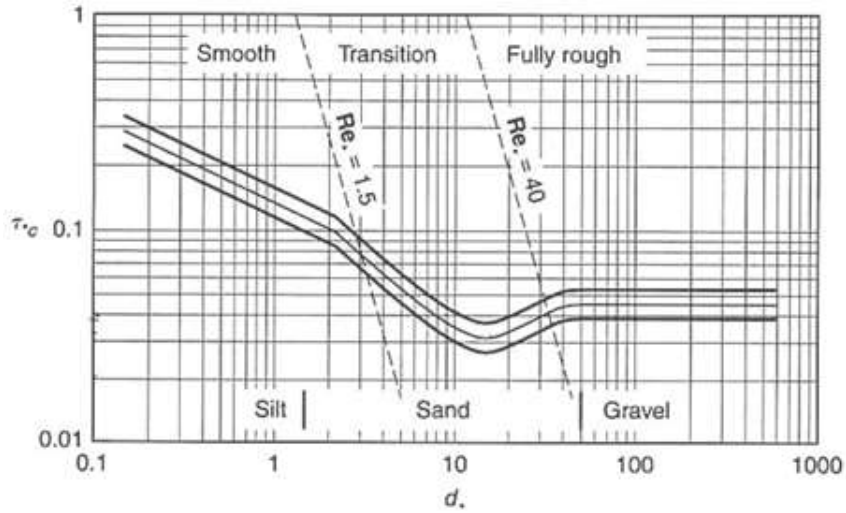

Figure 2-1 Shields' diagram

In a contracted bridge section, where velocity and shear stress both exceed the critical values of V_c and τ_c respectively, sediment motion is initiated resulting in an increase of flow depth by removal of sediments from the bed. This removal of sediment increases the flow area, which subsequently reduces both shear stress and velocity. Equilibrium is achieved through continuous increase in the flow area, which reduces the shear stress and velocity to the critical values. Critical velocity for fully-rough turbulent flow is given by Keulegan's equation (Sturm, 2001):

$$V_c = 5.75\sqrt{\tau_{*c}(SG-1)gd_{50}}\log\left(12.2R/k_s\right) \qquad (2\text{-}1)$$

in which τ_{*c} = Shields' parameter, SG = specific gravity of the sediment, g = gravitational acceleration, d_{50} = median sediment size, R = hydraulic radius, and k_s = equivalent sand-grain roughness which depends on the median sediment size, d_{50}.

2.3. Scour Processes and Types

Scour is classified into two basic types:

- Scour types based on upstream sediment transport conditions
- Scour types based on river and hydraulic structure geometry

2.3.1. *Scour Types Based on Upstream Sediment Transport Conditions*

Depending on upstream flow conditions, there are two types of scour: clear water scour (CWS) and live-bed scour (LBS). For CWS, water does not transport any sediment in the approach section (upstream flow) and the converse is true for the phenomenon of LBS. The main difference in both types is the magnitude of scour depth and the time required to reach equilibrium. Clear-water scour takes more time to reach equilibrium because all the sediment derives from the local scour hole until the velocity and shear stress have decreased to their critical values. Live-bed scour, on the other hand, reaches equilibrium when the sediment transport rate into the scour hole equals that out of the scour hole (sediment continuity equation is satisfied). Depth of scour in CWS is greater by about 10% as compared to LBS, as shown in Figure 2-2. To determine occurrence of LBS or CWS, the approach velocity is calculated and compared with critical velocity associated with median particle size d_{50}, with $V_1/V_c \leq 1.0$ for CWS and $V_1/V_c > 1.0$ for LBS.

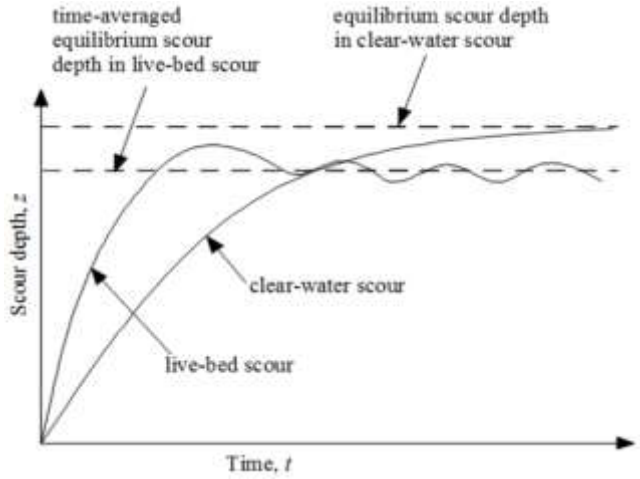

Figure 2-2 Clear water and live-bed scour (Kiraga and Popek 2016)

2.3.2. *Scour Types Based on River and Hydraulic Structure Geometry*

If the local sediment carrying capacity is more than the sediment carried by the river water then the scour is likely to occur. However, hydraulic structures such as bridge causes flow constriction, local flow separation, and turbulence, which contribute to scour. Three main types of scour based on river and bridge geometry are general scour, contraction scour, and local scour.

2.3.2.1. *General Scour*

A general scour may occur anywhere in the river, which may either be caused by change in river geometry or by the presence of any hydraulic structures such as bridges. This type of scour can be a long-term scour or a short-term scour. However, a general scour is normally defined by long-term geomorphic changes in the river (Coleman and Melville 2001).

- **Short-term General Scour:** A short-term general scour is a result of smaller duration events like short successive floods, scour due to shifting of bed forms, channel relocation due to braiding, merging of two streams or scour at bends.
- **Long-term General Scour:** A long-term general scour is sustained over extended time scales of the order of decades or even longer. This type of scour is exhibited by various events including lowering of the river bed, channel widening as a result of bank erosion, and change in river course either due to anthropogenic or natural changes.

2.3.2.2. *Contraction Scour*

Contraction scour results from a decrease in the cross section area of a river or stream, which leads to flow acceleration resulting in higher velocities, especially at a bridge site. Lowering of the bed, as a result of contraction scour may be uniform or varying along the width of the contracted section, depending on the physical conditions (Arneson et al. 2012). The contraction may either be lateral or vertical, causing lateral contraction scour or pressure flow scour, respectively.

- **Lateral Contraction Scour**: Flow through a contraction, such as a bridge, particularly during heavy flood events, results in an increase in velocity and shear stress beyond the critical limit, which generates scour. This type of scour is known as lateral contraction scour. This process is localized in nature and extends a considerable distance starting from the upstream edge of the abutment in the downstream direction. Lateral extent of the scour hole increases with increase in degree of geometric and flow contraction.

- **Pressure Scour/ Vertical Contraction Scour:** When water passes through the bridge section such that the lower chord of the bridge is submerged by the flowing water surface, the flow is subject to vertical contraction. This phenomenon creates additional vertical forces, induces turbulence, and increases velocity, which potentially increases scour known as vertical contraction scour. If water does not overtop the bridge but submerges the lower chord of the bridge deck, the condition is known as "submerged orifice flow" (SO Flow) whereas if the flow overtops the bridge, it is defined as "overtopping flow" (OT flow). However, SO flow is more critical in nature as the water passing over the bridge provides flow relief and reduces the pressure effect in case of OT flow (Hong 2013).

Most previous laboratory experiments have used free flow conditions for scour analysis (Ettema et al. 2006, Sturm 2006, Ataie-Ashtiani et al. 2010, Hager and Unger 2010, Kothyari and Kumar 2012, Lança et al. 2013, Ettema et al. 2015, Hong et al. 2015). In contrast to free flow, pressure flow induces more scour in a channel for given approach flow conditions, as the flow gets compressed under the bridge, which can only acquire stability by attaining critical shear stress and velocity through scouring of bed sediment (Junke et al. 2009).

2.3.2.3. *Local Scour*

Local scour is defined as the erosion of sediment around local objects like abutments, piers, and dikes. As defined in HEC-18, this type of scour is localized in nature. As the flow approaches the bridge section, it converges due to obstructions by

river training works resulting in acceleration and formation of vortices in interaction with abutments, piers, spurs, and embankments which cause local scour (Arneson et al. 2012).

- **Pier Scour:** Pier scour is a type of local scour around bridge piers, which are located away from the bank of the main channel and abutment, such that the influence of bank erosion and abutment scour do not affect the flow conditions and scour process. The scour phenomenon is an outcome of a horse-shoe vortex at the upstream end and a wake vortex at the downstream end of the pier which form due to flow obstruction. Pier scour follows a logarithmic progression with time, and equilibrium depth can only be achieved in weak approach flow conditions or in non-uniform sediments (Melville and Coleman 2000). Piers consisting of a combination of columns, pile cap, and pile group are known as complex piers. Prediction of scour depth is difficult in complex piers such as a pile group. The scour hole and vortices form at different piles of a pile group and interact with each other because they are in close proximity. As a result, the scour depth that develops at each pile is different than that for a single normal pier (Lança et al. 2013).
- **Abutment Scour:** The geometric contraction by an embankment terminating at an abutment causes flow acceleration and flow separation starting from the upstream edge of the abutment. This flow separation and contraction results in a flow field, which generates local scour around the abutment, known as abutment scour. Local flow fields result in the scour both on the upstream and downstream sides of the bridge abutments, but the maximum scour depth is either under the bridge across from the face of the abutment or directly downstream of the bridge.

2.4. Criterion for Equilibrium Scour

Clear-water scour development follows a logarithmic profile with time and most investigators agree that it asymptotically reaches an equilibrium condition. Thus, researchers have suggested criterion for equilibrium scour as a fraction of change in scour depth below a specified time limit. With minor variations, this criterion remains nearly the same for different researchers. For the experiments conducted for pier scour, equilibrium condition was defined as 1 mm or less change in scour depth in a 2 hour time period (Dey and Raikar 2007). Melville, for his experiments of pier scour, recommended a criterion for equilibrium scour as $\Delta d_s < 0.05a$ in 24 hours (Melville and Chiew 1999) where Δd_s = change in scour depth and a = pier diameter. Ettema used the criteria as Δd_s < 1 mm in 4 hours for the experiments of abutment and contraction scour (Ettema 1980). Lança, for his pier scour experiments, used a strict criterion and the experiments were stopped when the change in scour depth was less than 2mm = $2d_{50}$ in 24 hours and the experiment had continued at least over seven days (Lança et al. 2013). This resulted in experimental runs of about 2.5 times more duration than Melville and Chiew (1999) and Ettema (1980). Lança also concluded that the equilibrium scour given by Melville and Ettema represented 90% and 80% of the actual equilibrium scour, respectively. It was concluded that, for experiments lasting for less than 7 days, for the pile groups, certain implicit uncertainties are inherent in finding the equilibrium scour depth.

The criterion for equilibrium as used by Melville and Chew (1999) for a change in scour depth of less than 5% of pier diameter in 24 hours was further refined as 5% change in 24 hours for the smaller of pier diameter or abutment length (Coleman et al. 2003). Grimaldi used a more strict approach by reducing the limit with an additional

factor of 1/3, making it less than 0.05*a*/3 in 24 hours, where *a* = pier diameter (Grimaldi 2005). The factor of 5% is arbitrary, which if reduced further can significantly increase the time of experimentation (Simarro et al. 2011). Hong (2013) used a criterion of change in scour depth of less than 5% of the total scour in 24 hours for the study of interaction of abutment and contraction scour. Simarro et al. (2011) also showed that for certain experiments, equilibrium time criteria show significant errors in equilibrium scour (d_{se}). It was further concluded that the expressions of Lanca at al. (2010) provided good estimates of equilibrium scour depth if the experiment continued for 1-2 weeks. For experiments conducted over shorter durations, extrapolation of equilibrium scour (d_{se}) may give inaccurate results. A summary of the equilibrium criterion used by different researchers is presented in Table 2-1.

Table 2-1 Equilibrium criterion for different researchers

Researcher	**Equilibrium Criterion**	**Type of Scour**
Ettema (1980)	Δd_s< 1 mm in 4 hours	Abutment/ Contraction
Melville and Chiew (1999)	Δd_s< 5% of *a* in 24 hours; *a* = pier diameter	Pier
Coleman et al. (2003)	Δd_s< 5% of smallest of *a* or abutment length in 24 hours	Pier, Abutment/ Contraction
Girmaldi (2005)	Δd_s< 5%/3 in 24 hours	Abutment/ Contraction
Dey (2007)	Δd_s< 1 mm in 2 hours	Pier
Lanca et al. (2013)	Δd_s< 2 mm = 2*d50* in 24 hours	Pier
Hong (2013)	Δd_s< 5% in 24 hours	Abutment/ Contraction

2.5. Time Duration of Experiments

Laboratory experiments are performed for different time durations depending on the purpose of experimentation, ranging from acquiring equilibrium as per specified criteria, as discussed in para 2.4 above, to a shorter duration with extrapolation of time to estimate equilibrium scour depth. Dey continued pier scour experiments up to 80 hours, which was considered sufficient for attaining equilibrium scour (Dey and Raikar 2007). Umbrell conducted pressure flow experiments for vertical contraction scour for a duration of 3.5 hours. Experiments were stopped without reaching equilibrium and extrapolation of data was carried out as per Laursen's (1963) experiments (Umbrell et al. 1998). Junke conducted experiments for bridge pressure flow scour for a duration varying between 32-48 hours and claimed equilibrium scour (Junke et al. 2009), which is contrary to other researchers' results. Experiments by Oben and Ettema (2011), for pier and abutment scour interaction, continued until the equilibrium criterion was achieved. However some of the experiments continued only for 6 hours where the erodible embankment failed and for 24 hours where the main channel had a live-bed scour condition (Oben-Nyarko and Ettema 2011). It can safely be concluded that, for accurate estimation of equilibrium scour depth, the experiment should continue until the specified equilibrium criterion is achieved. For experiments conducted over shorter durations, extrapolation to equilibrium scour (d_{se}) results in an inaccuracy (Simarro et al. 2011).

2.6. Time Development of Scour

Time development of scour is necessary as some researchers follows that time required to reach equilibrium scour for the clear water scour case is infinite which can

only be reached asymptotically (Melville and Chiew 1999, Lopez et al. 2014). Another reason to monitor the time development is associated with flood duration, which may not produce an equilibrium scour resulting in a lesser scour depth. Therefore, researchers have focused on the time development of scour to estimate scour depth at times less than equilibrium (Mia and Nago 2003, Lu et al. 2008, Hahn and Lyn 2010, Arneson et al. 2012, Kothyari and Kumar 2012).

Time rate of scour development has been approximated by numerous researchers. Melville and Chiew (1999) observed that for pier scour less than 50% of the equilibrium scour develops in 10-12 hours after initiation of the scour process, and that for clear water conditions, 80% of the equilibrium scour develops in 5-40% of the time to equilibrium. Another investigation by Mia and Nago (2003) stated that in approximately 10% of the time to equilibrium scour, depending on the approach flow velocity, 50-80% of the equilibrium scour is reached (Mia and Nago 2003). In the experiments conducted by Hahn and Lyn (2010) significant changes in bed elevation just downstream of the bridge were observed within two to three hours which followed a logarithmic trend (Hahn and Lyn 2010).

2.7. Sediment Size Scaling Issues

In laboratory experiments, time and sediment coarseness limitations are major factors which contribute to discrepancies between field measurements and laboratory results (Lança et al. 2013). However, the field measurements also suffer from measurement accuracies because of accessibility issues in extreme events, thus denying the true maximum scour field measurement (Lee and Sturm 2009, Sturm et al. 2011).

Most researchers present bridge scour formulas based on experimental studies alone because relating the 3D interaction of the river flow with obstructions caused by a pier/foundation or an abutment using numerical models is very difficult. Field measurements made with the latest instrumentation exhibit more scattered data, whereas formulas based on laboratory experiments generally result in over-prediction. This difference is attributed to imprecise knowledge of field flow conditions, time development, and the scaling issues in the laboratory; however, the exact answer is yet to be ascertained. If we only apply the Froude Number criterion for similarity, choice of the sediment size in the laboratory distorts the pier width to sediment size ratio in the model (a/d_{50}) which gives smaller values as compared to the prototype. Despite extensive research on this subject the issue has not yet been resolved. In the laboratory experiments on pier conducted at the Georgia Institute of Technology it was observed that at a/d_{50}=25 (a/d_{50}=25 gives max scour, a = pier diameter), field values could be predicted as approximately 70% of the lab values (Lee and Sturm 2009).

In the field, sediment size is such that a/d_{50} is very large, thus the effect on normalized equilibrium scour (d_{se}/a) is not significant. In the lab, normalized equilibrium scour (d_{se}/a) tends to increase with a/d_{50}, up to $a/d_{50}=25$, and then becomes independent (Raudkivi 1986). However, Sheppard et al. (2004), based on experiments in large flumes, have stated that normalized equilibrium scour (d_{se}/a) tends to decrease at higher values of a/d_{50}. Therefore a/d_{50} is to be considered as an additional factor that affects the discrepancy between field and laboratory measurements.

Scaling sediment size (d_{50}) according to geometric ratio based on Shields' criterion may introduce inter-particle forces because particle size generally reduces to

cohesive particle sizes. To overcome this discrepancy, the flow intensity parameter (V_1/V_c) is reproduced in the model from the prototype, which can violate Froude number similarity because larger critical velocity values result from a larger particle size that is required to overcome inter-particle cohesive forces in models. Another distortion that occurs because of particle size selection constraint in the model is a/d_{50}, which accounts for large scale unsteadiness of the horseshoe vortex upstream of the pier. It was suggested that these two discrepancies can be accounted for by keeping the degree of Froude number distortion small while compensating for a/d_{50} (Lee and Sturm 2009).

In laboratory experiments, mainly uniform sediment is used with $\sigma_g < 1.5$ (Dey and Raikar 2007, Hahn and Lyn 2010). This gives the maximum scour effect for the given sediment size and is useful to find out the effect of sediment size on scour depth. Froude number similarity violation by a very narrow margin, by reproducing the same approach flow intensity variable (V_1/V_c) in the model as in the field, can help overcome the sediment size scaling issues if the selected material size gives the same scour value near the maximum clear water approach flow condition ($V_1/V_c \simeq 1$) as that of the field, as shown in Figure 2-3 (Hong and Abid 2016).

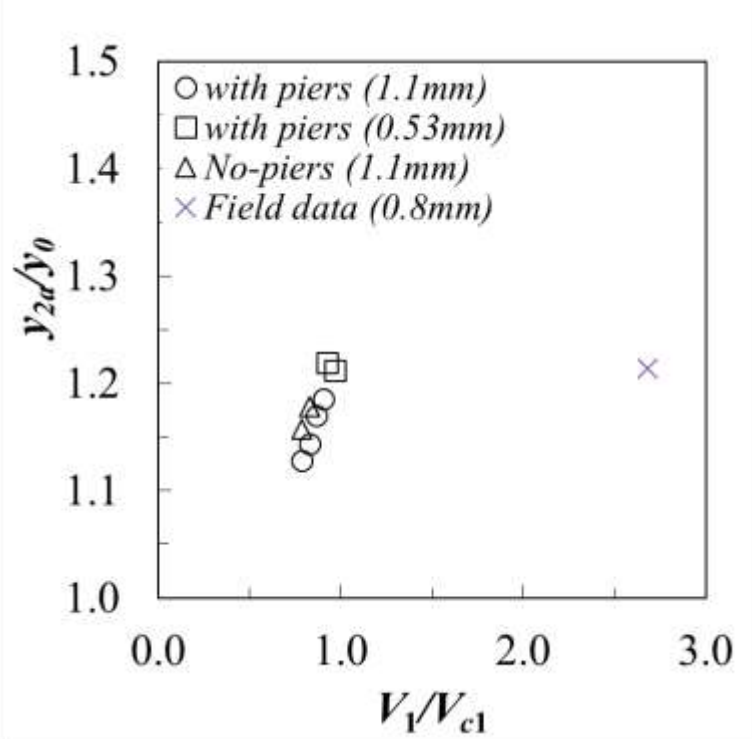

Figure 2-3 Sediment size selection and approach flow intensity effect for reproducing equilibrium scour, where y_{2a} = average water depth at equilibrium, y_o = tail-water depth, V_1 = approach velocity, and V_{c1} = critical velocity in approach section (Hong and Abid 2016)

2.8. Turbulence and Scour Relationship

Scour at a bridge section is a complex process, which depends on the three-dimensional turbulent forces within the scour hole and the properties of sediment in the river bed. Geometry of scour hole in cohesive soils is different from that in cohesion-less soils (Kothyari et al. 2014). Causes for development of scour are associated with complex turbulent flow fields defined by large-scale, unsteady turbulent configurations, which include horseshoe vortex, wake vortex, and surface rollers as shown in Figure 2-4.

Researchers have mainly focused on the equilibrium scour depth (Chreties et al. 2008, Guo et al. 2009, Junke et al. 2009, Ataie-Ashtiani et al. 2010, Hager and Unger 2010, Hong 2013). Time development of scour with regard to flow characteristics to

include velocity/flow variation and turbulence behavior in the horseshoe vortex has not been adequately addressed. Understanding this phenomenon is important to know the temporal variation and development of the scour hole. Experiments conducted by Dey gave an insight to understand the flow and turbulence characteristics in the horseshoe vortex and their effect on scour hole development (Dey and Raikar 2007). It was shown that the horseshoe vortex at the pier nose on the upstream side extends along the horizontal axis, whereas, the wake vortex downstream of the pier extends along the vertical axis. The reason for such geometry is partial blockage of the flow by the pier and a resultant down flow at the upstream pier face. Most of the scouring is caused by the horseshoe vortex, which leaves the wake vortex in live-bed condition, thus reducing the scour in the wake region.

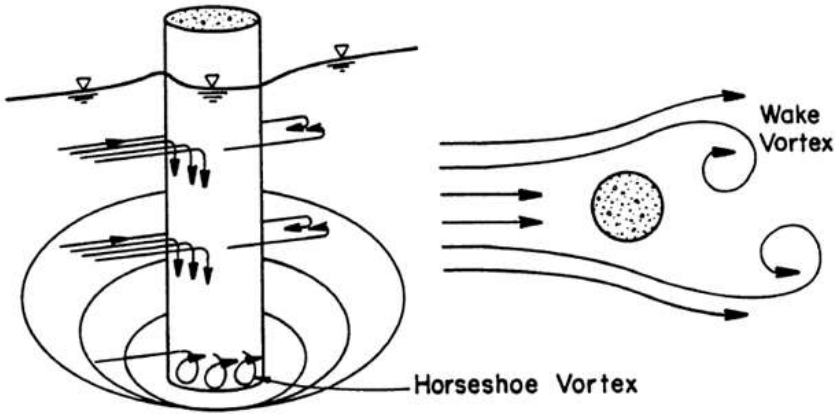

Figure 2-4 Horseshoe and wake vortex around piers (Arneson et al. 2012)

The study by Ettema (2006) represents influence of two parameters on the scour process: frequency of vortex shedding and magnitude of vorticity in the wake region of a pier. Three different length scales were highlighted as pier diameter, particle diameter, and flow depth, which lead to a dynamic similitude that cannot be satisfied

simultaneously. Sediment particles entrained by the horseshoe vortex are moved and lifted by the wake vortex, which carries them in a spiral path reaching as high as 80% of the flow depth behind the pier. The result is that they move them out of the scour hole (Ettema et al. 2006). Conclusions of the study were:

- For the same approach flow conditions, normalized equilibrium scour depth (d_{se}/a) decreases as the pier diameter increases.
- Shedding frequency and vorticity of wake vortices ($V_1{}^2/ga$), also decreases with increase in pier diameter. This decrease coincides with the decrease in normalized equilibrium scour depth (d_{se}/a).
- Vorticity of wake flow behind a smaller pier size is more than that of a larger one. This indicates that for same approach flow, smaller pier size has more capacity of removal of sediment.

Ettema suggested an adjustment factor (K_w) for similitude in the turbulent structures around the piers. This adjustment is required for the three length scales associated with local scour depth: pier diameter, particle diameter, and flow depth and is given by, $K_w = 0.95(D_o / a)^{-0.26}$, where $(D_o = 0.45)$. However, further verification of this adjustment factor was suggested.

Sturm and Lee (2009) conducted a study for particle motion in the horseshoe vortex formed by a pier. It was observed that secondary vortices are formed in the horseshoe vortex, which fluctuate haphazardly, stretch around the pier, and then combine in the primary vortex in a time scale of $10a/V_1$. The horseshoe vortex and the point of flow separation move back and forth in the streamwise direction, which accounts for the unsteady motion of sediment particles in front of the pier. The sediment motion was

oscillating and it took a time of $26a/V_1$ to wash out of the scour hole after initiation of motion. In contrast, the motion of coarser particles was different as they moved like bed load sliding and hopping and took a time of $30a/V_1$ to wash out from the scour hole (Lee and Sturm 2009).

Velocity measurements at x/a = -0.33 (where x = distance in flow direction, originating from upstream edge of the pier) were taken and dual peaks in the frequency distribution were observed for both streamwise and vertical velocities normalized by approach flow velocity V_1. It was observed that horseshoe vortex accounts for negative streamwise velocity, which converts into a positive streamwise velocity as the separation moves closer to pier, thus giving dual peaks. Maximum scour occurred when the frequency of suspension of the sediment due to turbulence (f_L) matched with the frequency of transporting events (f_T). Maximum scour depth (d_{se}/a) occurred for $f_L = f_T$ and a/d_{50}=25. With $f_L > f_T$ and a/d_{50}>25, value of normalized scour decreased with the increasing values of a/d_{50}, as increasing value of a/d_{50} means larger pier diameter, generally in the field, relative to the sediment size.

2.9. Dimensional Analysis

Dimensional analysis for predicting scour depth results in various combinations of non-dimensional groups having requisite significance. However, flow intensity parameter is the one which has most extensively been used (Melville and Coleman 2000). This parameter is of significant value where $V_1/V_c < 1$ indicates clear water scour conditions and $V_1/V_c > 1$ indicates live-bed scour conditions (Simarro et al. 2007). Because a large number of variables affect the scour process, it is very difficult to obtain an accurate

method of scour prediction. Before an experimental study, it is necessary to carry out dimensional analysis to identify and elucidate the effect of each variable and represent experimental data in unified terms. Sturm *et al*. (2011) conducted a detailed dimensional analysis of abutment and contraction scour in a compound channel, which is reproduced here (Sturm et al. 2011). Non-dimensional variables for the pier scour component used by Oben and Ettema (2011) have also been added to account for the pier scour contribution to total scour. Figure 2-5 shows the variables used in the dimensional analysis.

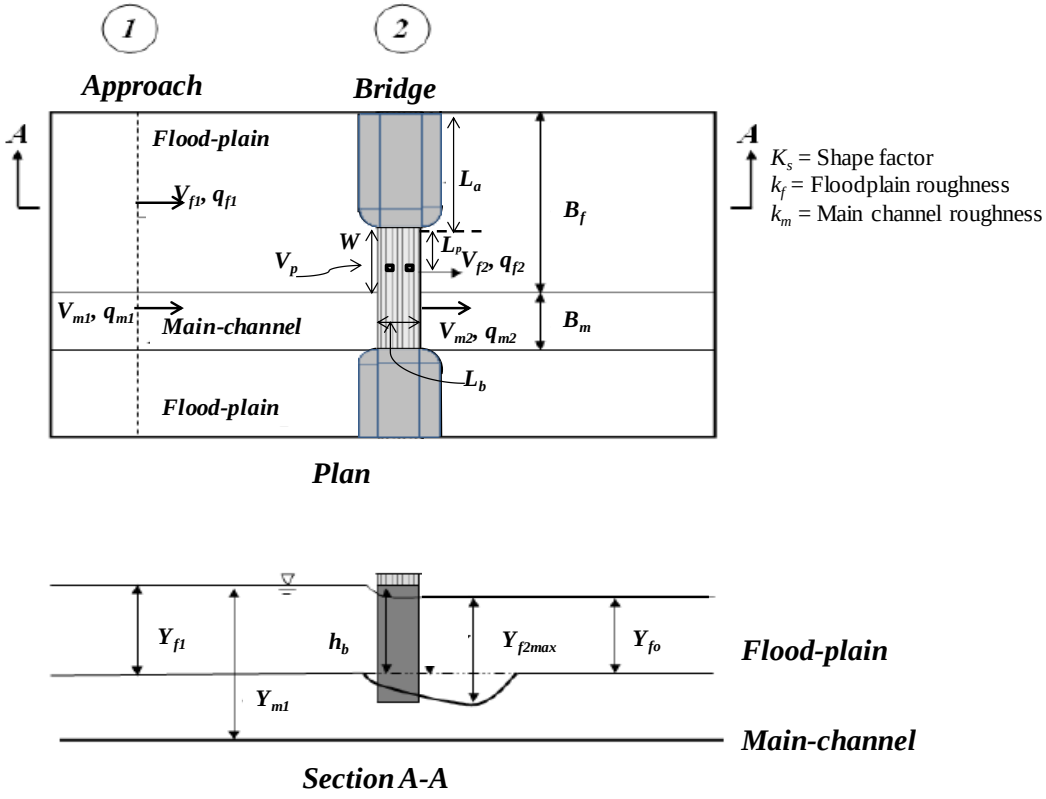

Figure 2-5 Definition sketch for variables of dimensional analysis

$$\frac{Y_{2\max}}{Y_1} = f\left(\frac{d_{50}}{Y_{f1}} or \frac{V_1}{V_c}, \frac{V_1^2}{gY_1}, \frac{\rho V_1 L_a}{\mu}, \frac{L_a}{d_{50}}, \frac{L_a}{Y_f}, \frac{L_b}{Y_f}, K_s, K_\theta, \frac{h_b}{Y_{f_1}}, \frac{Y_{m1}}{Y_{f_1}}, \frac{L_a}{B_f}, \frac{B_m}{B_f}, \frac{k_f}{k_m}, \frac{\sigma}{\gamma_e H_e}, \frac{V_{f1} t}{Y_{f1}}, \frac{L_p}{W}, \frac{L_p}{a}, \frac{L_p}{Y_{f1}}\right) \quad (2\text{-}2)$$

where Y_{2max} = flow depth at point of maximum scour, Y_1 = approach flow depth, d_{50} = median sediment size, V_1 = velocity of approach flow, V_c = approach critical velocity, ρ and μ are density and viscosity of fluid respectively, L_a = abutment length, K_s and K_Θ are shape and alignment factors respectively, h_b = flow depth under bridge with respect to undisturbed bed level, Y_{m1} and Y_{f1} are approach flow depth in main channel and floodplain respectively, B_m and B_f are main channel and floodplain width respectively, k_f and k_m are roughness height of floodplain and main channel respectively, σ = bulk shear strength of embankment, Υ_e = bulk density of embankment material, H_e = height of embankment, t = time, L_p = distance of pier from toe of abutment in transverse direction, W = width of floodplain in contacted section and a = pier width/ diameter.

The dimensionless parameters have been classified in five groups named as G1, G2, G3, G4 and G5 (Sturm et al. 2011). Details of all these groups have been reproduced as Table 2-2. Group G1 includes flow intensity, Froude number, and Reynolds number, which influence the stage of sediment transport, effect of gravity on water surface profile and effect of flow separation and bed roughness, respectively. Group G2 includes relative sediment size, which is related to sediment scaling issues. Group G3 includes flow and abutment geometry where Melville formula accounts for L_a/Y_{f1}. Group G4 includes abutment, flow and channel length scales. The geometric parameters taken together can be translated into discharge contraction ratio or q_2/q_1 for both main channel and floodplain. The abutment stability parameter in Group G5 is $\sigma/\Upsilon_e H_e$, which accounts for slope instability and is difficult to model in laboratory experiments.

Table 2-2 Classification of abutment scour parameters (Reproduced from Sturm *et al.* 2011)

Dimensionless Parameter Groups	***Parameter Names***	***Parameter Group***	***Influences***	***Comments***
u_{*1}/u_{*c} *or* V_1/V_c, $V_1/(gY_1)^{0.5}$, $\rho V_1 L/\mu$	Flow intensity, Froude number, Reynold number	G1 Flow/Sediment	*Stage of sediment transport; effect of gravity on water surface profile; effect of flow separation and bed roughness*	*Flow intensity indicates flow interaction with the sediment and can be used to classify clear-water vs live-bed scour*
L_a/d_{50}	Relative sediment size	G2 Abutment/ Sediment Scale	*Unclear but may be related to model scaling issues*	*Generally not included in abutment scour formulas*
L_a/Y_{f1}, W/Y_{f1}, K_s, K_Θ	Floodplain aspect ratio, relative contraction length, abutment shape and skewness factor	G3 Abutment/ Flow Geometry	*Measure abutment dimensions relative to scale of flow field, and shape and orientation of abutment relative to flow field*	*Abutment scour formulas classified by Melville according to value of* L_a/Y_{f1}
L_a/B_f, B_f/B_{m1}, B_{m2}/B_{m1}, Y_{f1}/Y_{m1}, Y_{f1}/k_f, k_f/k_m	Abutment, channel and flow length scales	G4 Abutment Flow distribution	*Taken together, these parameters can be translated into discharges per unit width of the flow in approach and test section*	*Discharge contraction ratio* (q_{f2}/q_{f1}) *determined by these parameters*
$\sigma/\Upsilon_e H_e$	Abutment stability parameter	G5 Scour/ Geotechnical Failure	*Scour that leads to slope instability*	*Difficult to model in laboratory*

2.10. Research Models Based on Experimental Results

Over the last few decades, researchers have extensively investigated the problem of scour prediction with different approaches, including study of effect of sediment and its properties, turbulent behavior, flow intensity effect, and Froude number approach, which resulted in different empirical formulas and mathematical models. The models for lateral contraction, vertical contraction, pier, and abutment scour are presented in the subsequent section.

2.10.1. *Lateral Contraction Scour*

A natural channel width reduction or a hydraulic structure blocking the channel causes flow acceleration resulting in contraction scour. Melville and Coleman (2000) specified that most of the scientists use a simple rectangular channel with a contraction long enough to assume uniform flow both in approach and contracted section. Laursen used the sediment continuity concept by incorporating both bed-load and suspended-load for live-bed scour (LBS) condition as given by Equation 2-3 (Laursen 1960). This is referred as the theoretical long contraction scour as shown in Figure 2-6.

$$\frac{Y_2}{Y_1} = \left(\frac{Q_t}{Q_c}\right)^{6/7} \left(\frac{B_{m1}}{B_{m2}}\right)^{P_1} \left(\frac{n_2}{n_1}\right)^{P_2} \qquad (2\text{-}3)$$

in which, Q_c = approach flow-rate in main channel, Q_t= total flow-rate through bridge opening main channel, n = Manning's resistance coefficient, P_1, P_2= exponents from Laursen's total sediment transport formula depending on whether sediment load is mostly bed-load, mixed load, or mostly suspended load, B_{m1}= approach-flow main channel width, and B_{m2} = contracted section main channel width.

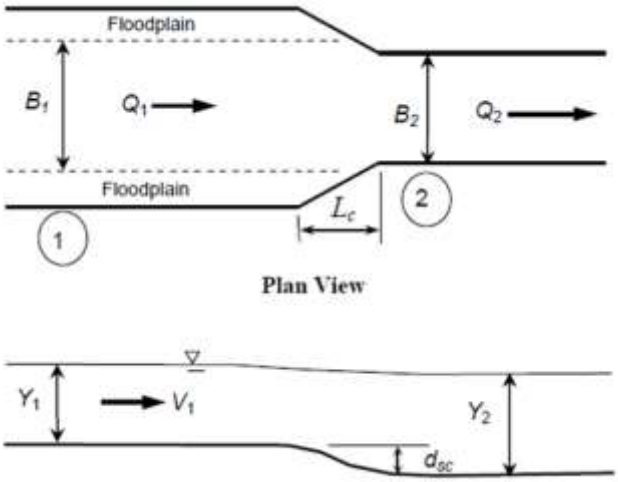

Figure 2-6 Definition sketch for theoretical long contraction scour (Q_1 = $Q_{channel}$= main channel flow-rate at approach flow section; Q_2= Q_t= total flowrate in main channel at contracted section; B_1 = B_{m1} = approach flow main channel width; B_2 = B_{m2} = contracted main channel width; d_{sc} = contraction scour depth; Y_1= approach flow depth and Y_2 = contracted section equilibrium depth). Reproduced from Sturm *et al*. (2011).

HEC-18 recommends the Equation (2-3) for LBS conditions with the exception of dropping the Manning's *n* ratio. If the head loss and change in velocity head is neglected between section 1 and 2, which is assumed in most of the cases, then $d_{sc} = Y_2 - Y_1$. Laursen (1963) applied the concept of theoretical long contraction scour for clear water scour (CWS) conditions and assumed a critical shear stress value in the contracted section at equilibrium as given by Equation 2-4 (Laursen 1963).

$$\frac{Y_2}{Y_1} = \left(\frac{B_{m1}}{B_{m2}}\right)^{6/7} \left(\frac{\tau_1}{\tau_c}\right)^{3/7} \tag{2-4}$$

Ettema (2010) related the geometric contraction ratio to the flow contraction ratio and rewrote the equation as Equation 2-5:

$$\frac{Y_2}{Y_1} = \left(\frac{q_2}{q_1}\right)^{6/7} \left(\frac{\tau_1}{\tau_c}\right)^{3/7} \tag{2-5}$$

HEC-18 however, suggests a modified approach by relating the shear stress in the contracted section to a critical value $\tau_2 = \tau_c$ and suggests incorporating Shields' parameter for solving for the critical shear stress by using Manning's equation. The modified equation by HEC-18 is in terms of contracted section variables and is given by Equation 2-6 (Arneson et al. 2012).

$$Y_2 = \left[\frac{n^2 q_2^2}{\tau_{*c}(SG-1)d_{50}} \right]^{3/7} \tag{2-6}$$

Gill (1981) suggested a relationship for the maximum contraction scour based on the long contraction theory and recommended a 58% increase in the scour depth to find a local maximum scour depth as given by Equation 2-7. His experiments cover a wide range of relative shear stress (τ_1/τ_c) which included both CWS and LBS conditions (Gill 1981).

$$\frac{Y_2}{Y_1} = 1.58\left(\frac{B_1}{B_2}\right)^{6/7}\left[\left(\frac{B_1}{B_2}\right)^{1/3}\left(1-\frac{\tau_c}{\tau_1}\right)+\frac{\tau_c}{\tau_1}\right]^{-3/7} \tag{2-7}$$

Application of the continuity equation for sediment transport and flow resulted in analytic formulation of Equation 2-8, which is applicable both for CWS and LBS conditions, (Lim and Cheng 1998).

$$\left(\frac{Y_1}{Y_2}\right)^{4/3}\frac{B_1}{B_2} = \frac{u_{*c}}{u_{*1}} + \left(1-\frac{u_{*c}}{u_{*1}}\right)\left(\frac{Y_1}{Y_2}\right)^{1/3}\left(\frac{B_1}{B_2}\right)^{1/4} \tag{2-8}$$

It was also concluded, analytically, that solution for equation exists only for:

$$\frac{Y_2}{Y_1} = \left(\frac{B_1}{B_2}\right)^{0.75} \tag{2-9}$$

2.10.2. *Vertical Contraction Scour*

Vertical contraction scour or pressure-flow scour is a comparatively new scour research area. For bridges, the phenomenon of vertical contraction results in an increase in the scour depth (Lyn 2008). Amongst more than 600,000 bridges listed in the U.S. National Bridge Inventory, a large number of bridges fall into pressure flow conditions under heavy floods or extreme events, which results in vertical contraction scour (Arneson and Abt 1998).

When the lower chord of the bridge is significantly in contact with water, there are two likely conditions: a) when only upstream section of lower chord of the bridge is in contact with water which creates orifice flow and b) when the complete lower chord is submerged in water, which converts a free flow into a submerged orifice flow known as pressure flow. Pressure flow results in a curvilinear flow under the bridge, which has a non-hydrostatic pressure distribution, so velocity and shear stress cannot be calculated from free surface formulas. Pressure flow increases the shear stress which results in vertical contraction scour (Arneson and Abt 1998).

In flood events, the type of flow changes with the rise of water in a channel. Initially a free flow case turns into pressure flow as the water level rises above the bottom of the bridge deck. Pressure flow increases as the degree of submergence increases. When water starts overtopping the bridge, it acts like a broad crested weir, and the flow is then a combination of weir/overtopping flow and submerged orifice flow (Umbrell et al. 1998). Maximum bridge scour depth under pressure flow conditions occurs near the downstream end of the bridge deck because maximum vertical flow contraction, in the submerged case, is at the end section of the bridge in the streamwise direction, and the

equilibrium condition corresponds to the attainment of critical velocity at minimum flow area. Figure 2-7 explains the variables for the vertical contraction scour models in which d_{se} = equilibrium scour depth, Y_1 = approach flow depth, h_b= water depth under the bridge for undisturbed bed level, V_b = velocity under the bridge for undisturbed bed condition, and V_c = critical velocity for the approach section.

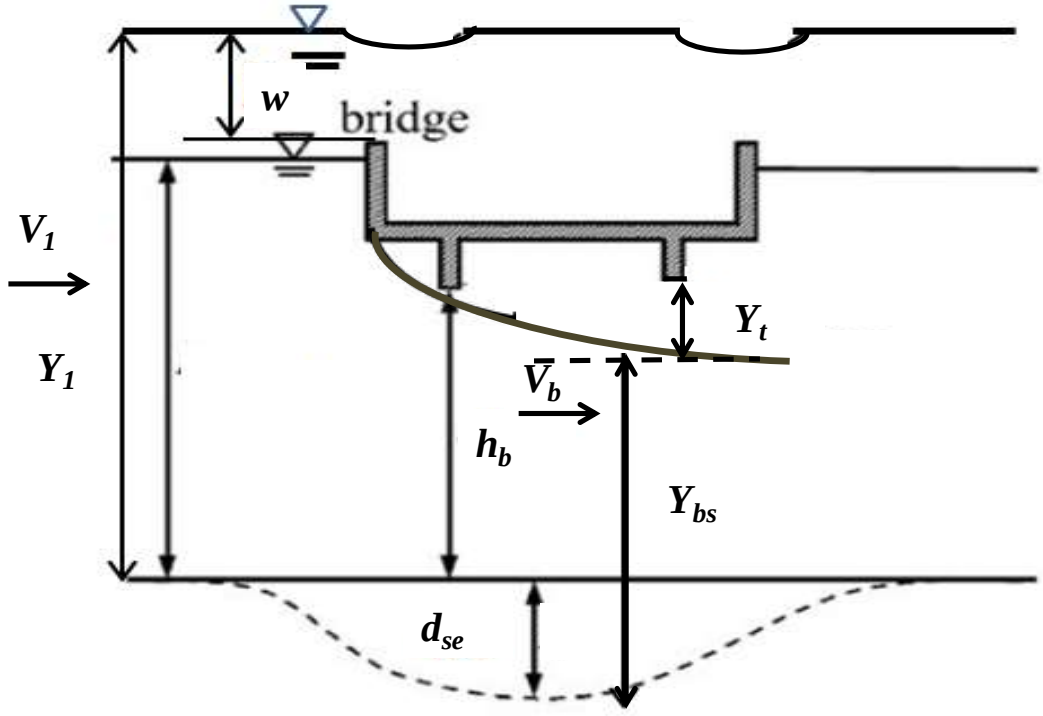

Figure 2-7 Schematic diagram of variables (Pressure flow)

In one of the initial investigations for vertical contraction scour Abed gave a limiting value of 2.3 to 10 times increased pier scour due to pressure flow but the scour components were not delineated (Abed 1991). Jones et al. (1993) gave a relationship, for calculation of pressure flow scour at piers which underestimated the field measurements. A revised formula assumed that pier scour (local scour component at pier) for pressure

flow and free flow is same and that the total scour is a sum of pier and pressure scour (Jones et al. 1993).

Arneson and Abt (1998) conducted a series of pressure flow experiments. His experimental approach followed Froude number similarity. The experiments were conducted for both for CWS and LBS conditions without incorporating any overtopping flow cases. Regression analysis using the least-squares technique was applied to the variable parameters that resulted in the relationship given by Equation 2-10 (Arneson and Abt 1998).

$$\frac{d_{se}}{Y_1} = -0.93 + 0.23\left(\frac{Y_1}{h_b}\right) + 0.82\left(\frac{d_{se} + h_b}{Y_1}\right) + 0.03\left(\frac{V_b}{V_c}\right) \qquad (2\text{-}10)$$

in which d_{se} = equilibrium scour depth, Y_1 = approach flow depth, h_b= water depth under the bridge for undisturbed bed level, V_b = velocity under the bridge for undisturbed bed condition, and V_c = critical velocity for the approach section. Rearranging the equation in terms of water depth under the bridge for undisturbed bed level (h_b) resulted in Equation 2-11.

$$\frac{d_{se}}{Y_1} = -5.08 + 1.27\left(\frac{Y_1}{h_b}\right) + 4.44\left(\frac{h_b}{Y_1}\right) + 0.19\left(\frac{V_b}{V_c}\right) \qquad (2\text{-}11)$$

In these experiments, the critical velocity for initiation of sediment motion was calculated using Neill's equation (Neill 1968, Arneson and Abt 1998). The median grain size, d_{50}, of the material was not used as an independent variable, but implicitly it was included in calculating critical velocity for sediment motion. The coefficient of determination of the regression analysis was 0.89 (Arneson and Abt 1998).

HEC-18 Methodology: In the submerged case, a flow separation zone contracts the flow where the effective depth in the bridge opening can be attributed to occurrence of the critical velocity in the equilibrium condition (refer to Figure 2-7 above). HEC-18 uses the concept of a separation zone at the downstream end of the bridge and applies the continuity equation as (Arneson et al. 2012):

$$h_b + d_{se} = Y_{bs} + Y_t \qquad (2\text{-}12)$$

in which Y_t = height of flow separation below the bottom of bridge deck, h_b = height of bottom chord of bridge above the undisturbed bed level, Y_{bs} = height of water column above the deepest scour point and d_{se} = equilibrium scour depth. For the submerged case without an overtopping component (refer to Figure 2-7 above), it was assumed by applying the continuity equation that at equilibrium:

$$V_1 * Y_1 = V_c (h_b - Y_t + d_s)$$

where Laursen's critical velocity is

$$V_c = K_u * Y_1^{1/6} * d_{50}^{1/3} \qquad K_u = 6.19 / 11.17 \text{ (SI/English Units)}$$

Substituting Laursen's equation into Equation 2.12 results in:

$$h_b + d_{se} = \left(\frac{V_1 * Y_1}{K_u * d_{50}^{1/3}} \right)^{6/7} + Y_t \qquad (2\text{-}13)$$

It is important to note that measurement of the separation zone thickness (Y_t) is difficult in the laboratory and especially in the field. So applying dimensional analysis, the following equation was formulated:

$$\frac{Y_t}{h_b} = 0.5 \left(\frac{h_b (Y_1 - h_b)}{Y_1^{\,2}} \right)^{0.2} \left(1 - \frac{w}{(Y_1 - h_b)} \right)^{-0.1} \qquad (2\text{-}14)$$

where w= depth of weir flow. Comparison between the predicted and the measured values show that the scour depth prediction gives an overestimate.

Umbrell et al. (1998) applied the continuity equation, assuming that flow over the bridge deck has the same velocity as that of the approach flow, and that the velocity under the bridge is critical (Umbrell et al. 1998). The application of the above-mentioned assumption to the continuity equation yields:

$$V_1 Y_1 B = V_1 w B + V_c (h_b + d_{se}) B \qquad \text{OR}$$

$$h_b + d_s = \frac{V_1}{V_c}(Y_1 - w)$$

However, the fitting of experimental results showed the best-fit relation to be Equation 2-15.

$$\frac{d_{se} + h_b}{Y_1} = 1.102\left[\frac{V_1}{V_c}\left(1 - \frac{w}{Y_1}\right)\right]^{0.603} \qquad (2\text{-}15)$$

Equation 2.15 contains Y_1 on both sides of equation, which shows that there is a spurious correlation. By involving the basic hydraulic concepts, in which for non-overtopping experiments, "w" = zero, leaves approach flow depth on one side of the equation only. The comparison of best-fit curve for overtopping and non-overtopping flows showed R^2 value as 0.77 and 0.81 respectively, which confirmed that correlation is not significant in this case.

Lyn (2008) analyzed pressure flow scour and pointed out unsatisfactory features of the HEC-18 equation, which shows that the original equation of Arneson (1997) has a spurious correlation. The range of parameters where this equation is to be applied has also not been given by HEC-18 (Lyn 2008). The value of V_b/V_c in the Arneson equation

is difficult to assess because V_b is associated with the bridge section, where the velocity distribution may be very different from the upstream section depending on Y_1/h_b. Lyn used a statistical technique of power law and applied limit to the flow conditions, by limiting it to clear water cases without pier only, keeping V_1/V_c <0.9. The suggested equation was:

$$\frac{d_{se}}{Y_1} = \min\left[A_1\left(V_b / V_c\right)^{2.95}, A_2\right] \qquad (2\text{-}16)$$

where the values of A_1 and A_2 are 0.105 and 0.5 respectively for the Arneson data. Lyn further examined the data including the pier experiments and suggested an envelope curve with values of A_1 and A_2 as 0.21 and 0.6, respectively. Scatter in the data has been attributed to local pier scour rather than pressure scour as the effect of V_b/V_c was small (Lyn 2008).

Experiments conducted by Hahn and Lyn (2010) investigated vertical contraction scour for the clear water cases with uniform sand (σ_g=1.15) and two approach velocities V_1 = 22.8 and 25.6 *cm/sec* over the range of experiments having L_b/h_b =7, where L_b = length of bridge in flow direction (Hahn and Lyn 2010). The parameter h_b/d_{50} was approximated to 36, which they argue to be sufficient for the sediment scaling effects not being important. The same is stated by Melville and Sutherland (1988) for bridge pier scour and Coleman *et al.* (2003) for pier or abutment length to sediment size ratios (to be larger than 25). For both the velocity sets, max scour occurred at x_m/L_b>1 (where x_m is the distance in downstream direction from the upstream edge of the bridge), however area under the bridge also produced significant scour from x_m/L_b=0. Other important observations were that upstream local slopes were observed much lesser than the particle

angle of repose, and although the equilibrium was not achieved in these experiments, still it clearly showed that models of Arneson (1997) and Umbrell *et al.* (1998) underestimate ultimate scour prediction.

2.10.3. *Pier Scour*

There are a number of widely used formulas for the effective assessment of scour depth around bridge piers. NCHRP project 24-32 (Sheppard et al. 2011) aimed to assess the existing pier scour equations for non-cohesive sediment. Findings of the report show that the then existing methods of the local scour prediction at bridge piers over predict the local scour including those recommended by the HEC-18 (Sheppard et al. 2011). The research proposed the combination of two models (Melville 1997, Sheppard and Miller Jr 2006) as the best performing equation which is referred as the Sheppard/Melville or S/M equation.

The latest version of HEC-18 recommends two equations for the prediction of pier scour, which are well recognized and are designated as the CSU (Colorado State University) equation and the Sheppard/Melville equation. The CSU model is given by Equation 2-17:

$$\frac{d_s}{a} = 2K_1K_2K_3K_4\left[\frac{Y_1}{a}\right]^{0.35} F^{0.43} \qquad (2\text{-}17)$$

where K_1 = pier shape factor, K_2 = pier skewness factor, K_3 = factor for bed condition, K_4 = bed armoring factor, and F = approach Froude number = $V_1/(gY_1)^{0.5}$. CSU equation was initially developed for cylindrical piers and has been improved over the time. The equation in its current form is being recommended by FHWA (Federal Highway Administration) for the estimation of pier scour around simple piers. An additional factor

(K_w) for wide piers in shallow flows was suggested for CSU equation (Johnson and Torrico 1994). The Sheppard and Melville equation is given as Equation 2-18:

$$\frac{d_{se}}{a^*} = 2.5 f_1 f_2 f_3 \qquad for \quad 0.4 \le \frac{V_1}{V_c} < 1.0$$

$$\frac{d_{se}}{a^*} = f_1 \left[2.2 \left(\frac{\frac{V_1}{V_c} - 1}{\frac{V_{1p}}{V_c} - 1} \right) + 2.5 f_3 \left(\frac{\frac{V_{1p}}{V_c} - \frac{V_1}{V_c}}{\frac{V_{1p}}{V_c} - 1} \right) \right] \qquad for \quad 1.0 \le \frac{V_1}{V_c} \le \frac{V_{1p}}{V_c}$$

$$\frac{d_{se}}{a^*} = 2.2 f_1 \qquad for \quad \frac{V_1}{V_c} > \frac{V_{1p}}{V_c}$$

$$f_1 = \tanh\left[\left(\frac{Y_1}{a^*} \right)^{0.4} \right]$$

$$f_2 = \left\{ 1 - 1.2 \left[\ln\left(\frac{V_1}{V_c} \right) \right]^2 \right\}$$

$$f_3 = \left[\frac{\left(\frac{a^*}{d_{50}} \right)}{0.4 \left(\frac{a^*}{d_{50}} \right)^{1.2} + 10.6 \left(\frac{a^*}{d_{50}} \right)^{-0.13}} \right]$$

$$V_{1p1} = 5 V_c \qquad (2\text{-}18)$$

$$V_{1p2} = 0.6 \sqrt{g Y_1}$$

$$V_{1p} = \begin{Bmatrix} V_{1p1} & for\ V_{1p1} \ge V_{1p2} \\ V_{1p2} & for\ V_{1p2} > V_{1p1} \end{Bmatrix}$$

where a_*= effective pier width, which is the projected width of the pier times the shape factor, V_{1p} = velocity of the live-bed peak scour, V_{1p1} and V_{1p2} = Velocities used in computing "live-bed peak velocity".

Large cylindrical piers are subject to an additional parameter affecting pier scour in the form of the sediment coarseness ratio, a/d_{50}. To analyze this factor, experiments conducted at the Georgia Institute of Technology used uniform bed materials with σ_g < 1.5. The approach flow section was defined at a distance of 10-pier widths upstream of the pier in the streamwise direction, where the pier approach velocity was measured

(exactly upstream of the pier location). Point velocities were measured from near the bed to the point 60% of depth above the bed and were fitted to a logarithmic velocity distribution to obtain the shear velocity, u_*. Critical velocity was calculated from Keulegan's equation with sand-grain roughness as $k_s=2d_{50}$ and Shields' diagram was used for the critical shear velocity (Lee and Sturm 2009). Results showed that for smaller values of a/d_{50}, scour hole was restricted in size but increased until $a/d_{50}=25$, which is a confirmation of Melville (1997). As the ratio a/d_{50} increased, there was a decrease in d_{se}/a. A regression applied to the data for Froude number < 0.4 resulted in the relationship as shown in Figure 2-8 and mathematical form is presented as Equation 2.19:

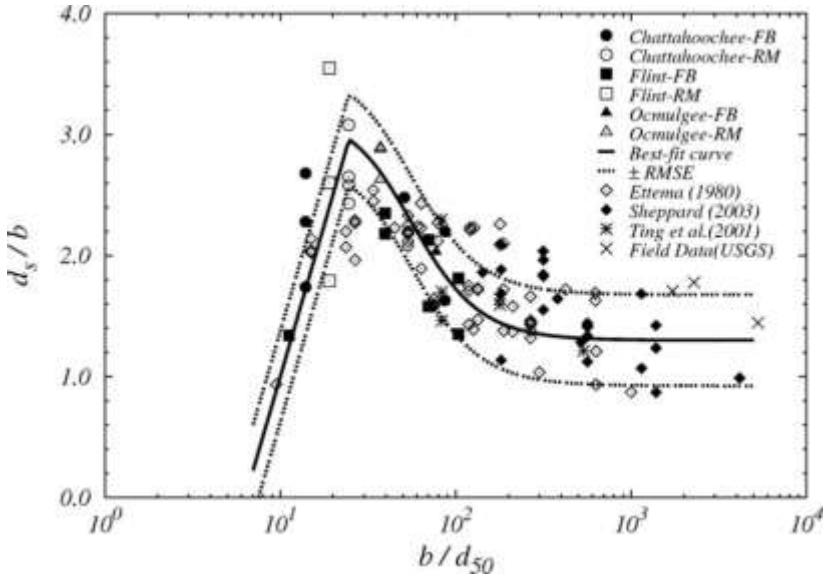

Figure 2-8 Effect of scour depth with sediment size, (Reproduced from (Lee and Sturm 2009)) where d_s = scour depth at equilibrium, d_{50} = median sediment size, and b = pier width.

$$\frac{d_{se}}{a} = 5\log\left(\frac{a}{d_{50}}\right) \quad for \quad 6 \le a/d_{50} \le 25$$
$$\frac{d_{se}}{a} = \frac{1.8}{\left(0.02a/d_{50} - 0.2\right)^2 + 1} + 1.3 \qquad for \quad 25 \le a/d_{50} \le 1*10^4 \tag{2-19}$$

where d_{se} = scour depth at equilibrium, d_{50} = median sediment size, and a = pier width.

Previously, it was concluded that normalized equilibrium scour depth d_{se}/a does not depend on the sediment coarseness ratio for $a/d_{50} > 50$ (Ettema 1980, Melville and Chiew 1999). However, the results in Figure 2-9 and those of Sheppard et al. (2004) show that "d_{se}/a" decreases with $a/d_{50} > 50$. This required additional information to verify any of the conclusions as for higher values of sediment size, larger pier diameter is required for larger a/d_{50}.

Lanca et al. (2013) carried out a study on CWS around piers and found that the parameter a/d_{50} influences the normalized equilibrium scour depth as d_{se}/a decreases with increase in a/d_{50} as indicated in Figure 2-9 (Lança et al. 2013). This corroborates the findings of Sheppard *et al.* (2004) and Lee and Sturm (2009) which associated the relation of horseshoe unsteadiness to different pier sizes and sediment coarseness. The equation given by regression analysis is:

$$\frac{d_{se}}{a} = \left\{ \begin{array}{ll} \frac{d_{se}}{a} = 7.3\left(\frac{a}{d_{50}}\right)^{-0.29}\left(\frac{Y_1}{a}\right)^{0.12} & for \quad 60 \le a/d_{50} \le 500 \\ \frac{d_{se}}{a} = 1.2\left(\frac{Y_1}{a}\right)^{0.12} & for \quad a/d_{50} \ge 500 \end{array} \right\} \qquad (2\text{-}20)$$

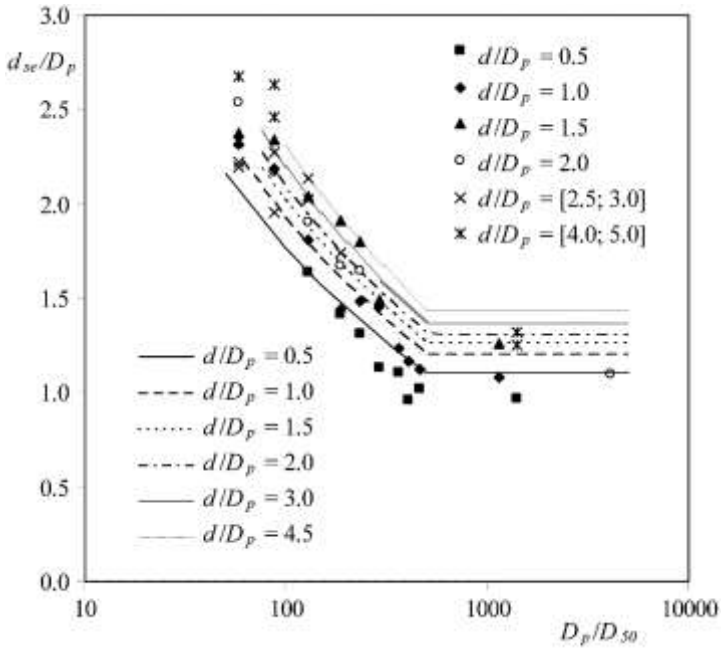

Figure 2-9 Normalized scour depth relationship to normalized pier dimeter (Reproduced from (Lanca et al. 2013)), where D_p = pier diameter, D_{50} = sediment size for 50% finer sediment, d_{se} = equilibrium scour depth and d = flow depth.

The results obtained in the study of Lanca *et al*. (2013) were applied to the data of Simarro et al. (2011) and Girmaldi (2005) and were found within 25% of the line of agreement. In another investigation, Lee and Sturm (2009) stated that $d_{se}/a \approx 1.3$ for $a/d_{50} > 400$. This finding is consistent with the equation proposed by Lanca et al (2013).

2.10.4. *Abutment Scour*

NCHRP 24-27 (Sturm et al. 2011) gives a comprehensive summary of the abutment scour prediction models. It was observed that most of the models have focused on the idealized studies in laboratory flumes. These models were graded as unreliable which generally lead to an over prediction of scour as compare to field measurement. It emphasized that none of the models described ideally, the abutment scour, as the process is difficult to model due to flow field complexity (Sturm et al. 2011). The most important factors to be taken into account were pointed as geotechnical failure of abutment,

consideration of compound channel geometry including floodplain and main channel rather than a simple rectangular channel, and addressing the riprap protection issue for the overtopping flow cases in order to prevent the complete embankment failure. NCHRP 24-20 project (Ettema et al. 2010) and NCHRP 24-27 project (Sturm et al. 2011) have addressed the geotechnical failure consideration in the respective research on the study of abutment scour in compound channels. Nevertheless, the earlier models still provide a good platform to investigate the abutment scour and interactive scour process. Figure 2-10 defines the variables to be used in the abutment scour prediction formulas to be presented in this section.

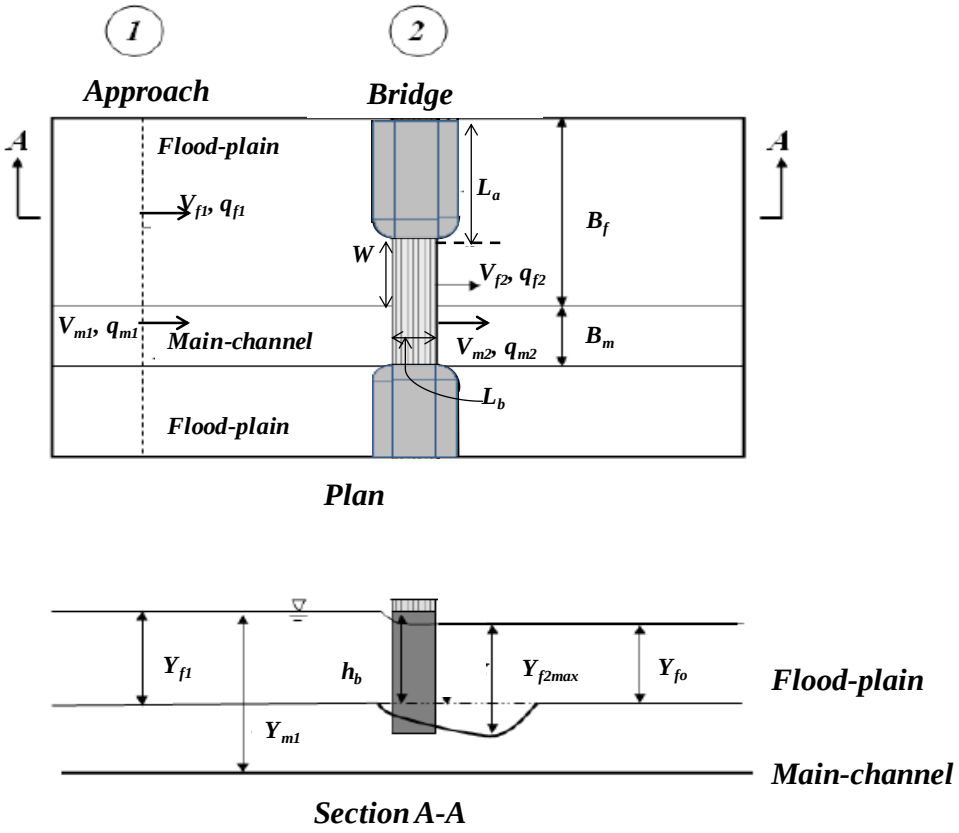

Figure 2-10 Definition sketch for abutment scour for a compound channel

For abutments, there is a variety of foundation designs. In sheet pile foundations, the abutment type is generally solid and non-erodible, while for buried abutment stubs supported on piles, the embankment itself is erodible. Therefore, it is very important to consider the geotechnical failure of an embankment/ abutment (Hong 2013).

Amongst different formulas for abutment scour, the most applicable formula for short, solid wall abutments, recommended by Sturm et al. (2011) is known as Melville Formula. This includes results from different researchers' investigations (Gill 1972, Wong 1982, Kwan 1984, Kandasamy 1985, Kwan 1988, Kandasamy 1989, Melville 1992, Dongol 1994, Melville 1997). The proposed formula is:

$$d_s = K_{yl} K_I K_d K_G K_\theta^* K_s^* \tag{2-21}$$

where K_{yl}= abutment length factor, K_I = Flow intensity factor for the approach flow, K_d= sediment size factor, K_s^*= abutment shape factor, K_θ^*= skewness factor and K_g = geometry factor, which accounts for short setback, long setback, bankline abutments and abutment in main channel (Sturm et al. 2011).

K_{yl} is given as

$$K_{yl} = \begin{cases} 2L_a & L_a/Y_1 \le 1 \\ 2(Y_1 L_a)^{0.5} & 1 \le L_a/Y_1 \le 25 \\ 10Y_1 & L_a/Y_1 > 25 \end{cases} \tag{2-22}$$

K_I is given by

$$K_I = \begin{cases} \dfrac{V-(V_a-V_c)}{V_c}) & V/V_c < 1 \\ 1.0 & V/V_c \ge 1 \end{cases} \tag{2-23}$$

in which V_a = mean flow velocity at the "armor peak" (V_a = V_c for uniform sediments). For live-bed conditions (V/V_c >1), the value of K_I remains less than "1", but to be conservative it is generally kept as 1.

K_d is given as

$$K_d = \begin{cases} 0.57\log\left(2.24\dfrac{L_a}{d_{50}}\right) & L_a/d_{50} < 25 \\ 1.0 & L_a/d_{50} \geq 25 \end{cases} \qquad \text{(2-24)}$$

For the fine sediments K_d is generally kept as unity and is only applicable when the L_a/d_{50} <25.

K_s^* is given as

$$K_s^* = \begin{cases} K_s & L_a/Y_1 < 10 \\ K_s + 0.67(1-K_s)\left(0.1\dfrac{L_a}{Y_1} - 1\right) & 10 \leq L_a/Y_1 \leq 25 \\ 1.0 & L_a/Y_1 \geq 25 \end{cases} \qquad \text{(2-25)}$$

for which K_s is unity for a vertical-wall abutment and the values for different types of the abutments are given in Table 2-3.

Table 2-3 Abutment shape factor (K_s)

Abutment Shape		***K*$_s$**
Vertical-Wall	Square End	1
	Semi-circular End	0.75
45^{o}Wing-wall		0.75
Spill-through	0.5:1.0 (H:V)	0.6
	1.0:1.0 (H:V)	0.5
	1.5:1.0 (H:V)	0.45

K_g is given as

$$K_G = \begin{cases} 1.0 & case\ A \\ \sqrt{1-\frac{B_f}{L_a}\left[1-\left(\frac{Y_f}{Y_m}\right)^{5/3}\frac{n_m}{n_f}\right]} & case\ B \\ 1.0 & case\ C \\ \left(\frac{Y_f}{Y_m}\right)^{5/6}\left(\frac{n_m}{n_f}\right)^{1/2} & case\ D \end{cases} \qquad (2\text{-}26)$$

in which B_f is the floodplain width, Y_m and Y_f are the flow depths in the main channel and on the floodplain, respectively; n_m and n_f are the Manning's roughness values in the main channel and on the floodplain. Figure 2-11 shows the geometry of all the four types of abutments, case A to D in a compound channel.

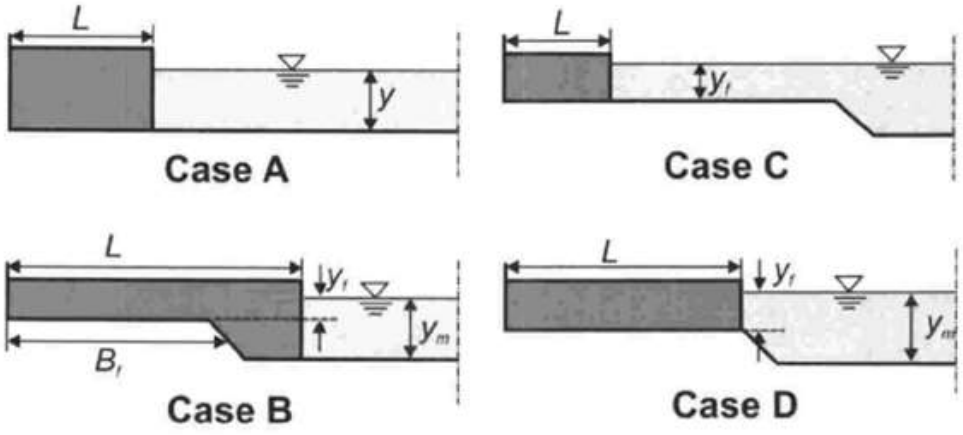

Figure 2-11 Abutment settings in compound channels (Melville and Coleman 2000)

Froehlich derived an equation both for CWS and LBS based on dimensional and regression analysis of experiments by others. Froehlich used 164 CWS laboratory

experiments for the regression of his CWS model. The CWS model is given by Equation 2-27:

$$\frac{d_{se}}{Y_1} = 0.78K_sK_\theta\left[\frac{L_a}{Y_1}\right]^{0.63} F^{1.16}\left[\frac{Y_1}{d_{50}}\right]^{0.43} \sigma_g{}^{-1.87} + 1 \qquad (2\text{-}27)$$

where K_s and K_θ are abutment shape and alignment factors, L_a is length of abutment, Y_1 is approach flow depth, F is approach Froude number, d_{50} is median sediment grain size and σ_g is the standard deviation of the sediment size distribution. Addition of "1" is a factor of safety (Froehlich 1989). This equation however overestimates the abutment scour if compared with the field measurements(Kandasamy 1989). HEC-18 suggests Froehlich's LBS equation because LBS is a common field occurrence and because it gives smaller scour values as compared to the CWS equation. Froehlich's LBS equation is the outcome of 170 LBS experiments and is given as:

$$\frac{d_{se}}{Y_1} = 2.27K_sK_\theta\left[\frac{L_a}{Y_1}\right]^{0.43} F^{0.61} + 1 \qquad (2\text{-}28)$$

The HIRE equation is based on field data obtained by the United States Army Corps of Engineers for spur dikes in the Mississippi River. The field data closely resembles laboratory observations where the discharge intercepted by the spur dike is a function of spur length. The HIRE equation is applicable for $L_a/Y_1>25$ and is given as:

$$\frac{d_{se}}{Y_1} = 4F^{0.33}\frac{K_s}{0.55}K_\theta \qquad (2\text{-}29)$$

where K_s and K_θ are abutment shape and alignment factors respectively.

The Maryland method applied Laursen's long contraction theory for abutment scour, both for CWS and LBS conditions, and the suggested formulas are given in Equation 2-33 (Chang and Davis 1998, Chang and Davis 1999):

$$d_{se} = K_s K_\theta \left[Y_1 k_p k_f \left(k_v \frac{q_2}{q_1} \right)^{k_2} - Y_{2o} \right] FS \qquad for \qquad CWS$$
$$d_{se} = K_s K_\theta \left[\left(k_p k_f k_v^{0.857} \frac{q_2}{V_c} \right) - Y_{2o} \right] FS \qquad for \qquad LBS \qquad (2\text{-}30)$$

in which d_{se} = equilibrium scour depth, K_s= abutment shape factor, K_θ = abutment/embankment alignment factor, Y_1= approach flow water depth, k_p= pressure flow coefficient, k_v= velocity adjustment factor, k_f= spiral flow adjustment factor, q_2= flow rate per unit width in the contracted section, q_1= flow rate per unit width in the approach flow section, V_c = critical velocity, Y_{2o}= flow depth at bridge before scour, and *FS*= factor of safety.

Abutment Scour in Compound Channels: Garde et al. (1961) suggested the geometric contraction ratio "*m*" for an idealized rectangular channel (Garde et al. 1961). Sturm and Janjua (1993, 1994) suggested that the same geometric ratio cannot be applied to compound channels as the dynamics of the flow interaction at the interface of floodplain and the main channel are different from an idealized rectangular flume. The authors suggested that the local abutment scour should depend on the flow redistribution rather than the earlier practice of using geometric contraction ratio and abutment length. The geometric contraction ratio was suggested to be replaced with the flow contraction ratio $M = Q_o/Q$ where Q_o is the proportion of the flow discharge in the approach flow section equal to the contracted opening and Q is the total approach flow discharge value

(Sturm and Janjua 1993, Sturm and Janjua 1994). It was assumed that discharge per unit width in the floodplain is uniformly distributed and that the change in the flow depth in the contracted section as compared to the approach section is negligible. The value of M was found to be a good estimate of the ratio of discharge per unit width of the floodplain in approach flow and contracted sections, q_{f1}/q_{f2}. Sturm and Janjua conducted a set of experiments in a flume with a compound channel and their suggested equation was:

$$\frac{d_{se}}{Y_1} = 7.70\left[\frac{F}{MF_c} - 0.35\right] = 7.70\left[\frac{q_{f2}V_1}{q_{f1}V_c} - 0.35\right] \qquad (2\text{-}31)$$

where d_{se} = maximum scour depth at the abutment, F= approach flow Froude number, F_c = critical Froude number, and Y_1 = approach flow water depth in the floodplain.

Further study at the Georgia Institute of Technology through a series of experiments for setback abutments and bankline abutments resulted in a model for abutment scour in compound channels (Sturm and Sadiq 1996, Sturm 2006). The equation given by the model is:

$$\frac{d_{se}}{Y_{f0}} = C_r\left[\frac{q_{f1}}{Mq_{f0c}} - C_0\right] \qquad (2\text{-}32)$$

in which d_{se} = equilibrium abutment scour depth; Y_{fo}= floodplain normal depth for un-constricted water surface elevation at the downstream end; C_r represents the scour amplification factor and C_o represents the equation intercept for no scour occurrence; q_{f1}= approach floodplain flow rate per unit width; q_{foc}= floodplain critical flow rate per unit width =V_{oc}*Y_{fo}; V_{oc}= critical velocity for un-constricted flow depth Y_{fo}, and M = discharge contraction ratio for the approach section. For the spill-though abutments, a shape correction factor "K_s" was suggested as:

$$K_S = 1.52\frac{\xi - 0.67}{\xi - 0.40} \quad for \quad 0.67 < \xi < 1.2 \tag{2-33}$$

in which $\xi = q_{f1}/(MV_{0c}Y_{f0})$, and K_s = 1.0 for $\xi \geq 1.2$ while K_s = 0 for $\xi \leq 0.67$. This corroborates the findings of Melville and Coleman (2000) that for longer abutments, the contraction effects overwhelm turbulence and the shape factor.

Abutment Scour for Erodible Abutments: Ettema et al. (2010) investigated the abutment scour for erodible abutments and adopted the approach similar to Sturm (2006) and Chang and Davis (1999). An envelope curve for the abutment scour was suggested for a dimensionless abutment scour as a ratio of maximum scour to the theoretical contraction scour (Ettema et al. 2010). For erodible abutments, three scour conditions have been investigated by Ettema in the conduct of experiments for a compound channel, which are widely accepted and are categorized as scour condition A, B, and C (Ettema et al. 2010, Yorozuya and Ettema 2015).

Scour Condition A: In this scour condition, erosion occurs in the main channel, for the reason either that the bed material in the main channel is more erodible than the floodplain or the abutment is covering more than ¾ of the floodplain width.

Scour Condition B: In this case the scour hole only takes place in the floodplain, because the abutment is far away from the main channel, thus there is no interaction between the main channel and the floodplain flows in a bridge contraction.

Scour Condition C: In this scour condition, the embankment breaches fully, such that the flow passes from both sides of abutment and the abutment column is exposed as if it is a pier.

The Ettema et al (2010) illustration for abutment scour conditions A, B, and C for the compound channel has been reproduced in Figure 2-12.

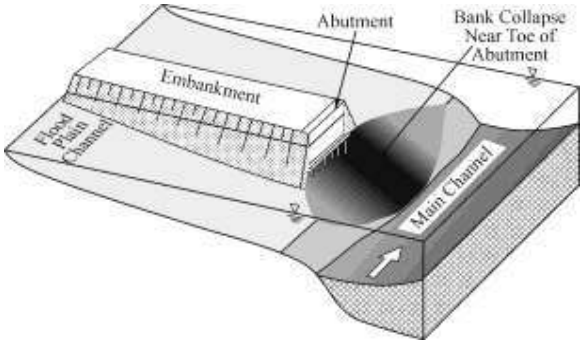

Scour condition A

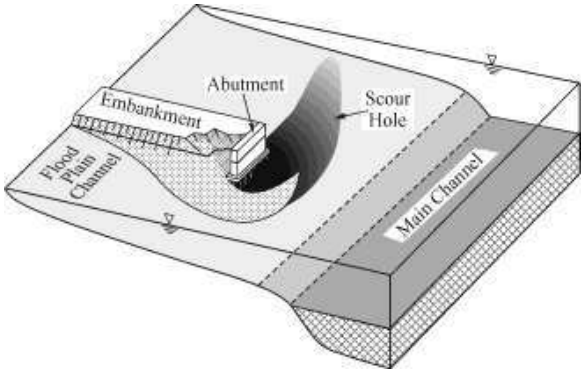

Scour condition B

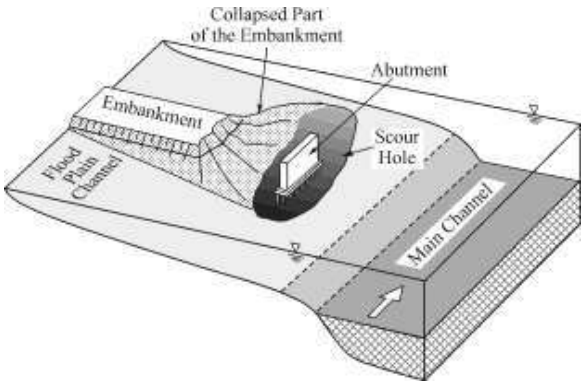

Scour condition C

Figure 2-12 Abutment scour conditions in a compound channel: Scour Condition A - bank failure and failure of the abutment face, Scour Condition B - failure of the abutment face, and Scour Condition C - breaching of the approach embankment (Reproduced from (Ettema et al. 2010))

Ettema et al. (2010) also investigated the important aspect of geotechnical failure of the embankment. However, if the geotechnical failure is not considered, then the abutment scour is related to the Laursen's theoretical long contraction scour both for clear-water as well as live-bed scour conditions with amplification factors (Laursen 1960, Laursen 1963).

$$Y_{MAX} = \alpha Y_C \tag{2-34}$$

in which Y_{max} is the flow depth corresponding to the maximum scour depth, Y_c is the mean flow depth of the theoretical contraction scour, and α is the amplification factor. Maximum scour depth for the abutment scour condition A and B are:

$$d_{se} = Y_{MAX} - Y_{m1} = Y_{m1}\left[C_{TA} m_A^{6/7}\left(\frac{q_{m2}}{q_{m1}}\right)^{6/7} - 1\right] \quad for \quad Scour \quad Condition \quad A$$

$$d_{se} = Y_{MAX} - Y_{f1} = Y_{f1}\left[C_{TB} m_B^{6/7}\left(\frac{\tau_f}{\tau_c}\right)^{3/7}\left(\frac{q_{f2}}{q_{f1}}\right)^{6/7} - 1\right] \quad for \quad Scour \quad Condition \quad B \qquad (2\text{-}35)$$

in which, d_{se}= scour depth, $Y_{max=}$ flow depth at the point of maximum scour depth, Y_{m1} = main channel approach depth, Y_{f1}= floodplain approach depth, C_{TA}= coefficient of turbulent influence (for scour condition A at the abutment), C_{TB}= coefficient of turbulent influence (for scour condition B at the abutment), m_A = value of q_{max}/q_2 for the scour condition A, m_B = value of q_{max}/q_2 for the scour condition B, q_{max}= discharge per unit width at the point of deepest scour in the main channel, q_{m1}= discharge per unit width in the approach section in the main channel , q_{m2}= discharge per unit width in the bridge section in the main channel, τ_f= shear stress for the floodplain in approach flow section, τ_c= critical shear stress for sediment movement; q_{f1}= discharge per unit width for the floodplain in the approach section, and q_{f2} = discharge per unit width for the floodplain in the bridge section.

2.10.5. *Abutment and Lateral Contraction Scour Interaction (Compound Channels)*

Bridges are mostly located in compound channels having flow in floodplains in flood conditions only. For shallow depth of floodplain flow, there is a great contrast between flow velocity in main channel and floodplain which results in shifting of longitudinal momentum from main channel to floodplain. Total flow in such cases is less than the sum of two estimated flow components (main channel and floodplain). In general, floodplain flow is underestimated and is somewhat compensated by

overestimation of main channel flow. Wormleaton ans Hadjipanos gave three divided channel methods to calculate the discharge in compound channels, out of which the diagonal interface method gives a better estimation (Wormleaton and Hadjipanos 1985).

In many laboratory experiments, the abutments are placed in rectangular channels, which experience different conditions than what exist in the field conditions of natural streams and prismatic channels. The experiments show that the length of abutment is a strong variable contributing to the scour around the abutment. However, it has also been observed that scour is a function of redistribution of flow between the main channel and floodplain, so for the same abutment length, scour depth can be different for different approach flow conditions and redistribution in the contracted section (Sturm 2006, Hong 2013). With the decrease in flow depth in floodplain the secondary currents and turbulent stresses contribute more in apparent shear stress (Sturm 2001). The scour conditions for bankline and setback abutments are also different, where bankline abutments are prone to live-bed scour and setback abutments are more likely to face clear water scour conditions.

Hong conducted experiments at the Georgia Institute of Technology, for free (F), submerged orifice (SO) and overtopping (OT) flow conditions with ratio of length of abutment to the floodplain as 0.53. 0.71, 0.88 and bankline abutments (Hong 2013). Results of all three flow conditions, with dimensionless parameters derived from the long contraction theory, were compared, and formulas for prediction of abutment scour depth were developed (Hong 2013, Hong et al. 2015) for long setback abutments (LSA), short setback abutments (SSA) and bankline abutments (BLA).

The key parameter for scour prediction in this approach was the ratio of discharge per unit width in the approach and bridge sections (q_2/q_1), where the bridge section

discharge per unit width for the OT flow cases was considered for the flow passing under the bridge only as the overtopping flow does not contribute to the scour. This method for SO and OT flows helped to combine the vertical and lateral contraction scour data into one prediction formula. For short setback abutments, the phenomenon is more complex as the scour hole is initially developed in the floodplain, but it then moves and reaches equilibrium in the main channel, so the formulas for long-setback abutments and bankline abutments were derived separately, as follows:

$$\frac{Y_{f2\max}}{Y_{fo}} = 0.96\frac{Y_{f1}}{Y_{fo}}\left[\frac{\overline{K}_b}{u_*^2}\right]^{0.31}\left[\left[\frac{q_{f2}}{q_{f1}}\right]\left[\frac{V_{f1}}{V_{fc1}}\right]\right]^{6/7} \qquad for \quad LSA \qquad (2\text{-}36)$$

$$\frac{Y_{m2\max}}{Y_{mo}} = 0.92\frac{Y_{m1}}{Y_{mo}}\left[\frac{\overline{K}_b}{u_*^2}\right]^{0.21}\left[\left[\frac{q_{m2}}{q_{m1}}\right]\left[\frac{V_{m1}}{V_{mc1}}\right]\right]^{6/7} \qquad for \quad BLA \qquad (2\text{-}37)$$

where, $\overline{K}_b$ = width-averaged bottom turbulent kinetic energy (TKE) in the scour hole along the downstream toe of the abutment, Y_{f1} and Y_{m1}= approach flow depth in floodplain and main channel, respectively, Y_{fo} and Y_{mo} = undisturbed flow depth in floodplain and main channel, respectively, Y_{f2max} and Y_{m2max} = flow depth at point of maximum scour in floodplain and main channel, respectively, q_{f1} and q_{f2} are approach and bridge section unit discharge values for the floodplain, q_{m1} and q_{m2} are approach and bridge section unit discharge values for the main channel, V_{f1} and V_{m1}= approach section velocity in floodplain and main channel, respectively, and V_{fc} and V_{mc}= approach section critical velocity in floodplain and main channel, respectively.

An important finding by Hong (2013) is that for higher discharge contraction ratios (q_2/q_1), the effect of $\overline{K}_b/u_*^2$ is smaller as compared to lower values of discharge

contraction ratios (q_2/q_1). This implies that, as we increase the discharge contraction ratio, dependence of scour development changes from the local turbulent structure as expressed by TKE to flow contraction ratio (q_2/q_1). Thus for LSA, the dependence on TKE is more as compared to SSA/BLA as shown previously in Equation 2-36 and Equation 2-37. Figure 2-13 gives a graphical representation of the same phenomenon.

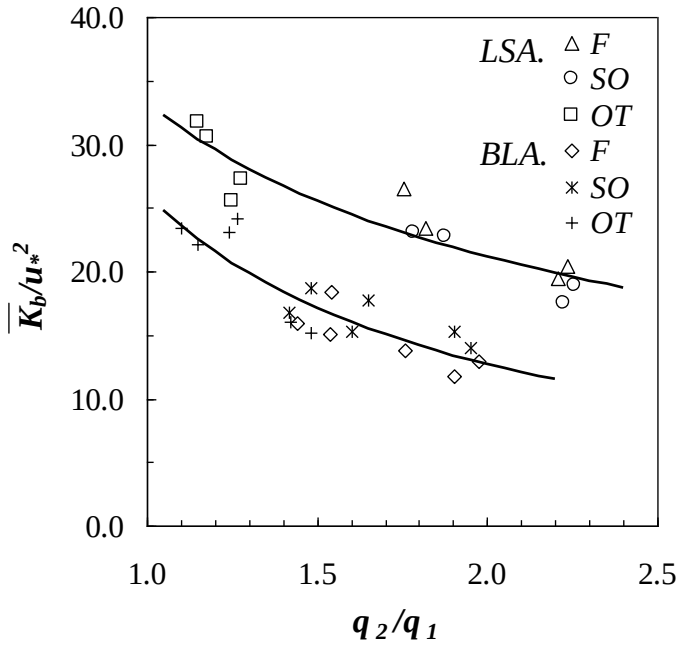

Figure 2-13 Effect of $\overline{K}_b/u_*^2$ on flow and geometric contraction (Reproduced from (Hong et al. 2015))

Other important findings of the research are given as:

- Length and location of the scour hole is dependent on the separation and recirculation region for free (F), submerged orifice (SO) and overtopping (OT) flow cases.
- For short setback abutment, severe flow contraction resulted in location of scour hole near the abutment in the main channel, which resulted in influencing the failure of abutment itself.

- Normalized equilibrium time is a weak function of $(q_2/q_1 * V_1/V_c)$ but depends more on the type of flow and abutment setback distance.
- For the formula given above, the proposed procedure for prediction of equilibrium scour was:
    1. Determine approach independent hydraulic variables, using WSPRO or HEC-RAS to compute water surface profiles through bridge.
    2. Calculate approach flow intensity (V_1/V_c) from results of the previous step and the sediment properties related to initiation of motion.
    3. Determine unit discharge contraction ratio (q_2/q_1) directly from HES-RAS or equation below:

$$M = \frac{Q_{un-obstructed}}{Q_{total}} = \frac{Q_{m1} + Q_{fo}}{Q_{m2} + Q_{f2}} \approx \frac{q_{m1}}{q_{m2}} \approx \frac{q_{f1}}{q_{f2}}$$

    4. For OT flow case, the broad crested weir equation can be used to calculate the overtopping discharge and the result can be used in step 3.
    5. Ratio of maximum abutment scour to theoretical contraction scour (r_T) can be estimated as a constant or as a function of computed turbulent kinetic energy from a 3D model or from (q_2/q_1) obtained from step 3.

2.10.6. *Pier and Abutment Scour Interaction*

Piers and abutments experience similar mechanisms responsible for the scour process but at different scales. Flow separation, turbulence, a horseshoe vortex, and a wake vortex are present in both cases, but the recirculation zone and the shear zone for an abutment are more prominent for an abutment. In addition, if the abutment is long enough, flow constriction results in acceleration and higher velocities responsible for the scour process. The interaction of the two processes is a complex phenomenon and is

difficult to model. Although there have been numerous studies of isolated pier and abutment scour, the interaction of the two scour processes require further investigation. A very few studies are available for the abutment and pier scour interaction. For example, Croad established a relationship for pier scour affected by abutment scour as $d_{s\ pier}=0.9d_{s\ max}$ ($d_{s\ max}$ is maximum abutment scour) (Croad 1989). Hong (2005) found that pier presence in the vicinity of an abutment affects the location of deepest scour point (Hong 2005).

Oben and Ettema (2011) carried out an interactive scour study of abutment and pier scour, both for spill-through and wing-wall abutments and wall pier. The flow conditions were kept constant and only free flow experiments were conducted, such that generally live-bed scour condition prevailed in the main channel and clear water scour condition in the floodplain (Oben-Nyarko and Ettema 2011). Experiments were run until the equilibrium criterion was achieved. Experiments for the fixed floodplain and live-bed condition in the main channel were run for 24 hours. For the experiments where the abutment failed in the floodplain the duration of experiment was about 6 hours. The following effects were observed:

Pier Effect on Abutment Scour: In the experiments, a pier did not have substantial effect on abutment scour, although some cases showed minor increases or decreases in equilibrium scour depth. Because the experiments were live-bed , this marginal difference was attributed to bed forms (Oben-Nyarko and Ettema 2011).

For spill-through abutments on fixed floodplain: The relative distance $L_p/Y_{f1} < 5$ was established as close proximity of the pier to the abutment, where L_p=distance between pier and abutment toe and Y_{f1} =water depth in the approach floodplain. Scour

region was defined as the area covered by the scour hole in lateral and longitudinal directions. For 2 $< L_p/Y_{f1} <$ 4, the scour region increased in size as compare to the size of scour region in absence of the pier. At L_p/Y_{f1} =3.20 the scour region doubled as compared to absence of pier.

For spill-through abutment on erodible floodplain: Pier in close proximity to the abutment reinforced it and confined the riprap near the toe of the abutment, thereby reducing the scouring. As L_p/Y_{f1} increased, the effect diminished.

For wing wall abutment on erodible floodplain: As there was no riprap to be accumulated, the scour depth increased 5-7%. This increase in the scour depth was associated with bed forms, owing to live-bed scour conditions.

Abutment Effect on Pier Scour: An abutment had significant effect on the pier scour, which varied with the pier location and type of abutment.

Pier near spill-through abutment on fixed floodplain: Maximum pier scour at the pier aligned with the flowing water and located away from the influence of abutment, was 15% of abutment scour, which increased considerably as the pier moved into the influence of abutment scour hole.

Pier near wing-wall abutment on erodible floodplain: The pier was placed in the main channel, but the floodplain was erodible, so erosion in the floodplain relieved the flow by an increase in the flow area through scouring which resulted in reduced velocities and thus smaller effect on the pier scour.

Pier near spill-through abutment on erodible floodplain: Two different scenarios developed where in the first condition, the pier at the toe of the abutment was protected by the riprap of the abutment, thus showing very little or no scour. In the other

condition, the pier at sufficient distance away from the toe of the abutment showed considerably more scour than a pier out of the influence of the abutment. It was observed that for spill-through abutments, the effect of embankment erosion reduced abutment scour and thus the influence of abutment on pier also reduced.

Conclusions of the study were:

- For spill-through abutments with the pier located in the near vicinity of abutment ($L_p/Y_{f1} \leq 3.0$), the abutment scour effect is significant and pier scour is governed by abutment scour.
- Pier presence does not produce a substantial effect on abutment scour.
- For short distances between pier and abutment, a larger scour hole is developed, which encircles both abutment and pier.
- Time development of scour shows deepest scour point movement from upstream corner of abutment to downstream corner. The pier, if closely located to the abutment, moves the maximum scour point near the centerline axis of the abutment.

2.11. Criterion for Long and Short Setback Abutments

In a compound channel the length of abutment is a significant variable to assess the flow interaction between the floodplain and the main channel. If the abutment is set well back into the floodplain, the flow redistribution in the contracted section will not result in any interaction of the floodplain and the main channel flow. However, an abutment, which is long enough to force an interaction between the floodplain and the main channel, involves flow redistribution between the floodplain and the main channel.

The flow passing over the bank between the floodplain and the main channel has complex flow mechanics and thus has different effects on the scour process. Therefore, classification of the abutment is very important. Abutments are categorized as long, intermediate, and short setback abutments where the deepest point of the scour hole is in the floodplain for the long setback abutments and in the main channel for the short setback abutments. Melville (1992) assumed that small abutments result in an abutment scour similar to that of the piers. He gave a classification of long, intermediate, and short setback abutments with a wide range covering the intermediate setback abutments (Melville 1992). The classification is as follows:

$$\begin{aligned} &0 \le L_a/Y_1 \le 1 && \text{Long setback abutments (Similar to pier)} \\ &1 \le L_a/Y_1 \le 25 && \text{Intermediate setback abutments} \\ &L_a/Y_1 > 25 && \text{Short setback abutments} \end{aligned} \qquad (2\text{-}38)$$

where L_a = length of abutment and Y_1 = approach flow depth.

As given by Chang and Davis (1998), ABSCOUR assumes the floodplain flow mixes with the main channel and redistributes uniformly for the short setback abutments (Chang and Davis 1998). The criterion for the classification of the abutments is:

$$\begin{aligned} &\text{Setback Distance} \le 5.0\, Y_{co} && \text{Short Setback} \\ &5.0\, Y_{co} \le \text{Setback Distance} \le 0.75W && \text{Intermediate Setback} \\ &0.75W \le \text{Setback Distance} && \text{Long Setback} \end{aligned} \qquad (2\text{-}39)$$

where Y_{co} = hydraulic depth in the main channel and W = floodplain width in the contracted section. For the long setback abutments, no interaction between the floodplain and main channel occurs so the discharge per unit width is same as that of the ratio of width in approach and contracted section (This does not apply to OT flow cases). For the

short setback abutments, the velocity under the bridge is assumed to be uniform for the entire cross-section, which is used to calculate the discharge per unit width. For the intermediate setback abutment an interpolation of the velocity is used:

$q_2 = V_{short} * Y_{co}$ for short setback abutments

$q_2 = q_1 * (W_2/W_1)$ for the long setback abutments

$V_{short} = Q/A$ at a setback distance of $5Y_{co}$

$V_{long} = Q/A_{sub}$ at a setback distance of $0.75W$

$$V_{intermediate} = V_{short} - [(V_{short} - V_{long}) * ((setback - 5Y_{co})/(0.75W - 5Y_{co}))]$$

where V_{short} = velocity under the bridge for the short setback abutments, V_{long} = velocity under the bridge for the long setback abutments, $V_{intermediate}$ = velocity under the bridge for the intermediate setback abutments, q_2 = discharge per unit width in the contracted section, q_1 = discharge per unit width in the approach section, W_1 = width in the approach section, and W_2 = width in the bridge section.

HEC-18 clasifies abutment setback according to the dimensionless variable W/Y_{f1} (where W = width of floodplain in the bridge section and Y_{f1} is approach flow depth in the floodplain). The criterion $W/Y_{f1}>5$ classifies the setback distance to be sufficient enough such that the deepest point of the scour hole remains in the floodplain and conversely for short setback abutments (Arneson et al. 2012). Hong (2013) suggested a further modification in the criterion as $W/Y_{f1} > 6$ for LSA and $W/Y_{f1} < 6$ for SSA.

2.12. HEC-18 Criterion for Interactive Scour Calculation

Hydraulic Engineering Circular-18 gives a criterion of addition of all the interacting components of scour by first plotting the long term aggradation or degradation

(aggradation is neglected, being on the conservative side), then plotting and adding the contraction scour from below the degradation of the bed level, and then adding the subsequent pier or abutment scour (Arneson et al. 2012). The criterion for the assessment of the size of the scour hole is 2 times the depth of the scour hole on each side of the pier or abutment. It further states that if the abutment and pier scour holes are overlapping then magnitude of the scour can increase. Therefore, it suggests to design the bridge span, bridge opening, and pier spans such that the overlapping of the scour holes is avoided.

2.13. Field Studies

Availability of field data for the extreme flood events is one of the most critical aspects in scour studies, as the scour is generally measured after the flood has passed, which gives the remnant scour value rather than the actual value (Sturm et al. 2011). However, in certain cases of bridge scour, where the instruments were placed for real time data collection, the field measurements are available and a few studies have been conducted to analyze these scour cases.

The field studies explored for this research were identified such that they include more than one scour component interaction, real time field data of velocity and scour measurement, and detailed geometric data. The summary of the field studies is presented in Table 2-4 which shows the scour type and interaction, channel shape, type of flow (F, SO, OT flow), type of data collected, and time of data collection (during flood or after flood). Almost all the studies give the scour measurement after the flood event has occurred which may not be a true representation of the actual scour at the peak of the

flood event. Almost all the studies summarized in Table 2-4 are free flow cases where the discharge has generally been measured based on the stage-discharge curve and the velocities have then been calculated from HEC-RAS, but no method has been specified for determining the tail-water level, which significantly affects the scour development.

Table 2-4 Summary of field scour studies

References	Scour Type			Channel Shape	Flow Type	Hydraulic &soil data			Measurements
	P	A	C			*V*	*Q*	*Soil*	
(Zhang et al. 2013)	x	x	x	Cmpd.	F		E	x	Interpolated
(Hong and Sturm 2011)	x		x	Cmpd.	F		M	x	After flooding
(Larsen et al. 2011)	x		x	Cmpd.	F	M	M	x	During flooding
(Ting et al. 2011)	x			Main	F		M	x	After flooding
(Hong and Sturm 2009)	x		x	Cmpd.	OT		M		After flooding
(Lombard and Hodgkins 2008)		x		Cmpd.	U		E	x	Not specified
(Lu et al. 2008)	x		x	Cmpd.	F	M	M	x	During flooding
(Shatanawi et al. 2008)		x		Cmpd.	U		E		Not specified
(Conaway 2007)		x	x	Cmpd.	F		M	x	During flooding
(Benedict et al. 2006)		x		Cmpd.	U		E	x	After flooding
(Conaway 2006)	x	x	x	Cmpd.	F		M	x	During flooding
(Wagner et al. 2006)	x	x	x	Cmpd.	F	M	M	x	During flooding
(Güven et al. 2005)	x		x	Cmpd.	F		M	x	After flooding
(Mueller and Wagner 2005)	x	x	x	Cmpd.	F	M	M	x	After flooding
(Sturm et al. 2004)	x		x	Cmpd.	F		M		After flooding
(Sturm 2004)		x		Cmpd.	F		M	x	After flooding
(Richardson and Trivino 2002)		x	x	Cmpd.	F		M	x	After flooding
(Coleman and Melville 2001)	x		x	Cmpd.	F		M	x	After flooding
(Holnbeck and Parrett 1997)	x	x	x	Cmpd.	U		E	x	Not specified
(Niehus 1996)	x	x	x	Cmpd.	F		M	x	After flooding
(Holnbeck et al. 1993)	x	x	x	Cmpd.	OT		E	x	After flooding
(Jarrett and Boyle 1986)	x	x	x	Cmpd.	F		E		During flooding

P: Pier scour; A: Abutment scour; C: Contraction scour; Cmpd: Compound channel; Main: Main channel only; F: Free flow; SO: Submerged-orifice flow; OT: Overtopping flow; M: Measured; E: Estimated; U: Unknown

An example of the interactive scour development which resulted in the failure is the Houfeng Bridge in Taiwan in 2008 (Hong et al. 2011). The bridge is located at a highly populated area with a wide floodplain on one side and is a slightly meandering channel. Causes identified for the excessive erosion were bed degradation after 1999 earthquake, exposure of the partially suspended pipeline on the upstream side of the bridge because of successive typhoons, which resulted in jet flow at the bridge location, and excessive scour because of jet flow itself. The failure was result of an integrated effect of local scour, jet scour, bend scour, contraction scour, and long term degradation.

Big Sioux River Bridge at Flandreau in South Dakota with multiple spans has a complex geometry which is located at a sharp bend in a compound channel (Larsen et al. 2011). As the bridge is located at a sharp bend so the flow is concentrated away from the bend, which generates a higher concentration of flow at a particular pier locations resulting in higher scour values for 1993 floods. As the flow distribution between the main channel and the floodplain varies with increase or decrease in the discharge so the behavior of the flow at the higher discharge varies from the lower discharge values. Thus, the dynamic flow distribution depends on the discharge in a compound channel. Higher scour value on the outer side of the river bend shows that the bend affects pier and abutment scour.

Current scour prediction methods were evaluated by Lombard and Hodgkins (2008) for 50 selected bridge sites in Maine with the use of field measurements and HEC-RAS simulations for the flow depths and velocities measurements based on the design discharge for the bridge life (Lombard and Hodgkins 2008). Zhang et al. (2013) also carried out the evaluation of current scour prediction models in Louisiana for which

seven bridge sites were selected (Zhang et al. 2013). LADOT bridge scour database was used for the field scour values. DEM (Digital Evaluation Model) and HEC-RAS were used for estimation of discharge through satellite imagery and hydraulic variables respectively.

Lombard and Hodgkins (2008) and Zhang et al. (2013) concluded that model estimates were one to two orders of the magnitude higher than the field measurements. Larsen et al. (2011) and Rossel and Ting (2013) found out that one-dimensional models are incapable of giving accurate estimates for complex field geometries. Another inherent factor for discrepancies of these studies in field and model results is the measurement of field scour after the flood event than the real time peak flood value. Conaway (2007), for his study of 17 bridge sites in Alaska, overcame the discrepancy of real time field data collection by taking measurements every 6 hours and came up with the results within reasonable tolerance limits (Conaway 2007). The difference in the results was attributed to the bed armoring factor and changes in flow distribution. Wagner et al (2006) concluded in his research that the laboratory research has failed to capture the field conditions an emphasized the need of reproducing the real time geometry and flow conditions from the field (Wagner et al. 2006).

2.14. Physical Model Studies

In the recent studies efforts have been made to close the gaps between the laboratory experiments and field studies by reproducing field events through physical models in laboratory. Important considerations for the physical model study are

geometric similarity, identification of the right dimensionless parameter, and sediment size scaling issue (discussed in para 2.7).

Hong (2005) conducted a scour study at the Fifth Street Bridge at Ocmulgee River in Macon, Georgia at a scale of 1:45 for 1998 flood event. The flood event was replicated with piers in place as well as without piers, so as to isolate the effect of contraction and pier scour (Sturm et al. 2004, Hong 2005, Hong and Abid 2015). The results suggest that rapid pier scour development makes a flow redistribution, which affects the scour process. Separation of pier scour component was approximated by the concurrent surface method (Landers and Mueller 1993). Figure 2-14 shows that scour measurements at pier locations were reproduced with good accuracy.

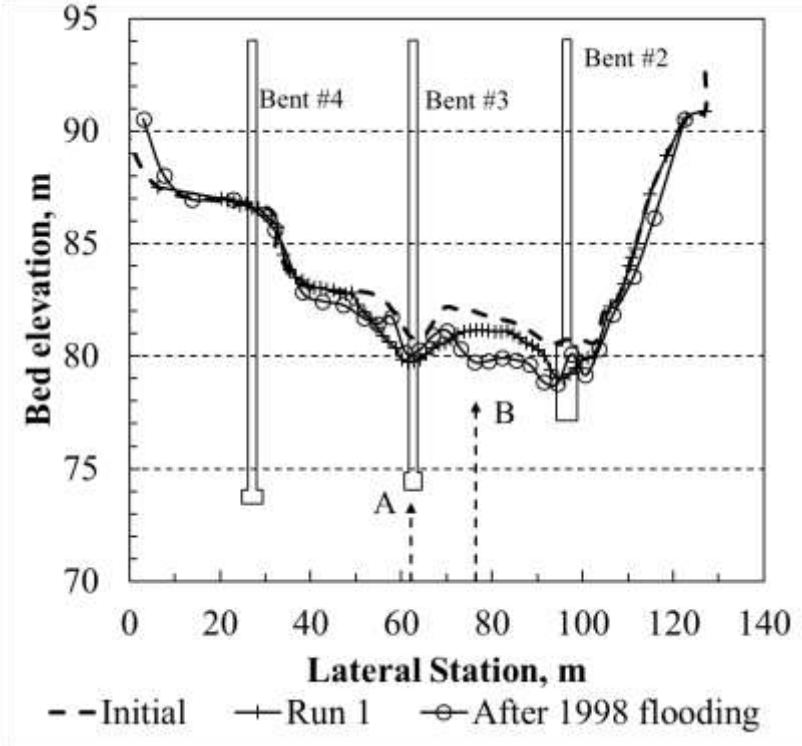

Figure 2-14 Comparison of field data and model study for 1998 Ocmulgee river flood (Hong 2005)

Towaliga River flood for Storm Alberto (1994) was replicated at the hydraulics engineering laboratory of the Georgia Institute of Technology at the scale of 1:60 as shown in Figure 2-15. The flood event was submerged orifice flow with erodible embankment in a compound channel. With the rating curve both submerged orifice and overtopping flow cases were run for different abutment conditions (Hong and Sturm 2009, Hong and Sturm 2010). Figure 2-16 shows that the model replicated the measured flood event values with reasonable accuracy. Hong and Sturm concluded that abutment scour is a combination of lateral and vertical flow contraction in addition to the local scour and computed the total scour as a multiple of the contraction component of the scour for all three types of flow including free, submerged orifice and overtopping flows. The additive method of total scour prediction in case of interactive scour results in over prediction.

Figure 2-15 Laboratory model of Towaliga river bridge (Hong and Sturm, 2010)

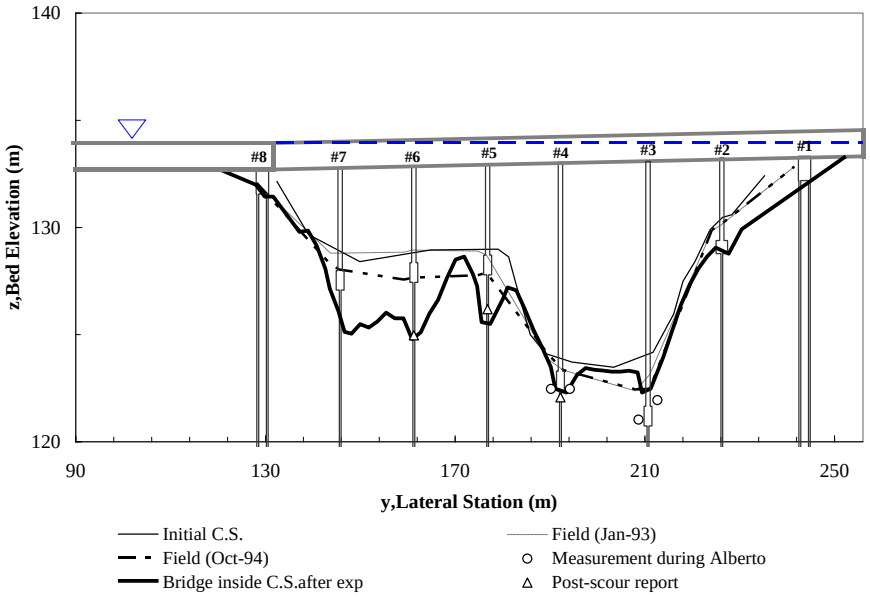

Figure 2-16 Comparison of bridge cross-section for field measurement and model study of Towaliga river flood (Hong and Sturm 2009)

Sturm (2004) analyzed the field data of April 1997 flood of Highway 22 Bridge of Pomme de Terre River in Swift County in Minnesota. The bridge had bankline abutments with two piers placed in the main channel at a spacing of 40 ft. The slope of the embankment was 2:1 with riprap protection (Sturm 2004). Flood discharge was 5150 ft^3/sec. The bridge had to be closed temporarily for repair after the flood. For the field geometry after scour, WSPRO run measurements were taken to verify the discharge, velocity and elevation. Figure 2-17 and Table 2-5 show the scour at the bridge and the summary of bridge scour parameters. Clear water scour model suggested by Sturm (2004) gives a fair estimation of the scour values based on the field measurements and the WSPRO model, where the dimensionless scour value (d_{se}/Y_{fo}) was predicted as 2.64 which was well within the standard error of the suggested model.

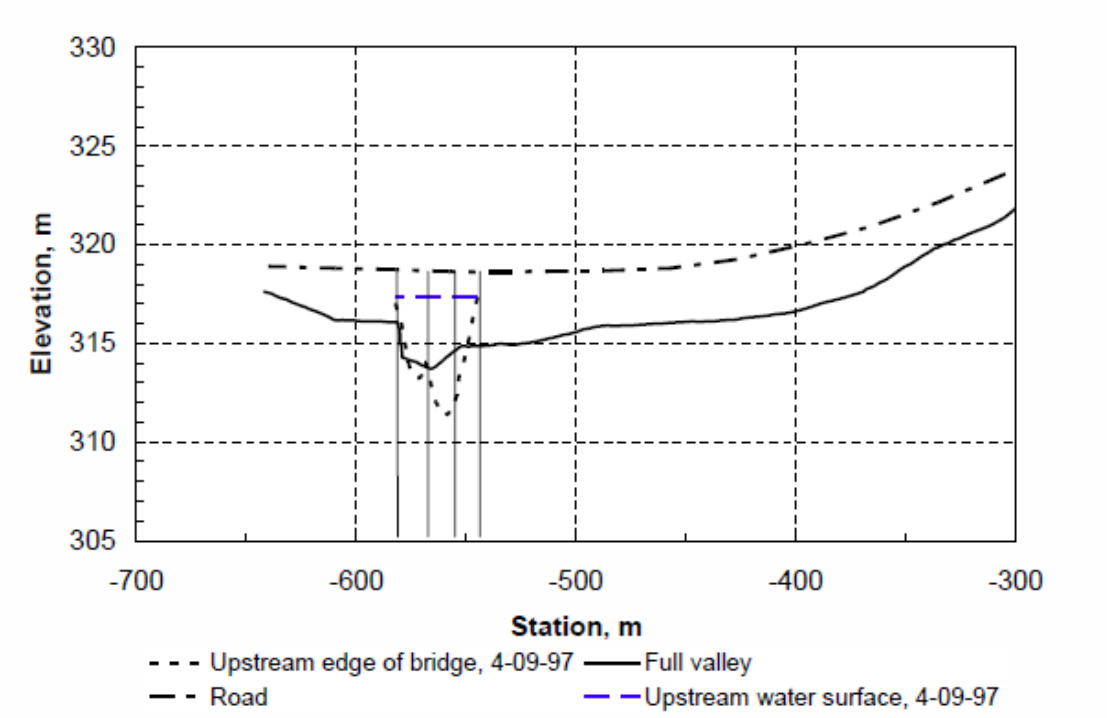

Figure 2-17 Highway 22 bridge cross section and scour elevation over Pomme de Terre river for 1997 flood (Sturm 2004)

Table 2-5 Field measurements for Pomme de Terre river flood data at Highway 22 for 1997 flood

$Q\ (ft^3/sec)$	V_{m1}/V_{mc}	M	q_{m2}/q_{m1}	$Y_{m2max}\ (ft)$	Y_{m2max}/Y_o
5150	1.2/2.85 (WSPRO)	0.336	2.976	19.84	1.75

For the same flood of April 1997 of Pomme de Terre River in Minnesota, at about 10 kilometers downstream of the Highway 22 bridge near Holloway, another bridge at Highway 12 with wing-wall abutments suffered heavy damage and scour extended down to the abutment footings. Flow was measured to be 5750 ft^3/sec and the minimum elevation after the scour was 963ft. Figure 2-18and Table 2-6 show the scour at the bridge and the summary of variables. Sturm (2004) analyzed the field data with the help of WSPRO model. The velocity measurements showed the threshold of the live-bed

scour with $V_1/V_c \simeq 1$. The predicted value resulted in an elevation of maximum scour about 10 ft lower than the ground measurements. For a conservative approach the estimate remains on the higher side but the discrepancy was attributed to sediment information limitation and that presence of both sand and gravel may have caused an armoring effect which is likely to result in lower scour values.

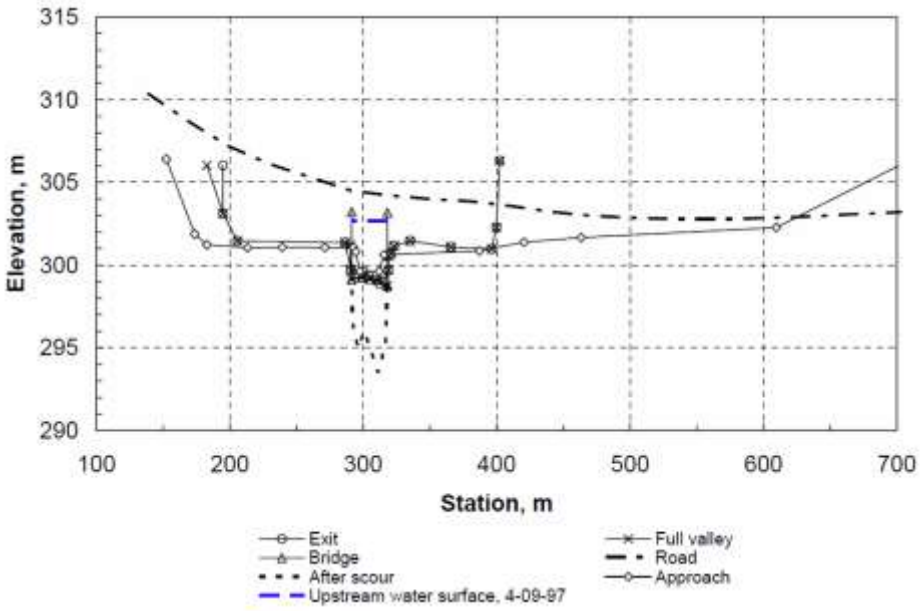

Figure 2-18 Highway 12 bridge cross section and scour elevation over Pomme de Terre river for 1997 flood (Sturm 2004)

Table 2-6 Field measurements for Pomme de Terre river flood data at Highway 12 for 1997 flood

Q (ft^3/sec)	V_{m1}/V_{mc}	M	q_{m2}/q_{m1}	Y_{m2max} (ft)	Y_{m2max}/Y_o
5750	2.76/2.89 (WSPRO)	0.335	2.985	29.8	2.94

2.15. Future Research Guidelines

Sturm reviewed the existing scour prediction methods under National Cooperative Highway Research Program for NCHRP 24-27 and gave recommendations for the

prediction of abutment scour (Sturm et al. 2011). They developed a set of five criteria to be satisfied for an idealized formula. This included:

1. Adequately addressing the parameters that affect the physical process governing the abutment scour.
2. Stating limitation on the formulas with respect to the parameters on which they are based.
3. Categorizing the laboratory experiments and research methods, which led to development of formulas (e.g. experimental duration, particle size variety, types of sediments, realistic geometries and scales, characterization of flow field, and degree of idealization).
4. Verifying formulas and comparison with other laboratory and field data, with which valid comparison can be made.
5. Applicability and ease of use for design.

It was concluded that none of the formulas developed until then, had adequately addressed all the five points. Therefore, it was emphasized that future research for abutment scour should particularly concentrate on three distinct aspects to include:

- Focus on better understanding of physical processes that cause abutment scour, which includes physical and numerical models.
- Inclusion of widespread use of reliable methods and scour countermeasures in the design.
- Emphasis on detailed real time flood event measurements and field data collection in comparison with the post flood surveys and measurement of

remnant scour hole with little or no knowledge of flow conditions that caused the scour.

The above mentioned criteria described in NCHRP 24-27 (Sturm et al. 2011), for future scour investigations does not only hold good for abutment scour but is an equally good guideline for all scour studies. Applicability of the laboratory models to the field conditions and real-time flood data at the time of peak of the event can help calibrate the model with maximum accuracy and can be used to validate the model results.

CHAPTER III

METHODOLOGY

3.1 General

Interaction among the types of bridge scour (i.e., lateral contraction scour, vertical contraction scour, abutment scour, and pier scour) may or may not occur depending on the geometric location, flow intensity, and flow type. To capture the interaction of scour components, this study consisted of experimental apparatus, experimental settings, and type of data to be measured such that both interactive and non-interactive scour could be developed and measured. The analyses of the data for interactive and non-interactive scour development helped identify the relationship for interaction of components of scour.

A compound channel with floodplain on each side of the main channel was set up with different floodplain to main channel ratio and different abutment lengths for each floodplain. The experiments consisted of two phases as fix bed experiments and movable bed experiments. Where movable bed experiments helped collecting the scour values for the time development and equilibrium scour bathymetry and fix bed experiments were used to measure the velocity, flow, and turbulence measurements. Details of the methodology for experimental setup, experimental settings, and data collection procedure are explained in this chapter.

3.2 Experimental Setup

Experiments were set up in the Hydraulic Laboratory at the Georgia Institute of Technology. The apparatus consists of a constant head overflow water tank that supplies water up to 9.5 cubic feet per second (cfs). The tank is linked to an 80 ft long and 14 ft wide flume through two 6- and 12-inch diameter pipes. To control the flow rate through the pipes, gate valves have been installed in both the pipes.

3.2.1. *Flume Setting*

Hong (2013) carried out a physical model study for the abutment and contraction scour on a modified model of the Towaliga River. The modification was carried out for the Towaliga River bridge site near Macon, Georgia, for which a separate physical model study for 1994 Tropical Storm Alberto was conducted, as discussed in Para 2.14. The modification resulted in a simplified compound channel to obtain more features of the flow field and wide applicability of the abutment/contraction scour model. This includes making floodplain horizontal on both sides of the main channel; however, the main channel original shape was preserved with an alteration of straight channel instead of the mild meandering river. The same model has been used in this study with different abutment ratios and addition of piers at different locations as per experimental settings. Abutment type was spill-through abutments having a side slope of 2:1 with riprap protection. Some of the experiments were repeated by replacing the spill-through abutments with wing-wall abutments. The modified model of the Towaliga River is shown in Figure 3-1.

Figure 3-1 Modified Towaliga river model

The experimental flume was 80 ft long, 14 ft wide, and 2.5 ft high. The flume had a concrete horizontal bed with steel walls bolted and sealed to prevent any water leakage. At the upstream end of the flume, a 12-inch diameter pipe from a large constant-head tank supplied water. The flume was divided into the following sections: the entrance, the approach, the test, the downstream, and the end/tailgate sections as shown in Figure 3-2.

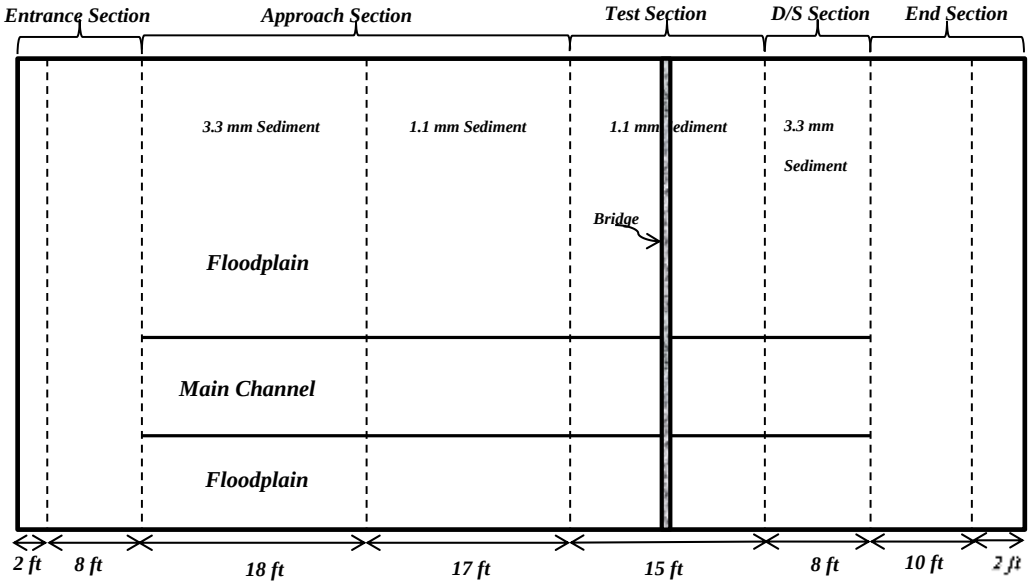

Figure 3-2 Definition sketch (Plan view of the flume)

The entrance section of the flume had an arrangement that eliminates excess turbulence so that water flowing in the flume was undisturbed. This arrangement consisted of a series of obstructions. The first element in the arrangement was a 12-inch diameter diffuser along the entire width of the flume for equal flow distribution. To reduce turbulence, an overflow weir was located 2 ft downstream of the headwall of the flume. Three chain fence rolls wound with horse-hair filters were placed in the gap between the headwall and overflow weir. One-foot further downstream, two baffles were installed, one consisting of wooden planks and the other of a steel plate with 3/8-inch diameter holes spaced 9/16-inches apart. Between the two baffles, another horse-hair filter was placed. This arrangement, shown in Figure 3-3, ensured a smooth flow entry to the flume.

An 8-foot-long transition area across the entire width of the flume, ahead of the entrance section, ensured smooth entry of water. This area leads to the approach section. The flume in the approach, the test, and the end sections consisted of horizontal floodplains on both sides separated by a main channel. To expand the range of geometric variables in the compound channel, the width ratios (B_f/B_m) of the floodplain to main channel were kept as 3:1 and 1:1 for the left and right floodplains, respectively, as shown in Figure 3-4. The left and right sides are defined while facing downstream. The approach section was 35 ft long with 3.3 mm diameter coarse sediment in the first 19 feet, which prevented any sediment entrainment in the upstream approach section and ensured a fully-rough turbulent flow with a fully-developed boundary layer. For the remaining approach section length of 16 ft, the sediment size was kept as 1.1 mm.

The test section was 15 ft long. In the middle of this section, the abutment, pier, and bridge settings were assigned to each experiment. Sediment size in this section remained 1.1 mm. The downstream section again consisted of 3.3 mm-diameter sediment with a section length of 8 ft. A 10 ft long end section for the sediment accumulation followed the downstream section, which terminated at the tailgate with a mechanical arrangement that controlled the tailgate position as shown in Figure 3-5. Water passing over the tailgate recirculated through the constant-head tank.

The flume had two additional features: First, a movable carriage was installed across the entire width of the flume with a crossbar to hold an acoustic Doppler velocimeter (ADV) and a point gauge to take measurements of depth, velocity, and turbulence at any point in the flume. Second, wooden templates were fixed in the flume at 8-10 ft intervals and at the start and the end of the test section at an undisturbed bed level, which helped accurately level the bed. A removable aluminum template was also used in the middle of the test section for accurate leveling.

Figure 3-3 Flume entrance section and arrangement for turbulence diffusion

(a) Looking downstream

(b) Looking upstream

Figure 3-4 Approach section

Figure 3-5 Tailgate section

3.2.2. *Flow Meter*

To measure the flow rate in the flume, magnetic flow meters are installed both in the 12-inch and 6-inch supply pipes leading to the flume. Uncertainty in the measurement of the flow meter is ± 0.005 ft^3/ sec (*cfs*).

3.2.3. *Bridge Design*

The model for this study replicates a standard two-lane bridge used by Georgia Department of Transportation (DOT) for rural-region bridges. The bridge was supported and attached by an upper support beam over the entire cross-section with an adjustable nut and bolt attachment. This arrangement ensured accurate bridge height for each experiment when the bridge was placed after leveling of the flume bed, as shown in Figure 3-6. A model-scale ratio of 1:45 was applied to the prototype bridge dimensions. Model dimensions are shown in Figure 3-7 and the prototype dimensions are as follows:

a. Road width = 40 ft (for two-lane roads without a sidewalk)

b. Bridge barrier 2 ft high with a 1.5 ft top width

c. Pavement and slab combined thickness = 1.5 ft

d. Girder dimensions are 1.4 ft, 1.5 ft, and 9 ft for width, thickness, and spacing, respectively.

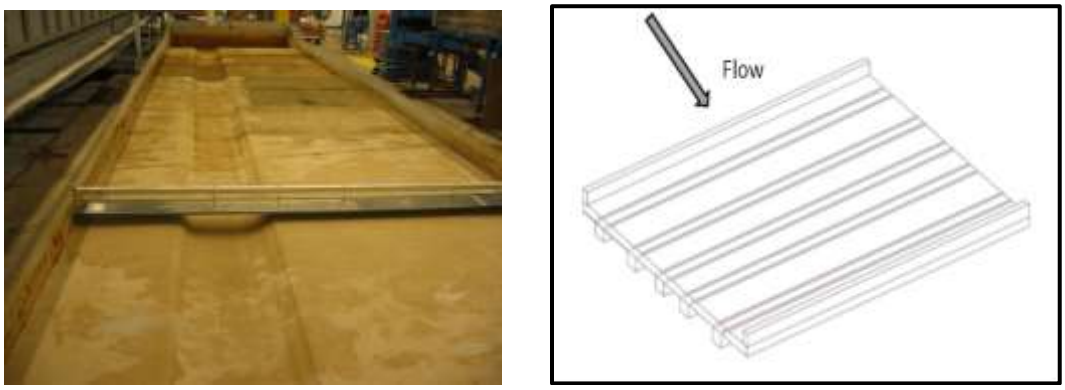

(a) Bridge placement in the flume (b) Schematic diagram of the bridge deck

Figure 3-6 Bridge deck model

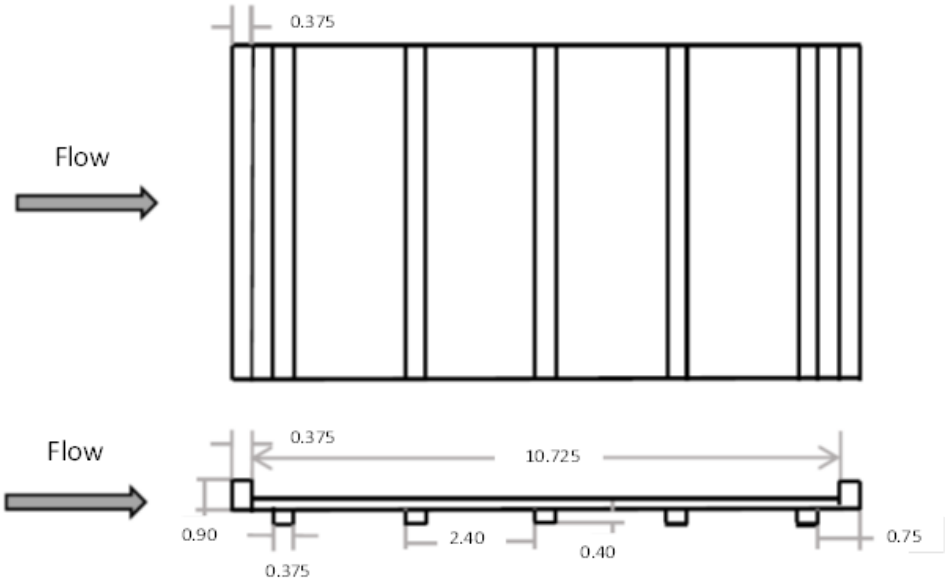

Figure 3-7 Model bridge dimensions for Georgia DOT bridge at a scale of 1:45 (All dimensions are in inches)

3.2.4. *Pier and Wing-wall Design*

Rectangular piers with a ratio of 1:45, in connection with the two-lane bridge design used by the Georgia DOT for rural regions were replicated in this study. A prototype bridge pier dimension of 42x42-inches had been used with a gap of 20 ft center to center between the upstream and downstream pier column. A pile cap that serves as a platform for bridge piers was assumed to be sufficiently deep such that it is not exposed even after maximum scouring. Exposure of the pile cap initiates an altogether different phenomenon (Kothyari and Kumar 2012) which is beyond the scope of this study. Therefore, the length of the pier below the undisturbed bed level was kept aligned with the assumed datum level. Free flow and SO flow experiments for the rectangular pier for long setback abutment (LSA) were repeated with wall piers having no other difference in the experimental setting such that the difference with the type of pier could be observed.

The dimensions of the wall-per were same as that of the rectangular pier with the only difference that the gap between the upstream and the downstream pier was covered as a solid wall. The fabricated model piers and wing-wall are shown in Figure 3-8 .

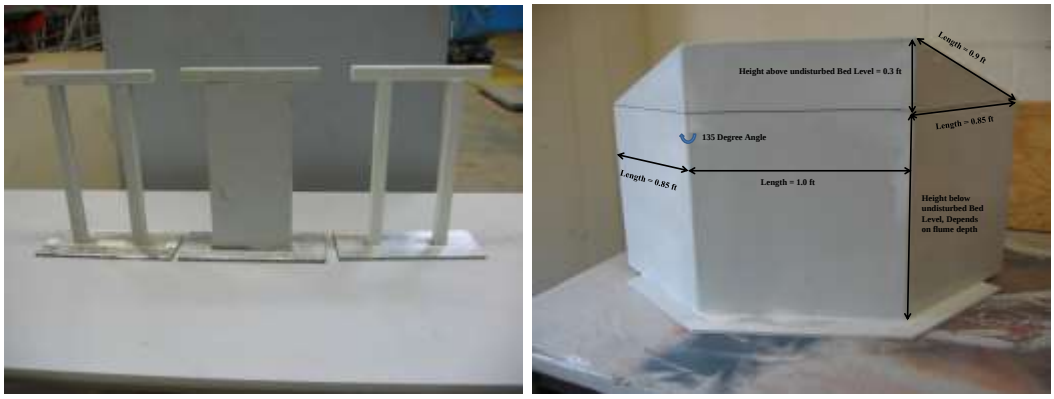

(a) Rectangular and wall piers (b) Wing-wall abutment

Figure 3-8 Fabricated models for rectangular pier, wall pier, and wing-wall abutment

3.2.5. *Bed Material and Riprap*

For the test section, two types of materials, river bed material and riprap material, were selected. Uniformly graded materials were used in this study with a geometric standard deviation as $\sigma_g \leq 1.35$. A sieve analysis of the river bed material shows uniformly graded sand with a geometric standard deviation of $\sigma_g = (d_{84}/d_{16})^{0.5} = 1.13$. The value of the critical Shields' parameter, τ_{*c} , was calculated with Shields' diagram (as shown in Figure 2-1) as 0.032. The size distribution of the sediment is characterized by the sieve diameter at which 50% of the material is finer by weight, (d_{50}). For this study, the bed material had a d_{50} = 1.1 mm sand.

The HEC-23 design criterion, as given by Equation 3-1, for the riprap design has been used for the riprap size selection to protect the embankment and toe of the

embankment from erosion. This equation depends on the contracted section depth, the contracted section Froude Number, and the abutment shape factor.

$$\frac{d_{50}}{Y_2} = \frac{K_s}{(SG-1)} F_{r2}^{\ 2} \qquad (3\text{-}1)$$

where d_{50} = median diameter of the riprap, and SG = specific gravity of the riprap material. In this study Y_2 = flow depth in the contracted section, F_{r2} = contracted section Froude number, and K_s = abutment shape factor (i.e. 1.02 for F_{r2} <0.8). The contracted section Froude number was well below 0.8 for the experiments in the study. The riprap size varied between 7.4 and 8.6 mm for all abutments. The conservative choice of riprap for the experiments was kept as d_{50} = 9.2 mm with σ_g=1.25. Table 3-1and Figure 3-9 show the important sediment properties and the size distribution of both the materials. HEC-23 design includes a riprap apron at the toe of abutment, which prevents toe failure. During the scour process, the riprap apron provides an armoring effect and reduces scour within the abutment toe area. The width of riprap apron was based on HEC-23 recommendations and was chosen to be 0.4 ft for all flow conditions.

Table 3-1 Sediment properties for the study

Sediment	d_{50} (mm)	σ_g	d_*	τ_{*c}	u_{*c} *(ft/sec)*
Bed Material	1.1	1.13	26.6	0.032	0.0765
Riprap	9.2	1.25	232.7	0.045	0.269

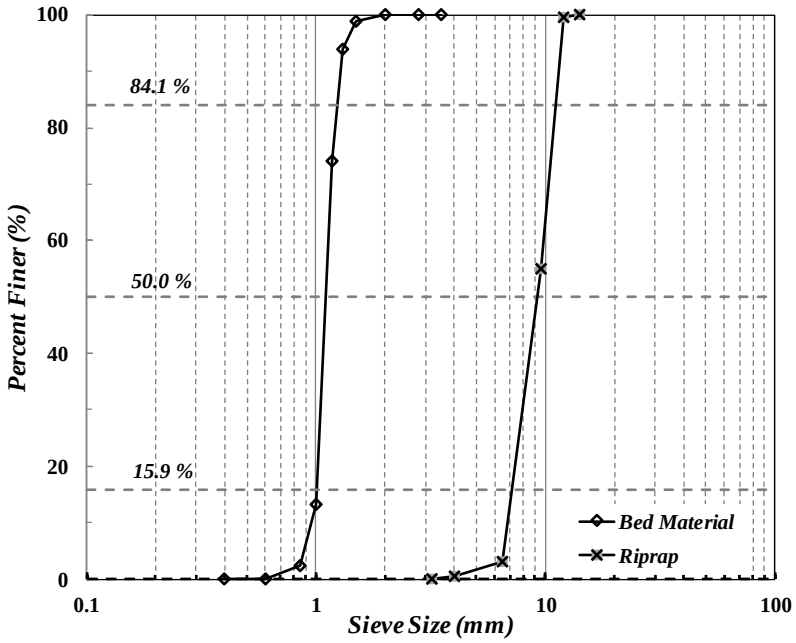

Figure 3-9 Size distribution for bed sediment and riprap

3.2.6. *Instruments for Measurements*

The data were measured by two instruments: a point gauge and a 16 MHz Micro Acoustic Doppler Velocimeter (16 MHz microADV). At the start of experiments, the point gauge with an accuracy of ±0.001 ft was used for water-surface profile measurements. For the point velocity measurements, a 3-D down-looking ADV and a 2-D side-looking ADV were used. A 16 MHz microADV can measure distances up to 25 cm from the center of a sampling volume with an accuracy of ±1mm. For near-bed measurements, the 3-D down-looking instrument was used, while for near-surface measurements, a 2-D side-looking instrument was deployed. Near the water surface, a 3-D down-looking ADV was unable to take measurements because of instrument limitations. Thus, velocity and fluctuation components in the vertical direction could not be measured by the 2-D side-looking instrument in the near surface measurements. Both the point gauge and ADV were calibrated with respect to datum level such that there is no

difference in the measurements of elevation level. Figure 3-10 shows the comparison between the measurements taken by point gauge and the ADV.

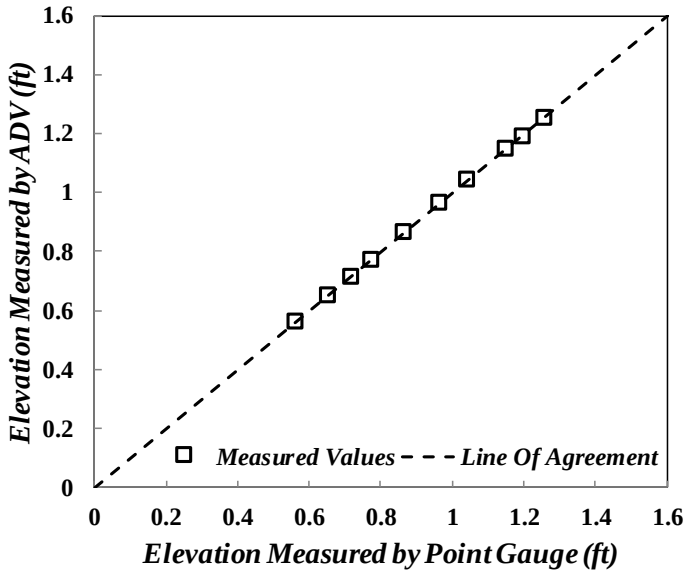

Figure 3-10 Comparison of elevation measurement of point gauge and ADV

The ADV works on the principle that the reflections of sound waves by the small particles in the fluid (which are assumed to be moving with the velocity of fluid) shift the Doppler frequency of the emitted acoustic signals. The analysis of the accuracy of the ADV shows that the ADV can accurately measure the velocity and Reynold stresses in the fluid (Voulgaris and Throwbridge 1998). The noise in the measurements can still exist either by the reflections of the previous signals getting reflected by the uneven surfaces in complex geometries or if the velocity to be measured exceeds the pre-set velocity range. This difficulty can be overcome by filtering the measured data. The data was thus filtered by applying the protocol for a minimum correlation of 70% for all three components of velocity and keeping the signal to noise ratio (SNR) above 15 which is recommended for both velocity and turbulence measurements (SonTek 2001). During the

measurements, it was ensured that measured velocity did not exceed the pre-set velocity range as shown in Table 3-2, so that better accuracy was achieved. Kaolin clay particles were used to improve the correlation factor and SNR ratio where there was a difficulty in measurement of velocity within the pre-set velocity range. In addition, the phase-space despiking algorithm was applied to remove any spikes in the time record caused by aliasing of the Doppler signal which may occur closer to a boundary (Goring and Nikora 2002). Only those measurements were kept where the filtered time data retained was more than 60% of the total measured time data. Typical values of correlation of the velocity components were greater than 90% with SNR>15 and retained filter data more than 85%.

Table 3-2 Velocity range settings for ADV (SonTek 2001)

Velocity Range Setting (cm/s)	**Max Horizontal Velocity (cm/s)**	**Max Vertical Velocity (cm/s)**
±3	±30	±8
±10	±60	±15
±30	±120	±30
±100	±300	±75
±250	±360	±90

For an ADV, at higher frequencies, the Doppler noise increases but at the same time maximum feasible frequency is recommended for better accuracy. Sampling duration is also case-specific which can be determined by long-term sampling at a single point (García et al. 2005, Chanson et al. 2007). Based on the previous experiments conducted at the Georgia Institute of Technology the minimum sampling frequency was kept as 25Hz and sampling duration was kept as a minimum of 2 min with as high as 5

min for near-bed measurements on case-to-case basis (Lee et al. 2004, Ge et al. 2005, Hong 2005). A comparison of the velocity and fluctuation measurements over time as presented in Table 3-3and Figure 3-11 shows that velocity and fluctuation measurements (for normal flow condition) gives satisfactory results if measured for a minimum duration of 2 minutes.

Table 3-3 Comparison of velocity and fluctuation measurements by a 3-D down-looking ADV for a time duration ranging from 1 to 5 Minutes for the same flow condition

Time	***u (ft/s)***	***v (ft/s)***	***w (ft/s)***	***u′ (ft/s)***	***v′ (ft/s)***	***w′ (ft/s)***	***COR***	***SNR***	***Data Retained %age***
1 min	0.999	-0.055	0.004	0.225	0.132	0.107	79.380	16.450	74.450
2 min	1.008	-0.056	0.005	0.224	0.127	0.105	79.070	16.935	73.025
3 min	1.003	-0.053	0.006	0.226	0.127	0.104	79.020	17.003	72.927
4 min	1.004	-0.053	0.005	0.227	0.127	0.104	78.858	17.318	73.095
5 min	1.006	-0.052	0.005	0.227	0.127	0.105	78.794	17.630	73.472

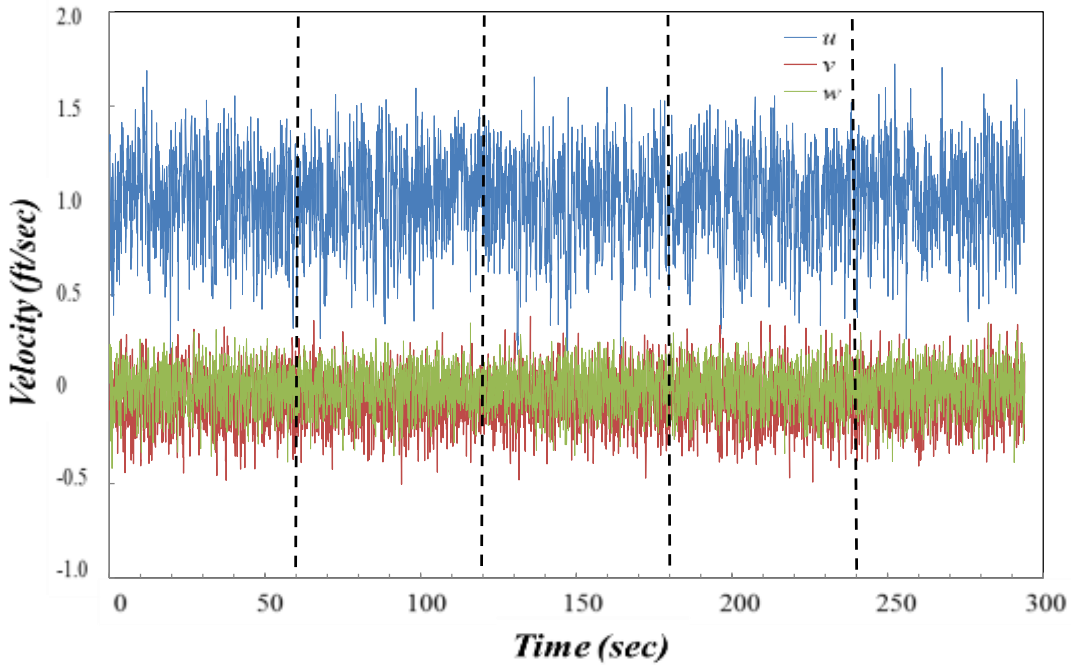

Figure 3-11 Filtered data for point velocity measurements in X, Y, and Z directions for the data shown in Table 3-3

3.3 Experimental Setting

A long setback abutment (LSA) is one for which the scour hole is within the floodplain; whereas, for a short setback abutment (SSA) the setback distance is small, such that the scour hole the deepest point of the scour hole is in the main channel For a bankline abutment (BLA), abutment covers the whole of the floodplain thus the complete scour hole is in the main channel. The variables used in this study are shown in Figure 3-12 and Figure 3-13. Dimensionless parameters used as independent variables in the experiments are approach flow intensity (V_1/V_c) both in the main channel and in the floodplain, relative depth in main channel to the floodplain (Y_{m1}/Y_{f1}), the type of flow (free (F), submerged orifice (SO), and overtopping (OT)), the relative length of the abutment (L_a/B_f), and the presence and the location of the pier, L_p/W. Figure 3-14 show the schematic diagram of the experimental settings and the profile view of section A-A respectively.

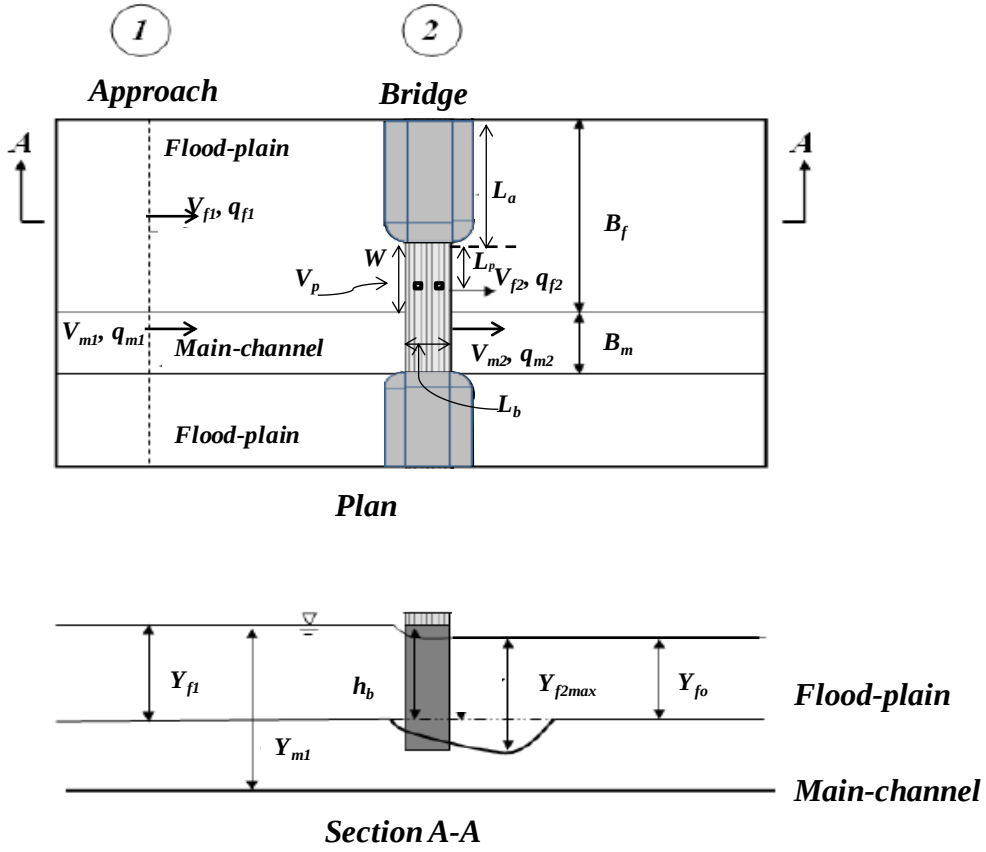

Figure 3-12 Definition sketch of the variables (Plan view)

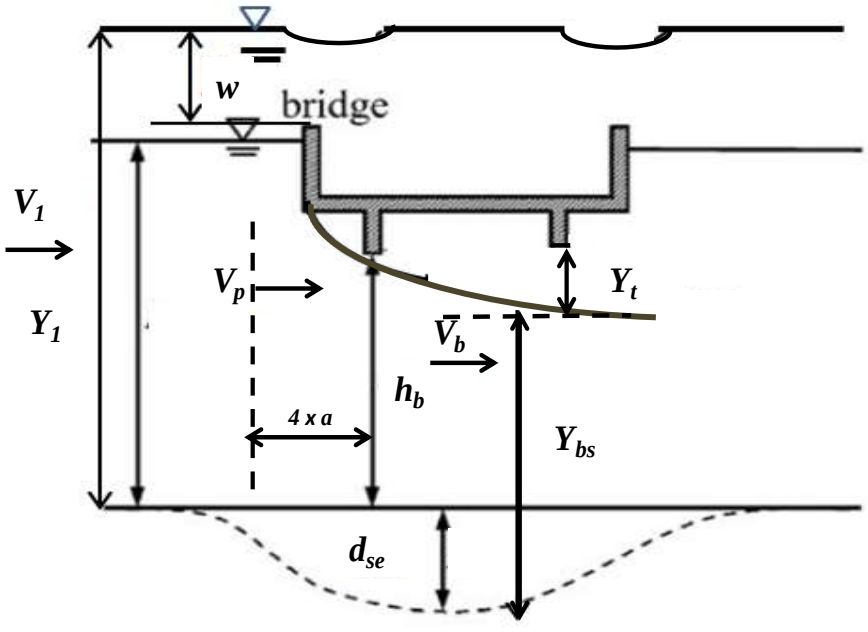

Figure 3-13 Definition sketch for the variables in the bridge section (Profile view)

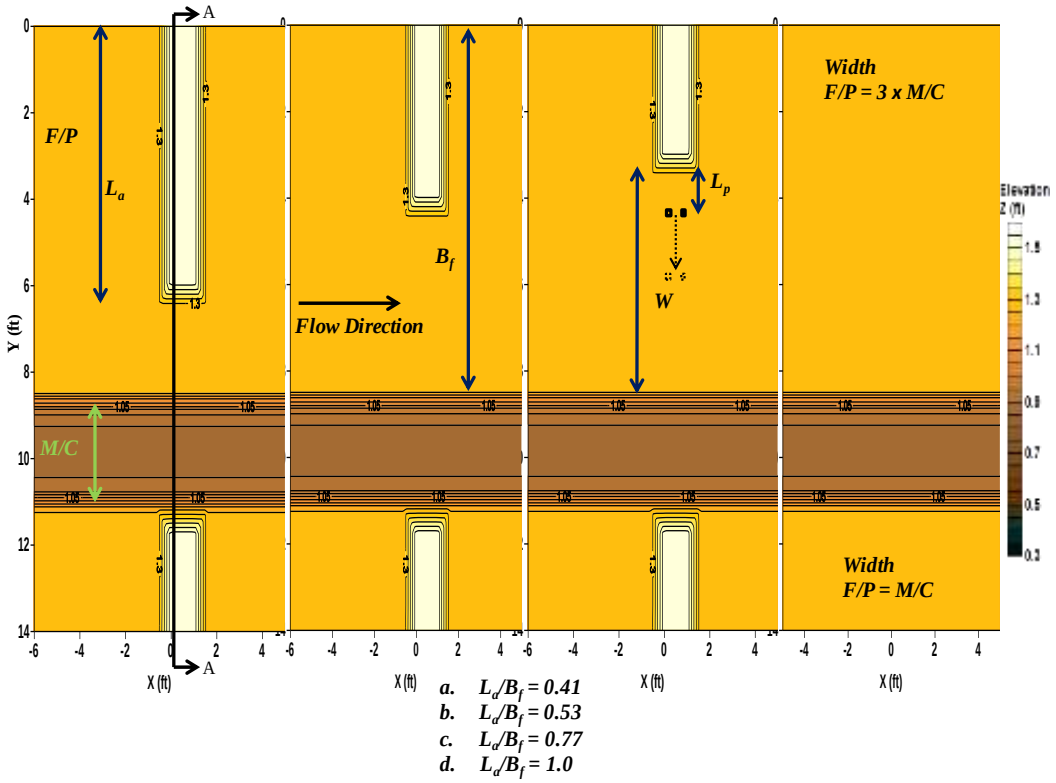

(a) Plan view

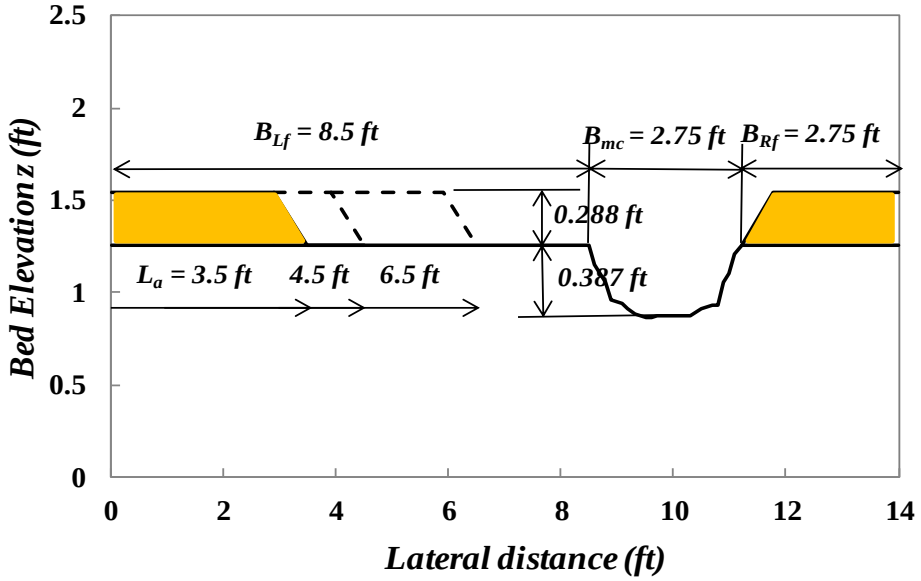

(b) Section A-A (Cross section elevation)

Figure 3-14 Schematic diagram for experimental settings

This study entailed 45 experiments, listed in Table 3-4. For the larger setback distance (i.e. L_a/B_f = 0.41), experiments (without the pier) were repeated having pier in place, for the investigation of the effect of the pier. The pier location was set closer to the abutment in one experimental setting and was replaced with the pier location away from the abutment such that the pier still remained in the influence of the abutment and contraction scour hole (i.e. L_p/W=0.18 and 0.35). The same setting was applied to all three flow types by changing the tail water (TW) and discharge (Q). For the relatively shorter setback distance of abutment (i.e. L_a/B_f = 0.77), the scour hole in the floodplain entered into the main channel (for the experiments without piers). Thus the setting of the pier, in the repeated experiments, was set such that in one case the pier was sufficiently away from the bank of main channel and floodplain, such that the bank does not affect the interactive pier scour (i.e. L_p/W=0.40). For the other case pier was placed at the critical location of the junction of the floodplain and the main channel, referred to as a bankline pier (i.e. L_p/W=1.0). For the intermediate abutment size (L_a/B_f = 0.53) two piers were placed in the floodplain, for each experiment, such that the distance between the pier was sufficient that their scour holes did not interact with each other. One pier was located in the influence of the abutment and contraction scour hole and the other was located out of the influence of abutment and contraction scour hole. This second pier was used to capture pier scour only in F flow case and pier and vertical contraction scour in SO and OT flow cases.

Experiments with spill-through abutments for L_a/B_f = 0.41 and 0.77 (Run 1, 2, 3, 10, 11, and 12) were repeated with wing-wall abutments (Run 22, 23, 24, 25, 26, and 27). Some of the experiments with rectangular piers (Run 6, 8, 28, and 29) were repeated with

wall piers (Run 39, 40, 41, and 42). Detail of dimensionless variables used in the set of experiments is given in Table 3-4.

Isolated vertical contraction scour was measured by experiments without abutments. The absence of abutments eliminated abutment and lateral contraction scour components. Three different values of dimensionless variables Y_{m1}/Y_{f1} and V_1/V_c, both in the main channel and in the floodplain were used in SO and OT flow conditions. Observations of the interaction between pier and vertical contraction scour were collected through repetition of these experiments with piers. However, because of the absence of abutment and contraction scour, these experiments involved no relocation of the pier. Therefore, to compare the results with all three abutment lengths (L_a/B_f = 0.41, 0.53, and 0.77), these experiments entailed two sets of the piers: one in the floodplain and one on the bankline.

Three experiments, one each for the L_a/B_f = 0.41, 0.53, and 0.77, were conducted for experimental settings of SO flow but without the bridge deck (i.e., refer to experiment numbers 18, 19, and 20 in Table 3-4). The purpose of these experiments was to observe the effect of vertical contraction resulting from the bridge.

For L_a/B_f = 0.41, the wider floodplain in the contracted section had sufficient space in the lateral direction, next to the abutment scour region, in which no scour was observed for the free flow experiment and only vertical contraction scour was yielded in the case of SO and OT flow experiments. Isolated vertical contraction scour was thus measured in the experiments with L_a/B_f = 0.41. Figure 3-15 explains this phenomenon.

Table 3-4 List of experiments and variable parameters

Run	L_a/B_f	***Flow type***	$\frac{V_{f1}}{V_{fc1}}$	$\frac{V_{m1}}{V_{mc1}}$	$\frac{Y_{f1}}{Y_{m1}}$	$\frac{L_p}{W}$	$\frac{Q_{ot}}{Q}$	***Q, cfs***	***T.W. elev., ft***	***Scour components***			
										A	***P***	***L***	***V***
1	0.41	F	0.542	0.723	0.487	-	-	3	1.48	*		*	
2		SO	0.589	0.725	0.556	-	-	4	1.547	*		*	*
3		OT	0.561	0.653	0.651	-	0.303	5.5	1.714	*		*	*
4		F	0.655	0.841	0.493	-	-	3.7	1.477	*		*	
5		OT	0.683	0.823	0.657	-	0.340	7	1.717	*		*	*
6		F	0.648	0.820	0.495	0.18	-	3.7	1.477	*	*	*	
28		SO	0.589	0.725	0.557		-	4	1.547	*	*	*	*
7		OT	0.683	0.822	0.658		0.340	7	1.717	*	*	*	*
8		F	0.648	0.820	0.494	0.35	-	3.7	1.477	*	*	*	
29		SO	0.589	0.725	0.557		-	4	1.547	*	*	*	*
9		OT	0.683	0.822	0.658		0.340	7	1.717	*	*	*	*
18		F	0.586	0.712	0.554	-	-	4	1.547	*		*	
10	0.77	F	0.659	0.879	0.509	-	-	3.8	1.47	*		*	
11		SO	0.579	0.711	0.585	-	-	4.4	1.522	*		*	*
12		OT	0.623	0.784	0.662	-	0.406	6.5	1.714	*		*	*
14		F	0.660	0.879	0.509	0.4	-	3.8	1.47	*	*	*	
30		SO	0.579	0.711	0.585		-	4.4	1.522	*	*	*	*
15		OT	0.622	0.784	0.663		0.407	6.5	1.714	*	*	*	*
16		F	0.659	0.878	0.509	1.0	-	3.8	1.47	*	*	*	
31		SO	0.579	0.711	0.585		-	4.4	1.522	*	*	*	*
17		OT	0.622	0.784	0.664		0.407	6.5	1.714	*	*	*	*
19		F	0.590	0.791	0.557	-	-	4.4	1.522	*		*	
32	0	SO	0.831	0.974	0.522	-	-	5	1.522				*
33		SO	0.902	1.041	0.529	-	-	5.5	1.522				*
35		OT	0.74	0.802	0.648	-	0.385	7	1.714				*
36		SO	0.832	0.974	0.522	0.4 & 1.0	-	5	1.522		*		*
37		SO	0.902	1.041	0.527		-	5.5	1.522		*		*
38		OT	0.731	0.801	0.649		0.385	7	1.714		*		*
22	0.41 WW	F	0.542	0.723	0.486	-	-	3	1.48	*		*	
23		SO	0.589	0.725	0.556	-	-	4	1.547	*		*	*
24		OT	0.561	0.653	0.651	-	0.307	5.5	1.714	*		*	*
25	0.77 WW	F	0.659	0.879	0.507	-	-	3.8	1.47	*		*	
26		SO	0.579	0.711	0.585	-	-	4.4	1.522	*		*	*
27		OT	0.623	0.784	0.662	-	0.406	6.5	1.714	*		*	*

Run	L_a/B_f	Flow type	$\frac{V_{f1}}{V_{fc1}}$	$\frac{V_{m1}}{V_{mc1}}$	$\frac{Y_{f1}}{Y_{m1}}$	$\frac{L_p}{W}$	$\frac{Q_{ot}}{Q}$	Q, cfs	T.W. elev., ft	Scour components			
										A	P	L	V
39	0.41	F	0.648	0.82	0.495	0.18	-	3.7	1.477	*	*	*	
40		SO	0.589	0.725	0.557	w	-	4	1.547	*	*	*	*
41		F	0.648	0.82	0.494	0.35	-	3.7	1.477	*	*	*	
42		SO	0.589	0.725	0.556	w	-	4	1.547	*	*	*	*
43	0.53	F	0.613	0.831	0.487	0.23, 0.65	-	3.3	1.475	*	*	*	*
44		SO	0.590	0.726	0.575	0.48, 0.78	-	4.1	1.572	*	*	*	*
45		SO	0.569	0.682	0.581	0.43, 0.85	-	3.9	1.582	*	*	*	*
20		F	0.600	0.730	0.471	-	-	4.1	1.572	*		*	

Note: F=free flow; SO=submerged orifice flow; OT=overtopping flow; L_p=distance from the toe of the abutment to the centre of the pier; W=setback distance (=B_f-L_a); y_{f1}= approach the floodplain water depth; y_{m1}= water depth in the approach section of the main channel; B_f = floodplain width; B_m= main channel width; L_a/B_f=ratio of the abutment length to the floodplain width; V_{f1}/V_{fc1} = ratio of the approach flow velocity to the critical velocity in the floodplain; V_{m1}/V_{mc1} = ratio of the approach flow velocity to the critical velocity in the main channel; Q_{ot} = overtopping discharge; Q = discharge; *T.W.* = tail water. *A*= abutment scour; *P*= pier scour; *L*=lateral contraction scour, *V*=vertical contraction scour. Also refer to Figure 3-12 for definition of variables.

The type of scour developed in a given experimental setting, is given in last four columns of Table 3-4. The experiments were designed such that multiple observations of interactive scour and individual scour components could be observed simultaneously. Thus one experimental setting having either a long setback or a short setback abutment on the left floodplain had a bankline abutment on the right floodplain which resulted in development of different scour interactions and scour components both in the floodplain and in the main channel.

Experiments organized by the type of scour show a representation of the experimental methodology as given in Table 3.5. In the table, the first column shows the combination of scour components in an experiment. For this purpose, four combinations

of the scour interaction have been identified and color coded in the table as category I, II, III, and IV to coincide with the specific scour procedures developed in the study, as shown in Figure 3-16. For all four categories in this study, Free flow (F) cases have been combined with submerged orifice (SO) and overtopping (OT) cases to investigate the interactive scour as already established in the experiments carried out at the Georgia Institute of Technology (Hong 2013, Hong et al. 2015). Isolated pier scour and vertical contraction scour observations were also collected to make a comparison with the existing scour prediction models. The symbol "Y" appearing in each box shows the scour categories that were observed in an experiment. The last column of the table shows the total number of observations that were collected for each category of the experiments from the complete set of experiments in this study.

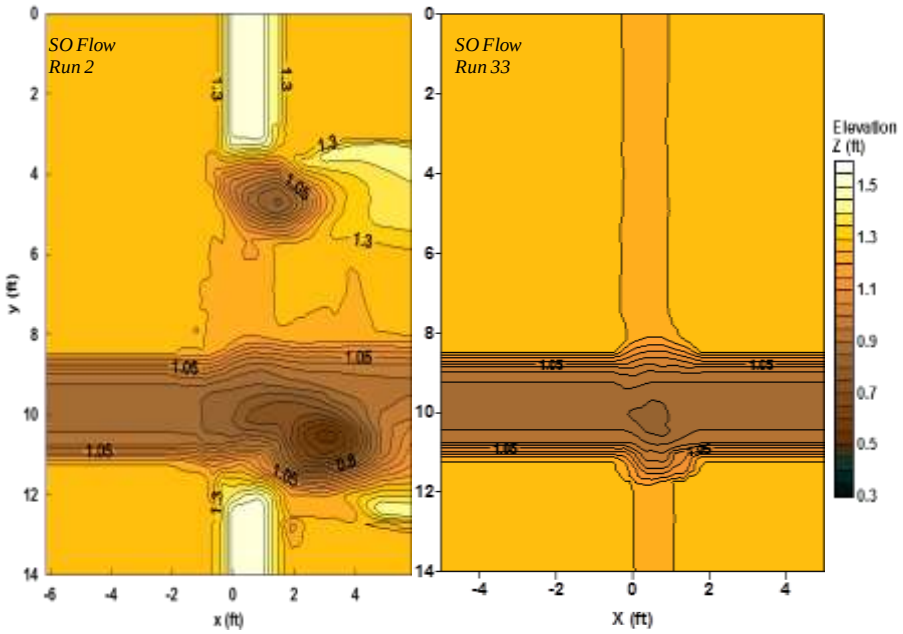

Figure 3-15 Vertical contraction scour with and without abutment

Table 3-5 Table of experiments showing the combination of scour components

Scour Component/s	Experiment Number																																										Total Observations
	(La/Bf) = 0.41									(La/Bf) = 0.77							0.41	0.77	0.41/WWA			0.77/WWA			0.41		0.77		W/O Abutment						0.41 Walled Pier				(La/Bf) = 0.53			
	1	2	3	4	5	6	7	8	9	10	11	12	14	15	16	17	18	19	22	23	24	25	26	27	28	29	30	31	32	33	35	36	37	38	39	40	41	42	43	44	45	
Type of Flow	F	SO	OT	F	OT	F	OT	F	OT	F	SO	OT	F	OT	F	OT	No Br		F	SO	OT	F	SO	OT	SO	SO	SO	SO	SO	SO	OT	SO	SO	OT	F	SO	F	SO	F	SO	SO	
Pier Location *(Lp/W)*						0.18	0.18	0.35	0.35				0.4	0.4	1	1									0.18	0.35	0.4	1				0.4&1.0			0.18	0.18	0.35	0.35	0.23	0.48	0.45	
I-Abutment/Contraction Scour LSA (Free Flow)	Y			Y				Y		Y							Y	Y	Y			Y															Y						7+2
II-Abutment/Contraction Scour BLA/SSA (Free Flow)	Y			Y		Y		Y		Y			Y		Y		Y	Y	Y			Y													Y		Y		Y			12+2
Vertical Contraction Scour		Y	Y		Y		Y		Y											Y	Y				Y	Y			Y	3Y	Y	Y	3Y	Y		Y		Y				21
Pier Scour								Y																								Y+Y		Y+Y			Y		Y			4+2+1
I-Abutment/Contraction Scour LSA + Vertical Contraction Scour (SO/OT Flow)		Y	Y		Y							Y								Y	Y		Y	Y													Y		Y	Y	7+4
II-Abutment/Contraction Scour BLA/SSA + Vertical Contraction Scour (SO/OT Flow)		Y	Y		Y		Y		Y		2Y	Y		Y		Y				Y	Y		Y	Y	Y	Y	Y	Y							Y		Y		Y	Y	18+4
III-Abutment/Contraction Scour + Pier Scour (Free Flow)						Y							Y		Y																			Y				Y			4+1
IV-Vertical Contraction + Pier Scour																																Y+Y					Y		Y	Y	3+1+1
III-All Components Together (SO/OT Flow)							Y		Y					Y		Y									Y	Y	Y	Y								Y				Y	Y	10+1

LEGEND	
Y	WING WALL ABUTMENT READINGS
Y	BANK LINE PIER READINGS
Y	WALL PIER RADINGS

Suggested categories for the scour interaction in Table 3.5 are:

Category I. Abutment/Lateral Contraction Scour for LSA (with or without vertical contraction scour): This category is a combination of local scour around the abutment resulting from the turbulent structure of the flow and flow acceleration by the width constriction because of the embankment terminating at abutment for free flow around LSA. Vertical contraction scour is also added in case of SO and OT flows;

Category II. Abutment/Lateral Contraction Scour for SSA/BLA (with or without vertical contraction scour): The definition is same as that of Category I, but for SSA and BLA;

Category III. Abutment/Lateral Contraction Scour for LSA with pier scour (in the floodplain) in free flow cases and it includes vertical contraction scour for SO and OT flows;

Category IV. Vertical Contraction Scour and Pier Scour in the floodplain outside the zone of influence of the abutment.

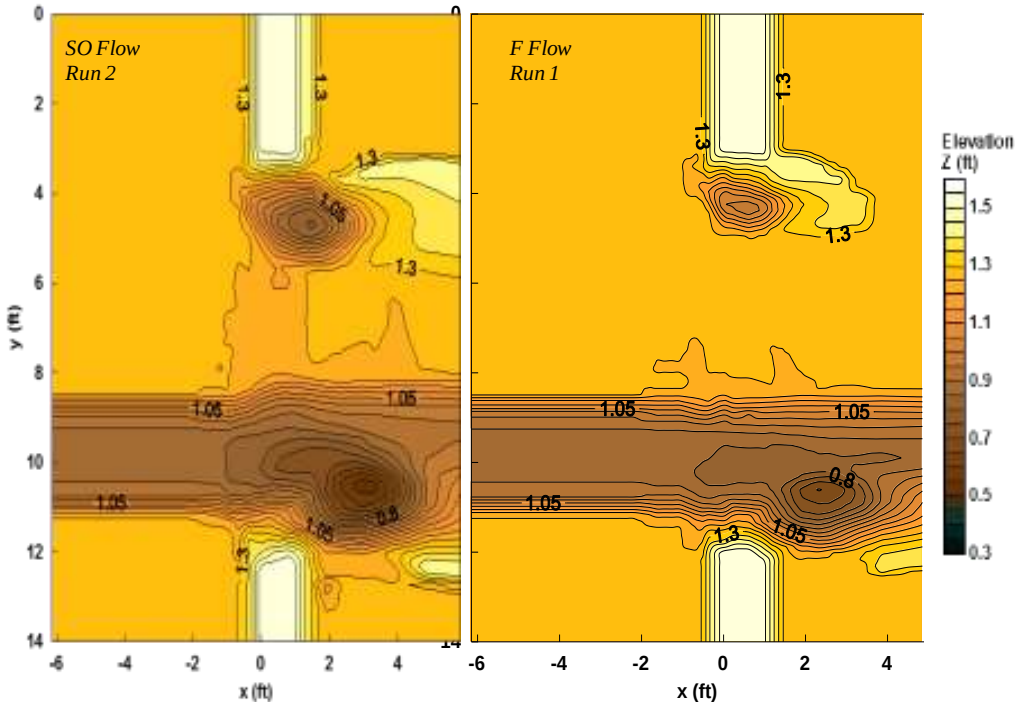

(a) Category I & II (Abutment and contraction scour LSA & SSA/BLA)

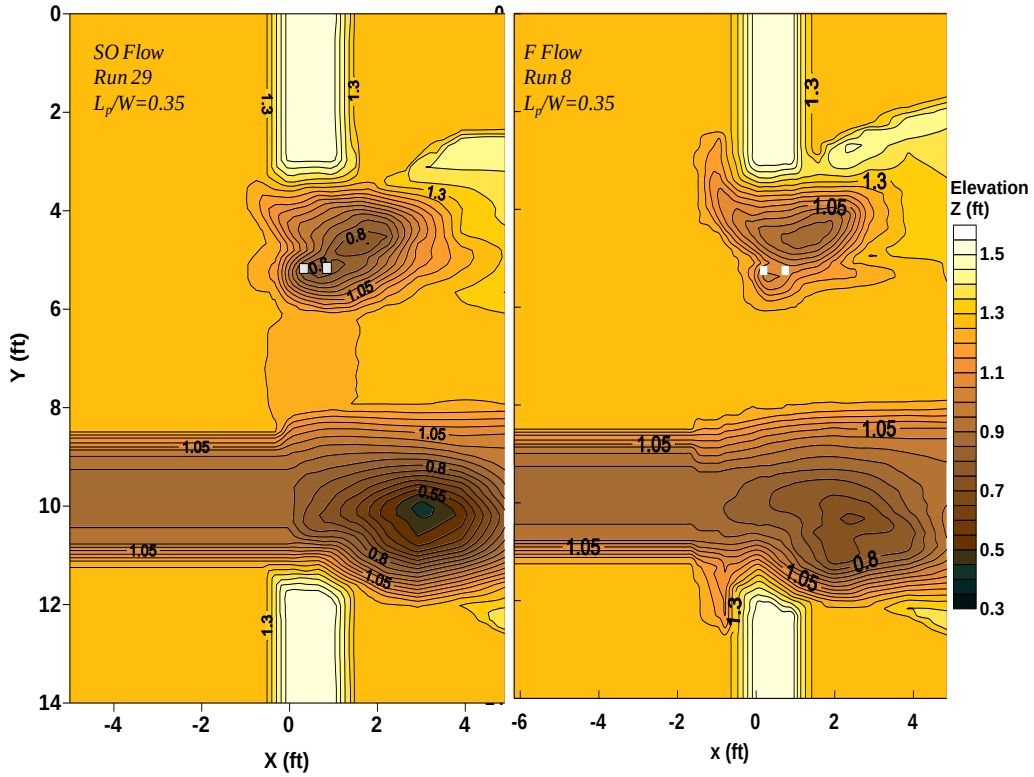

(b) Category III (Abutment, contraction and pier scour LSA)

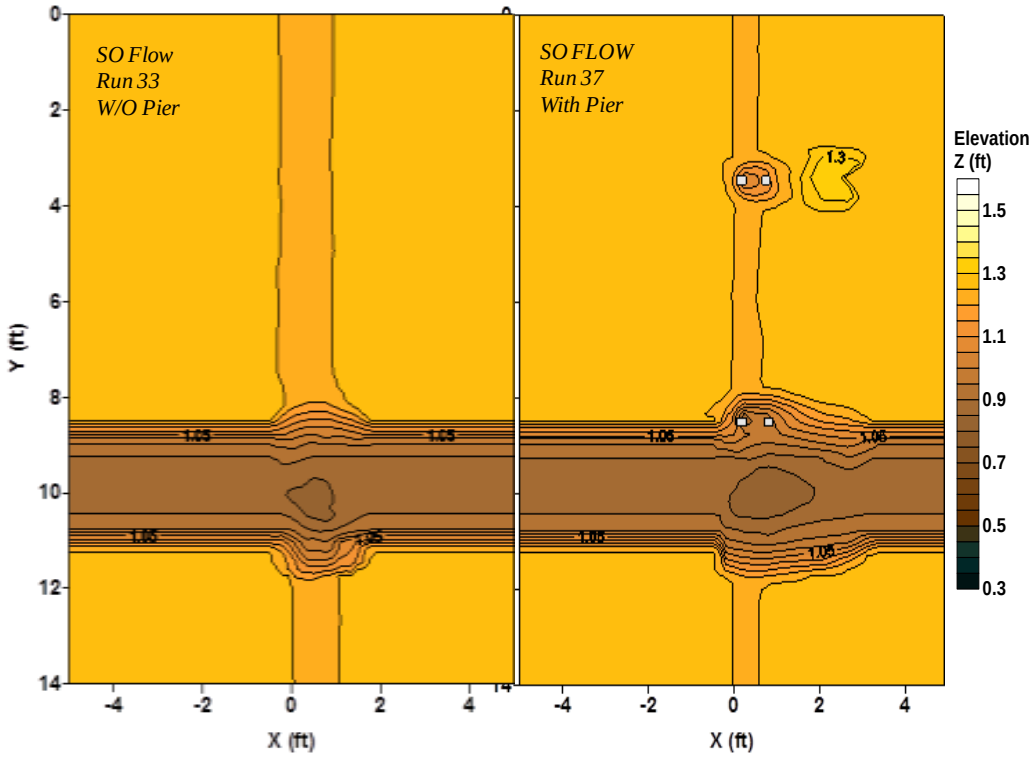

(c) Category IV (Pier and vertical contraction scour only)

Figure 3-16 Pictorial representation of categories of interactive scour

Critical velocities calculated from Keulegan's equation varied between 1.10 to 1.22 ft/sec for the floodplain and 1.20 to 1.25 ft/sec for the main channel due to varying flow depth for different experiments. Critical shear stress value for the test section sediment, d_{50} = 0.0036 ft (1.1 mm), was 0.012 lb/ft^2 as calculated from Shields' diagram.

3.4 Experimental Procedure and Data Collection

The experiments consisted of two phases: Phase one of the experiments was named "Movable Bed Experiments", whereas phase two of the experiments was termed "Fixed Bed Experiments." In the movable bed experiments, the scour hole developed with time, and the readings of the time development of the deepest scour point and final

bathymetry at equilibrium were measured. For fixed bed experiments, velocity and turbulence measurements were taken in the approach and test sections.

3.4.1. *Movable Bed Experiments*

At the start of an experiment, the flume was filled with water at a very slow rate such that the bed material did not move. Once the flume was filled to the desired level, the water flow rate increased gradually at a tail water elevation higher than the required experimental setting, such that scour did not start to develop until the desired discharge was attained. Tail water was then adjusted to the required experimental setting. A scour hole developed at a very fast rate in the beginning, so the time development readings for the initial 12 hours were taken at very short time intervals of 0.16, 0.33, 0.5, 1, 2, 4, 6, 8, 10, and 12 hours, respectively. Subsequently, time development readings were taken at 12-hour time intervals until the equilibrium criterion was achieved. Figure 3-17 shows the time development of the location and magnitude of the deepest scour point for Run 1. The equilibrium criterion was defined as explained in Section 2.42.4 that is, when the rate of change in the scour depth at the deepest scour point in 24 hours was less than 5% of the total scour.

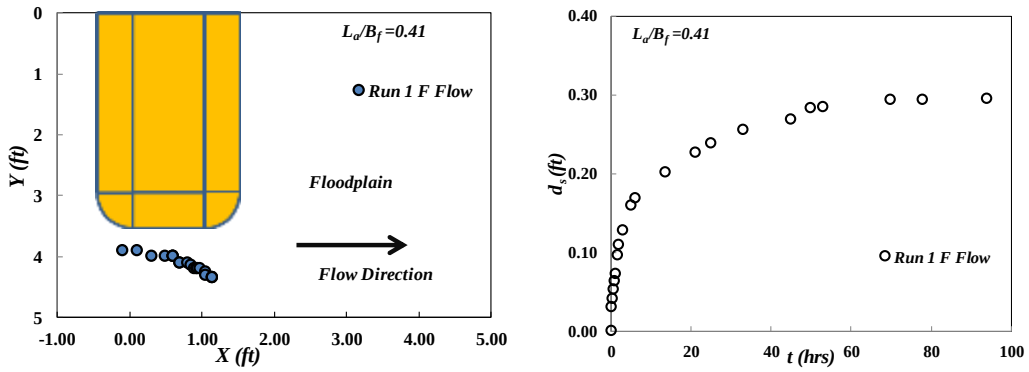

(a) Special variation with time (b) Scour depth with time

Figure 3-17 Time development of deepest scour point (Run 1)

After the equilibrium condition was achieved, the water flow rate was reduced and the tail gate was raised such that any further movement of the bed material stopped, and the bathymetry of the test section was measured with the ADV. For the bathymetry measurements, a fine resolution of 0.1 ft in lateral direction and 0.3 ft in the flow direction was maintained in the bridge section and in deeper scour hole areas. For the farther reaches of the main channel and the floodplain lateral direction, resolution was still kept as 0.1 ft whereas the resolution was increased to 0.5 ft in the flow direction.

In order to assess the uncertainty in the experimental results, some of the experiments were repeated for the bankline abutment case for the spill-through abutments. Experiments for all three types of flows (F, SO, and OT flow) were repeated thrice and the variation in results was less than 10%. This is a reasonably high accuracy owing to the uncertainties involved in the experiments in the form of turbulence characteristics, armoring effects, errors in re-leveling of the flume bed, and experimental and instrumental errors. Table 3-6 shows the comparison of results for the repeated experiments.

Table 3-6 Comparison of results for repeated experiments

BLA	**M/C**			
Run	V_{m1}/V_{mc}	Y_{mo} **(ft)**	Y_{m2max} **(ft)**	Y_{m2max}/Y_{mo}
Free Flow L_a/B_f =1				
4	0.84	0.48	0.81	1.71
6	0.82	0.48	0.85	1.79
8	0.82	0.48	0.79	1.67
SO Flow L_a/B_f =1				
2	0.72	0.55	1.02	1.87
28	0.72	0.55	1.06	1.94
29	0.72	0.55	1.12	2.04
OT Flow L_a/B_f =1				
5	0.82	0.72	1.14	1.59
7	0.82	0.72	1.12	1.56
9	0.82	0.72	1.08	1.50

3.4.2. *Fixed Bed Experiments*

In the second phase of the experimental procedure, with the help of wooden and removable templates, the flume bed was set to the undisturbed bel level. It was then sprayed with five to six successive coats of polyurethane over five days until the bed material became fixed and hard enough to sustain the initial flow condition over long durations without developing any scour, as shown in Figure 3-18. This procedure was implemented to measure velocity and turbulence for the initial experimental conditions in the approach and bridge sections.

Velocity and turbulence readings were taken at the approach section, the bridge downstream end, and the abutment downstream toe, referred to as sections 1, 4, and 5 respectively, as shown in Figure 3-19. Water surface profile readings were also taken with the point gauge in the initial stage of the experiments. In the approach section (C.S. 1), point velocities were measured at multiple vertical profiles at an interval distance of 1

ft in the floodplain (at a distance of 0.5 ft near the wall) and at a distance of 0.4 ft in the main channel. In the floodplain, 8-10 point velocities were measured in each vertical profile and 13-15 point velocities were measured in the main channel for each vertical profile. In the bridge section (C.S. 4), point velocities were measured every 0.5 ft and 0.3 ft for the floodplain and the main channel, respectively. Time averaged point velocities were integrated over the depth and then over the entire cross section to obtain the width-averaged discharge values (q_2/q_1) in the approach section (C.S. 1) and bridge downstream section (C.S. 4) for floodplain and main channel. Turbulence measurements for the near-bed region were measured at the bridge downstream section (C.S. 4) and downstream toe of the abutment (C.S. 5). For some of the experiments (without piers) turbulence measurements at the downstream toe of the abutment (C.S. 5) were also measured at 20% and 40% of the water depth.

Figure 3-18 Fixing of the flume bed

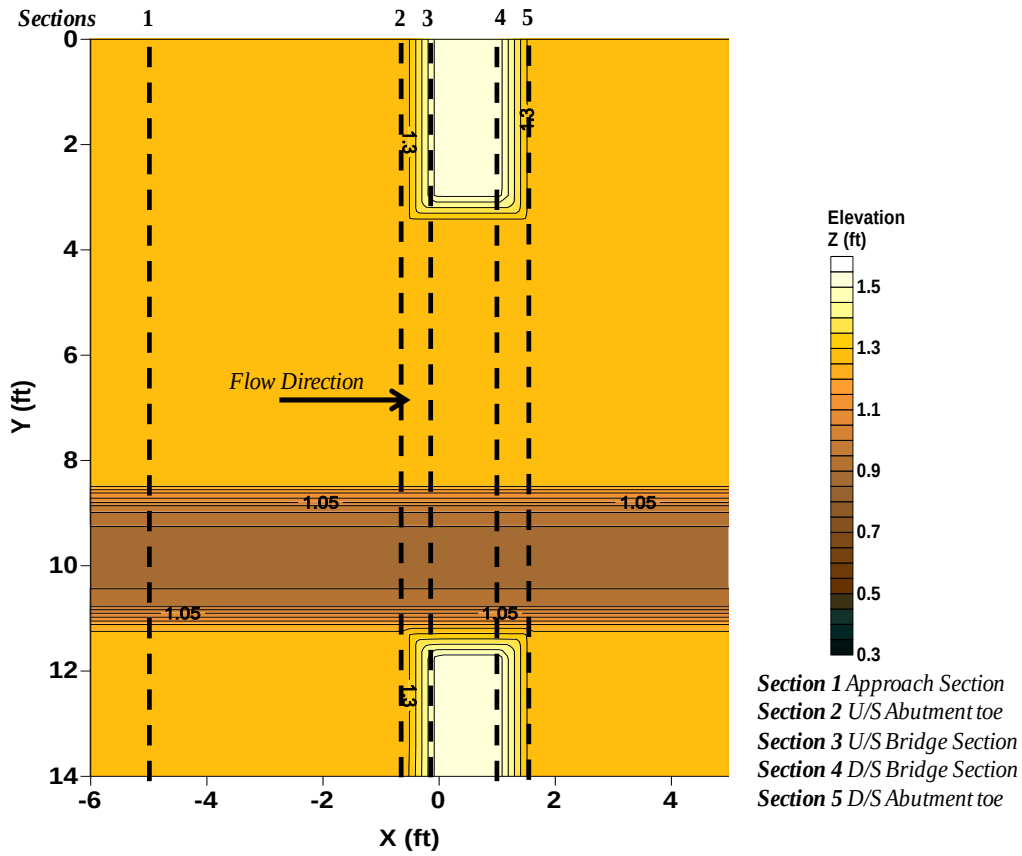

Figure 3-19 Schematic diagram for turbulence measurements

3.4.2.1. *Velocity and Turbulence Measurements*

Mean velocity profile is affected by the presence of the wall; however, out of the "near-wall region", the time averaged velocity profile follows the relationship given in Equation 3.2 for a steady flow in an open channel both for smooth and rough boundaries (Ligrani and Moffat 1986, Krogstadt and Antonia 1999, Rahman and Webster 2005).

$$\frac{U(z)}{u_*} = \frac{1}{k}\ln\left(\frac{zu_*}{\nu}\right) + A - \Delta U^+ + \frac{2\Pi}{\kappa}\omega\left(\frac{z}{\delta}\right) \qquad (3\text{-}2)$$

where $U(z)$ = time average point velocity, u^* = shear velocity k = Von Karman constant having a value of 0.41, A = constant with a value of 5, U^+ = roughness function, Π =

Coles wake parameter, and ω = wake function. For near-bed measurements, the viscous length scale is replaced by grain size roughness k_s and for the near-surface measurements the wake correction is neglected. The equation thus transforms to:

$$\frac{U(z)}{u_*} = \frac{1}{k}\ln\left(\frac{z}{k_s}\right) + C \qquad (3\text{-}3)$$

where k_s is the equivalent grain roughness and the value of C varies with flow regime from smooth to fully rough flow depending on k_s^+ (where $k_s^+ = k_s\, u_*/\nu$). For the fully rough flow ($k_s^+ > 70$) value of C is 8.5, and for the smooth region ($k_s^+ < 5$) the value of C is (Hermann 1979).

$$C = \frac{1}{k}\ln\left(k_s^+\right) + A \qquad (3\text{-}4)$$

The definition of the relationship for the transition regime ($5 < k_s^+ < 70$) is given by (Ligrani and Moffat 1986):

$$C = \frac{1}{k}\ln\left(k_s^+\right) + A + \left[8.5 - A - \frac{1}{k}\ln\left(k_s^+\right)\right]\sin\left(\frac{\pi}{2}g\right)$$
$$where \quad g = \frac{\ln\left(k_s^+/5\right)}{\ln(70/5)} \quad for \quad 5 < k_s^+ < 70 \qquad (3\text{-}5)$$

Putting the value of $g = 1$ for $k_s^+ > 70$ in Equation 3.5 returns the value of C = 8.5 and for smooth regime $k_s^+ < 5$ returns equation 3.4 as defined by (Hermann 1979). It was suggested in the experiments in a uniform open channel for a smooth bed that the log-law can be followed up to 60% of the depth (Nezu and Rodi 1986). The value of shear velocity (u_*) in Equation 3.3 was calculated using the best-fit logarithmic velocity profile in the log layer for which the velocity measurements up to 60% of the depth from the bed

were used. Time-averaged point velocities in the log layer at the normal scale were plotted against the depth (z) on the log scale and a best-fit line was drawn by the method of least squares. The value of the shear velocity was then calculated by using the product of the slope of the best fit line and κ =0.41. An example is shown in Figure 3-20 (L_a/B_f = 0.41, Q = 3 cfs, Free Flow Case, Run 1).

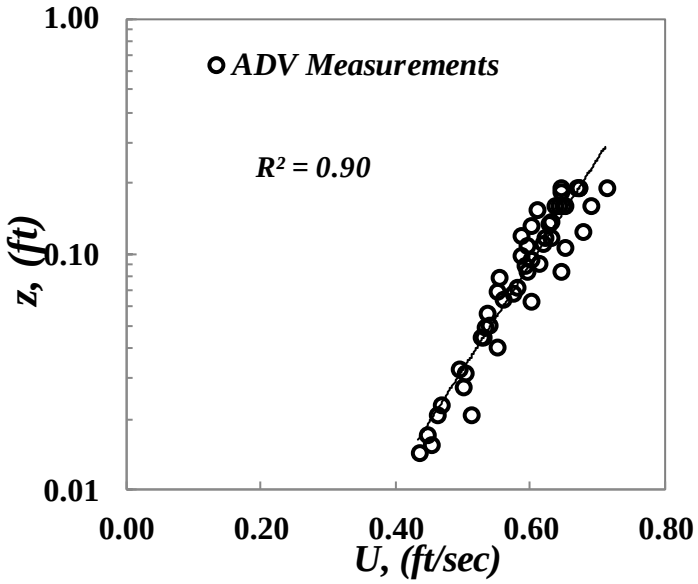

Figure 3-20 Best fit line for velocity distribution over the depth (Left floodplain Run 1, u_* = 0.042 ft/sec)

Value of the shear velocity obtained was used to calculate the equivalent roughness height by use of Equation 3.3 and Equation 3.5 by trial and error. The measured vertical velocity profile showed good agreement with Equation 3.3 as shown in Figure 3-21

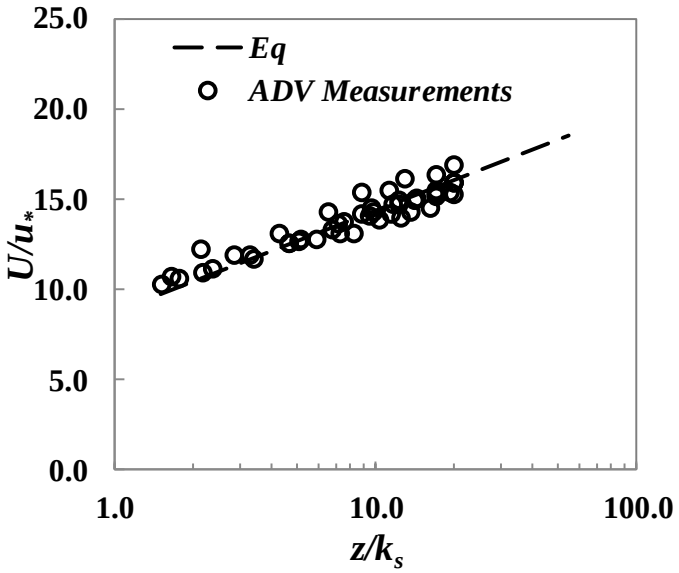

Figure 3-21 Vertical velocity profile comparison with Equation 3.3 (Run 1, u_* = 0.042 ft/s, k_s/d_{50} = 2.63 and C = 8.80)

The procedure for obtaining the value of shear velocity u_* and k_s/d_{50} was repeated for all the experiments conducted without the piers as the experiments with the piers were the repetition of the same experimental conditions with addition of pier, which does not affect the approach flow condition. A summary of the values of shear velocity u_*, k_s/d_{50}, and constant C obtained for the left floodplain, main channel and right floodplain is presented in Table 3-7. Critical velocities were calculated from the Keulegan's equation, which requires a vale of k_s/d_{50}. The value of k_s/d_{50} has been consistent for all the experiments with minor variation, which can be attributed to experimental uncertainty and instrumental error. Average values of k_s/d_{50} based on the experimental results shown in Table 3-7 were used as 2.65, 2.82, and 2.00 for left floodplain, main channel, and right floodplain, respectively, for calculation of critical velocity in Keulegan's equation.

Table 3-7 Summary of flow characteristics in approach flow

Run	Left F/P			M/C			Right F/P		
	k_s/d_{50}	u* (ft/s)	C	k_s/d_{50}	u* (ft/s)	C	k_s/d_{50}	u* (ft/s)	C
1	2.630	0.042	8.800	2.898	0.054	8.550	1.910	0.042	9.080
2	2.601	0.046	8.730	2.895	0.056	8.536	2.002	0.048	8.943
3	2.696	0.041	8.816	2.814	0.049	8.624	1.975	0.041	9.110
4	2.649	0.056	8.579	2.836	0.066	8.502	2.042	0.055	8.790
5	2.639	0.054	8.602	2.891	0.062	8.506	2.016	0.055	8.802
10	2.822	0.044	8.702	2.964	0.058	8.515	2.103	0.048	8.893
11	2.544	0.045	8.782	2.943	0.054	8.544	1.938	0.044	9.070
12	2.681	0.050	8.650	2.956	0.060	8.511	2.134	0.050	8.838
18	2.535	0.048	8.719	2.890	0.055	8.545	2.043	0.048	8.922
19	2.631	0.046	8.772	2.897	0.062	8.506	1.930	0.052	8.908
32	2.450	0.070	8.520	2.789	0.079	8.500	2.037	0.072	8.585
33	2.658	0.078	8.500	2.806	0.082	8.500	2.279	0.074	8.522

3.4.2.2. *Pier Approach Velocity*

Hydraulic Engineering Circular-18 defines that the pier approach velocity should be measured directly upstream of the pier. However no specific criterion has been mentioned for the location and distance of the point of measurement (Arneson et al. 2012). HEC-RAS uses the option of maximum velocity in the cross section outside and just upstream of the bridge. The maximum velocity is used as the pier approach velocity for all the piers (Brunner 2001). For this study, pier approach velocity measurements (depth-averaged velocity) were taken directly upstream of the pier at different points ranging from two pier-widths upstream of the edge of the upstream pier to ten pier-widths upstream of the edge of the upstream pier for all three types of flow (F, SO, and OT flow cases). The procedure was repeated for two abutment ratios, L_a/B_f = 0.41 and 0.77, and location of the maximum velocity was found four pier-widths upstream of the edge of the upstream pier as shown in Figure 3-22.

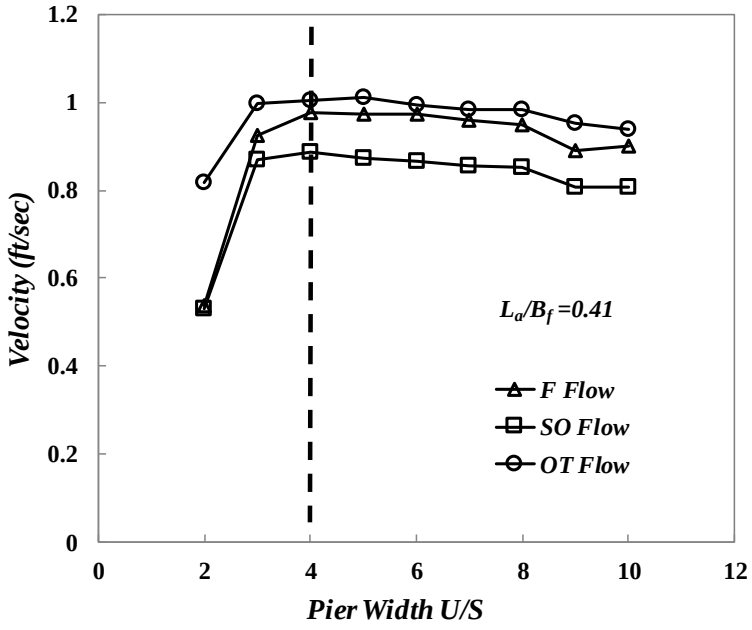

(a) Pier Approach Velocity for L_a/B_f = 0.41

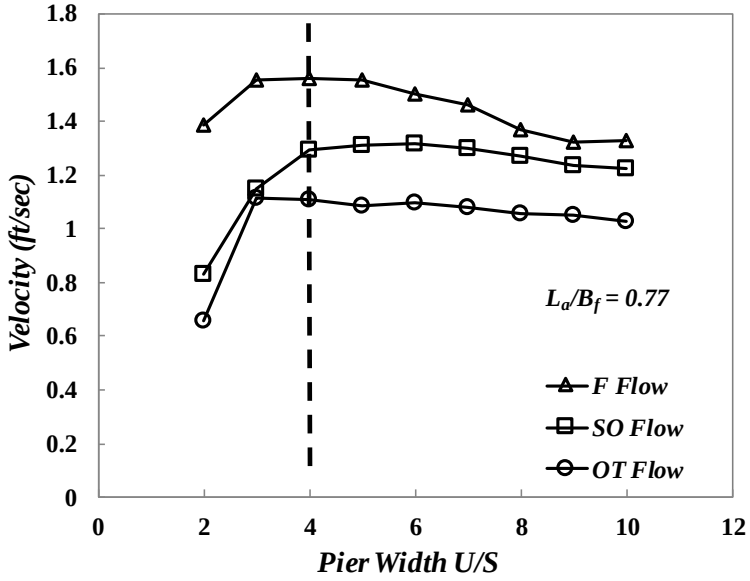

(b) Pier Approach Velocity for L_a/B_f = 0.77

Figure 3-22 Pier approach velocity measurements directly upstream of the pier for L_a/B_f = 0.41 and 0.77

CHAPTER IV

ANALYSIS OF ABUTMENT AND CONTRACTION SCOUR INTERACTION

4.1. Introduction

Abutment and contraction scour interaction for all three types of flows (F, SO, and OT flow) is analyzed and presented in this chapter. This covers LSA and SSA/BLA scour interaction with contraction scour, namely Category I and Category II types of scour interaction (as mentioned in Table 3.5). Experiments conducted at the Georgia Institute of Technology for a model scale ratio of 1:45 (this also includes the experiments conducted by Hong (2013)), experiments conducted at the University of Auckland (Xiong 2017) for a model scale ratio 1:30, and experiments conducted for NCHRP 24-20 (Ettema et al. 2010) have been used for the analysis. Criteria for the classification of abutment length as long and short setback abutment are covered in the subsequent chapters; however, the short setback abutment is defined as the length of the abutment for which the major portion of the scour hole remains in the main channel in addition to the floodplain and the deepest point of the scour hole is located in the main channel.

Hong (2013) developed the hypothesis that interactive abutment and contraction scour for free flow cases (F flow) can be combined with the cases

involving vertical contraction scour (SO and OT flows). Therefore, experiments for the free flow condition have been considered in the same category with the experiments involving vertical contraction scour.

4.2. Qualitative Observations

Scour is a function of geometric/flow contraction ratio, relative backwater depth ratio (Y_1/Y_o), initial flow intensity in the contracted section (where the depth average velocity is higher than the critical velocity), and turbulent kinetic energy (TKE) for the near-bed measurements which will be referred to as bottom TKE (K_b). For a higher magnitude of scour parameters, both the extent and depth of scour hole increase which also governs the location of the point of deepest scour.

A scour hole develops near the toe of the abutment and expands both in flow and transverse directions. A flow separation zone develops along the abutment, which starts from the upstream edge of the abutment and expands in the transverse direction as it moves downstream of the bridge contraction. This flow separation zone merges with the recirculation region in the downstream direction. The pictorial representation of flow separation zone and recirculation region is presented in Figure 4-1.

Velocity in the flow separation zone is small (a stagnant or fluctuating zone) compared to the highest values within the same cross-section. In the transverse direction moving away from the abutment face, this flow separation region adjoins a high velocity region developed by the flow convergence in the contracted section. Velocity in the contracted section is highest at the junction between the flow separation region and the contracted high velocity flow. The value of bottom TKE

(K_b) is also at the highest value at this point (within the same cross-section) due to the shear between the two flow regions. As the flow moves in the downstream direction, the flow separation zone expands; thus, the highest bottom TKE (K_b) value tends to move away from the abutment. The normalized bottom TKE value (K_b/u_{*c}^2) is highest in the cross section at the toe of the abutment for all flow types and abutment ratios. This observation is consistent with Hong (2013).

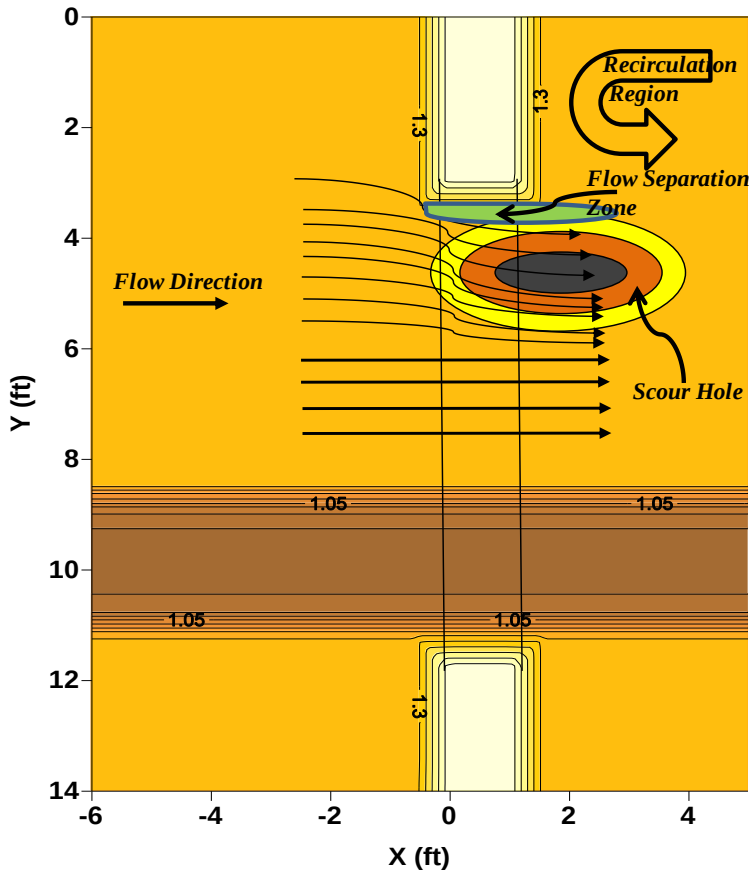

Figure 4-1 Definition sketch explaining the flow separation zone and recirculation region

The deepest scour point in the lateral direction is either aligned with the same point of highest bottom TKE (K_b) and highest velocity, or in some cases even further away from the abutment. The reason for the deepest scour point to occur further away

from the point of highest bottom TKE (K_b) and highest velocity is the riprap apron, which collapses as the scour hole develops and provides the bed armoring effect in the area near the toe of the abutment. This leaves the region closer to the abutment experiencing less scour as compared to the adjacent region further away from the abutment in the transverse direction. However, in the flow direction the point of deepest scour continues to move in the downstream direction with increase in the scour depth, which is dependent on the flow contraction ratio (q_2/q_1), backwater depth ratio (Y_1/Y_o), and approach flow intensity (V_1/V_c). The phenomenon of elevated velocity and bottom TKE (K_b) in the vicinity of the scour hole holds good for all three type of abutments to include LSA, SSA and BLA, and all three types of flows including free (F) submerged-orifice (SO) and overtopping (OT) flow cases. Figure 4-2 presents the graphical representation of the phenomenon for L_a/B_f=0.41 and 0.77.

Flow rate per unit width in the contracted section at the downstream end of the bridge normalized by the average approach flow rate per unit width ($q_2/q_{1(avg)}$) changes with approach flow intensity (V_1/V_c) and setback distance of the abutment, both for the main channel and the floodplain. Thus, for lower approach flow intensity (V_1/V_c) and higher setback distance for the abutment, the value of normalized flow contraction ratio ($q_2/q_{1(avg)}$) is less in the floodplain. As the approach flow intensity (V_1/V_c) increases, the normalized flow contraction ($q_2/q_{1(avg)}$) is observed to increase more rapidly in the floodplain than in the main channel (compare Figure 4-2 (a) with (d) and (c) with (e)).

For short setback abutments, the floodplain flow faces a larger degree of contraction and also tends to interact with the main channel flow which results in

higher flow rates both in the floodplain and in the main channel. Comparable increases occur in normalized flow contraction ratio ($q_2/q_{1(avg)}$) both in the floodplain and the main channel. In other words, for shorter setback abutments, the floodplain and main channel flow interaction is significant. The equilibrium scour depths for the floodplains and the main channel were observed to be comparable for the short setback abutments. Figure 4-2 graphically represents the phenomena explained above both for longer and shorter setback distances of the abutments and for different approach flow intensities in all three flow types (F, SO, and OT flows). The figure includes initial bridge section geometry at the downstream end of the bridge, equilibrium scour at the downstream toe of the abutment, bottom TKE (K_b) normalized by the critical shear velocity (K_b/u_{*c}^2) both for downstream end of the bridge and downstream toe of the abutment, and normalized flow contraction ratio ($q_2/q_{1(avg)}$) both for the floodplain and the main channel.

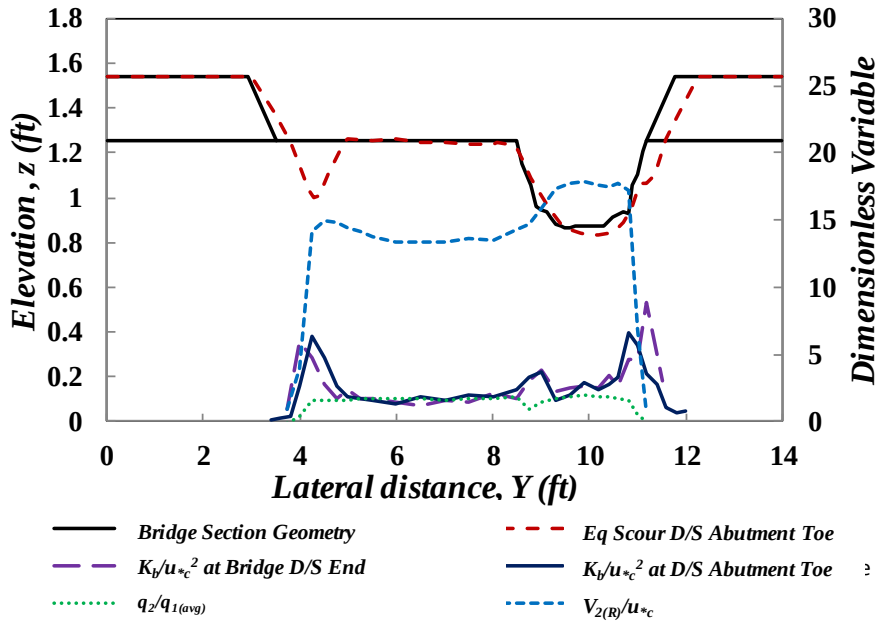

(a) Run 1, Free flow L_a/B_f = 0.41, V_{f1}/V_{fc} =0.542, V_{m1}/V_{mc} =0.723

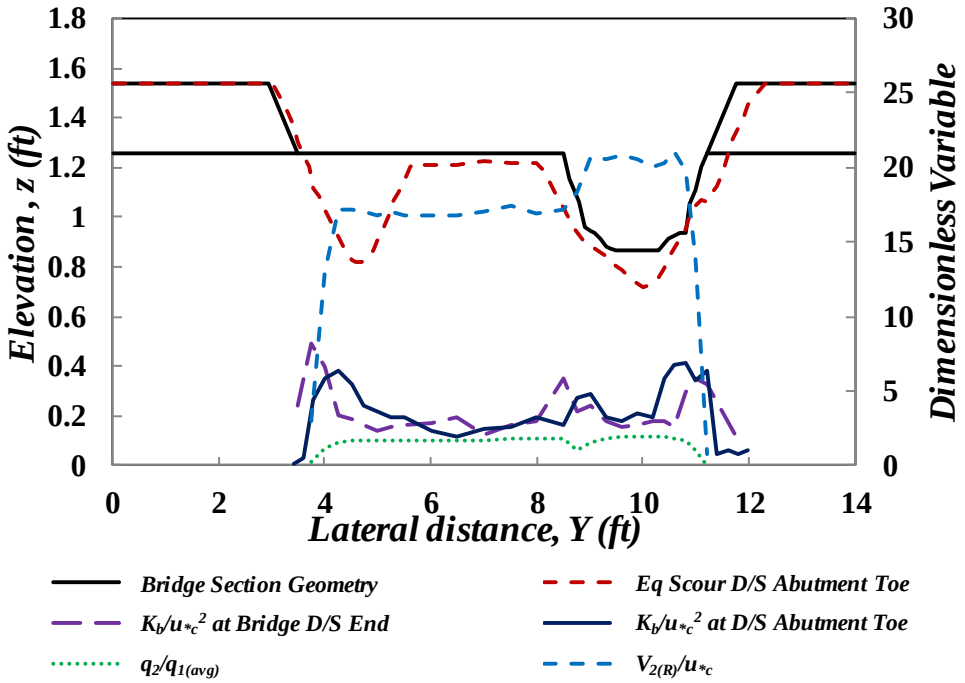

(b) Run 2, SO Flow L_a/B_f = 0.41, V_{f1}/V_{fc} =0.589, V_{m1}/V_{mc} =0.725

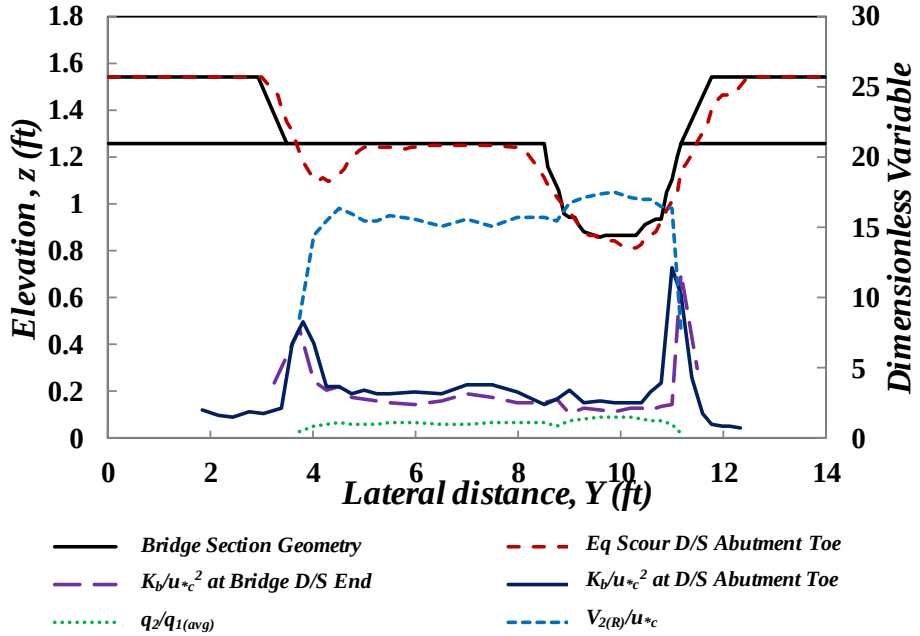

(c) Run 3, OT Flow L_a/B_f = 0.41, V_{f1}/V_{fc} =0.561, V_{m1}/V_{mc} =0.653

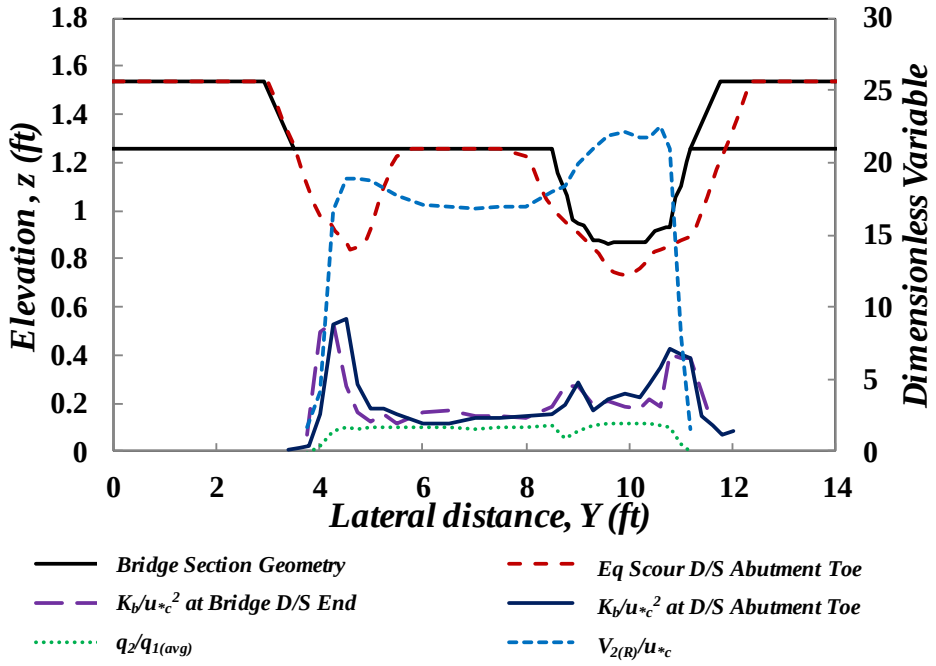

(d) Run 4, Free Flow L_a/B_f = 0.41, V_{f1}/V_{fc} =0.655, V_{m1}/V_{mc} =0.841

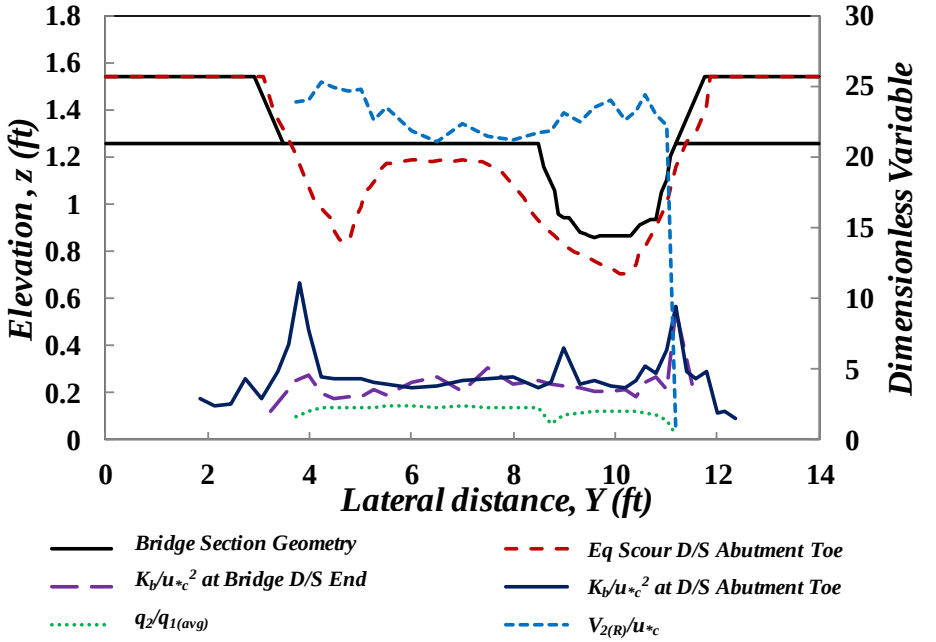

(e) Run 5, OT Flow L_a/B_f = 0.41, V_{f1}/V_{fc} =0.683, V_{m1}/V_{mc} =0.823

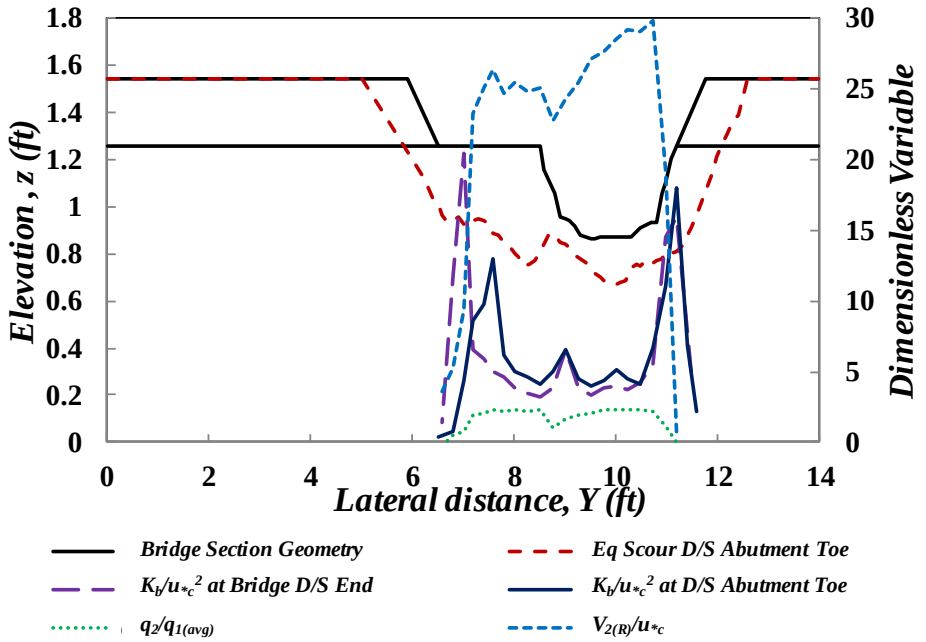

(f) Run 10, Free Flow L_a/B_f = 0.77, V_{f1}/V_{fc} =0.659, V_{m1}/V_{mc} =0.879

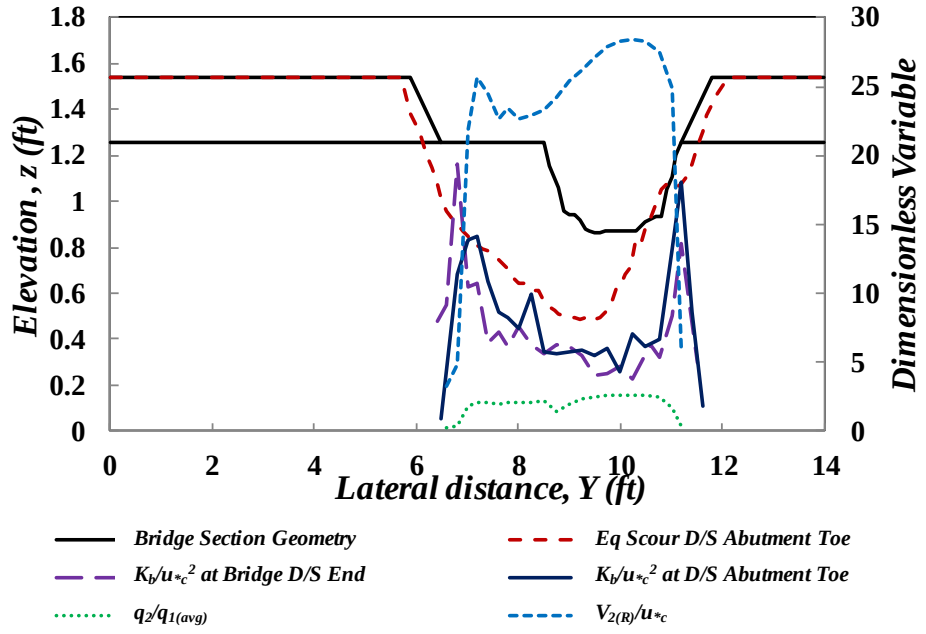

(g) Run 11, SO Flow L_a/B_f = 0.77, V_{f1}/V_{fc} =0.579, V_{m1}/V_{mc} =0.711

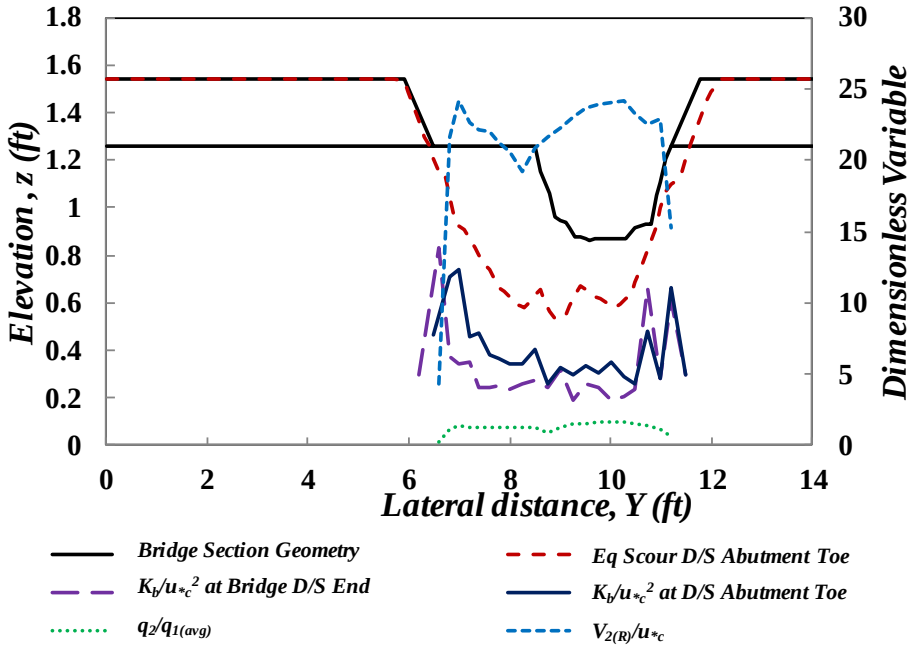

(h) Run 12, OT Flow L_a/B_f = 0.77, V_{f1}/V_{fc} =0.623, V_{m1}/V_{mc} =0.784

Figure 4-2 Dimensionless variables for L_a/B_f = 0.41 and 0.77, bottom TKE (K_b) normalized by the critical shear velocity (K_b/u_{*c}^2) for downstream end of the bridge and downstream toe of the abutment, normalized flow contraction ($q_2/q_{1(avg)}$) for the floodplain and the main channel, initial bridge section geometry at the downstream end of the bridge, and Equilibrium scour at the downstream toe of the abutment.

At the interface of the floodplain and main channel, the velocity reduces because of the flow interaction between floodplain and main channel, which generates turbulent eddies resulting in higher bottom TKE (K_b) values. This phenomenon occurs regardless of the scour parameters as shown in Figure 4-2. The higher bottom TKE (K_b) value may result in failure of the main channel bank.

4.2.1. *Velocity Profiles*

Approach section and contracted section (downstream face of the bridge) velocities were measured as point velocities in different vertical profiles. Point velocities were then integrated vertically over the entire depth of flow (for the

contracted section, OT flow cases' velocities were measured for the flow passing under the bridge only and integrated for the water depth under the bridge) and then divided by the flow depth to calculate the depth-averaged velocity. Although the approach flow velocity follows the logarithmic curve for the vertical profile, the measurements were taken over the entire depth and integrated to obtain a more accurate result rather than applying the approximation of a best-fit curve.

In a compound channel, the velocity distribution is different form a simple rectangular channel where interaction between the floodplain and the main channel flow affects the flow distribution. A shallow depth in the floodplain results in a higher velocity difference between the floodplain and the main channel, which decreases with increase in the relative flow depth (Y_{f1}/Y_{m1}). Figure 4-3 shows that the approach flow section velocity difference is higher between the floodplain and the main channel for a free flow case (which has relatively shallow depth in floodplain resulting in smaller value of Y_{f1}/Y_{m1}). As the relative flow depth (Y_{f1}/Y_{m1}) increases, for SO and OT flow case, the velocity in the floodplain increases more rapidly than in the main channel; thus, differences between the floodplain and the main channel velocity decrease resulting in higher values of the relative velocity (V_{f1}/V_{m1}). For a contracted section, the measurements have been taken for the flow passing under the bridge only (which does not account for the weir flow passing over the bridge in OT flow cases). The phenomenon still follows the same principle as in the approach section, but the relative velocity (V_{f1}/V_{m1}) for an OT flow case shows a higher difference, especially for the longer abutment length ($L_a/B_f = 0.77$) as shown in Figure 4-3. This difference is subject to other contributing factors including the increase in the tail water, increase in

the flow rate, flow interaction and redistribution between the floodplain and the main channel in case of L_a/B_f = 0.77. In contrast, for L_a/B_f = 0.41, flow relief available to OT flow cases in comparison to SO flow cases (where all the flow passes under the bridge), results in sharp converging flow producing a wider flow separation zone in SO flow cases as compared to OT flow cases. There is also a difference in contribution of the right-floodplain flow to the main channel between F/SO and OT flow cases. The bankline abutment causes convergence of the complete right floodplain flow in to the main channel for the F/SO flow cases, but some of this flow passes over the bridge in OT flow cases. Distribution of the discharge per unit width over the entire cross section for the approach flow and test section (downstream end of the bridge) shows a better representation of the effect of change in the relative flow depth (Y_{f1}/Y_{m1}) for LSA, SSA, and BLA as shown in Figure 4-4.

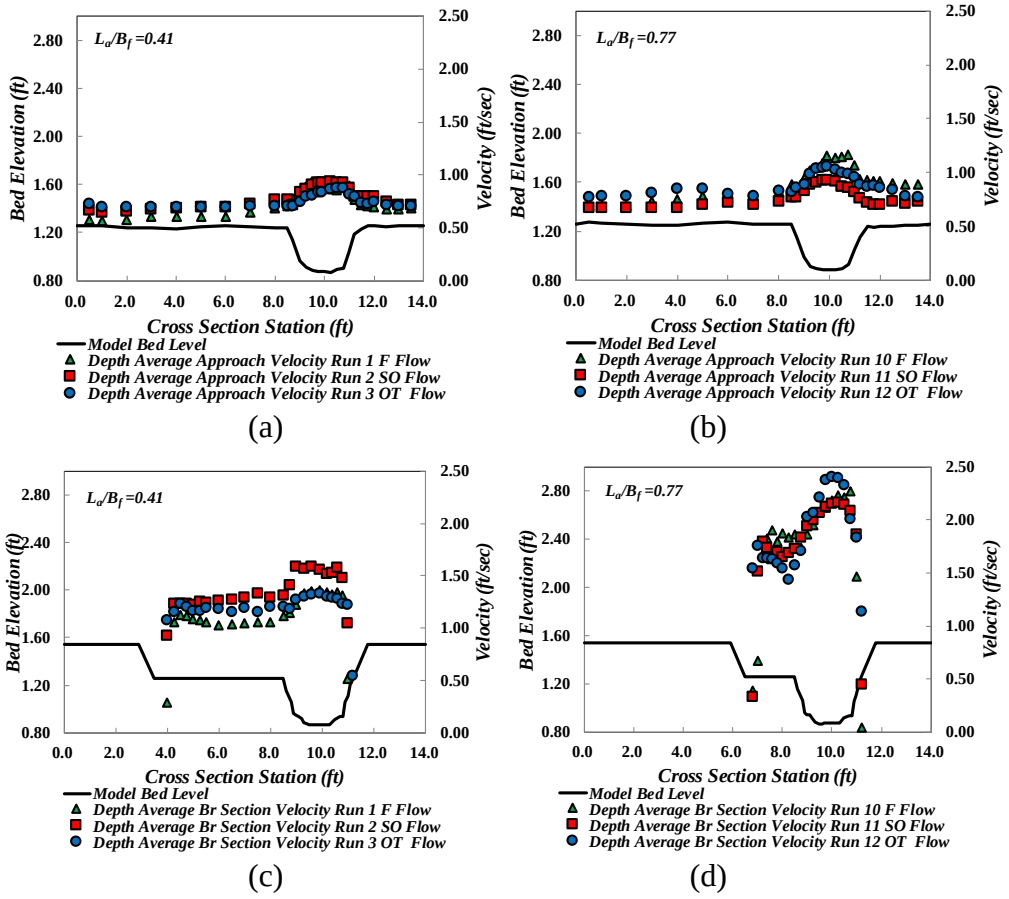

Figure 4-3 Depth averaged flow velocity for free submerged orifice and overtopping flow for L_a/B_f = 0.41 and 0.77, (a) Approach flow velocity for Run 1, 2, and 3 with L_a/B_f = 0.41, (b) Approach flow velocity for Run 10, 11, and 12 with L_a/B_f = 0.77, (c) Contracted section velocity for Run 1, 2, and 3 with L_a/B_f = 0.41, and (d) Contracted section velocity for Run 10, 11, and 12 with L_a/B_f = 0.77

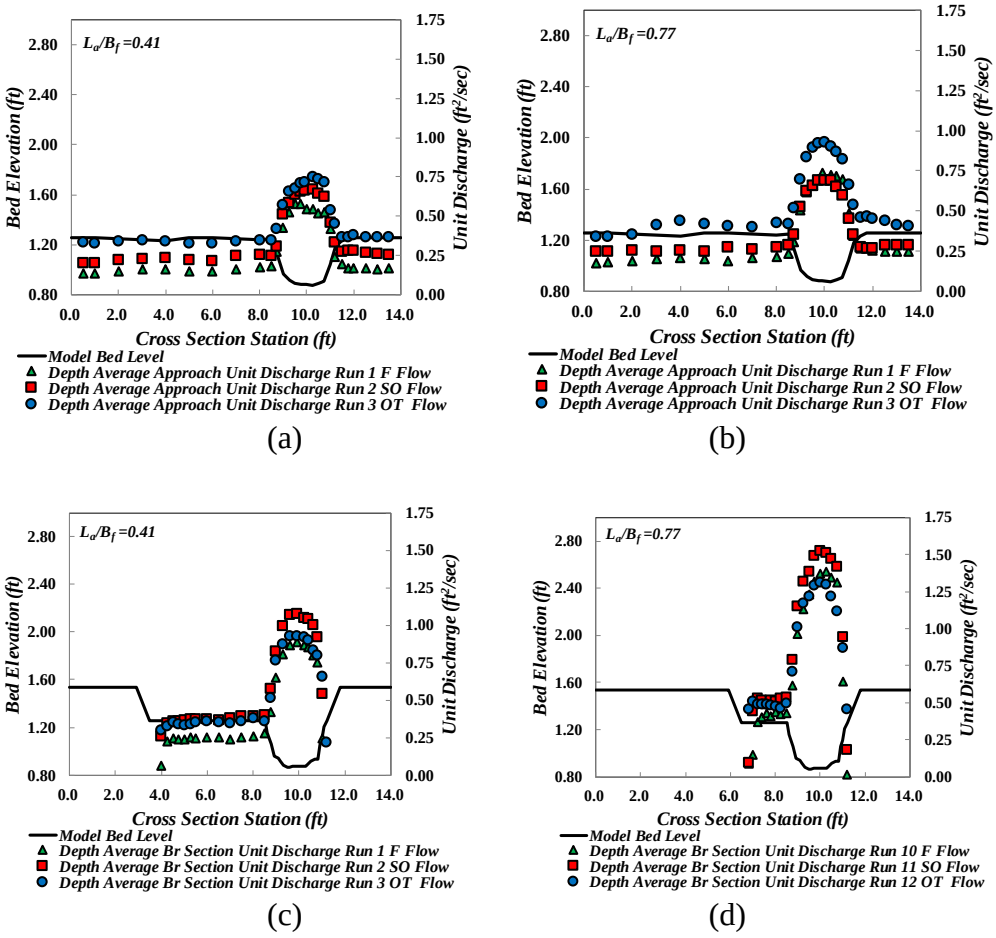

Figure 4-4 Depth averaged flow rate per unit width for free submerged orifice and overtopping flow for L_a/B_f = 0.41 and 0.77, (a) Approach flow rate per unit width for Run 1, 2, and 3 with L_a/B_f = 0.41, (b) Approach flow rate per unit width for Run 10, 11, and 12 with L_a/B_f = 0.77, (c) Contracted section flow rate per unit width for Run 1, 2, and 3 with L_a/B_f = 0.41, and (d) Contracted section flow rate per unit width for Run 10, 11, and 12 with L_a/B_f = 0.77

The increase in relative velocity (V_{f1}/V_{m1}) between floodplain and the main channel with increase in relative flow depth (Y_{f1}/Y_{m1}) specifies that relatively larger flow is accommodated in the floodplain than in the main channel as the relative flow depth (Y_{f1}/Y_{m1}) increases. This postulates an increasing trend of relative unit discharge (q_{f1}/q_{m1}) with increase in relative flow depth (Y_{f1}/Y_{m1}). Theoretically, as the relative flow depth (Y_{f1}/Y_{m1}) approaches unity, the relative unit discharge (q_{f1}/q_{m1}) should also

approach unity. This theoretical agreement transforms the compound channel into a simple rectangular channel at the limit of very large depths. Figure 4-5 shows the relationship between relative unit discharge (q_{f1}/q_{m1}) with relative flow depth (Y_{f1}/Y_{m1}) which includes results for the current research and experiments conducted by Hong (2013) and Sturm (2004).

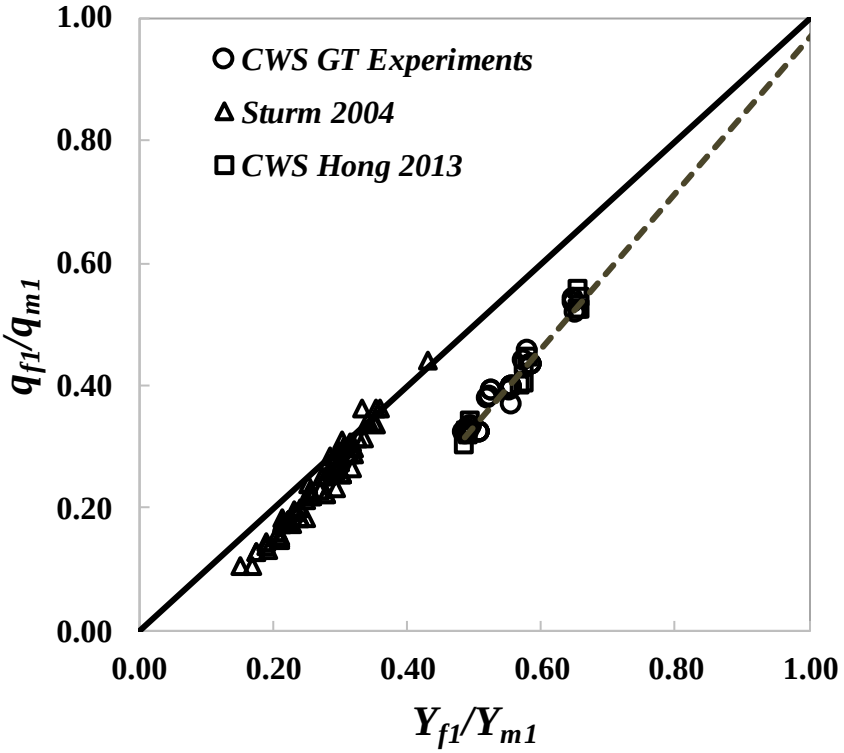

Figure 4-5 Relationship of relative discharge per unit width (q_{f1}/q_{m1}) and relative flow depth (Y_{f1}/Y_{m1}) in the main channel and in the floodplain

4.2.2. *Water Surface Profiles*

Water surface profiles were measured at multiple locations in the floodplain and in the main channel ranging from near the abutment to away from the abutment in the floodplain in case of long-setback and short-setback abutments and in the main channel for bankline abutments. Range of the water surface profile covered the

distance from the approach section in the upstream direction to the test section and further downstream in the tailwater section of the flume. Total range of the distance was 15 ft upstream and 20 ft downstream of the bridge section.

Water surface profiles show the head loss and the backwater effect (Y_1/Y_o) in the bridge contraction as shown in Figure 4-6 (water surface profiles are for the centerline of the main channel, i.e. 10 ft away from the edge of the left floodplain, looking in downstream direction). The backwater effect in the floodplain is more significant than in the main channel for the obvious reason of higher relative flow depth of the main channel as compared to the floodplain. The range of the backwater effect in the floodplain is $1.03 < Y_1/Y_o < 1.36$ and for main channel is $1.02 < Y_1/Y_o < 1.18$.

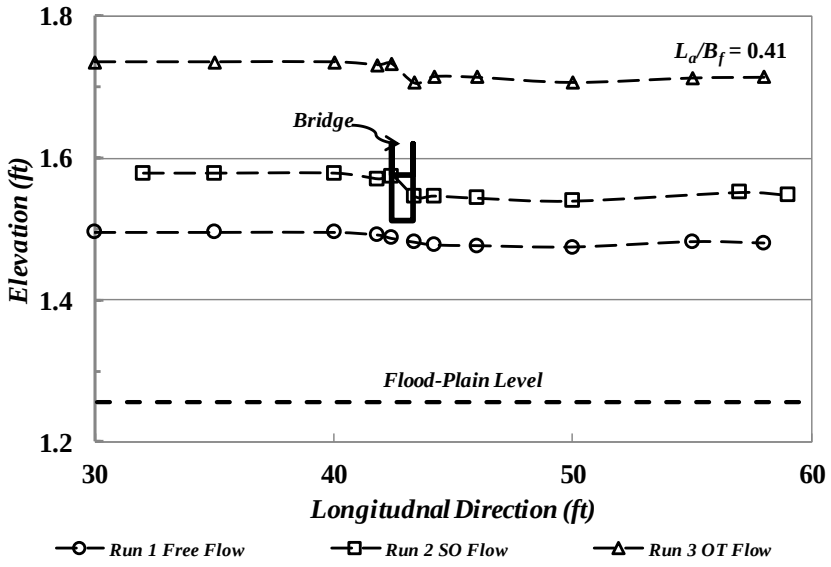

(a) Water surface profiles for Run 1, 2, and 3 with L_a/B_f = 0.41

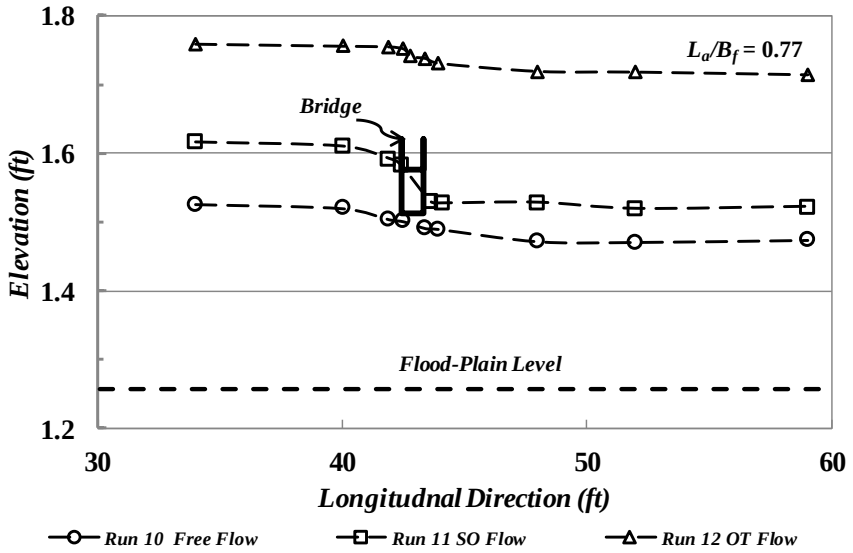

(b) Water surface profiles for Run 10, 11, and 12 with L_a/B_f = 0.77

Figure 4-6 Water surface profiles for centerline of the main channel for Free, SO, and OT Flows for L_a/B_f = 0.41 and 0.77

4.2.3. *Turbulent Kinetic Energy (TKE) and Velocity Measurements*

Velocity and velocity fluctuation measurements were taken for all the experiments at the downstream face of the bridge (Section 4) and downstream toe of the abutment (Section 5). For a few experiments, the velocity measurements were also taken at the upstream end of the bridge (Section 3). The approach section was long enough for the flow to fully develop; therefore, a relatively smooth water surface was observed in the approach section. As the flow passed through the bridge contraction, a non-uniform flow surface was observed near the bridge in the downstream direction.

At the upstream edge of the bridge, a relatively smooth flow was observed with flow converging into the bridge contraction. As the flow passed through the bridge section, a complex flow developed due to a flow separation zone and high velocity region adjacent to the flow separation zone (as explained in Figure 4-1). This

phenomenon produces flow with higher velocity fluctuations and higher velocities as compared to the upstream end of the bridge, as the flow is more contracted in comparison to the upstream end of the bridge due to expansion of the flow separation zone, both for the floodplain and the main channel. Flow contraction effects through the bridge are presented in Figure 4-7, Figure 4-8, and Figure 4-9 which show the time-averaged velocity vectors containing the transverse (v) and vertical (w) component of the velocity (i.e. $sqrt(<v^2>+<w^2>)$). These velocity components are plotted at the bridge upstream end, bridge downstream end and downstream toe of the abutment for Runs 1, 2, and 3, respectively, both for the floodplain and the main channel. Figure 4-10 shows the velocity vectors for Runs 11, 12, and 13 at the downstream end of the bridge. As the flow moves further downstream of the bridge at the toe of the abutment, the flow starts to interact with the recirculation region, which can be observed for the cross sections at the downstream toe of the abutment.

As compared to the free flow case (Run 1) an additional vertical contraction of the flow can also be observed in Run 2 (SO Flow) and Run 3 (OT Flow) at the upstream edge of the bridge where a downward velocity vector shows the vertical flow contraction. As the flow passes though the bridge and exits at the downstream end of the bridge, an upward velocity component is also prominent both for SO and OT flow cases.

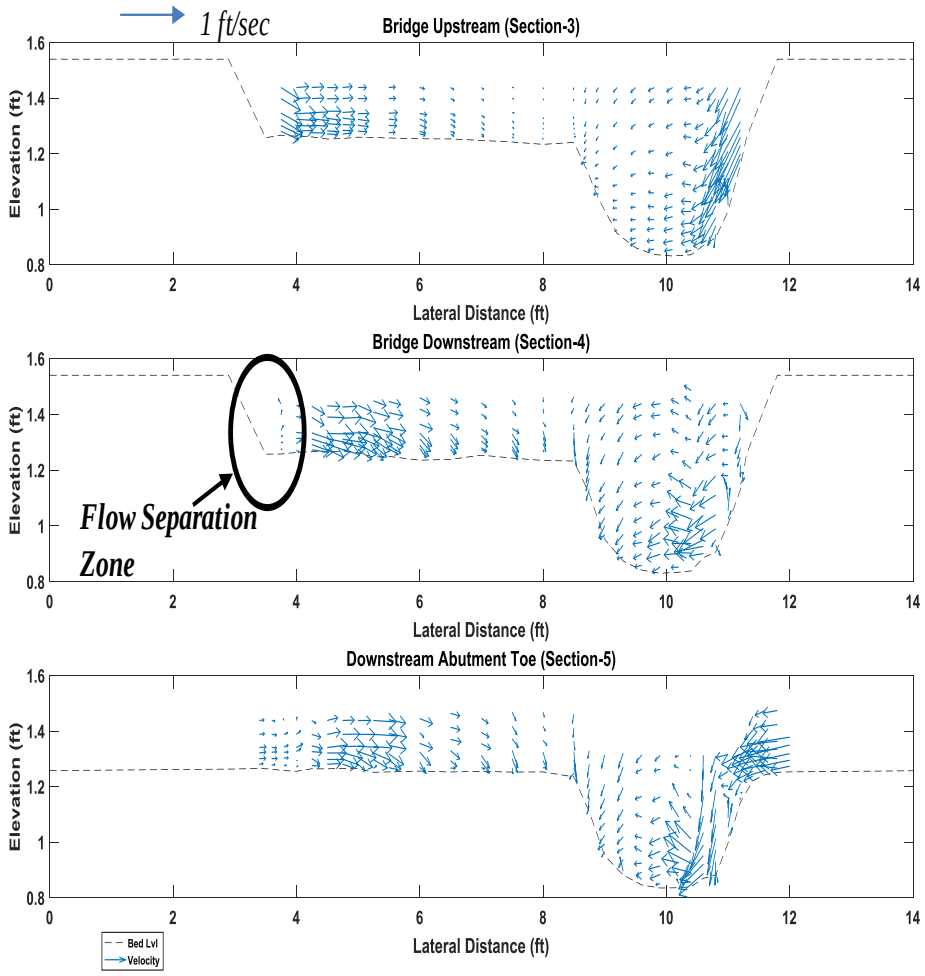

Figure 4-7 Velocity vectors containing the transverse (v) and vertical (w) components of the velocity at the bridge upstream end, bridge downstream end, and downstream toe of the abutment for Run 1 (Free Flow case)

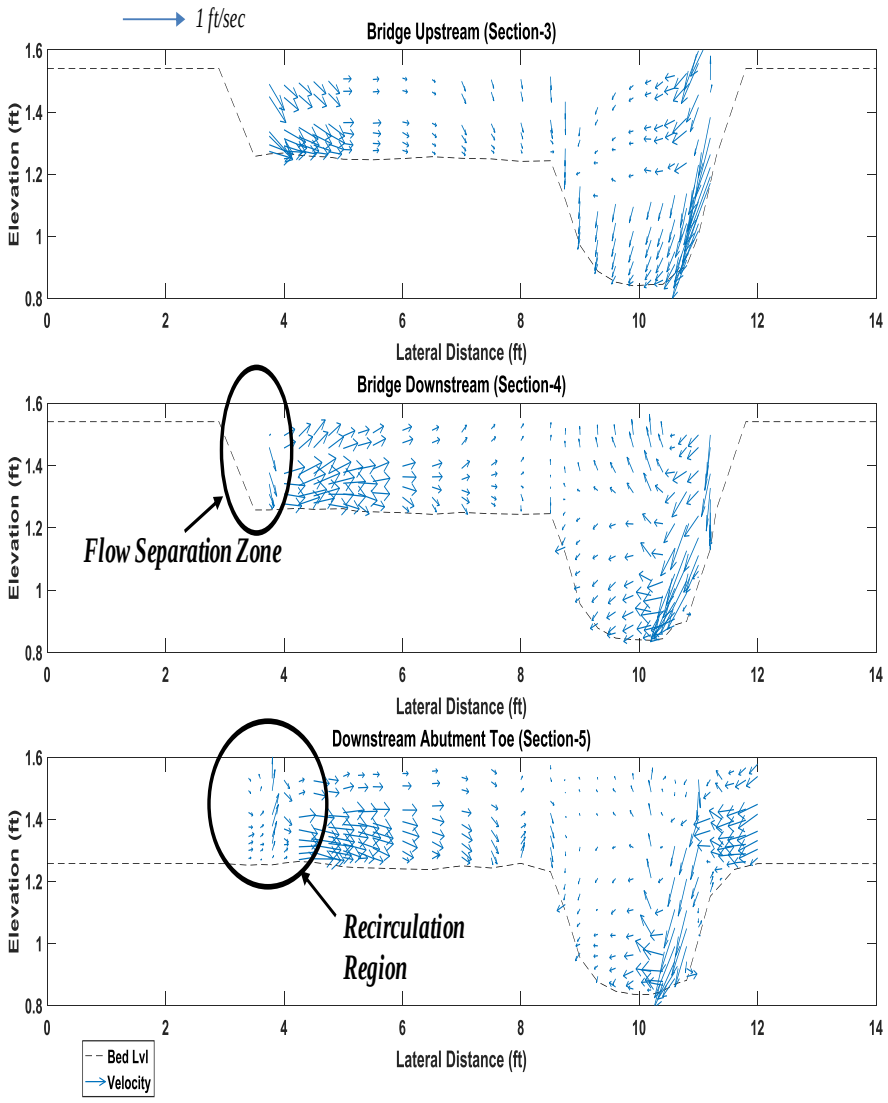

Figure 4-8 Velocity vectors containing the transverse (*v*) and vertical (*w*) components of the velocity at the bridge upstream end, bridge downstream end, and downstream toe of the abutment for Run 2 (SO Flow case)

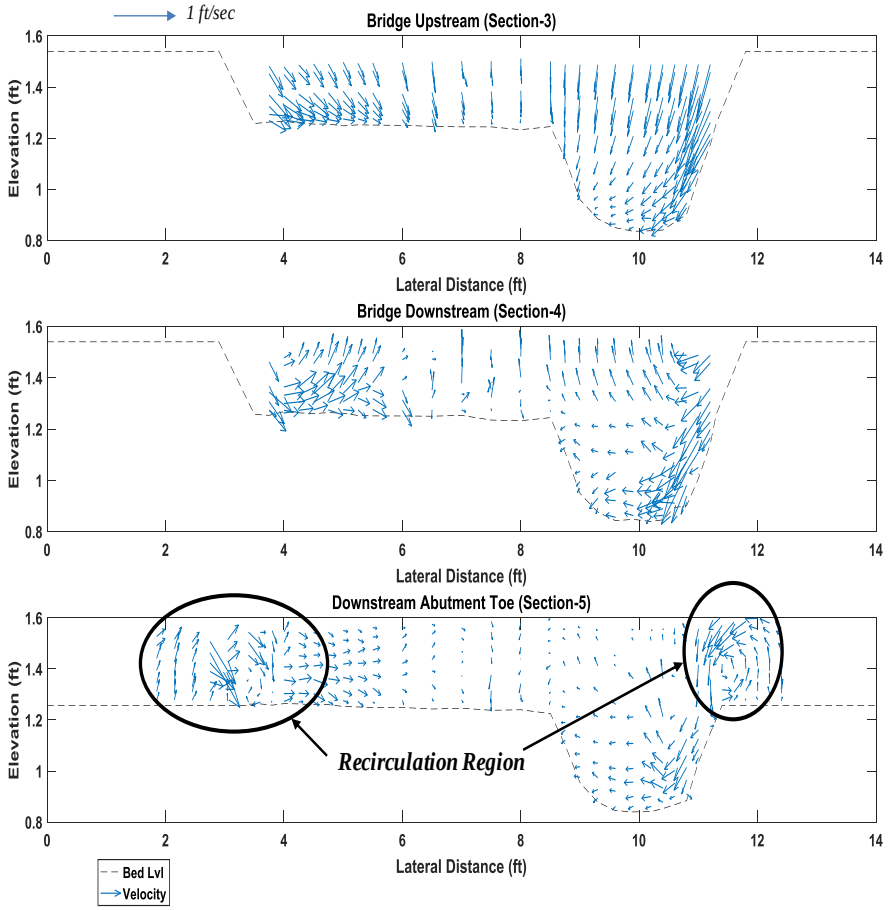

Figure 4-9 Velocity vectors containing the transverse (v) and vertical (w) components of the velocity at the bridge upstream end, bridge downstream end, and downstream toe of the abutment for Run 3 (OT Flow case)

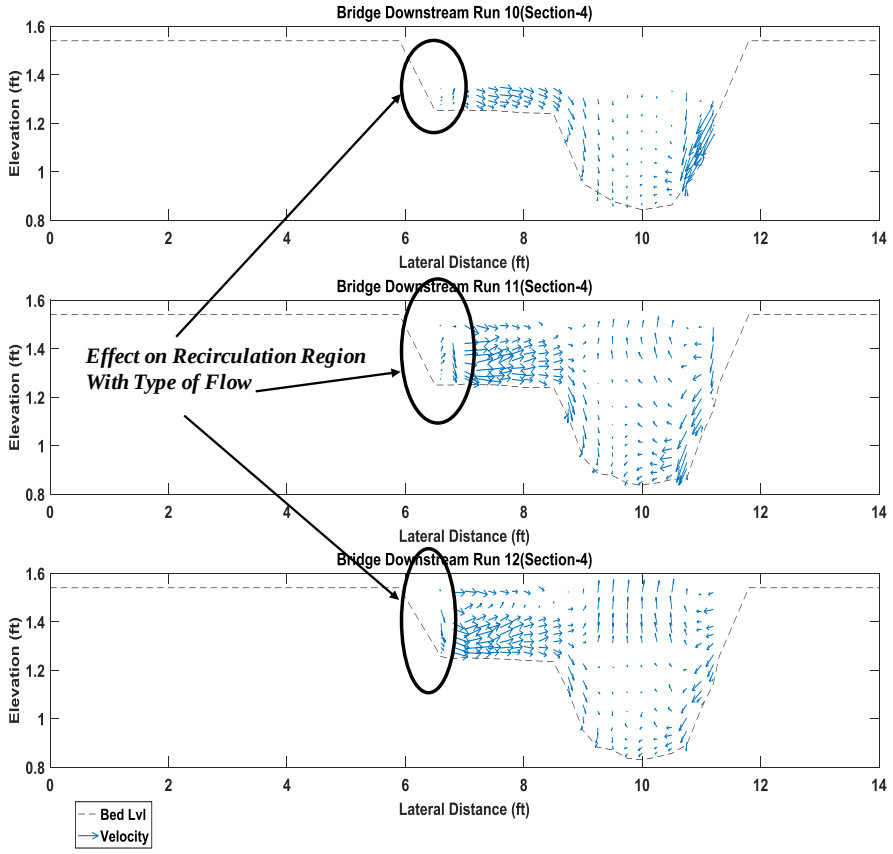

Figure 4-10 Velocity vectors containing the transverse (*v*) and vertical (*w*) component of the velocity at the bridge downstream end for Run 10, 11, and 12 (Free, SO, and OT Flow case respectively)

Figure 4-11 shows time-averaged bottom velocity vectors containing the transverse (v) and flow direction (u) components of the velocity (i.e. $sqrt(<v^2>+<u^2>)$) in the bridge section, showing the development of the flow separation zone as it moves downstream in the bridge contraction for Runs 1 , 2 , and 3 (F, SO, and OT flow, respectively). The separation zone is more prominent in F and SO flow, whereas the weir flow in OT flow cases provides relief to the flow passing under the bridge, resulting in a more narrow flow separation region.

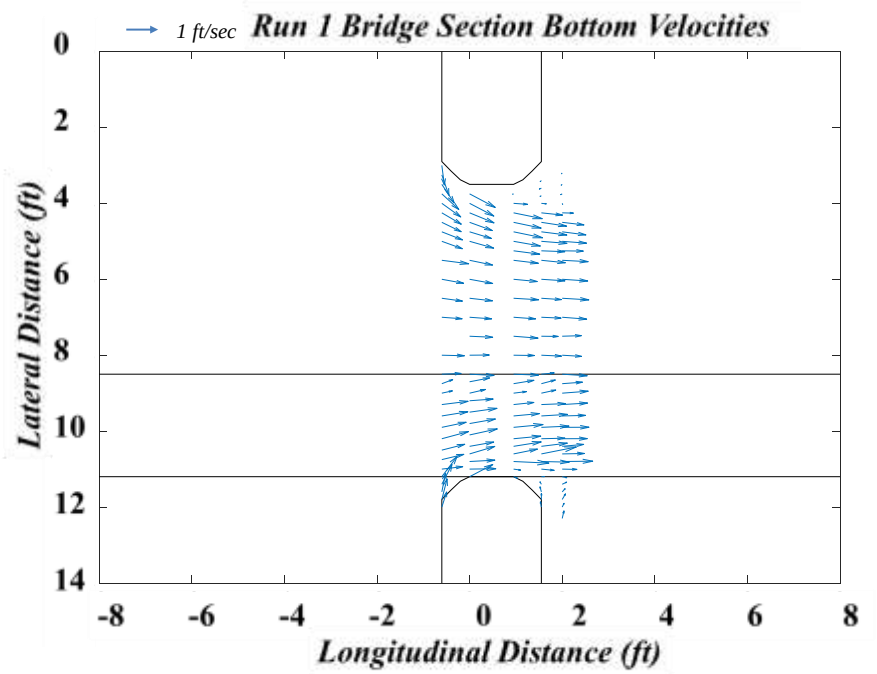

(a) Run 1 F Flow, bottom velocity vectors in the bridge section

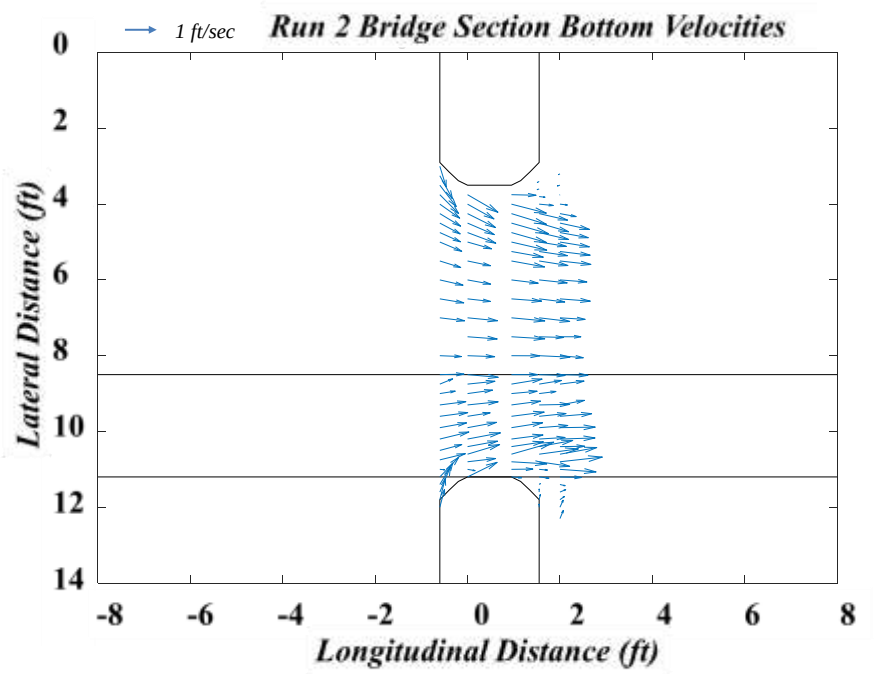

(b) Run 2 SO Flow, bottom velocity vectors in the bridge section

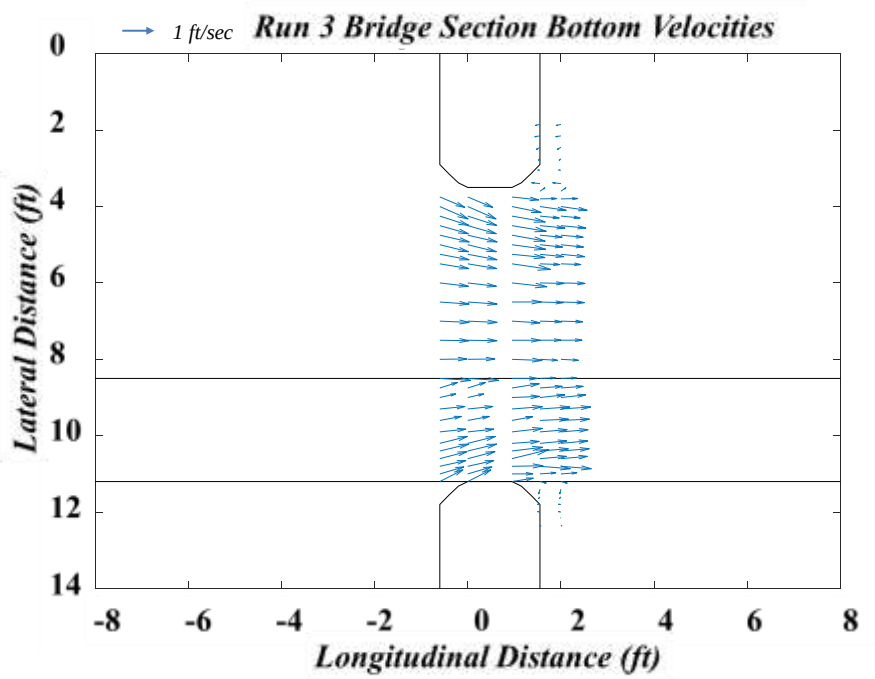

(c) Run 3 OT Flow, bottom velocity vectors in the bridge section

Figure 4-11 Bottom velocity vectors in the bridge section for the transverse (v) and flow direction (u) components of the velocity for Run 1, 2 , and 3 (Free, SO, and OT flow cases, respectively)

The flow geometry in the bridge section is complex and it generates turbulence structures that are responsible for forming the interactive abutment and contraction scour hole. Because of the smooth flow upstream of the bridge, the turbulence measurements were taken at the downstream end of the bridge and at the downstream toe of the abutment. The turbulent kinetic energy (TKE) is defined as the half of the sum of squares of time-averaged velocity fluctuation components of longitudinal (u'), transvers (v'), and vertical (w') components of the velocities (i.e. TKE = $0.5(<u'^2><v'^2>+<w'^2>)$).

For the scour process, the near-bed turbulence measurements are important because they contribute to the development of the scour hole. Therefore, the turbulent kinetic energy (TKE) was measured at the minimum possible distance from the bed (5 mm/0.017 ft from the bed). Measurements were taken at the downstream end of the bridge (Section 4) and at the downstream toe of the abutment (Section 5). It was found that the TKE value was higher at the downstream toe of the abutment. This observation was consistent for all the experiments. Figure 4-12 shows the bottom TKE ($(K_b) = 1/2(<u'^2><v'^2>+<w'^2>)$, for the near-bed measurements) normalized by the square of the critical shear velocity (K_b/u_{*c}^2) for section 4 and 5 for Run 1 (F Flow) along with the contour plot for the equilibrium scour condition.

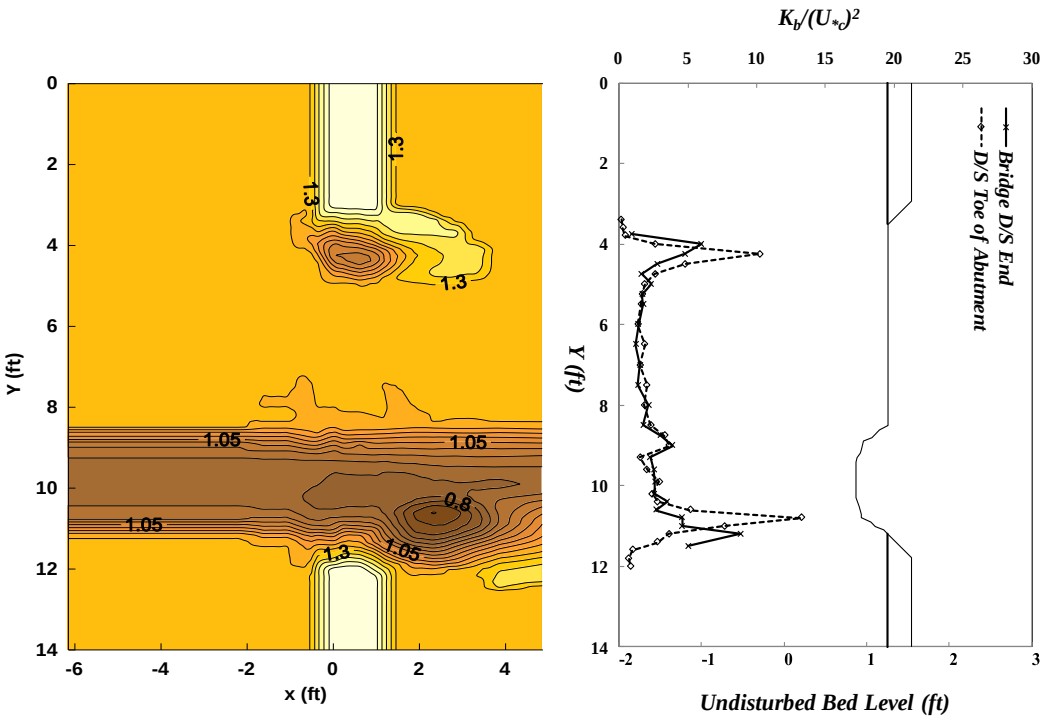

Figure 4-12 Normalized bottom TKE (K_b/u_{*c}^2) for section 4 and section 5 and equilibrium contour plot of Run 1, (F Flow, L_a/B_f = 0.41, V_{f1}/V_{fc} =0.542, V_{m1}/V_{mc} =0.723)

Turbulence kinetic energy measurements for the downstream toe of the abutment were also taken at 20% and 40% of the water depth from the undisturbed bed level in addition to the near-bed measurements for some of the experiments. It was observed that the TKE value was highest for the near-bead measurements, which reduced with increase in distance from the bed. This observation is consistent with Hong (2013). Figure 4-13 shows the TKE values normalized by square of the critical shear velocity (K/u_{*c}^2) for Run 1 (F Flow) for near bed, at 20% of flow depth, and 40% of flow depth for section 5.

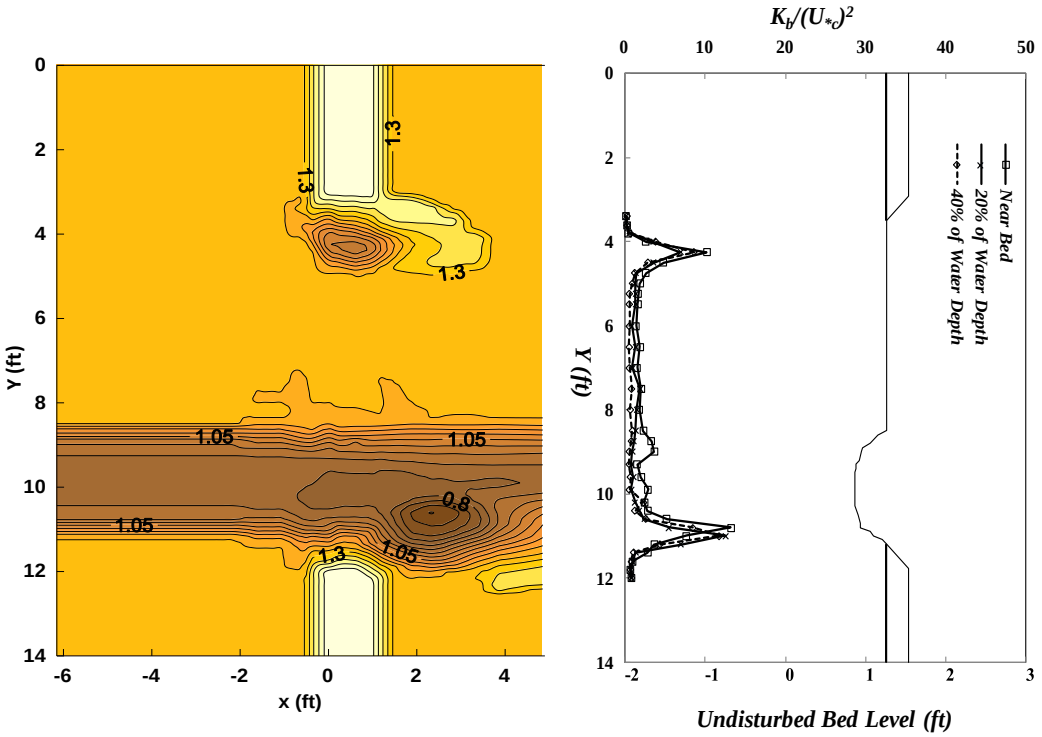

Figure 4-13 Normalized bottom TKE (K_b/u_{*c}^2) for section 5 of Run 1 for near bed, 20%, and 40% of the water depth and equilibrium contour plot (F Flow L_a/B_f = 0.41, V_{f1}/V_{fc} =0.542, V_{m1}/V_{mc} =0.723)

4.2.4. *Scour Measurements*

Scour measurements were taken at the time of scour development as described in Para 3.4.1. The time development will be analyzed in the subsequent chapter. However, the equilibrium scour measurements were taken for the complete test section as a mesh grid. Final bathymetry at the equilibrium scour was plotted as contour plots using Surfer-8 (Golden software Inc. Colorado) at a contour interval of 0.05 ft to analyze the location, shape and extent of the scour hole.

It was found that the scour hole started from the upstream edge of the abutment and expanded in the transverse direction as it moved downstream. The location of the point of deepest scour varied depending on the type of flow and the scour parameters,

including flow contraction ratio (q_2/q_1), backwater depth ratio (Y_1/Y_o), and approach flow intensity (V_1/V_c). After the point of deepest scour in the downstream direction, the scour hole starts to reduce its lateral extent. As the scour hole meets the undisturbed bed level in the downstream direction, the deposition region starts where the scoured material is deposited. The scour hole has a distorted oval shape with the deepest point in the middle of the scour hole. The distorted shape is an outcome of the complex flow geometry in the contracted section, armoring effect of the riprap apron, and the type of flow. For F and SO flow cases, the shape of the scour hole remained elongated and it moved away from the abutment in the downstream direction. However, for the OT flow cases the extent of the scour hole was larger in the flow direction. The scour hole was observed relatively closer to the abutment in OT flow cases as compared to F and SO flow cases as it moved in the downstream direction. This difference between the F/SO and OT flow cases is attributed mainly to three reasons: (1) flow separation zone is affected by the weir flow passing over the bridge for OT flow cases resulting in a more narrow flow separation zone (refer to previous Figure 4-11); (2) weir flow passing over the bridge adds vertical confinement to the flow downstream of the bridge; and (3) weir flow affects the recirculation region due to the vertical confinement. This phenomenon is presented in Figure 4-14 which shows the equilibrium scour contours and the photographs of the equilibrium scour for all three types of flow for two different abutment ratios L_a/B_f = 0.41 and 0.77. Scour Contours and photographs of all the experiments are attached as Appendix-A.

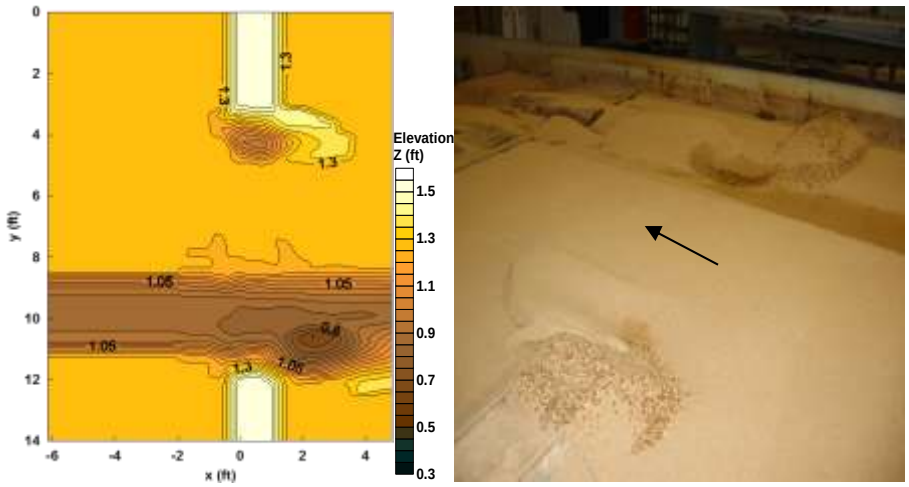

(a) Run 1, Free flow L_a/B_f = 0.41, V_{f1}/V_{fc} =0.542, V_{m1}/V_{mc} =0.723

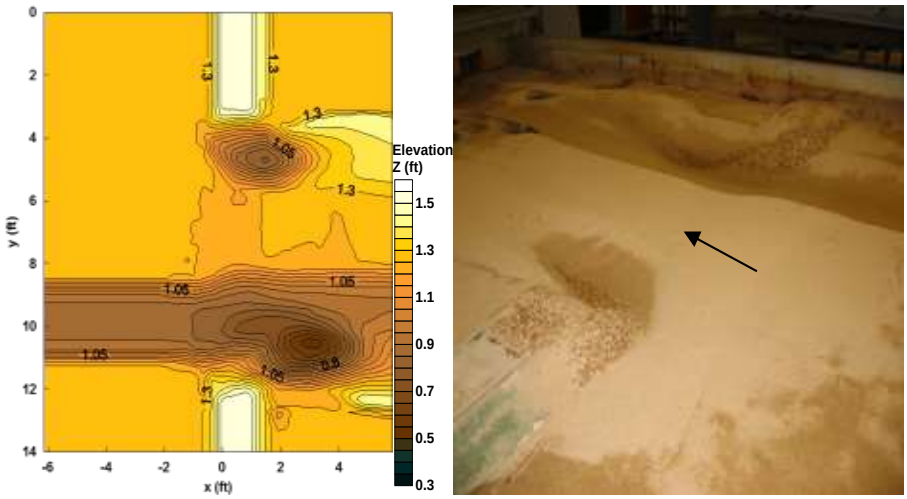

(b) Run 2, SO flow L_a/B_f = 0.41, V_{f1}/V_{fc} =0.589, V_{m1}/V_{mc} =0.725

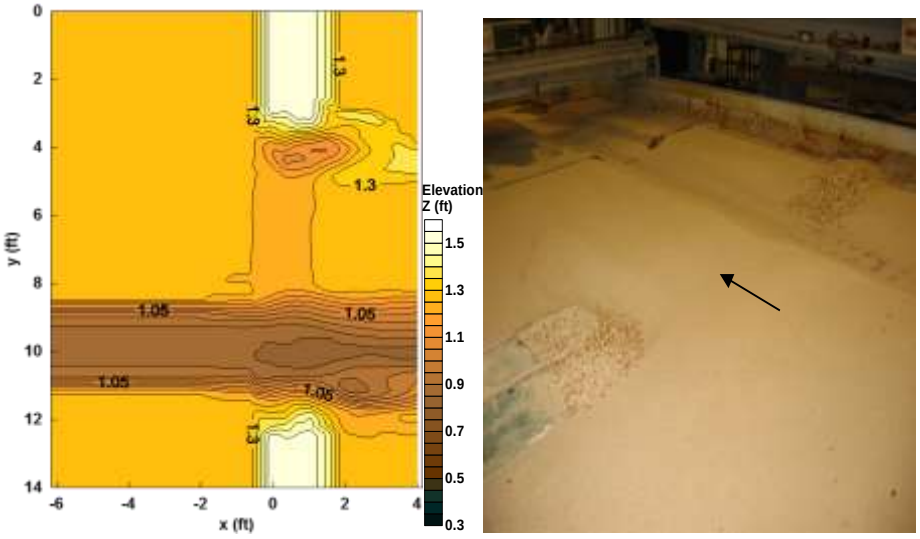

(c) Run 3, OT flow L_a/B_f = 0.41, V_{f1}/V_{fc} =0.561, V_{m1}/V_{mc} =0.653

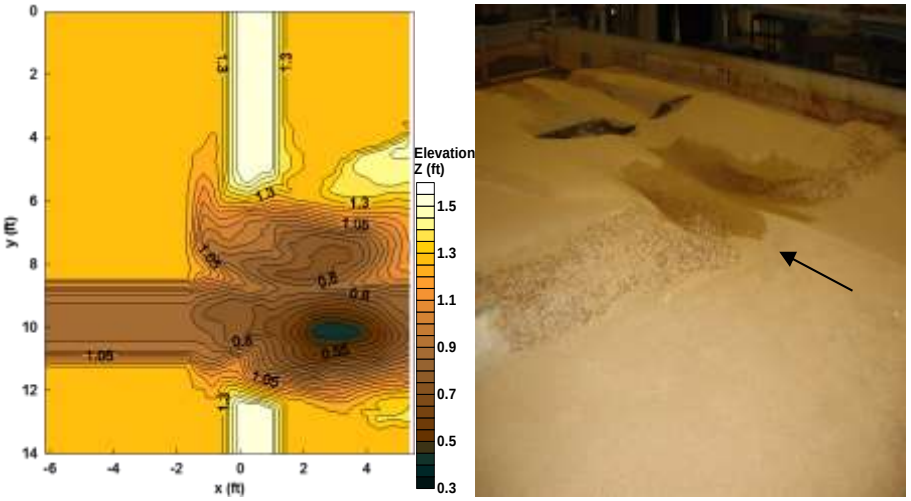

(d) Run 10, Free flow L_a/B_f = 0.77, V_{f1}/V_{fc} =0.659, V_{m1}/V_{mc} =0.879

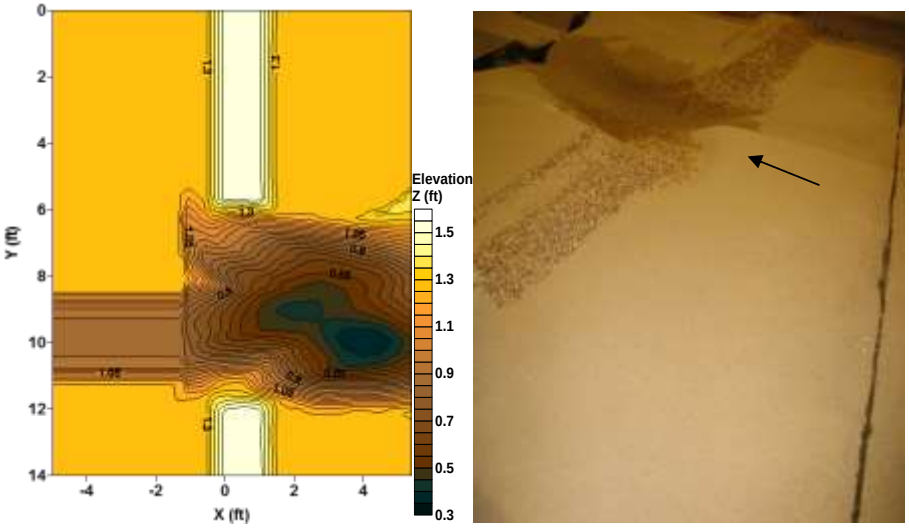

(e) Run 11, SO flow L_a/B_f = 0.77, V_{f1}/V_{fc} =0.579, V_{m1}/V_{mc} =0.711

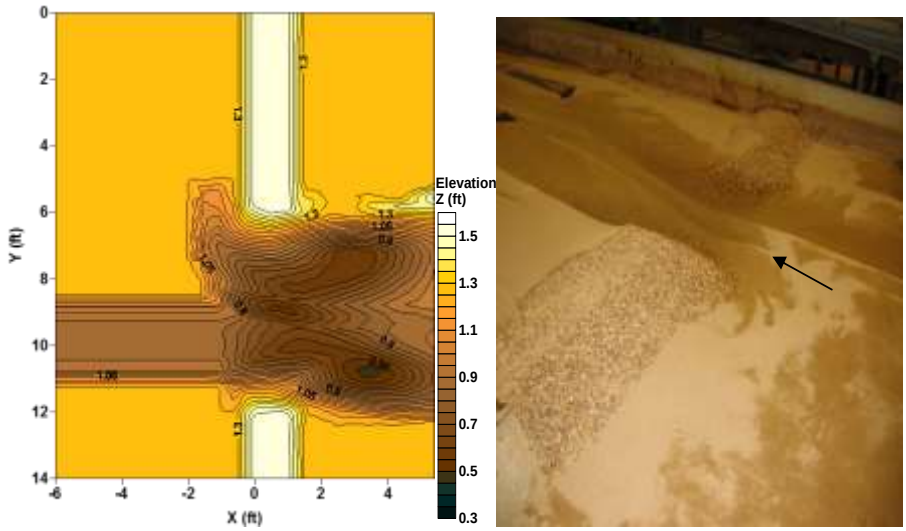

(f) Run 12, OT flow L_a/B_f = 0.77, V_{f1}/V_{fc} =0.623, V_{m1}/V_{mc} =0.784

Figure 4-14 Equilibrium bed bathymetry of test section for all three types of flows for L_a/B_f = 0.41 (Run 1, 2, and 3) and L_a/B_f = 0.77(Run 10, 11, and 12)

4.3. Interactive Abutment and Contraction Scour Prediction for LSA (Type-I Scour)

In a bridge contraction, an embankment terminating at the abutment gives the effect of both abutment and lateral contraction. Thus, the scour at an abutment does not develop as an isolated abutment scour but rather includes both components. It has also been observed in this study that lateral contraction scour may or may not span over the entire width of the contracted section (refer to Figure 3-15) depending on the length of the abutment and the degree of contraction.

Hong (2013, 2015) analyzed abutment and lateral contraction scour and showed that combined lateral contraction and abutment scour can be expressed as an amplification of the theoretical contraction scour proposed by Laursen (1960). Laursen and Sturm (2006) applied a constant amplification factor to calculate abutment scour

alone for a solid abutment. Ettema et al. (2010) applied a variable amplification factor to free flow around an erodible abutment, but Hong included vertical contraction scour as well in submerged orifice and overtopping flows. Hong suggested using as scour prediction parameters the approach flow intensity V_1/V_c, backwater depth ratio (Y_1/Y_o), and ratio of unit discharge in approach and bridge sections (q_2/q_1). A constant scour amplification factor (r_T) was given as 2.51 for LSA with a coefficient of determination of 0.86 and standard error of the estimate as 0.173. In a second formulation, it was shown that the amplification factor decreased with increases in the flow contraction ratio (q_2/q_1) which corresponded to decreases in bottom TKE (K_b) as local turbulence effects became less important than flow constriction in producing scour.

A non-dimensional theoretical contraction scour (Y_{2max}/Y_1) depends on two parameters which include a flow contraction ratio (q_2/q_1) and the approach flow intensity (V_1/V_c). However, if the contraction scour is normalized by the undisturbed flow depth (Y_o) at the bridge an additional factor of backwater effect (Y_1/Y_o) adds to the theoretical contraction scour as shown in Equation 4-1.

$$\frac{Y_{f2\max}}{Y_{f1}} = \left[\left[\frac{q_{f2}}{q_{f1}}\right]\left[\frac{V_{f1}}{V_{fc1}}\right]\right]^{6/7} \qquad OR$$
$$\frac{Y_{f2\max}}{Y_{fo}} = \left[\frac{Y_{f1}}{Y_o}\right] * \left[\left[\frac{q_{f2}}{q_{f1}}\right]\left[\frac{V_{f1}}{V_{fc1}}\right]\right]^{6/7} \qquad (4\text{-}1)$$

A dimensional analysis by Sturm *et al.* (2011) as explained in Para 2.9 shows that for a given type, alignment, and shape of the abutment, an abutment scour is a function of the variables as shown in Equation 4-2 (for definition of variables, refer to Figure 2-5).

$$\frac{Y_{f2\max}}{Y_{fo}} = f\left(\frac{Y_{f1}}{Y_{m1}}, \frac{h_b}{Y_{f1}}, \frac{L_a}{B_f}, \frac{B_f}{B_m}, \frac{W}{Y_{f1}}, \frac{n_f}{n_m}, \frac{L_a}{d_{50}}, \frac{V_{f1}}{V_{fc1}}, \frac{Y_{f1}}{Y_{fo}}, \frac{V_{f1}}{\sqrt{gY_{f1}}}\right) \quad (4\text{-}2)$$

A geometric contraction ratio (L_a/B_f) and all geometric ratio variables including those related to compound channel geometry and roughness (first six dimensionless parameters on the right hand side of Eq. (4-2)) can be combined into one parameter as the flow contraction ratio (q_2/q_1) related to flow distribution as given by Sturm and Janjua (1993,1994) and Sturm et al. (2011). The ratio of abutment length to sediment size, L_a/d_{50}, is very large and thus does not affect the scour process (Melville and Coleman 2000).Neglecting Froude number effects as second order, especially for submerged bridges, the abutment scour equation can be rewritten as:

$$\frac{Y_{2\max}}{Y_o} = f\left(\frac{V_1}{V_{c1}}, \frac{Y_1}{Y_o}, \frac{q_2}{q_1}\right) \quad (4\text{-}3)$$

Following the theoretical contraction scour approach in terms of arrangement of parameters but with unknown coefficients, a best-fit of the experimental data is proposed in the form:

$$\frac{Y_{2\max}}{Y_o} = a * \left(\frac{Y_1}{Y_o}\right)^b * \left(\frac{V_1}{V_{c1}} * \frac{q_2}{q_1}\right)^c \quad (4\text{-}4)$$

A constant "*a*" has been added to the equation in order to account for the amplification factor and the theoretical contraction scour parameters have been kept as a single variable. In addition, Y_1/Y_o represents backwater effects. Experiments were conducted at the Georgia Institute of Technology and University of Auckland (Xiong 2017) for which the measured scour parameters and the non-dimensional equilibrium scour are

presented in Table 4-1. Experiments conducted by Hong (2013) and Ettema et al. (2011) have also been included in the regression analysis (these have not been included in the table).

Table 4-1 Measured scour parameters and normalized equilibrium scour for LSA experiments, includes both set of experiments from the Georgia Institute of Technology and University of Auckland

Run	***Flow Type***	L_a/B_f	***F/P***				Y_{f2max}/Y_{fo}
			q_2/q_1	Y_1/Y_o	V_1/V_c	Y_o (ft)	
1 GT	F	0.41	1.549	1.081	0.542	0.223	2.408
2 GT	SO	0.41	1.520	1.107	0.589	0.290	2.638
3 GT	OT	0.41	1.044	1.046	0.561	0.457	1.373
4 GT	F	0.41	1.501	1.132	0.655	0.220	2.950
5 GT	OT	0.41	1.014	1.067	0.684	0.460	1.943
8 GT	F	0.41	1.479	1.136	0.648	0.220	2.800
10 GT	F	0.77	1.821	1.244	0.659	0.213	3.469
12 GT	OT	0.77	1.154	1.098	0.622	0.457	2.554
18 GT	F	0.41	1.670	1.097	0.586	0.29	2.438
19 GT	F	0.77	2.103	1.215	0.589	0.265	3.287
22 GT	F	0.41 WW	1.578	1.076	0.541	0.223	2.204
23 GT	SO	0.41 WW	1.556	1.107	0.589	0.290	2.024
24 GT	OT	0.41 WW	1.042	1.044	0.561	0.457	1.612
25 GT	F	0.77 WW	1.867	1.239	0.659	0.213	3.277
26 GT	SO	0.77 WW	2.001	1.362	0.579	0.265	3.584
27 GT	OT	0.77 WW	1.214	1.098	0.622	0.457	2.342
41 GT	F	0.41	1.486	1.141	0.648	0.220	2.915
11 UOA	FS	0.50	1.78	0.985	0.48	0.27	2.536
13 UOA	OT	0.50	0.98	1.003	0.49	0.54	1.613
14 UOA	FS	0.50	1.52	1.018	0.66	0.32	2.625
16 UOA	OT	0.50	0.94	1.033	0.79	0.60	2.446
17 UOA	SO	0.50	1.07	1.117	0.57	0.34	2.189
18 UOA	SO	0.5 WW	1.15	1.117	0.55	0.34	2.145
19 UOA	OT	0.5 WW	0.98	1.003	0.49	0.54	1.538
20 UOA	OT	0.5 WW	0.94	1.108	0.81	0.46	2.847
21 UOA	OT	0.5 WW	0.94	1.033	0.79	0.60	2.341

Note: F = free flow, SO = submerged orifice flow, OT = overtopping flow, WW = wing-wall abutments, GT = Georgia Institute of Technology experiments, and UOA = University of Auckland experiments

4.3.1. *Comparison with Ettema's Contraction Scour Model*

Ettema conducted free flow experiments for LSA under clear water scour conditions and analyzed the equilibrium scour by normalizing the maximum scour depth (Y_{2max}) with theoretical contraction scour (Ettema et al. 2010). Ettema gave an upper envelope curve for the maximum non-dimensional abutment and contraction scour (Y_{f2max}/Y_{fc}). Figure 4-15 shows the comparison of the current set of experiments with the envelope curve suggested by Ettema.

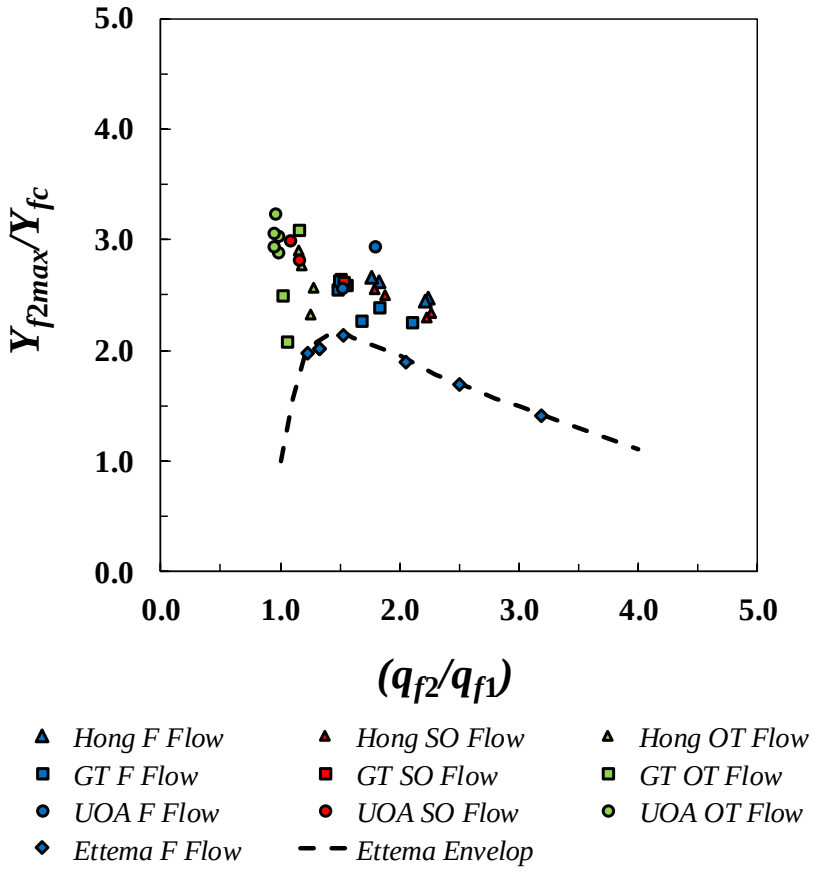

Figure 4-15 Comparison of Ettema's envelope curve for the maximum non-dimensional abutment and contraction scour (Y_{f2max}/Y_{fc}) with current set of experiments (where Hong shows experiments by Hong (2013) , GT shows the latest set of experiments at The Georgia Institute of Technology, and UOA Shows the experiments conducted at the University of Auckland)

The envelope curve shows the relationship of the ratio of discharge per unit width in approach and test section (q_{f2}/q_{f1}) with the normalized total equilibrium scour. Experiments show that the equilibrium scour is higher in case of the new experiments as compared to the envelope curve, with higher values in case of SO and OT flows. This result validates the observation that contribution of abutment scour component is much higher (ranging up to a factor of 3.5) as compared to the lateral contraction scour component. A higher approach flow intensity, greater backwater effect, and the inclusion of SO and OT flows are the other contributing factors to larger scour values than observed by Ettema et al. (2010).

4.3.2. *Statistical Analysis and Suggested Model*

The set of experiments, including the experiments conducted by Hong (2013), Ettema et al. (2011), the experiments conducted for the current research at the Georgia Institute of Technology, and experiments conducted at the University of Auckland (Xiong 2017), was compared with the model suggested by Hong (2013) and showed a reasonable agreement with a coefficient of determination of 0.64 and a standard error of the estimate as 0.312. The modified Hong's model which includes the effect of turbulent stresses on the amplification factor showed a better agreement with a coefficient of determination of 0.68 and a standard error of the estimate of 0.289. A stepwise approach was adopted in this research for the regression of the data using Eq. 4-4 as a model. Initially, all the three parameters including approach flow intensity (V_1/V_c), the discharge contraction ratio per unit width (q_{f2}/q_{f1}), and backwater effect (Y_1/Y_o) were kept as separate variables. This resulted in the relationship given by Equation 4-5:

$$\frac{Y_{f2\max}}{Y_{fo}} = 2.345 * \left(\frac{Y_{f1}}{Y_{fo}}\right)^{1.51} * \left(\frac{q_{f2}}{q_{f1}}\right)^{0.50} * \left(\frac{V_{f1}}{V_{fc1}}\right)^{0.51} \quad (4\text{-}5)$$

A better coefficient of determination (R^2) of 0.82 was achieved with a standard error of the estimate (SEE) of 0.233. The regression resulted in almost identical exponents (within the standard error of the parameter) of approach flow intensity (V_1/V_c) and the discharge contraction ratio per unit width (q_{f2}/q_{f1}) as 0.51 and 0.50, respectively, which confirms that theoretical contraction scour parameters can be combined as a single variable. This result also validates the formulation of Equation 4-4. The theoretical contraction scour parameters were kept as a single variable for the subsequent regression which resulted in the same coefficient of determination of 0.82 and the standard error of the estimate as 0.230 with b = 3/2 and c = 1/2. The rounding of the exponents was within their standard error. The final model is given by Equation 4-6:

$$\frac{Y_{f2\max}}{Y_{fo}} = 2.363 * \left(\frac{Y_{f1}}{Y_{fo}}\right)^{3/2} * \left(\frac{q_{f2}}{q_{f1}} * \frac{V_{f1}}{V_{fc1}}\right)^{1/2} \quad (4\text{-}6)$$

Figure 4-16 shows the regression model for LSA under clear-water scour conditions. A comparison with the theoretical contraction scour (Theoretical CS) plotted in the figure shows a much higher equilibrium scour as compared to theoretical contraction scour. The details of each regression are given in Table 4-2, with residual vs. fitted values plotted in Figure 4-17 for the suggested model, which show an unbiased trend. The summary is presented in Table 4-3. The lower limit for initiation of scour process determined by the model is $(Y_{f1}/Y_{fo})^3 * (V_{f1}/V_{fc} * q_{f2}/q_{f1})$ = 0.20. The maximum normalized scour for spill-through erodible abutments has been defined as

Y_{f2max}/Y_{fo} = 3.6, as shown by the experimental results of Ettema et al. 2010. After attaining the maximum value, the scour remains the same with increases in the scour parameters, but abutment failure may result.

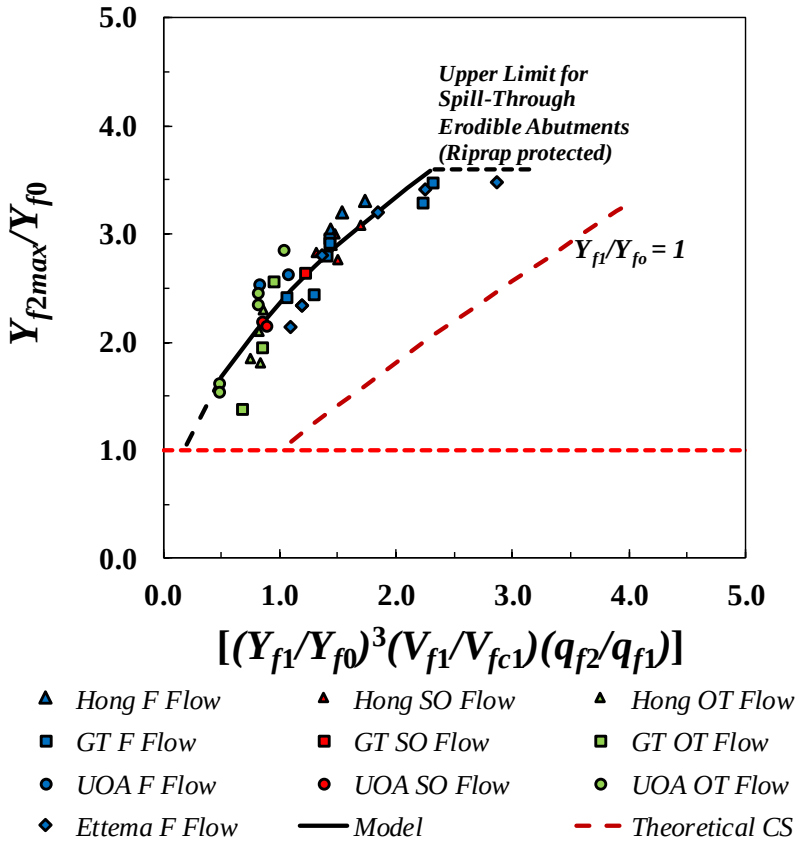

Figure 4-16 Suggested LSA regression model along with theoretical contraction scour line

Table 4-2 Details of the regression analysis for LSA

Hong (2013) Model	$\frac{Y_{f2\max}}{Y_{fo}} = \left(\frac{Y_{f1}}{Y_{fo}}\right)^{1.0} * 2.51 * \left(\frac{V_{f1}}{V_{fc1}} * \frac{q_{f2}}{q_{f1}}\right)^{6/7}$		
R^2	0.64	SEE	0.312
Hong (2013) Modified Model	$\frac{Y_{f2\max}}{Y_{fo}} = \left(\frac{Y_{f1}}{Y_{fo}}\right)^{1.0} \left(\frac{q_{f2}}{q_{f1}}\right)^{-0.16} * 2.75 * \left(\frac{V_{f1}}{V_{fc1}} * \frac{q_{f2}}{q_{f1}}\right)^{6/7}$		
R^2	0.68	SEE	0.289
Separate Powers of Variables	$\frac{Y_{f2\max}}{Y_{fo}} = \left(\frac{Y_{f1}}{Y_{fo}}\right)^{1.51} * 2.345 * \left(\frac{V_{f1}}{V_{fc1}}\right)^{0.50} \left(\frac{q_{f2}}{q_{f1}}\right)^{0.51}$		
R^2	0.82	SEE	0.233
Standard Error of Parameters	Parameter	Value	SE
	Coefficient	2.345	0.105
	Exponent of Y_{f1}/Y_{fo}	1.514	0.300
	Exponent of q_{f2}/q_{f1}	0.513	0.069
	Exponent of V_{f1}/V_{fc}	0.499	0.096
Taking Theoretical Contraction Scour as single Variable	$\frac{Y_{f2\max}}{Y_{fo}} = \left(\frac{Y_{f1}}{Y_{fo}}\right)^{1.53} * 2.356 * \left(\left(\frac{V_{f1}}{V_{fc1}}\right)\left(\frac{q_{f2}}{q_{f1}}\right)\right)^{0.51}$		
R^2	0.82	SEE	0.230
Standard Error of Parameters	Parameter	Value	SE
	Coefficient	2.356	0.006
	Exponent of Y_{f1}/Y_{fo}	1.534	0.057
	Exponent of $q_{f2}/q_{f1} * V_{f1}/V_{fc}$	0.509	0.037
Fixing the Powers Within Error Term	$\frac{Y_{f2\max}}{Y_{fo}} = \left(\frac{Y_{f1}}{Y_{fo}}\right)^{1.50} * 2.363 * \left(\left(\frac{V_{f1}}{V_{fc1}}\right)\left(\frac{q_{f2}}{q_{f1}}\right)\right)^{0.50}$		
R^2	0.82	SEE	0.230
Standard Error of Parameters	Parameter	Value	SE
	Coefficient	2.363	0.069

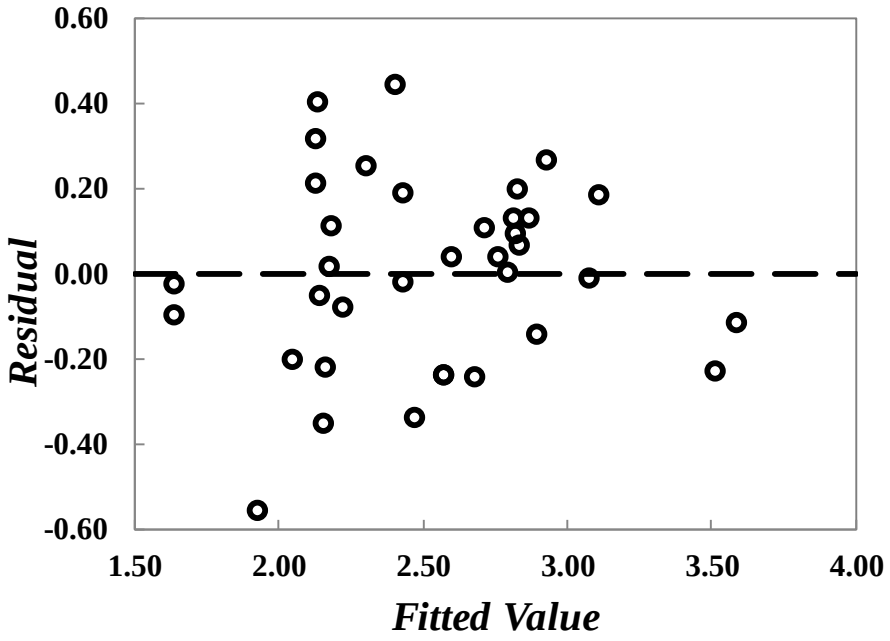

Figure 4-17 Residuals of the fitted values for the interactive abutment and contraction scour suggested model LSA

Table 4-3 Summary of the regression results for LSA

Model	Best Fit Formula	R^2	SEE	Comments
Hong (2013) Model	$\frac{Y_{f2\max}}{Y_{fo}} = \left(\frac{Y_{f1}}{Y_{fo}}\right)^{1.0} * 2.51 * \left(\frac{V_{f1}}{V_{fc1}} * \frac{q_{f2}}{q_{f1}}\right)^{6/7}$	0.64	0.312	
Hong (2013) Modified Model	$\frac{Y_{f2\max}}{Y_{fo}} = \left(\frac{Y_{f1}}{Y_{fo}}\right)^{1.0} \left(\frac{q_{f2}}{q_{f1}}\right)^{-0.16} * 2.75 * \left(\frac{V_{f1}}{V_{fc1}} * \frac{q_{f2}}{q_{f1}}\right)^{6/7}$	0.68	0.289	
Separate Variable Powers	$\frac{Y_{f2\max}}{Y_{fo}} = \left(\frac{Y_{f1}}{Y_{fo}}\right)^{1.51} * 2.345 * \left(\frac{V_{f1}}{V_{fc1}}\right)^{0.50} \left(\frac{q_{f2}}{q_{f1}}\right)^{0.51}$	0.82	0.233	
Taking Theoretical Contraction Scour as Single Variable	$\frac{Y_{f2\max}}{Y_{fo}} = \left(\frac{Y_{f1}}{Y_{fo}}\right)^{1.53} * 2.356 * \left(\left(\frac{V_{f1}}{V_{fc1}}\right)\left(\frac{q_{f2}}{q_{f1}}\right)\right)^{0.51}$	0.82	0.230	
Fixing the Powers Within Error Term	$\frac{Y_{f2\max}}{Y_{fo}} = \left(\frac{Y_{f1}}{Y_{fo}}\right)^{1.50} * 2.363 * \left(\left(\frac{V_{f1}}{V_{fc1}}\right)\left(\frac{q_{f2}}{q_{f1}}\right)\right)^{0.50}$	0.82	0.230	Suggested Model

4.3.3. *Backwater Effect*

Backwater effect (Y_1/Y_o) is the measure of the degree of contraction, which is the head required to negotiate the bridge obstruction. The bridge obstruction includes a geometric contraction in form of an embankment and bridge girders and deck spanning over the entire cross section, posing an obstruction to the flow striking the bridge (in case of SO and OT flows). The backwater effect is the most significant parameter in case of LSA (as given by regression analysis). A shallower depth in the floodplain as compared to the main channel results in a higher value of backwater (Y_1/Y_o) in the floodplain. An increasing degree of flow contraction (q_2/q_1) and higher approach flow intensity (V_1/V_c) also contribute directly to the magnitude of scour as shown in Figure 4-18.

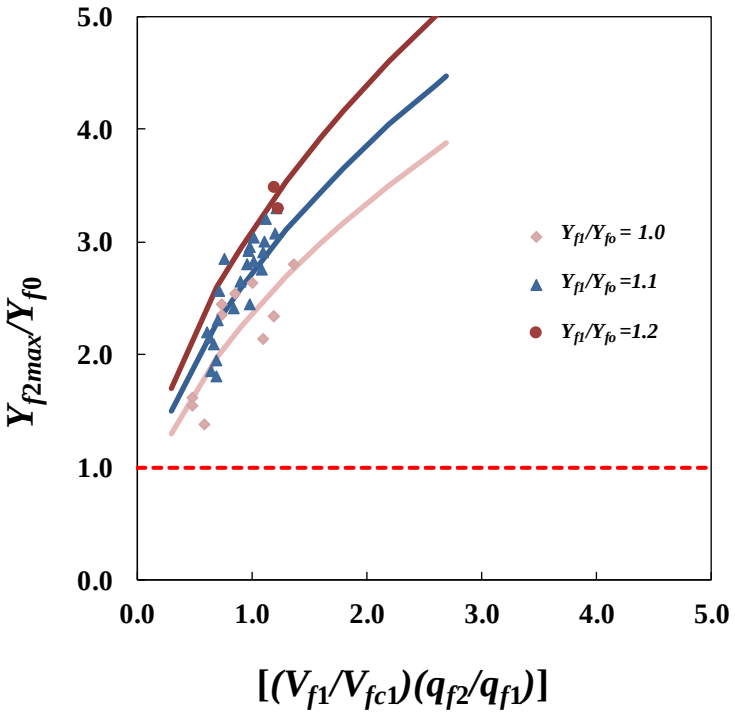

Figure 4-18 Backwater effect (Y_{f1}/Y_{fo}) for the LSA under CWS conditions

4.3.4. *Wing-Wall Abutments For LSA (Type –I Scour)*

Experiments were also conducted for the wing-wall abutments under the same flow conditions as that of spill-through abutments to make a comparison of wing-wall and spill-through abutments. Experiments were conducted for all the three types of flows (F, SO, and OT flows) and for three different abutment ratios with L_a/B_f = 0.41, 0.50, and 0.77 (experiments for L_a/B_f = 0.50 were conducted at University of Auckland). Table 4-1 also shows the measured scour parameters and normalized equilibrium scour for wing-wall abutment experiments (where "WW" shows the wing-wall experiments). A separate regression for wing-wall abutments, by keeping only the coefficient as variable, to find the shape factor, results in a coefficient of 2.311, standard error of the estimate of 0.329, and coefficient of determination of 0.70. However, the application of spill-through abutment model with a coefficient of 2.363 results in a coefficient of determination of 0.69 and a standard error of the estimate of 0.334. Thus, the variation in the coefficient is less than 2%, which can be attributed to experimental uncertainty, and it is concluded that wing-wall abutments also follow the CWS LSA model for interactive abutment and contraction scour with a little higher scatter. This higher scatter can be attributed to the limited number of wing-wall experiments. Figure 4-19 shows that the wing-wall abutment experiments conform to the CWS LSA spill-through abutment model. However, no upper limit is suggested owing to the presence of solid wing-walls.

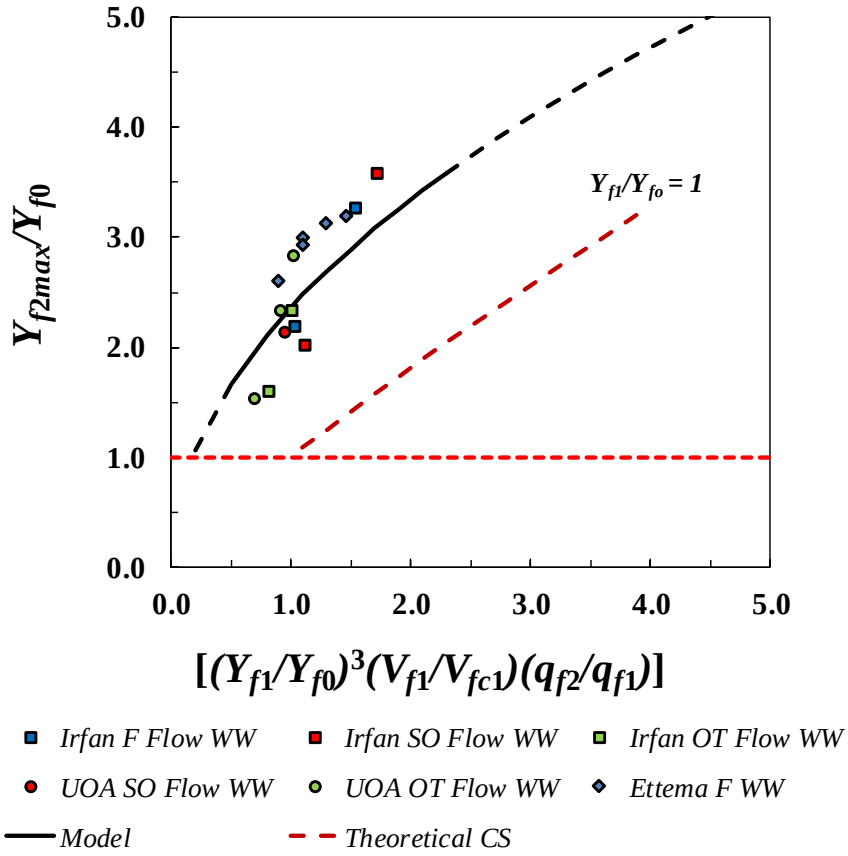

Figure 4-19 Comparison of wing-wall abutment experiments with CWS LSA interactive abutment and contraction scour model

4.3.5. *Comparison of HEC-18 Model with Suggested Interactive Abutment and Contraction Scour Model for LSA (Type-I Scour)*

The interactive scour development is affected by simultaneous development of different scour components, which affects the total interactive scour. This results in less equilibrium scour than the arithmetic sum of the scour components, which is recommended by HEC-18. A comparison of the HEC-18 and suggested model is shown in Figure 4-20 for LSA. The scour components for HEC-18 have been calculated by equations suggested in HEC-18 where contraction scour for CWS uses equation derived from Laursen (1963) contraction scour theory (Equation 2-6);

vertical contraction scour uses equation based on flow separation thickness under the bridge (Equation 2-14) (Shen et al. 2012); and abutment scour is calculated from Froehlich's equation (Equation 2-28). Abutment scour is the most significant contributor to the total scour with an average of about 76% of the total scour. Vertical contraction scour contributes 16 %, and contraction scour is 8% of the total scour as per HEC-18 methodology calculations. HEC-18 predicts much higher values as compare to suggested model, which predicts the interactive abutment and contraction scour for LSA within 10% of physical measurements.

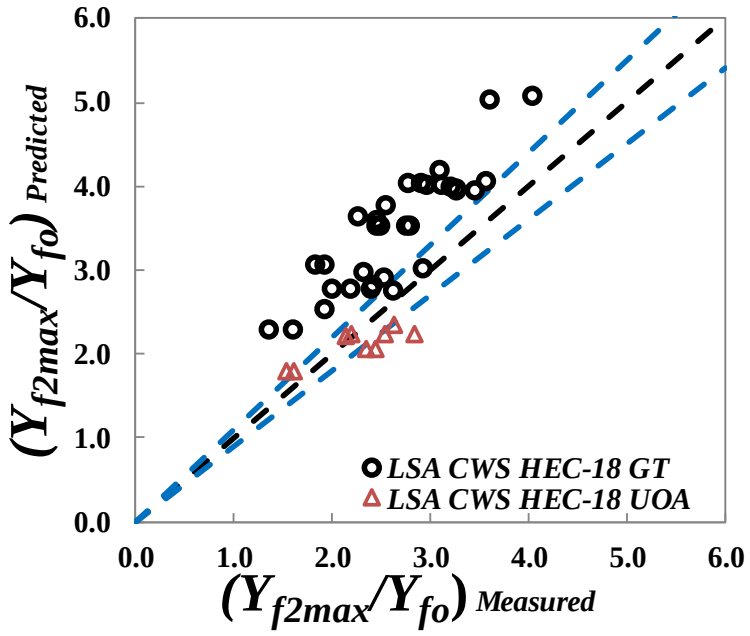

(a) Clear water interactive abutment and contraction scour prediction HEC-18

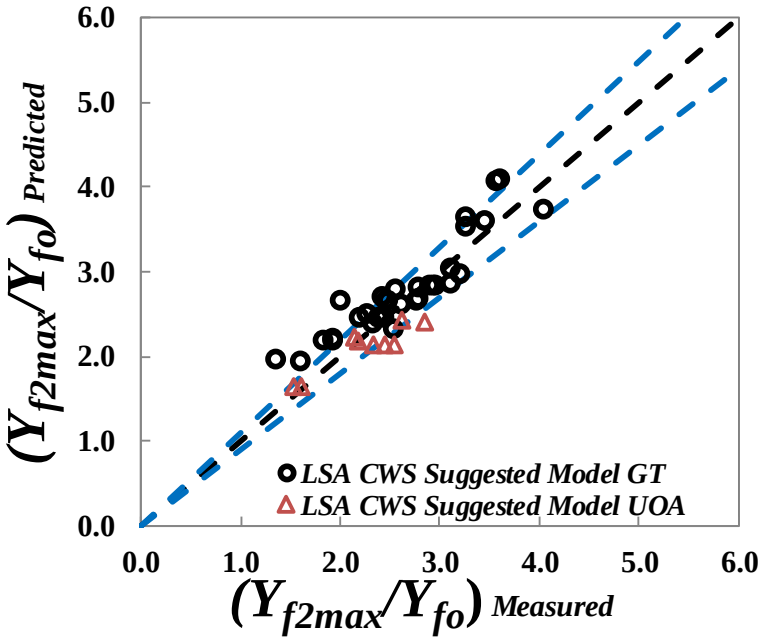

(b) Clear water interactive abutment and contraction scour prediction (Suggested model)

Figure 4-20 Comparison of clear water interactive abutment and contraction scour between HEC-18 and suggested model (LSA)

4.4. Interactive Abutment and Contraction Scour Prediction for BLA and SSA under CWS Conditions (Type-II Scour)

Hong (2013, 2015) analysis shows that interactive abutment and lateral contraction scour for a bankline abutment (BLA) is an amplification of the theoretical contraction scour given by Larson (1960). The model suggests an amplification factor (r_T) of 1.66 for CWS cases.

The similarity explained in Para 4.3 and Equation 4-4 also applies to BLA interactive abutment and contraction scour. Measurements of the experiments conducted for the current research for the dimensionless scour parameters and the normalized equilibrium interactive abutment and contraction scour for BLA are given in Table 4-4.

Table 4-4 Measured scour parameters and normalized equilibrium scour for BLA experiments

Run	*Flow Type*	L_a/B_f	*M/C*				Y_{m2max}/Y_{mo}
			q_2/q_1	Y_1/Y_o	V_1/V_c	Y_o (ft)	
1 GT	F	1.0	1.487	1.033	0.723	0.479	1.745
2 GT	SO	1.0	1.501	1.057	0.725	0.546	1.874
3 GT	OT	1.0	1.241	1.029	0.653	0.713	1.265
4 GT	F	1.0	1.452	1.061	0.841	0.476	1.708
5 GT	OT	1.0	1.140	1.043	0.823	0.716	1.585
6 GT	F	1.0	1.456	1.065	0.820	0.476	1.790
7 GT	OT	1.0	1.135	1.046	0.822	0.716	1.560
8 GT	F	1.0	1.456	1.063	0.820	0.476	1.668
9 GT	OT	1.0	1.137	1.045	0.822	0.716	1.501
10 GT	F	1.0	1.805	1.111	0.879	0.469	2.256
11 GT	SO	1.0	2.178	1.184	0.711	0.521	2.250
12 GT	OT	1.0	1.433	1.063	0.784	0.713	1.746
14 GT	F	1.0	1.945	1.111	0.878	0.469	2.102
15 GT	OT	1.0	1.372	1.066	0.784	0.713	1.736
16 GT	F	1.0	1.933	1.113	0.878	0.469	2.058
17 GT	OT	1.0	1.351	1.067	0.784	0.713	1.537
18 GT	F	1.0	1.419	1.051	0.712	0.546	1.749
19 GT	F	1.0	1.980	1.109	0.791	0.521	2.142
22 GT	F	1.0WW	1.451	1.031	0.723	0.479	1.952
23 GT	SO	1.0WW	1.501	1.057	0.725	0.546	1.660
24 GT	OT	1.0WW	1.175	1.028	0.653	0.713	1.305
25 GT	F	1.0WW	1.906	1.109	0.879	0.469	1.912
26 GT	SO	1.0WW	2.199	1.184	0.711	0.521	2.080
27 GT	OT	1.0WW	1.401	1.063	0.784	0.713	1.663
28 GT	SO	1.0	1.505	1.059	0.725	0.546	1.936
29 GT	SO	1.0	1.503	1.058	0.725	0.546	2.044
30 GT	SO	1.0	2.213	1.184	0.711	0.521	2.063
31 GT	SO	1.0	2.170	1.184	0.711	0.521	2.163
39 GT	F	1.0	1.454	1.069	0.820	0.476	1.948
40 GT	SO	1.0	1.503	1.058	0.725	0.546	1.962
41 GT	F	1.0	1.455	1.067	0.820	0.476	1.921
42 GT	SO	1.0	1.502	1.057	0.725	0.546	1.951
43 GT	F	1.0	1.542	1.053	0.831	0.474	1.889
44 GT	SO	1.0	1.482	1.056	0.726	0.571	1.923
45 GT	SO	1.0	1.417	1.052	0.682	0.581	1.878

Note: F = free flow, SO = submerged orifice flow, OT = overtopping flow, WW = wing-wall abutments, GT = Georgia Institute of Technology experiments.

The water depth in the main channel is higher as compared to the floodplain, which depends on the overbank flow (Y_{f1}/Y_{m1}). The scour hole for a bankline abutment develops in the main channel where the approach flow depth (Y_{m1}) is higher as compared to the floodplain; therefore, the backwater effect (Y_1/Y_o) is much less. Intuitively, the significance of the backwater effect (Y_1/Y_o) on the scour development should also be less as compared to other contributing parameters.

Regression analysis was applied to the data presented in Table 4-4 and the experimental results of Hong (2013) for BLA CWS experiments. Application of Hong model and modified Hong model (accounting for bottom TKE (K_b)) did not produce a good result and showed the biased residuals with higher standard error of the estimate. Application of Equation 4-4 by keeping theoretical contraction scour parameters as a single variable resulted in a better regression model with a coefficient of determination of 0.71 and standard error of the estimate of 0.151. The regression results also verified that the backwater (Y_1/Y_o) does not affect the scour in case of a bankline abutment. The model was adjusted within the standard error of the parameter, which gave minor adjustments in the coefficient of determination, and standard error of the estimate. The final model is given by:

$$\frac{Y_{m2\max}}{Y_{mo}} = 1.725 * \left(\frac{q_{m2}}{q_{m1}} * \frac{V_{m1}}{V_{mc1}} \right)^{1/2} \qquad (4\text{-}7)$$

Figure 4-21 shows the regression model for BLA abutment and contraction scour under clear water scour conditions. A comparison with the theoretical contraction scour (Theoretical CS) plotted in the figure shows a higher equilibrium scour as compared to theoretical contraction scour and the dotted black line shows the

extrapolation of the model results. The details of each regression are given in Table 4-5 and the summary is presented in Table 4-6. The lower limit for initiation of scour process determined by the model is $(V_{m1}/V_{mc}*q_{m2}/q_{m1}) = 0.20$.

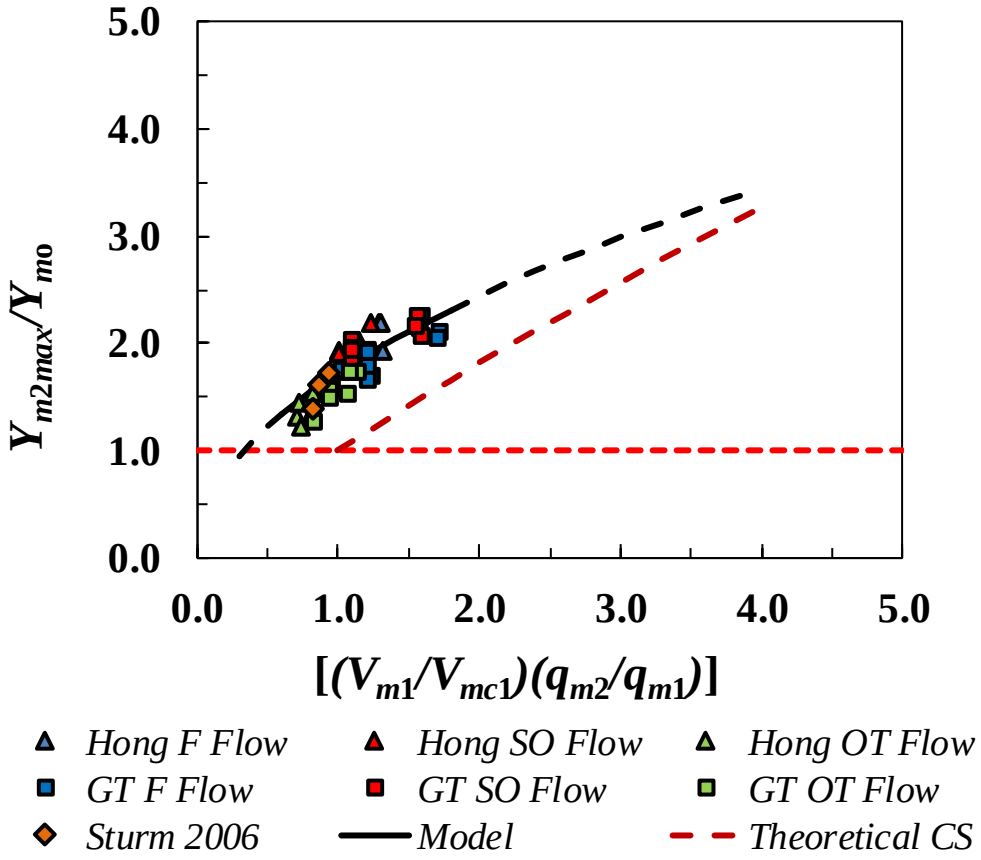

Figure 4-21 Suggested BLA regression model along with theoretical contraction scour

Table 4-5 Details of the regression analysis for BLA

Hong (2013) Model	$\frac{Y_{m2\max}}{Y_{mo}} = \left(\frac{Y_{m1}}{Y_{mo}}\right)^{1.0} * 1.66 * \left(\frac{V_{m1}}{V_{mc1}} * \frac{q_{m2}}{q_{m1}}\right)^{6/7}$		
R^2	-	SEE	0.319
Hong (2013) Modified Model	$\frac{Y_{m2\max}}{Y_{mo}} = \left(\frac{Y_{m1}}{Y_{mo}}\right)^{1.0} * \left(\frac{q_{m2}}{q_{m1}}\right)^{-0.12} * 1.75 * \left(\frac{V_{m1}}{V_{mc1}} * \frac{q_{m2}}{q_{m1}}\right)^{6/7}$		
R^2	-	SEE	0.292
Taking Theoretical Contraction Scour as single Variable	$\frac{Y_{m2\max}}{Y_{mo}} = \left(\frac{Y_{m1}}{Y_{mo}}\right)^{0} * 1.712 * \left(\frac{V_{m1}}{V_{mc1}} * \frac{q_{m2}}{q_{m1}}\right)^{0.55}$		
R^2	0.71	SEE	0.151
Standard Error of Parameters	Parameter	Value	SE
	Coefficient	1.712	0.025
	Exponent of $q_{m2}/q_{m1} * V_{m1}/V_{mc}$	0.55	0.056
Fixing the Powers Within Error Term	$\frac{Y_{m2\max}}{Y_{mo}} = 1.725 * \left(\frac{V_{m1}}{V_{mc1}} * \frac{q_{m2}}{q_{m1}}\right)^{0.50}$		
R^2	0.70	SEE	0.153
Standard Error of Parameters	Parameter	Value	SE
	Coefficient	1.725	0.026
	Exponent of $q_{m2}/q_{m1} * V_{m1}/V_{mc}$	0.50	0.093
Combined Regression of BLA, SSA	$\frac{Y_{m2\max}}{Y_{mo}} = 1.722 * \left(\frac{V_{m1}}{V_{mc1}} * \frac{q_{m2}}{q_{m1}}\right)^{0.50}$		
R^2	0.59	SEE	0.183
Standard Error of Parameters	Parameter	Value	SE
	Coefficient	1.722	0.004
	Exponent of $q_{m2}/q_{m1} * V_{m1}/V_{mc}$	0.50	0.091

Table 4-6 Summary of the regression results for BLA

Model	Best Fit Formula	R^2	SEE	Comments
Hong (2013) Model	$\frac{Y_{m2\max}}{Y_{mo}} = \left(\frac{Y_{m1}}{Y_{mo}}\right)^{1.0} * 1.66 * \left(\frac{V_{m1}}{V_{mc1}} * \frac{q_{m2}}{q_{m1}}\right)^{6/7}$	-0.35	0.319	
Hong (2013) Modified Model	$\frac{Y_{m2\max}}{Y_{mo}} = \left(\frac{Y_{m1}}{Y_{mo}}\right)^{1.0} * \left(\frac{q_{m2}}{q_{m1}}\right)^{-0.12} * 1.75 * \left(\frac{V_{m1}}{V_{mc1}} * \frac{q_{m2}}{q_{m1}}\right)^{6/7}$	-0.13	0.292	
Taking Theoretical Contraction Scour as Single Variable	$\frac{Y_{m2\max}}{Y_{mo}} = \left(\frac{Y_{m1}}{Y_{mo}}\right)^{0} * 1.712 * \left(\frac{V_{m1}}{V_{mc1}} * \frac{q_{m2}}{q_{m1}}\right)^{0.55}$	0.71	0.151	
Fixing the Powers Within Error Term	$\frac{Y_{m2\max}}{Y_{mo}} = 1.725 * \left(\frac{V_{m1}}{V_{mc1}} * \frac{q_{m2}}{q_{m1}}\right)^{0.50}$	0.70	0.153	Suggested Model
Combined Regression of BLA, SSA	$\frac{Y_{m2\max}}{Y_{mo}} = 1.722 * \left(\frac{V_{m1}}{V_{mc1}} * \frac{q_{m2}}{q_{m1}}\right)^{0.50}$	0.59	0.183	

The BLA CWS model of interactive abutment and contraction was applied to the short-setback abutments (SSA) for the set of experiments conducted at the Georgia Institute of Technology and the University of Auckland for which the measured scour variables and measured normalized equilibrium scour is presented in Table 4-7. BLA CWS interactive abutment and contraction scour model fits well with the SSA CWS experimental results as shown in Figure 4-22 (This includes experiments conducted by Hong (2013) as well). Figure 4-23 shows the residual plot for the BLA and SSA experiments where the SSA experiments show a higher scatter as compared to BLA, possibly because of the reason that the scour hole covers the area both in the main channel and in the floodplain for short-setback abutments. The standard error of the estimate (SEE) for SSA was 0.205. This higher error is attributed to experimental

uncertainty, lower number of experiments, and existence of scour hole partly both in the floodplain and the main channel.

Table 4-7 Measured scour parameters and normalized equilibrium scour for SSA experiments

Run	***Flow Type***	L_a/B_f	***M/C***				Y_{m2max}/Y_{mo}
			q_2/q_1	Y_1/Y_o	V_1/V_c	Y_o (ft)	
1 UOA	FS	0.8	1.389	1.044	0.750	0.523	1.492
2 UOA	SO	0.8	1.507	1.058	0.796	0.625	2.073
3 UOA	OT	0.8	1.382	1.006	0.712	0.856	1.887
4 UOA	FS	0.8	1.358	1.052	0.980	0.538	2.027
5 UOA	SO	0.8	1.653	1.065	0.912	0.686	2.304
6 UOA	OT	0.8	1.481	1.053	0.858	0.812	2.352
7 UOA	OT	0.8	1.460	1.051	0.893	0.894	2.206
8 UOA	OT	0.8	1.412	1.028	0.605	0.887	1.667
9 UOA	FS	0.8	1.450	1.003	0.747	0.578	1.951
22 UOA	OT	0.8WW	1.492	1.000	0.717	0.737	2.080
23 UOA	FS	0.8WW	1.406	1.023	0.789	0.554	2.081
24 UOA	OT	0.8WW	1.490	1.005	0.495	0.841	1.336
25 UOA	OT	0.8WW	1.421	1.026	0.759	0.891	1.915
11 GT	SO	0.77	2.178	1.184	0.711	0.521	2.096

Note: F = free flow, SO = submerged orifice flow, OT = overtopping flow, WW = wing-wall abutments, GT = Georgia Institute of Technology experiments, and UOA = University of Auckland experiments

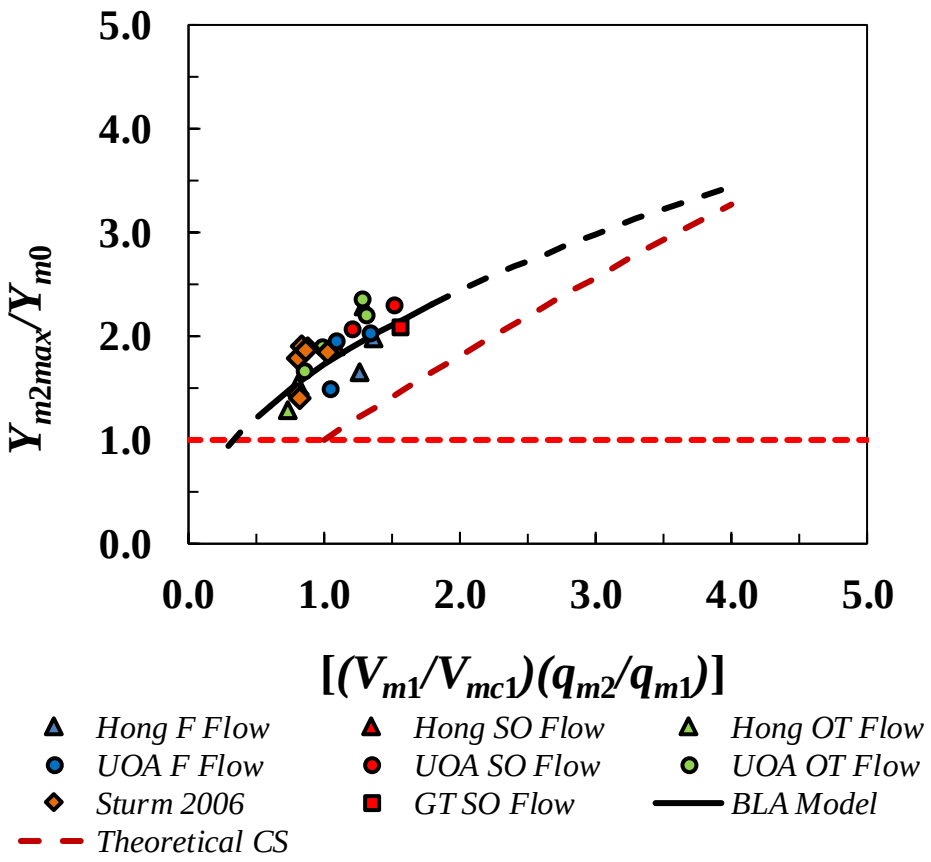

Figure 4-22 Suggested BLA CWS interactive abutment and contraction scour model applied to SSA CWS experiments

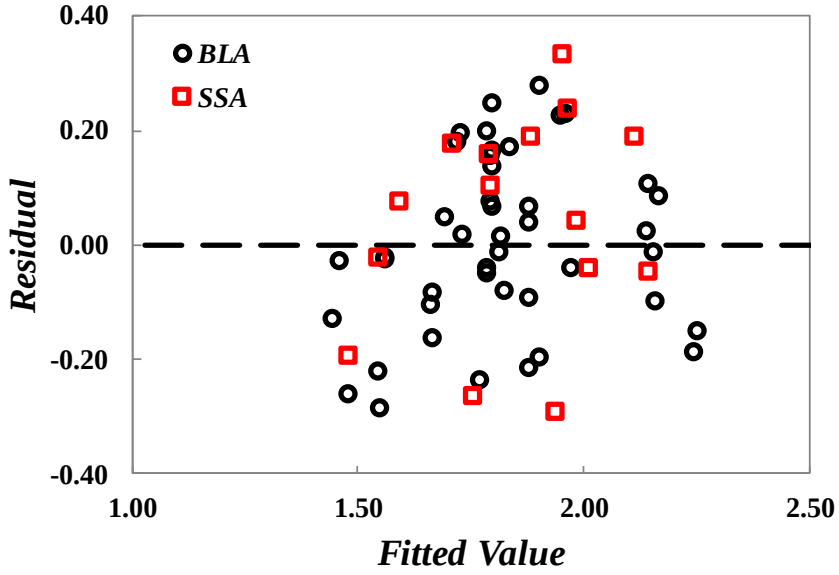

Figure 4-23 Residuals of the fitted values for the interactive abutment and contraction scour suggested model LSA

4.4.1. *Wing-Wall Abutments BLA/SSA (Type –II Scour)*

Experiments were also conducted for the wing-wall abutments under the same flow conditions as that of spill-through abutments to make a comparison of wing-wall and spill-through abutments. Experiments were conducted for all three types of flows (F, SO, and OT flows) and for three different abutment ratios with L_a/B_f = 0.77, 0.80, and 1.0 (experiments for L_a/B_f = 0.80 were conducted at the University of Auckland). Table 4-4 and Table 4-7 show the measured scour parameters and normalized equilibrium scour for wing-wall abutment experiments for BLA and SSA, respectively (where "WW" shows the wing-wall experiments). It was found that wing-wall abutments also follow the CWS BLA model for interactive abutment and contraction scour with a little more scatter (this little higher scatter can be attributed to limited number of experiments).

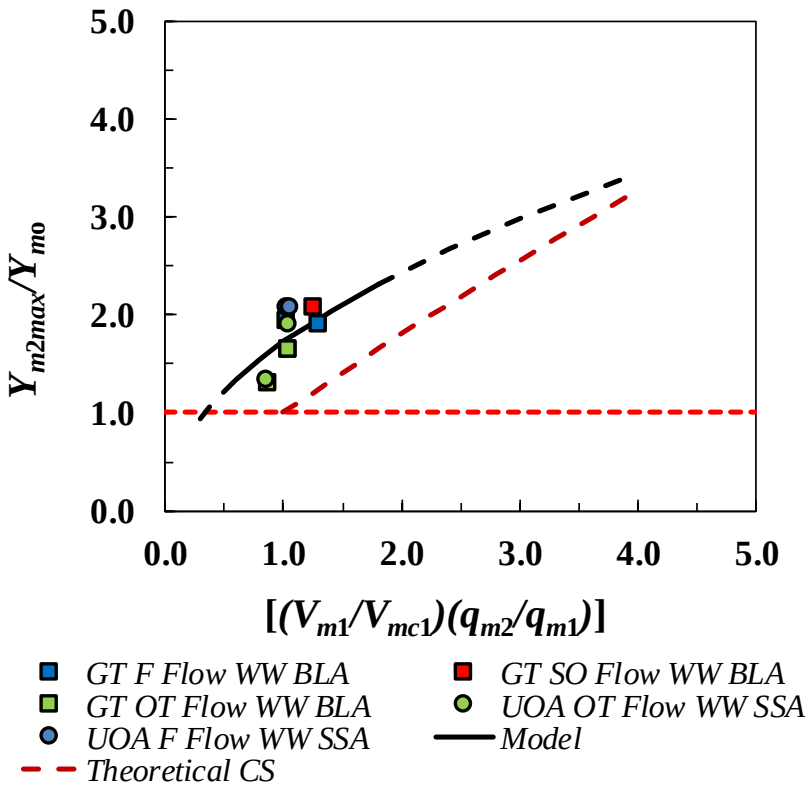

Figure 4-24 Comparison of wing-wall abutment experiments with CWS BLA interactive abutment and contraction scour model

4.4.2. *Comparison of HEC-18 Model with Suggested Interactive Abutment and Contraction Scour Model for BLA/SSA (Type-II Scour)*

The interactive scour development is affected by simultaneous development of different scour components, which affects the total interactive scour. This results in a smaller equilibrium scour than the arithmetic sum of the scour components recommended by HEC-18. A comparison of the HEC-18 and suggested model is shown in Figure 4-20 for BLA/SSA. The scour components for HEC-18 have been calculated by equations suggested in HEC-18 where contraction scour for CWS uses the equation derived from Laursen (1963) contraction scour theory (Equation 2-6);

vertical contraction scour uses the equation based on flow separation thickness under the bridge (equation 2-14) (Shen et al. 2012); and abutment scour comes from the Froehlich equation (Equation 2-28). Abutment scour is the most significant contributor to the total scour with an average of about 78% of the total scour, vertical contraction scour as 15%, and contraction scour as 7% of the total scour as per HEC-18 methodology calculations. HEC-18 predicts much higher values as compared to the suggested model, which predicts the interactive abutment and contraction scour for BLA/SSA within 10% of physical measurements.

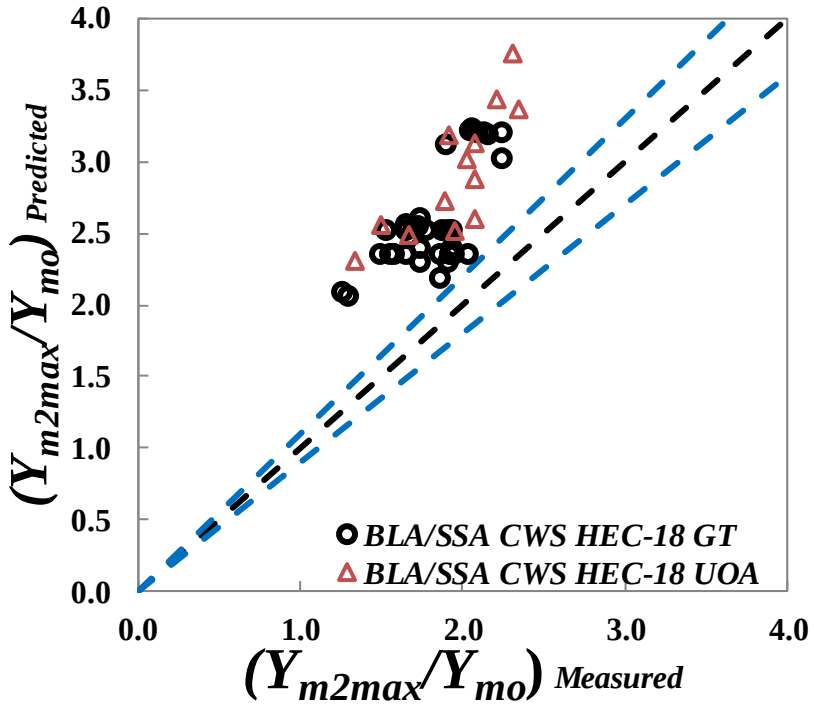

(a) Clear water interactive abutment and contraction scour prediction BLA/SSA HEC-18

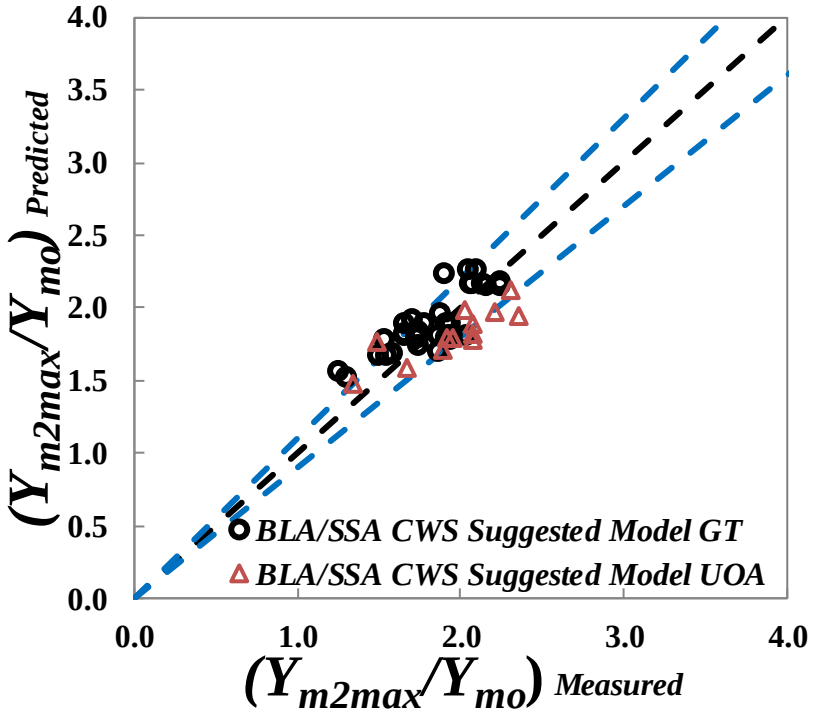

(b) Clear water interactive abutment and contraction scour prediction BLA/SSA – suggested model

Figure 4-25 Comparison of clear water interactive abutment and contraction scour between HEC-18 and suggested model (BLA/SSA)

4.5. Comparison of the Suggested Models with Field Examples

Towaliga River flood for Tropical Storm Alberto (1994) was reproduced in the hydraulics laboratory of the Georgia Institute of Technology as mentioned in Para 2.13. The flood was submerged orifice flow case with erodible embankment in a compound channel with a long setback abutment on one side and a bankline abutment on the other side. The field scour measurements and the scour parameter measurements from the laboratory model based on Froude number similarity show good agreement with the suggested model.

Missouri River flood (1993) at Interstate 70 near Rocheport, Missouri, for a long setback solid wall abutment with field scour measurements after the flood event and available flow and scour parameters at the peak of flood event (calculated, based on the upstream gauging station data) also show an agreement with the suggested model. The presence of solid wall tend to follow the extrapolated dash-line of the model.

The other two field examples are for April 1997 flood of Highway 22 at Pomme de Terre River in Swift County in Minnesota and Highway 12 (wing-wall abutment bridge) in the same area 10 kilometers downstream of Highway 22. In both the cases, the field scour measurements and scour/hydraulic parameters measurements from the WSPRO model obtained from Sturm (2004) and Mueller and Wagner (2005) have been used to compare with the suggested model.

Details of the field scour examples along with the source of measurements for the hydraulic parameters and the predicted/ measured values are summarized in Table 4.8. The equilibrium scour depths for LSA (Towaliga River and Missouri River) have been plotted on the suggested model of interactive abutment and contraction scour for LSA as shown in Figure 4-26. The equilibrium scour for BLA (Towaliga River, Highway 12, and Highway 22) have been plotted on the suggested model of interactive abutment and contraction scour for BLA as shown in Figure 4-27. The field measurements for all four cases have been captured within 10% accuracy by the suggested model as shown in Figure 4-28 with the predicted value a little higher than the observed, thus giving a conservative estimate of the equilibrium scour.

Table 4-8 Details of the field examples data

Event	Method of Hydraulic parameter measurement	Scour measurements	Abutment type	Flow type	Y_{max} (*ft*) Predicted/ measured	Abutment length/ Category
Towaliga River storm Alberto 1994	Physical model (Hong and Sturm 2010)	Field/ after flood	Erodible Spill-through	SO flow	31.7/ 30.9 (F/P) 37.6/36.8 (M/C)	LSA & BLA/ Category I & II
Pomme de Terre River flood 1997 (Highway 22)	WSPRO (Sturm 2004)	Field/ after flood	Erodible Spill-through	F flow	20.9/19.8	BLA/ Category II
Pomme de Terre River flood 1997 (Highway 12)	WSPRO (Sturm 2004)	Field/ after flood	Wing-wall abutment	F flow	29.8/29.5	BLA/ Category II
Missouri River flood 1993	Field (extracted from u/s gauging station and post-flood field reconnaissance)	Field/ after flood	Solid wall abutment with guide bank	F flow	20.8/21.3	LSA/ Category I

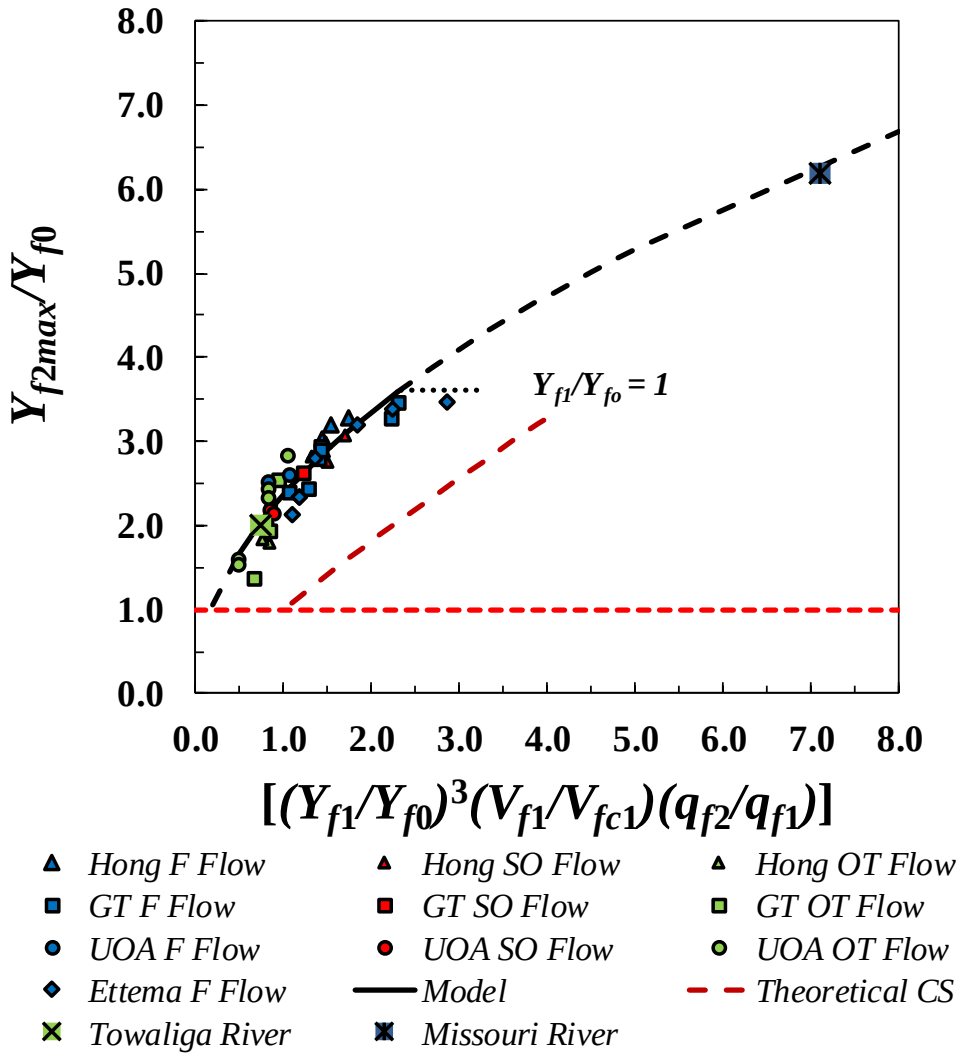

Figure 4-26 LSA field examples plotted with suggested model

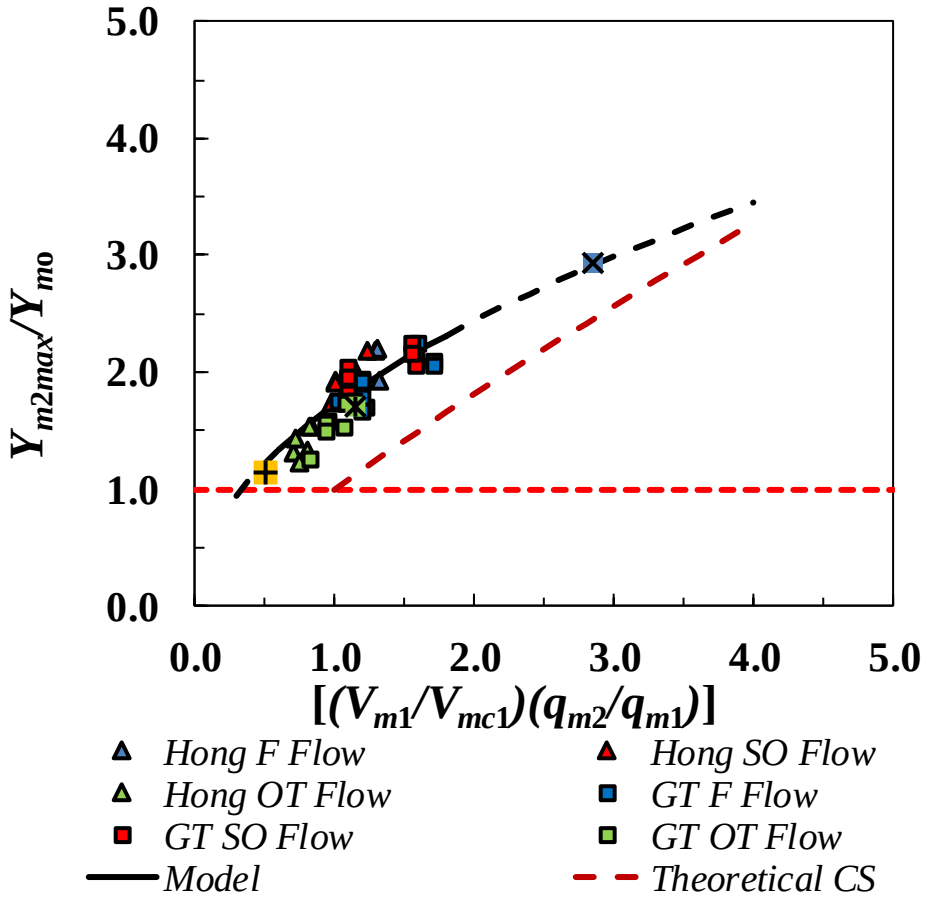

Figure 4-27 BLA field examples plotted with suggested model

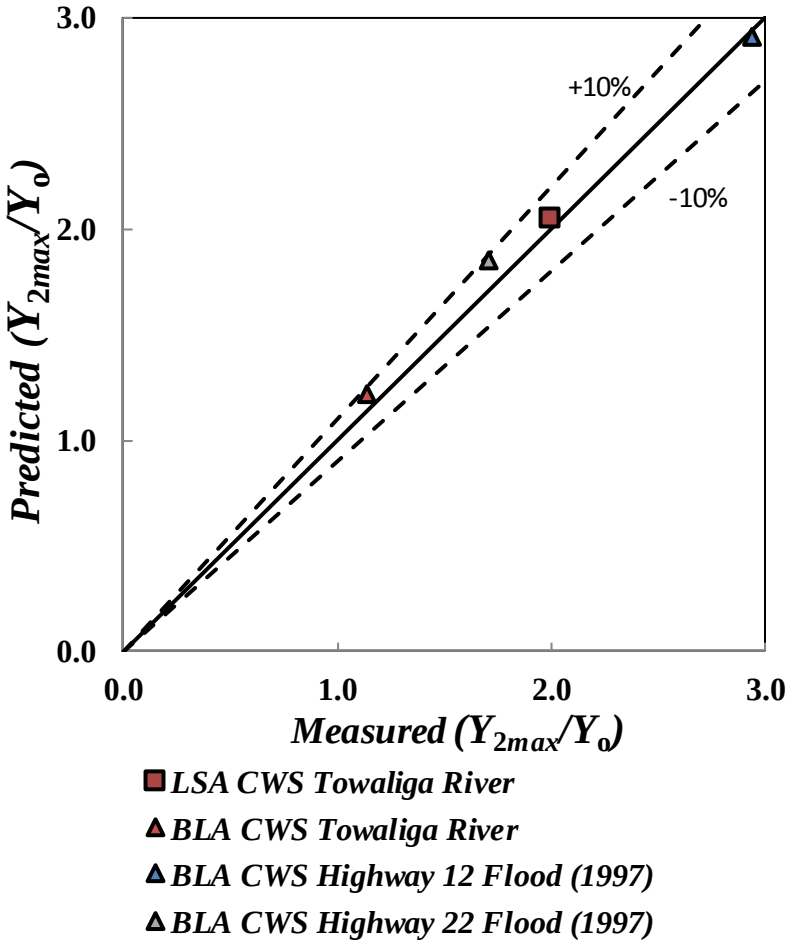

Figure 4-28 Measured vs predicted values of all field examples LSA and BLA

CHAPTER V

ANALYSIS OF INTERACTION OF PIER SCOUR WITH OTHER COMPONENTS OF SCOUR

5.1. Introduction

In a bridge contraction, in addition to the interaction of abutment and contraction (both lateral and vertical contraction) scour components, pier in the zone of abutment and contraction scour also contributes to the total interactive scour. This chapter deals with the interaction of other scour components with pier scour. This includes category III (abutment and contraction scour interaction with pier scour in floodplain) and category IV (interaction of pier and vertical contraction scour) as described in Table 3.5, for which experiments were conducted to capture the respective scour interactions.

5.2. Individual Scour Component Models

Researchers have analyzed individual scour components over the last few decades and numerous scour prediction models are available for the experimental studies; some of those include field observations. The details have already been discussed in Chapter 2. Pier scour models have developed and crystalized the most over this time period and they are generally viewed as giving a higher degree of

accuracy in scour prediction than for other types of scour. However, vertical contraction scour is a relatively new topic for which comparatively fewer research models are available. It occurs when bridges are subject to submerged orifice flow or overtopping during extreme floods. Researchers have focused on providing an envelope approach to cover the larger scatter and variability in vertical contraction scour measurements.

5.2.1. *Pier Scour*

Numerous pier scour models are available; however, HEC-18 recommends the Colorado State University equation (CSU Equation) and Sheppard and Melville equation (S & M Equation). The equations were developed from a large data set and cover a wide range of parameters. In the current research, a few experiments were designed to capture the individual pier scour component in order to validate the observations of the current experimental setup with pier scour models recommended by HEC-18. The measured normalized scour depth relative to the pier width, $(d_{se}/a)_{measured}$, is plotted against the calculated normalized scour, $(d_{se}/a)_{calculated}$, in Figure 5-1 for both the equations recommended by HEC-18. It was observed that experimental results fall within 10% of the model values for both CSU equation and S & M equation, which validates the current experimental set up with respect to recommended models.

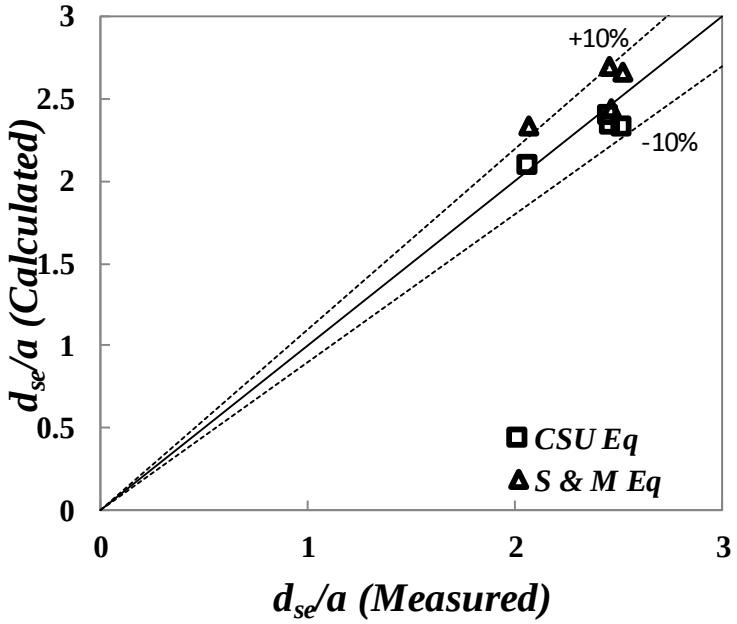

Figure 5-1 Normalized pier scour comparison of the measured and calculated values for CSU equation and S & M equation for the experiments conducted for current research

5.2.2. *Vertical Contraction Scour*

Models for vertical contraction scour, as discussed in Para 2.10.2, generally take the approach flow intensity (V_1/V_c) variable as the vertical contraction scour parameter as most researchers have conducted the experiments without any lateral contraction. However, in case of a bridge contraction where the lateral contraction is caused by the embankment, the result is a much higher flow intensity in the contracted section (V_b/V_c) as compared to that caused by a vertical contraction only. This higher contracted section flow intensity (V_b/V_c) produces a higher value of the vertical contraction scour as compared to the vertical contraction scour without lateral contraction for the same approach flow intensity (V_1/V_c).

Lyn (2008) used contracted section flow intensity (V_b/V_c) for his model and gave the envelope curve which was further modified by a higher envelope curve for the experiments conducted with piers. Experiments conducted for the current study were designed such that individual vertical contraction scour component was captured in most of the experiments. Experiments were also conducted at the University of Auckland (UOA) for vertical contraction scour, which included both clear water and live-bed scour conditions (Melville 2017).

Experiments for the current study were compared with Lyn model as shown in Figure 5-2. The comparison shows that the Lyn Model (marked as black line in the figure) does not serve as an envelope for all the experimental observations. In particular, data points with a contracted section flow intensity (V_b/V_c) near the boundary line between clear water and live-bed conditions ($0.8< V_b/V_c <1.3$) do not fall under the envelope curve. However, the Lyn modified model (shown as dark brown line in the figure) envelopes all the experimental results including experiments used by Lyn for his model envelope curve (data of experiments conducted by Arneson (1997)), clear water scour experiments at the Georgia Institute of Technology, clear water scour experiments by Shan et al. (2012), clear water scour experiments at the University of Auckland, and live-bed scour experiments at the University of Auckland. Therefore, Lyn modified model has been adopted for vertical contraction scour for this study.

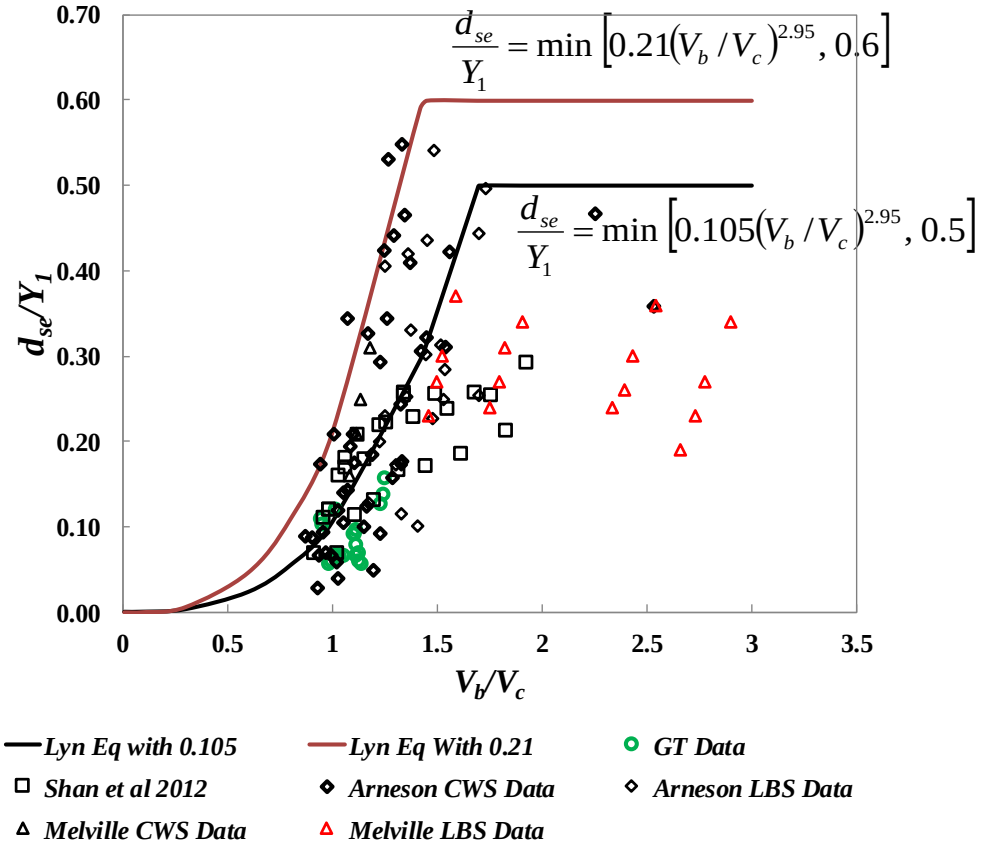

Figure 5-2 Comparison of normalized vertical contraction scour with Lyn (2008) model and modified model (also includes Arneson data)

5.3. Scour Measurements and Qualitative Observations

Experiments conducted without piers were repeated with different pier locations for all three types of flows (F, SO, and OT flows) with the pier located near the abutment and displaced away from the abutment such that it remains in the area of influence of the abutment and contraction scour hole. The pier location was set as L_p/W = 0.18 and 0.35 for L_a/B_f = 0.41 and in case of L_a/B_f = 0.77, the pier location was set as L_p/W = 0.40 and 1.0.

It was observed that the size of the scour hole at equilibrium conditions as a result of addition of the pier scour component was slightly less in cases where the pier

was located closer to the abutment. Pier presence channelized the high velocity zone between the abutment and the pier (channelization of high velocity will be shown in the subsequent discussion of depth-averaged velocity distribution) which helped reduce the extent of the scour hole. This phenomenon also affected the shape of the scour hole by drifting the downstream side of the scour hole closer to and curved around the abutment in comparison to the experiments without piers. In case of the pier located sufficiently away from the abutment (still in the zone of influence), the size of the scour hole increased for total interactive scour (Type III). Figure 5-3 shows a comparison of the equilibrium scour hole for a free flow case for L_a/B_f =0.41, with a pier (at two different locations) and without a pier. For combined pier and vertical contraction scour (Type IV), the extent of the scour hole increased as there was no geometric confinement involved to channelize or restrict the high velocity flow; thus, the deepening of the scour hole by addition of two types of scour (pier and vertical contraction scour) increased the extent of the scour hole.

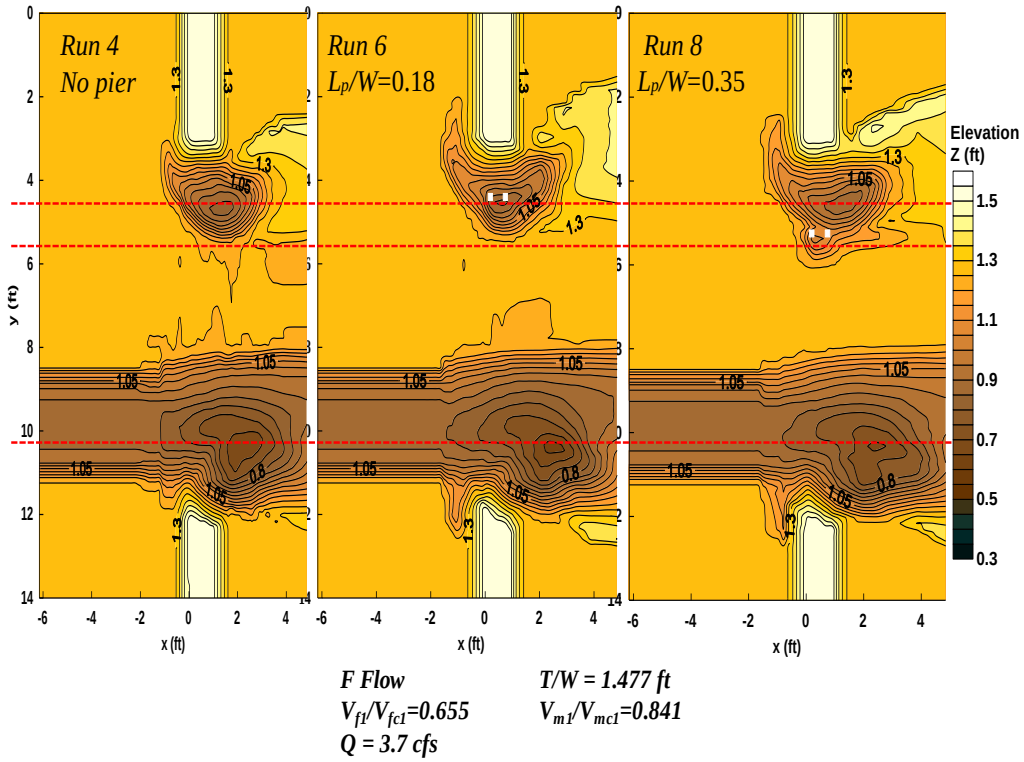

Figure 5-3 Run 4, 6, and 8 (F flow cases) showing the effect of the pier on shape and size of the abutment scour hole

For isolated pier scour, the upstream edge of the upstream pier is the deepest point of the scour hole. In contrast, the deepest point in abutment and contraction scour varies depending on the scour parameters. Thus, the interaction of pier scour with abutment and contraction scour results in two distinct points of interest. One point of interest is the effect of abutment and contraction scour on pier scour (this accounts for the scour at the upstream edge of the upstream pier). The other point of interest is effect of pier scour on abutment and contraction scour (this accounts for the deepest point of the scour hole anywhere other than the pier upstream edge). Figure 5-4 gives a pictorial representation of these two cases of interactive abutment and contraction scour with pier scour.

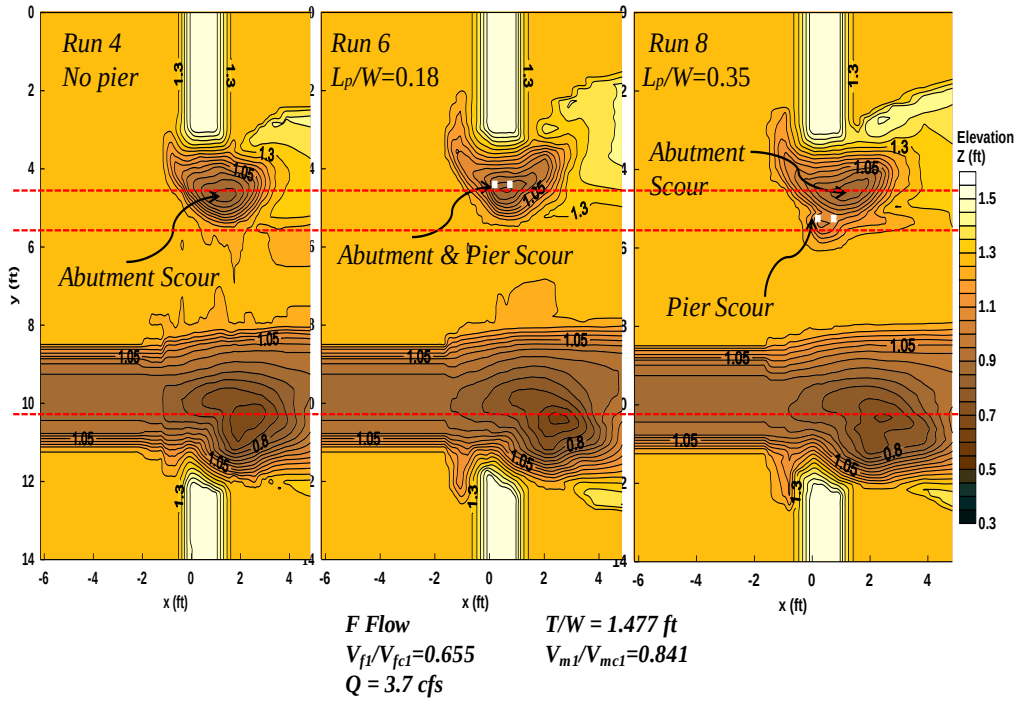

Figure 5-4 Interactive pier scour with abutment and contraction scour showing the effect of abutment and contraction scour on pier scour and effect of pier on abutment and contraction scour

Effect of Pier Location and Riprap Armoring on Pier Scour in the Influence of Abutment and Contraction Scour Hole:

For a pier located in the area of influence of the abutment and contraction scour hole, the magnitude of the scour at the upstream end of the pier is observed to be higher than the abutment and contraction scour at the same location (for the case without pier). This increase in scour is because of the flow dynamics around the pier and the high velocity flow trapped between abutment and the pier. Figure 5-5 gives a pictorial representation of this observation. The initial bed elevation is compared with the measured equilibrium scour bed elevation at the cross section of the upstream edge of the pier. The comparison is made for an SO flow case in Run 2, 28, and 29, which

is without pier, pier located close to the abutment, and pier located away from the abutment, respectively, for L_a/B_f =0.41.

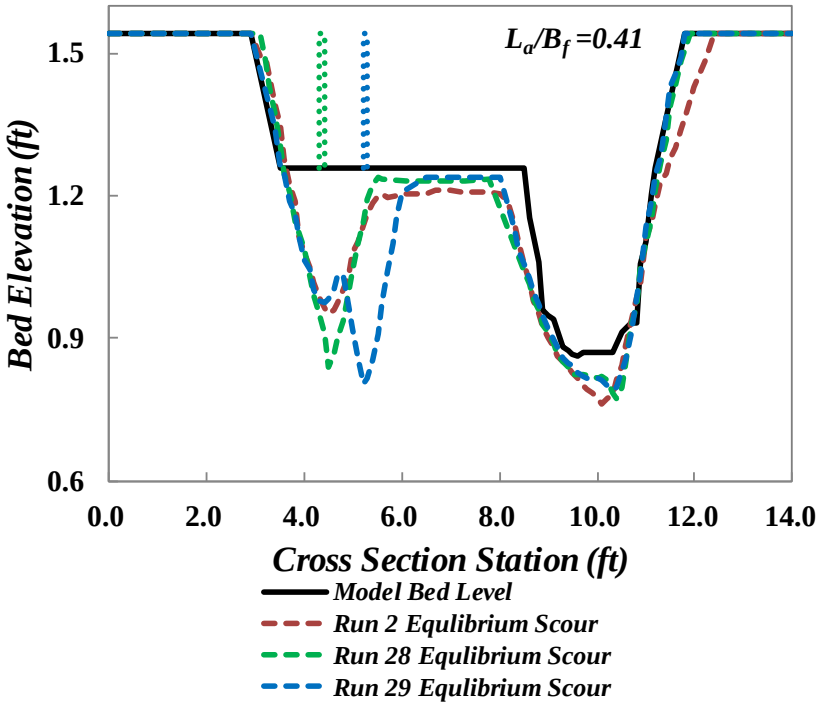

Figure 5-5 Effect of pier on equilibrium scour depth at pier upstream cross section, SO flow, L_a/B_f = 0.41, V_{f1}/V_{fc} =0.589, V_{m1}/V_{mc} =0.725 (Pier is color coded with scour line)

For the interaction of abutment and contraction scour with pier scour, where the pier location is closer to the abutment, the upstream face of the pier was the deepest point of the scour hole for the initial phase of the experiment. Depending on the flow parameters, including the approach flow intensity (V_1/V_c) and unit discharge contraction ratio (q_2/q_1), the deepest point of scour moved across the pier away from the abutment as time progressed. The riprap apron also started to accumulate around the pier giving an armoring effect, which resulted in less scour at the upstream end of the pier. In the experiments where the pier was relatively far away from the abutment,

the scour at the upstream end of the pier increased, and the armoring effect also diminished as less riprap material was able to accumulate around the pier. For a pier location sufficiently far away from the abutment such that no riprap material collapsed around the pier, initially the pier was the deepest point of the scour hole, but as the scour developed the abutment scour also started to get deep enough to be comparable with the pier scour depth. Bed elevation contours and photographs of the bed for the cases of no pier, pier near the maximum depth in the abutment and contraction scour hole, and pier at the outer edge of the abutment and contraction scour hole are shown in Figure 5-6 and Figure 5-7 for OT and SO flow, respectively.

Effect of Pier and its Location on Interactive Abutment and Contraction Scour Hole: Pier location not only affects the magnitude of the scour hole depth but also the location of the scour hole. For a pier location relatively close to the abutment, the deepest point of the abutment and contraction scour hole is laterally across from the pier away from the abutment. The pier presence and higher scour magnitude at the pier upstream edge shifts the streamwise location of the point of deepest scour of the abutment and contraction scour hole in the upstream direction. However, no significant effect is observed for the transverse direction of the point of deepest scour (in comparison to the scour location without pier).

The relocation of the pier further away from the abutment shifts the deepest point of interactive abutment and contraction scour in the zone between pier and abutment. The flow dynamics around the pier and the high velocity flow trapped between the abutment and the pier act to elongate the scour hole in the streamwise direction; thus, the streamwise location of the point of deepest abutment and

contraction scour also shifts in the downstream direction as compared to the case without pier, for the same experimental conditions. No change in the transverse component of the location of point of deepest scour is observed. In addition to the effect of riprap on the pier scour interaction, Figure 5-6 and Figure 5-7 show the effect of pier location on the deepest point of abutment and contraction scour for OT flow and SO flow, respectively.

At the stage where the abutment and contraction scour deepest point shifts in the zone between abutment and the pier, the interactive pier scour (at upstream edge of the pier) and the interactive abutment and contraction scour (deepest point of the abutment and contraction scour hole) magnitudes at the equilibrium condition become comparable. However, separate distinct points of deepest scour at the two locations exist within the same scour hole (refer to Figure 5-6 and Figure 5-7).

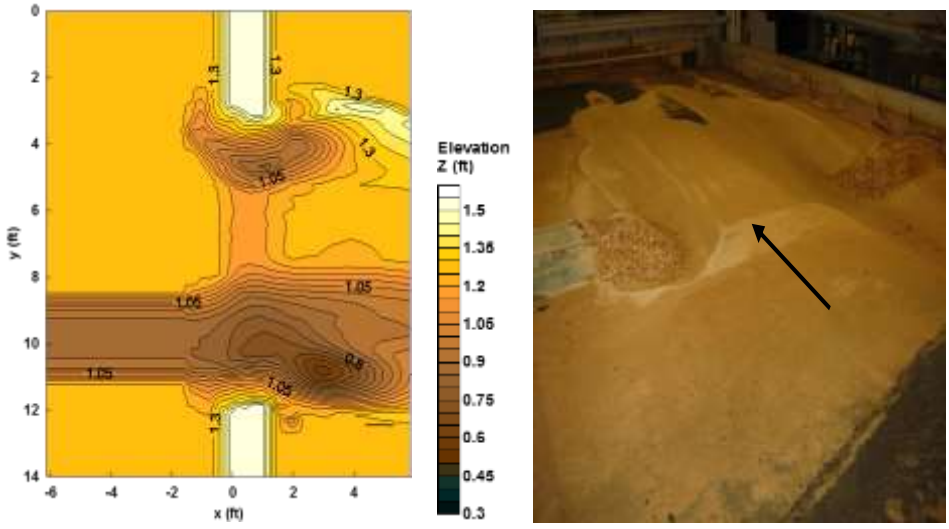

(a) Run 5 OT flow, without pier, L_a/B_f = 0.41, V_{f1}/V_{fc} =0.683, V_{m1}/V_{mc} =0.823

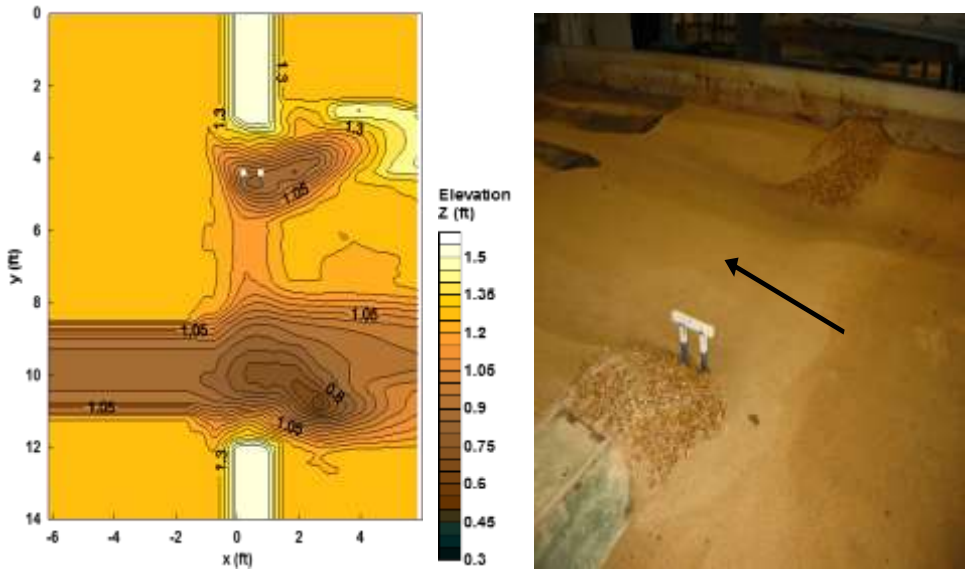

(b) Run 7 OT flow, L_p/W = 0.18, L_a/B_f = 0.41, V_{f1}/V_{fc} =0.683, V_{m1}/V_{mc} =0.823

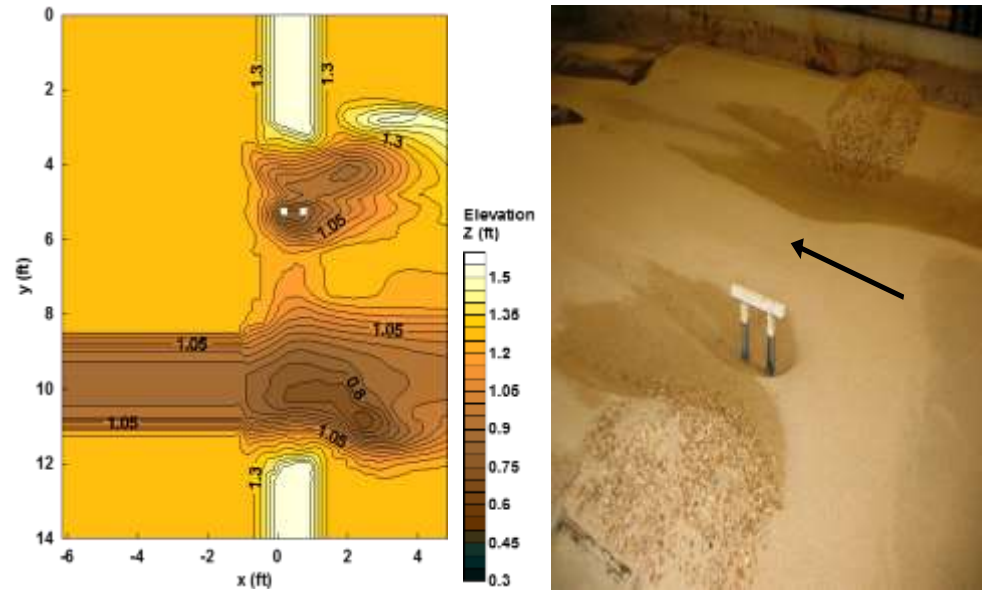

(c) Run 9 OT flow, L_p/W = 0.35, L_a/B_f = 0.41, V_{f1}/V_{fc} =0.683, V_{m1}/V_{mc} =0.823

Figure 5-6 Armoring effect of riprap on interactive pier scour in an abutment and contraction scour hole (Run 5, 7, and 9 with L_a/B_f = 0.41, V_{f1}/V_{fc} =0.683, V_{m1}/V_{mc} =0.823)

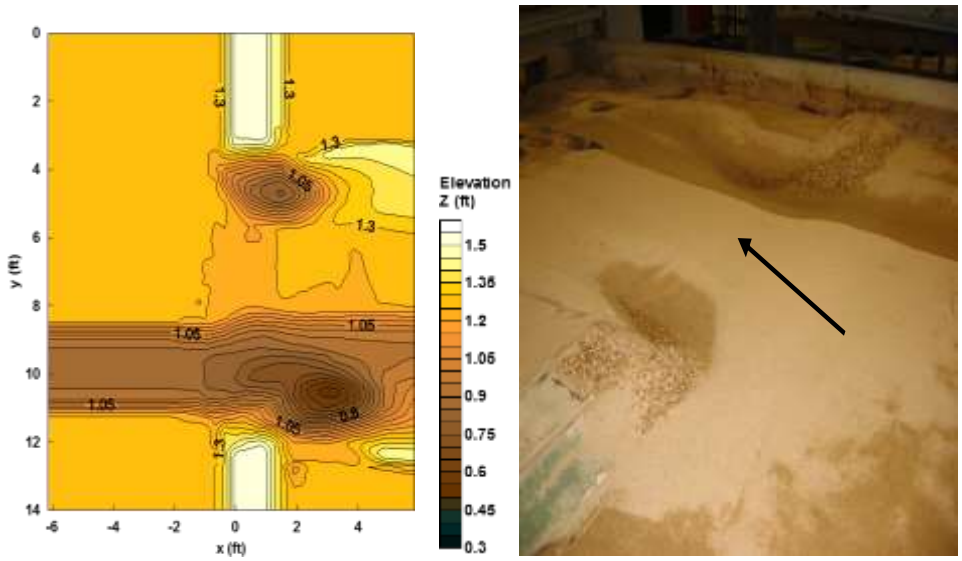

(a) Run 2 SO flow, without pier, L_a/B_f = 0.41, V_{f1}/V_{fc} =0.589, V_{m1}/V_{mc} =0.725

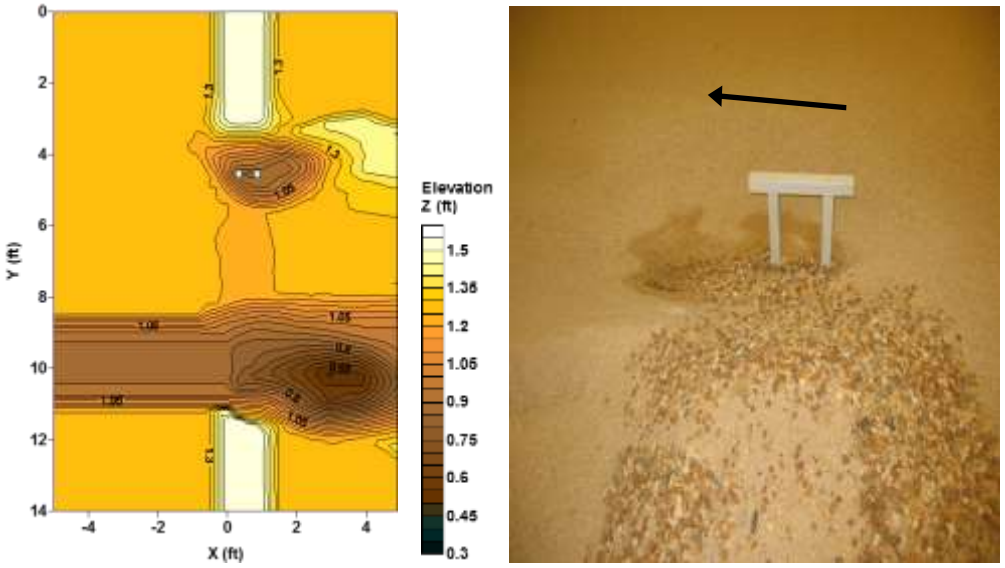

(b) Run 28 SO flow, L_p/W = 0.18, L_a/B_f = 0.41, V_{f1}/V_{fc} =0.589, V_{m1}/V_{mc} =0.725

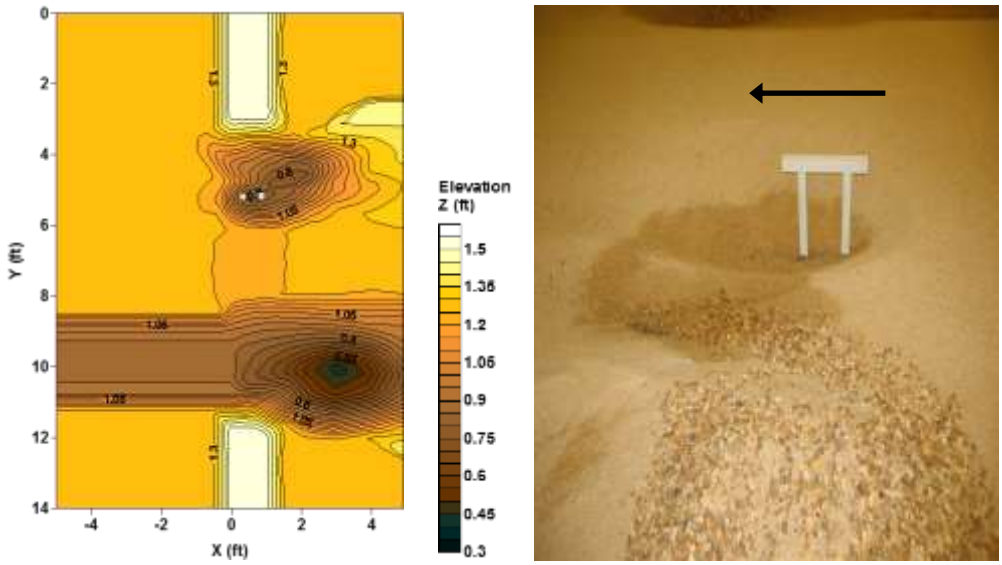

(c) Run 29 SO flow, L_p/W = 0.35, L_a/B_f = 0.41, V_{f1}/V_{fc} =0.589, V_{m1}/V_{mc} =0.725

Figure 5-7 Effect of pier location on deepest point of abutment and contraction scour hole

5.4. Velocity and Turbulence Measurements

Depth-averaged velocity profiles were measured at regular intervals both in the floodplain and in the main channel, in the approach and in the test section. In each vertical profile, 8 -10 measurements of the velocity were taken for the floodplain and 12-15 measurements for the main channel. In the approach section, the velocity profiles are the same as that of the experiments without piers as the addition of a pier does not affect the approach flow section. The relative approach velocity of the floodplain to the main channel (V_{f1}/V_{m1}) increases with increase in the depth ratio (Y_{f1}/Y_{m1}) of the floodplain to the main channel which results in an increase of the relative discharge per unit width (q_{f1}/q_{m1}) between the floodplain to the main channel (Already shown in chapter 4 as Figure 4-5). Depth-averaged pier approach velocity was also measured immediately upstream of the pier, and the highest depth-averaged

approach velocity was used for pier scour prediction which was at four pier-widths upstream of the edge of the upstream pier.

In a contracted section velocity, the presence of the pier affects the flow converging near the abutment by channelizing the flow into the area between abutment and the pier resulting in a higher velocity and reducing the width of the flow separation zone along the abutment face. The relocation of the pier further away from the abutment eases out the channelized flow, still giving a high velocity flow in the channelized region. The comparison of the depth-averaged velocity profile in the contracted section at the downstream edge of the bridge (with and without pier) is shown in Figure 5-8. This high velocity region coupled with the flow dynamics around the pier results in a higher scour in this region. However, the contribution of the armoring effect of the riprap slows down the time development of the scour as well as the magnitude of the equilibrium scour at the upstream end of the pier. For the pier moved laterally away from the abutment, where the pier upstream edge is free of riprap material, a higher scour depth is observed with a faster time development.

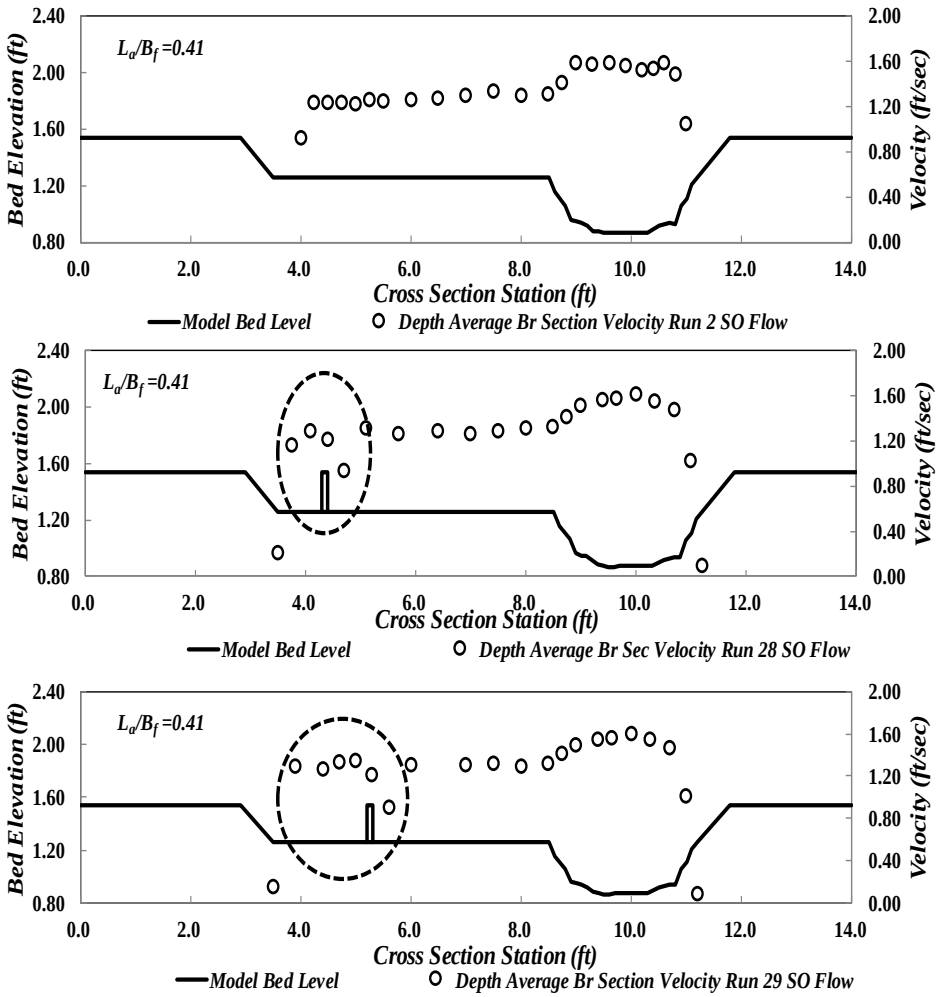

Figure 5-8 Effect of pier presence and location on velocity profile at bridge downstream end, SO flow, L_a/B_f = 0.41, V_{f1}/V_{fc} =0.589, V_{m1}/V_{mc} =0.725

Measurements of TKE near the bed were taken at section 4 (downstream edge of the bridge) and section 5 (downstream toe of the abutment) for all the experiments conducted with a pier. However, TKE measurements at 20% and 40% of the depth from the initial bed level were also taken for a few experiments at section 5. It was found that bottom TKE (K_b) was higher at section 5, however, the point value at the location immediately downstream of the pier was much higher at section 4 than at section 5 which makes normalized width averaged bottom TKE (K_b/u_{*c}^2) comparable for section 4 and section 5. This observation is different from the experiments

conducted without a pier. However, the comparable magnitude still allows the use of bottom TKE (K_b) at section 5 for consistency. Comparison of bottom TKE normalized by the square of critical shear velocity (K_b/u_{*c}^2) for Run 28 (SO Flow, L_a/B_f =0.41), between section 4 and section 5 and comparison of near bed measurements with 20% and 40% depth from bed level is presented in Figure 5-9 and Figure 5-10, respectively.

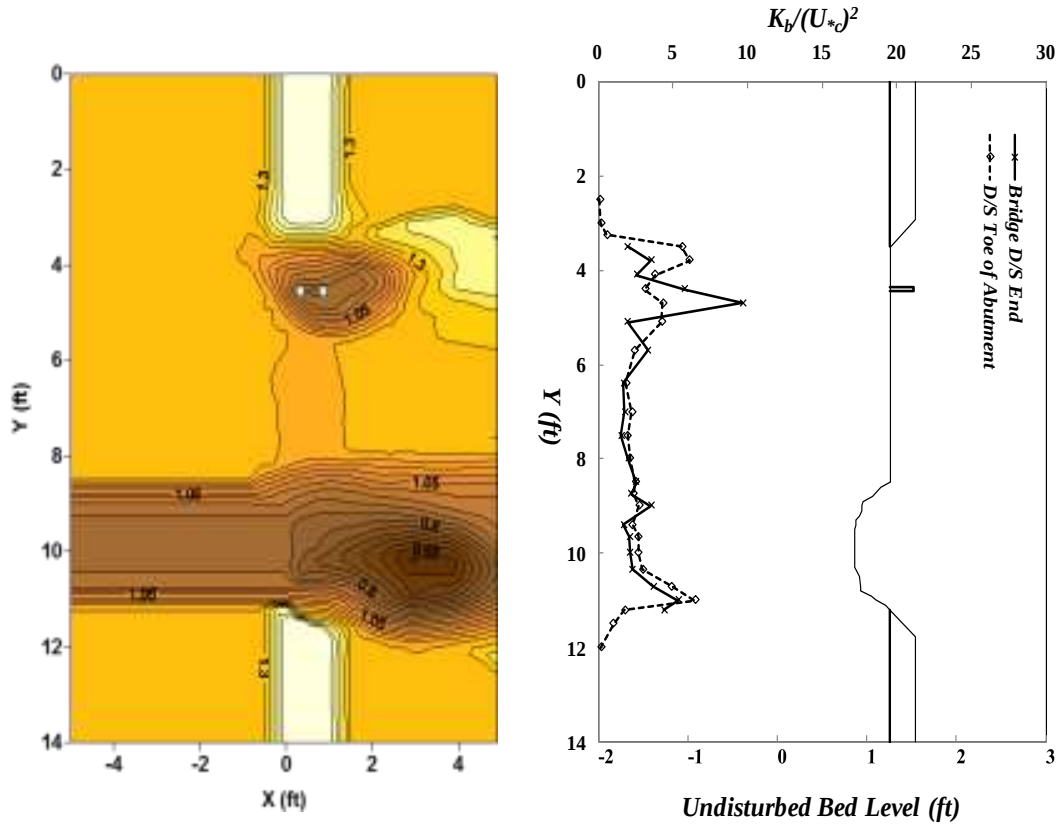

Figure 5-9 Comparison of normalized bottom TKE (K_b/u_{*c}^2) for section 4 and section 5 of Run 28 (SO flow L_a/B_f = 0.41, V_{f1}/V_{fc} =0.589, V_{m1}/V_{mc} =0.725)

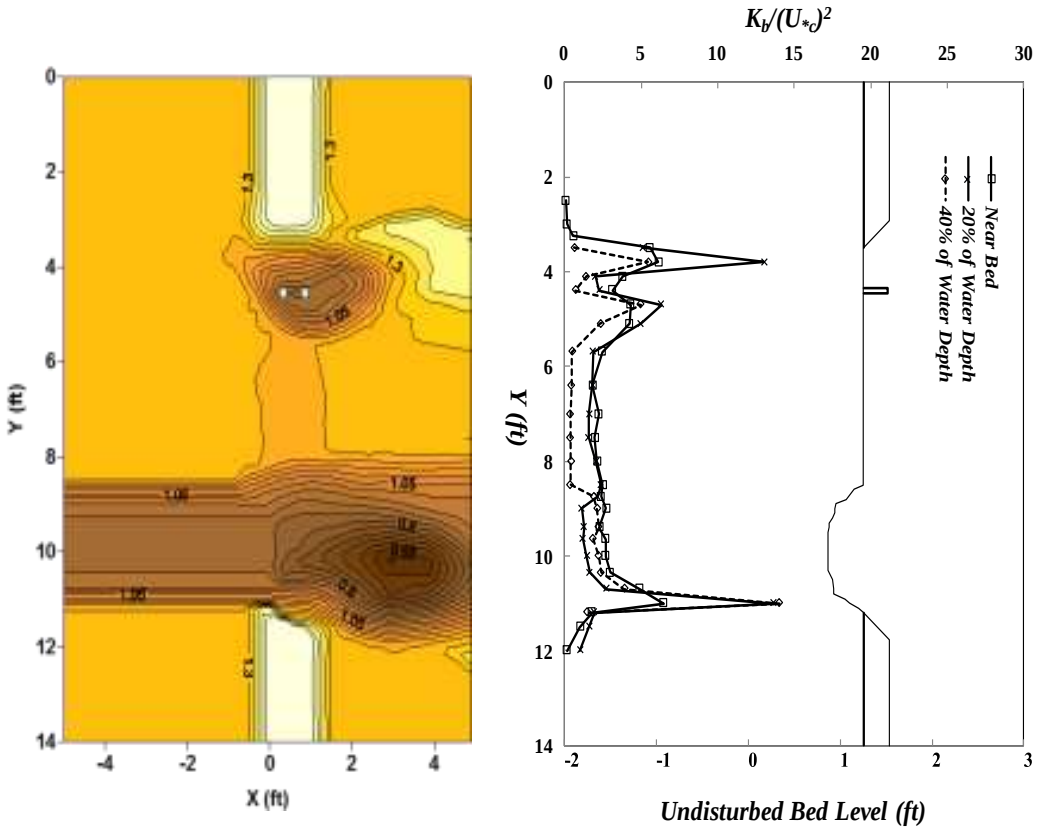

Figure 5-10 Normalized bottom TKE (K_b/u_{*c}^2) for section 5 of Run 28 for near bed, 20%, and 40% of the water depth and equilibrium contour plot (SO flow L_a/B_f = 0.41, V_{f1}/V_{fc} =0.589, V_{m1}/V_{mc} =0.725)

5.5. Interaction of Pier and Vertical Contraction Scour (Type –IV Scour)

The interaction of pier and vertical contraction scour was captured in the experiments, which were either conducted without abutments or the pier location was out of influence of the abutment and contraction scour hole. As already discussed (Para 5.2.1), isolated pier scour experiments satisfy both the CSU equation and Sheppard and Melville equation for simple rectangular piers. Lyn modified model, which uses the contracted section velocity under the bridge, best represents the isolated vertical contraction scour (as an envelope curve) with a coefficient of 0.21

and an upper limit for the dimensionless scour as 0.6. This contracted section velocity satisfies the cases with an additional involvement of lateral contraction (as discussed in Para 5.2.2). It was found that for this case (Category IV), the sum of the two scour components represents approximately the total interactive scour, where the predicted scour is generally slightly higher as compared to measured scour as a conservative approach. Figure 5-11 shows the comparison of interactive pier scour with vertical contraction scour (Category IV) between measured and predicted values. The figure includes experiments from the current study (for which pier scour was calculated with both the equations, i.e. CSU equation and Sheppard and Melville equation), experiments conducted at the University of Auckland for cylindrical piers (for which pier scour was calculated with Sheppard and Melville equation), and a field example from the Towaliga River flood for Tropical Storm Alberto (1994) for a compound pier, for which the pier scour was calculated from the method presented for the compound piers (Melville and Raudkivi 1996). The set of experiments and field data points cover a range of dimensionless scour of $0.7 < d_{se}/Y_1 < 1.3$.

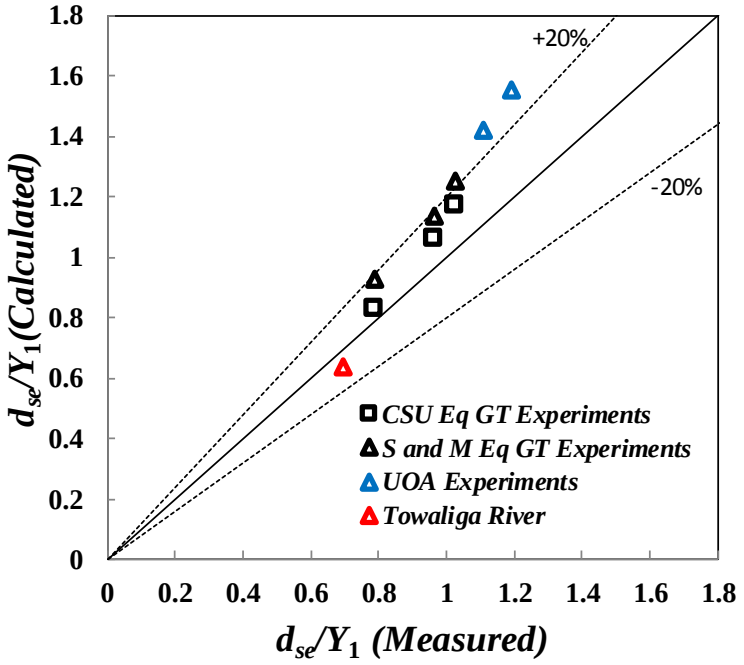

Figure 5-11 Comparison of measured and predicted interactive pier and vertical contraction scour

5.6. Interaction of Pier Scour with Abutment and Contraction Scour (Type-III Scour)

This section deals with pier scour interaction with abutment and contraction scour (Category III) as two sub groups. These sub groups are effect of pier scour on abutment and contraction scour and effect of abutment and contraction scour on pier scour. Table 5-1 shows the scour parameters measured for the experiments conducted with pier placed in the influence of the abutment scour hole along with the location of pier, type of flow, abutment length, and the equilibrium scour depth measured for both the locations including pier upstream edge (Y_{2max}/ Y_o *(Pier)*) and the abutment scour hole deepest point (Y_{2max}/ Y_o *(Ab)*).

Table 5-1Measured scour parameters and normalized equilibrium scour at the upstream edge of the pier and at the deepest point of abutment and contraction scour hole, for interactive pier scour experiments

Run	*Flow Type*	L_a/B_f	L_p/Yf_1	*F/P (M/C for Run 30 & 31)*				Y_{2max}/Y_o *(Ab)*	Y_{2max}/Y_o *(Pier)*
				q_2/q_1	Y_1/Y_o	V_1/V_c	Y_o *(ft)*		
6 GT	F	0.41	3.59	1.481	1.141	0.648	0.220	2.981	2.867
7 GT	OT	0.41	1.83	1.020	1.072	0.684	0.460	1.937	1.887
8 GT	F	0.41	7.20	1.479	1.136	0.648	0.220	2.800	2.000
9 GT	OT	0.41	3.65	1.009	1.071	0.683	0.460	1.848	2.026
14 GT	F	0.77	3.02	1.951	1.244	0.660	0.213	4.065	3.267
15 GT	OT	0.77	1.59	1.268	1.103	0.622	0.457	2.466	1.966
17 GT	OT	0.77	3.96	1.319	1.105	0.622	0.457	2.280	2.676
28 GT	SO	0.41	2.80	1.547	1.110	0.589	0.290	2.476	2.445
29 GT	SO	0.41	5.60	1.549	1.109	0.589	0.290	2.778	2.564
30 GT	SO	0.77	2.22	2.210	1.184	0.711	0.521	1.842	2.857
31 GT	SO	0.77	5.54	2.170	1.184	0.711	0.521	2.456	4.393
39 GT	F	0.41	3.57W	1.483	1.145	0.648	0.220	3.122	3.110
40 GT	SO	0.41	2.80W	1.571	1.109	0.589	0.290	2.807	2.782
41 GT	F	0.41	7.17W	1.486	1.141	0.648	0.220	2.915	2.454
42 GT	SO	0.41	5.07W	1.567	1.107	0.589	0.290	2.504	2.824
43 GT	F	0.53	3.72	1.914	1.115	0.613	0.218	3.120	3.129
44 GT	SO	0.53	5.48	1.975	1.102	0.590	0.315	3.218	3.108
45 GT	SO	0.53	4.8 &9.6	1.875	1.092	0.569	0.325	2.571	2.557

NOTE: For Run 30 and 31, Y_{2max}/Y_o *(Ab)* is in the main channel and Y_{2max}/Y_o *(Pier)* is in the floodplain.

5.6.1. *Effect of Pier on Abutment and contraction Scour*

Pier presence and its location in the zone of influence of the abutment and contraction scour hole affects the location and depth of the scour hole. In the set of experiments for the current research, the location of the pier varied such that the pier distance normalized by the approach flow depth (L_p/Y_{f1}), ranged between 1.5 and 11 for three abutment lengths (L_a/B_f = 0.41, 0.53, and 0.77) and for three types of flows (F, SO, and OT flows). The effect of pier and its position on the location of the deepest scour point of abutment and contraction scour has been discussed in Para 5.3.

The magnitude of the measured abutment and contraction scour affected by pier presence (Y_{f2max}) was compared with the calculated abutment and contraction scour (Y_{f2maxo}) by the suggested model presented in Chapter 4 (which gives the abutment and contraction scour without any pier effect). Figure 5-12 shows that the variation in the measured scour remained within ±15% of the calculated scour which approximates the standard error of the estimate of the suggested model as compared to the measured values and can be attributed to experimental uncertainty. Experiments with pier for L_a/B_f = 0.41 for F and SO flows were repeated with wall piers having the same flow conditions, which gave consistent observations as shown in Figure 5-13. It is concluded that the effect of a pier on abutment and contraction scour magnitude is negligible for the pier located in the floodplain and abutment and contraction scour can be calculated by the LSA abutment and contraction scour formula. It was also observed that for a pier location $L_p/Y_{f1} > 11$, the pier doses not remain in the influence of the abutment and contraction scour hole.

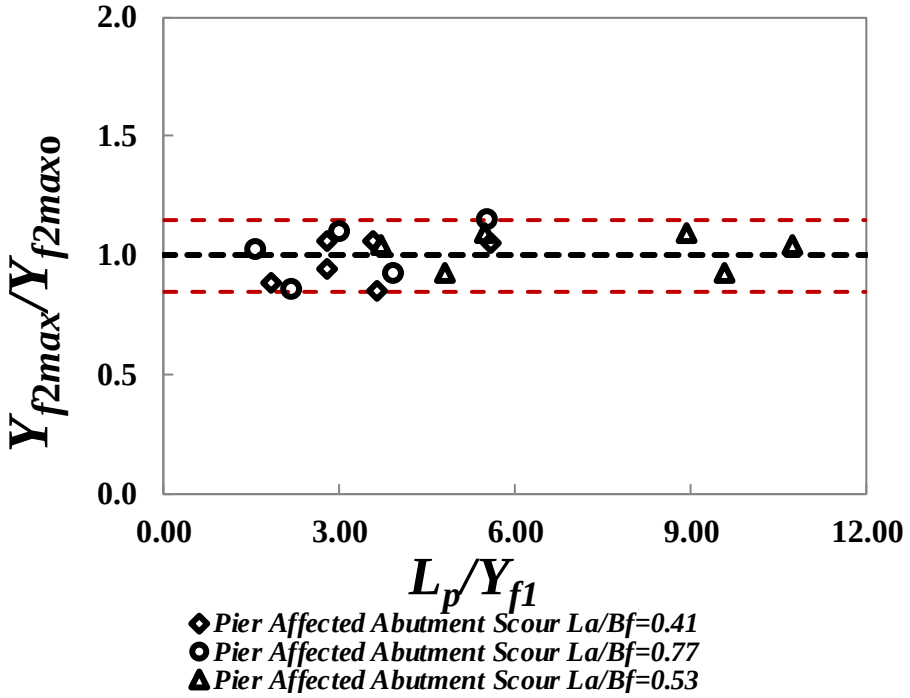

Figure 5-12 Effect of pier location on abutment and contraction scour

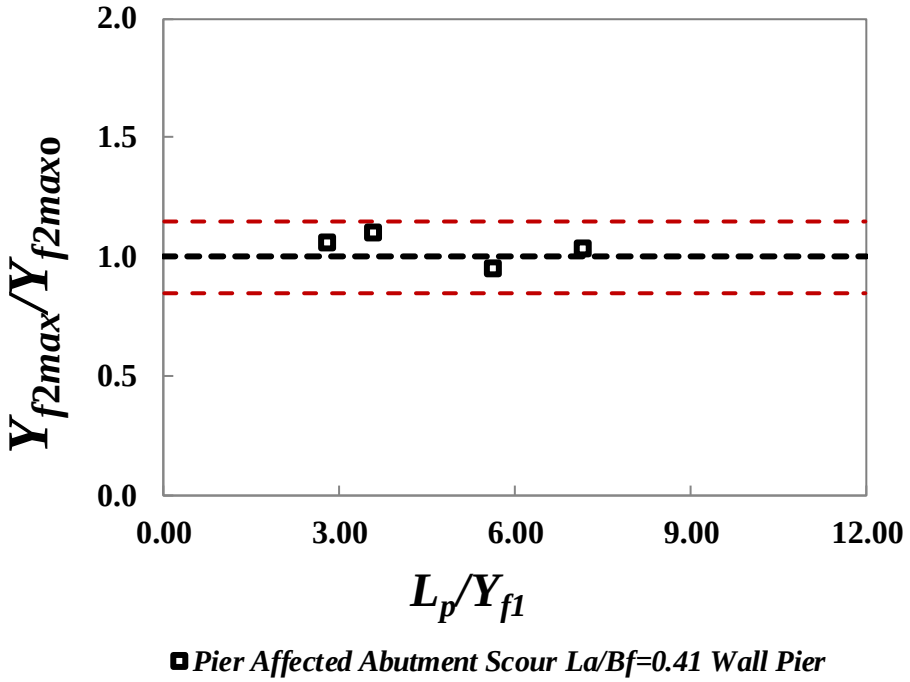

Figure 5-13 Effect of wall pier location on abutment and contraction scour

5.6.2. *Effect of Abutment and Contraction Scour on Pier Scour*

Piers placed at the toe of the abutment do not produce any scour, as it is a very low velocity area (almost stagnant or recirculating water) in the flow separation zone with additional effect of riprap armoring. Oben and Ettema (2011) also concluded the same for the experiments conducted for their research. This conclusion is used as a base line and no experiments were performed with pier placement at the toe of the abutment. Experiments were conducted for three abutment lengths with L_a/B_f = 0.41, 0.53, and 0.77 for F, SO, and OT flow cases. Pier placed closer to the abutment produced less equilibrium scour due to armoring effect. The pier scour depth increased by increasing the distance of the pier from the abutment, and after reaching a maximum value, the equilibrium scour again started to decrease with further increase in the distance of the pier from the abutment.

The amplification factor for the pier scour was determined by dividing the measured total scour at the upstream edge of the pier (d_{smax}) by the isolated pier scour (d_{smaxo}) calculated by CSU or S & M equation as given in Equation 5.1. Figure 5-14 shows that the pier scour is zero at the toe of the abutment for all the abutment lengths. As the pier is moved away from the abutment across the floodplain, the scour depth increases to the isolated pier scour depth (as calculated by CSU or S & M equation) at L_p/Y_{f1} = 1.5). The pier scour amplification factor increases as the pier is moved further away from the abutment and reaches a maximum value at $L_p/Y_{f1} \approx 6$ for all the abutment lengths (L_a/B_f = 0.41, 0.53, and 0.77). The pier scour amplification factor starts to reduce as the pier is moved further away from the abutment and reduces to the isolated pier scour at L_p/Y_{f1} = 11. Thus the pier scour amplification factor is divided

into two zones with respect to the normalized distance (L_p/Y_{f1}) from the abutment: (1) lower region for 3.0> L_p/Y_{f1}>7.5 and (2) higher region for 3.0< L_p/Y_{f1}<7.5. The pier scour amplification factor is defined by

$$Pier \quad Scour \quad Amplification \quad Factor = \frac{d_{s\max}}{d_{s\max o}} \tag{5-1}$$

where d_{smax0} is the maximum isolated pier scour depth.

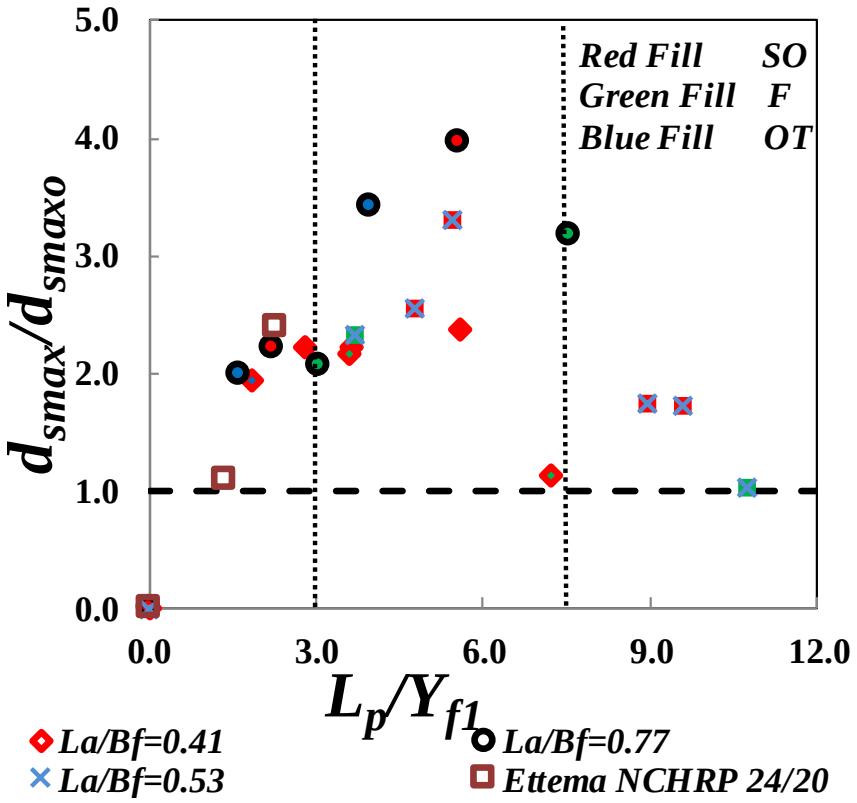

Figure 5-14 Variation of pier amplification factor with normalized distance from the abutment for different abutment lengths (L_a/B_f = 0.41, 0.53, and 0.77)

The magnitude of the highest amplification factor for an interactive pier scour at $L_p/Y_{f1} \approx 6$, as shown in Figure 5-14, increases with increase in the abutment length (L_a/B_f). This observation suggests a separate equation for each abutment length, which will be cumbersome and difficult since there are only three abutment lengths. In order

to address this limitation, interactive pier scour was compared with the abutment and contraction scour model, which covers all the lateral contraction ratios under one formula, by using unit discharge contraction ratio (q_{f2}/q_{f1}). Interactive pier scour was divided in two components as a pier scour component and an abutment and contraction scour component. The pier scour is calculated by CSU equation or S & M equation (both are recommended in HEC-18, and give comparable results for given range of experimental data) and is subtracted from total observed scour which leaves the remaining observed scour as an excess component contributed by abutment and contraction scour $(Y_{f2max}/Y_{fo})_{excess}$. Thus, the interactive abutment and contraction scour at the upstream edge of the pier can be written as show in Equation 5.2.

$$\left(\frac{Y_{f\,2\max}}{Y_{fo}}\right)_{excess} = \left(\frac{d_{se-pier(measured)} - d_{se-pier(calculated)} + Y_{fo}}{Y_{fo}}\right) \qquad (5\text{-}2)$$

The pier excess scour, which is the contribution of abutment and contraction scour, is shown in Figure 5-15 for three separate ranges as $L_p/Y_{f1} < 3.0$, $L_p/Y_{f1} > 7.5$, $3.0 < L_p/Y_{f1} < 7.5$ for all abutment lengths ($L_a/B_f = 0.41$, 0.53, and 0.77) and flow types (F, SO , and OT Flows). The lower region for $3.0 > L_p/Y_{f1} > 7.5$ and higher region for $3.0 < L_p/Y_{f1} < 7.5$ was regressed separately for pier excess scour (the abutment and contraction scour component) by keeping LSA abutment and contraction scour parameters and their exponents as constant and only determining the coefficient as a variable. This regression resulted in a coefficient of abutment and contraction scour contribution to pier scour as 1.906 and 1.283 for the higher and lower region, respectively, if pier scour is calculated from the CSU equation. However, if the pier scour is calculated from S & M equation, the regression results in a coefficient of

abutment and contraction scour as 1.871 and 1.253 for the higher and lower region, respectively. Thus, the difference is negligible, and either of the pier scour equations, recommended by HEC-18 can be used for pier scour calculation. Equation 5.3 and Equation 5.4 give the excess pier scour model for higher and lower region, respectively.

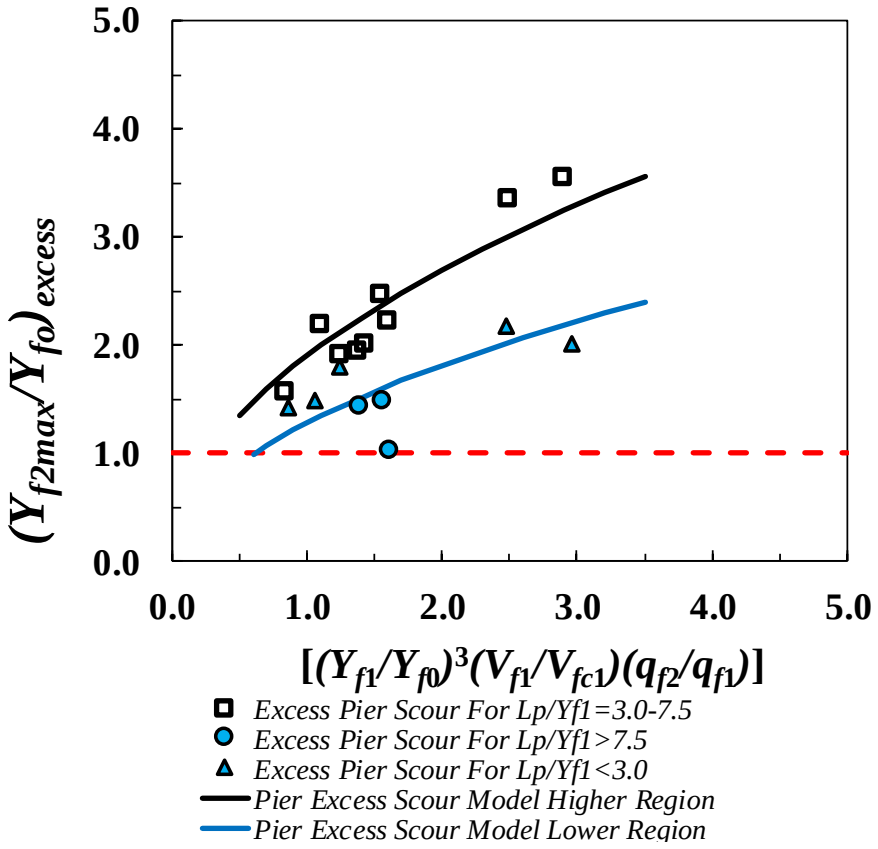

Figure 5-15 Pier excess scour for higher and lower region for interactive pier scour with abutment and contraction scour

$$\left(\frac{Y_{f2\max}}{Y_{fo}}\right)_{excess} = 1.906 * \left(\frac{Y_{f1}}{Y_{fo}}\right)^{3/2} * \left(\frac{q_{f2}}{q_{f1}} * \frac{V_{f1}}{V_{fc1}}\right)^{1/2} \quad For \quad 3 < \frac{L_p}{Y_{f1}} < 7.5 \qquad (5\text{-}3)$$

$$\left(\frac{Y_{f2\max}}{Y_{fo}}\right)_{excess} = 1.283 * \left(\frac{Y_{f1}}{Y_{fo}}\right)^{3/2} * \left(\frac{q_{f2}}{q_{f1}} * \frac{V_{f1}}{V_{fc1}}\right)^{1/2} \quad For \quad 3 > \frac{L_p}{Y_{f1}} > 7.5 \qquad (5\text{-}4)$$

The total interactive pier scour at the upstream edge of the pier can thus be obtained by calculating and adding the two components as the pier scour with CSU or S & M equation and excess scour (abutment and contraction scour contribution ($Y_{f2max}/Y_{fo})_{excess}$) with Equation 5.3 for higher region for 3.0< L_p/Y_{f1}<7.5 or with Equation 5.4 for lower region for 3.0> L_p/Y_{f1}>7.5. The method was also applied to the wall pier experiments conducted for L_a/B_f =0.41 for F and SO flow cases which showed good agreement with the same model for wall pier experiments as shown in Figure 5-16.

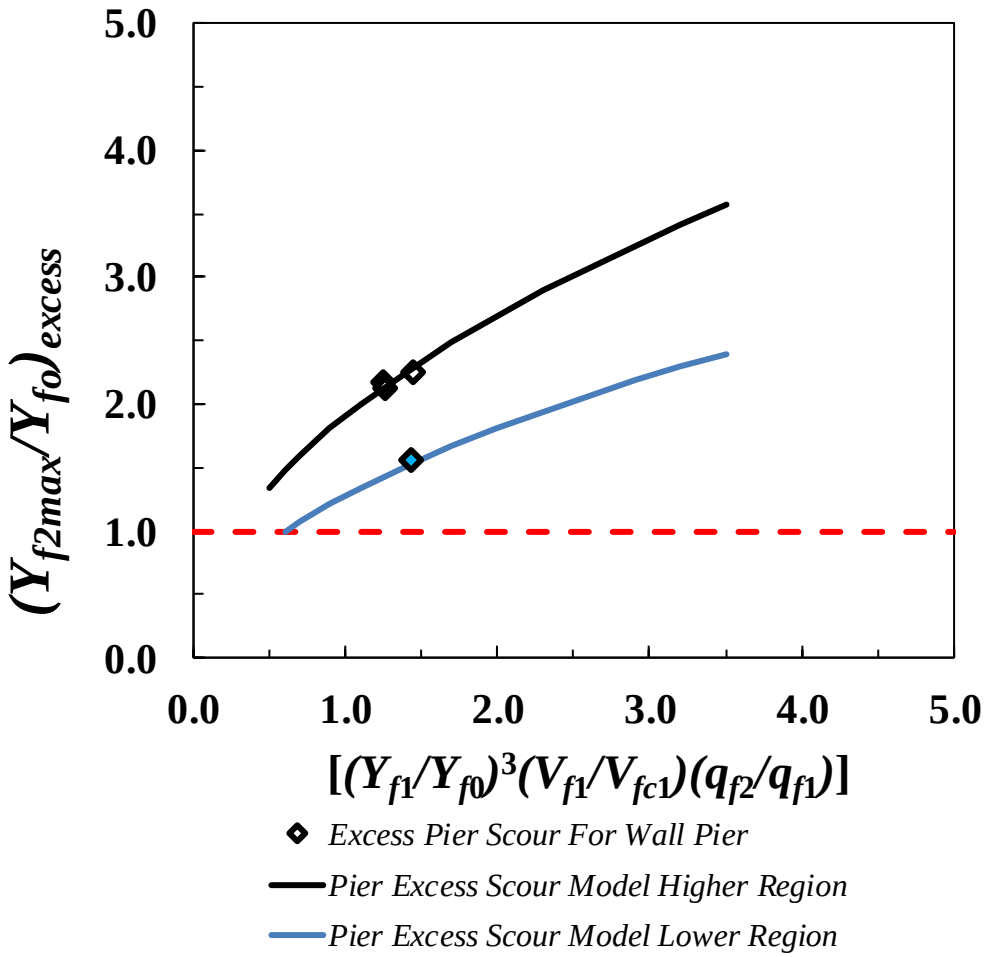

Figure 5-16 Interactive pier scour model application to wall pier experiments (L_a/B_f = 0.41 for F and SO flow cases)

5.7. Comparison of HEC-18 Model with Suggested Interactive Pier and Abutment and Contraction Scour Model (Type-III Scour)

The interactive scour development is affected by simultaneous development of different scour components; hence, the total interactive scour depends on interaction of various scour processes. This results in less equilibrium scour than the arithmetic sum of the scour components. HEC-18 suggests calculating the sum of individual scour components which overestimates the total interactive scour. A comparison of the

HEC-18 and suggested model is shown in Figure 5-17, part (a), for interactive pier scour with abutment and contraction scour. The scour components for HEC-18 have been calculated by equations suggested in HEC-18 where contraction scour for CWS uses the equation derived from Laursen (1963) contraction scour theory (Equation 2-6), vertical contraction scour uses equation based on flow separation thickness under the bridge (Equation 2-14) (Shen et al. 2012), abutment scour from Froehlich equation (Equation 2-28), and pier scour form CSU equation (Equation 2-17) or S & M equation (Equation 2-18) (both the equations for pier scour show comparable results in the given range of experimental data). Abutment scour is most significant contributor to the total scour with an average of about 65% of the total scour, vertical contraction scour as 10%, contraction scour as 5%, and pier scour as 20% of the total scour as per HEC-18 methodology calculations. HEC-18 predicts much higher values as compare to the suggested model, which predicts the interactive pier scour with abutment and contraction scour within the 10% of physical measurements as shown in Figure 5-17, parts (b) and (c).

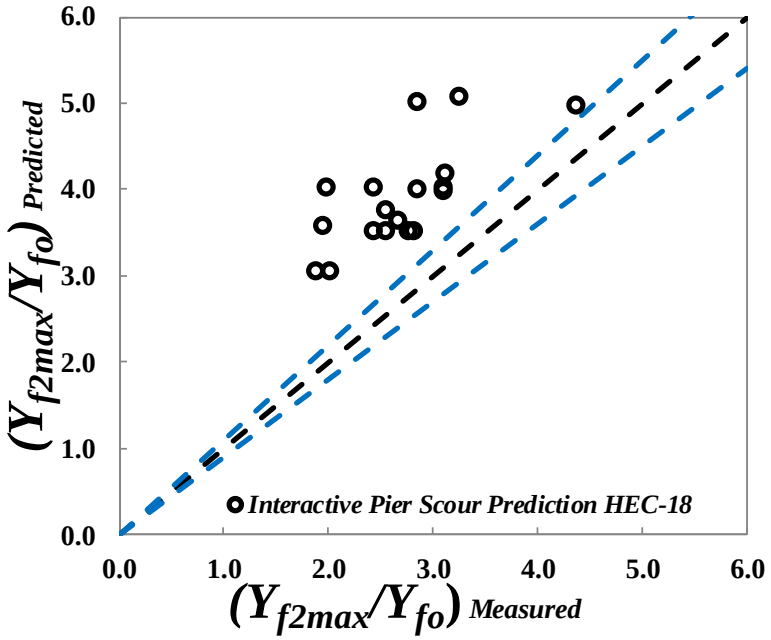

(a) Clear water interactive pier, abutment, and contraction scour prediction LSA, HEC-18

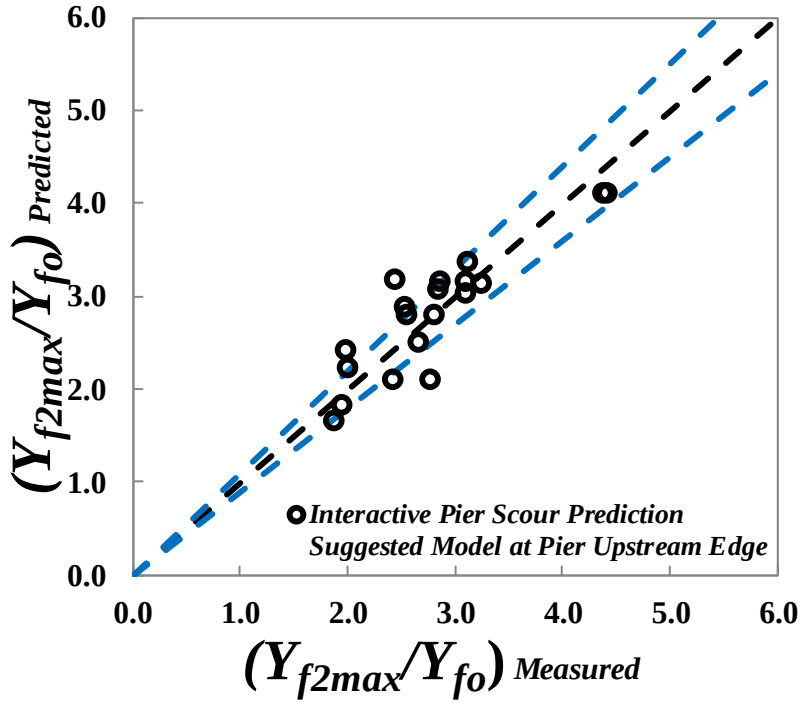

(b) Clear water interactive pier, abutment, and contraction scour prediction LSA, suggested model at upstream edge of the pier

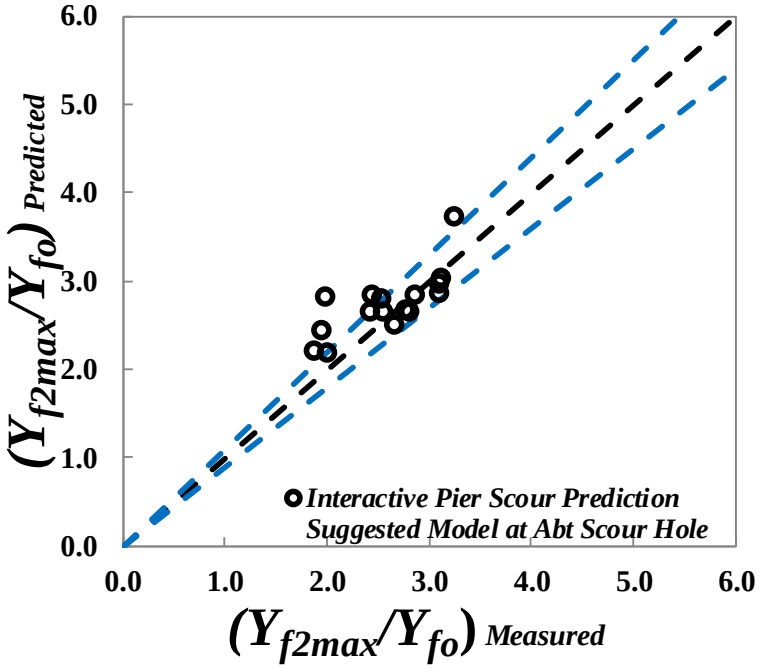

(c) Clear water interactive pier, abutment, and contraction scour prediction LSA, suggested model at abutment scour hole deepest point

Figure 5-17 Comparison of clear water interactive pier, abutment, and contraction scour between HEC-18 and suggested model

5.8. Comparison of the Suggested Model with Field Example

The Towaliga River flood for Tropical Storm Alberto (1994) was reproduced in the hydraulics laboratory of the Georgia Institute of Technology as mentioned in Para 2.13. The flood was submerged orifice flow case with erodible embankment in a compound channel with a long setback abutment on one side and a bankline abutment on the other side. The field scour measurements and the proposed model calculations based on scour parameter measurements from the laboratory Froude similarity model show good agreement with the suggested model in Figure 5-18. Pier number 7, 6, and 5 (as marked in Figure 2-16) are in the lower scour region, higher scour region, and pier and vertical contraction scour (Category IV), respectively. The equilibrium scour

for LSA with pier in the influence of abutment and contraction scour hole (Towaliga River) has been marked on the suggested model of interactive pier, abutment, and contraction scour for LSA as shown in Figure 5-18. The field measurements for all three cases were captured within 10% accuracy by the suggested model as shown in Figure 5-19.

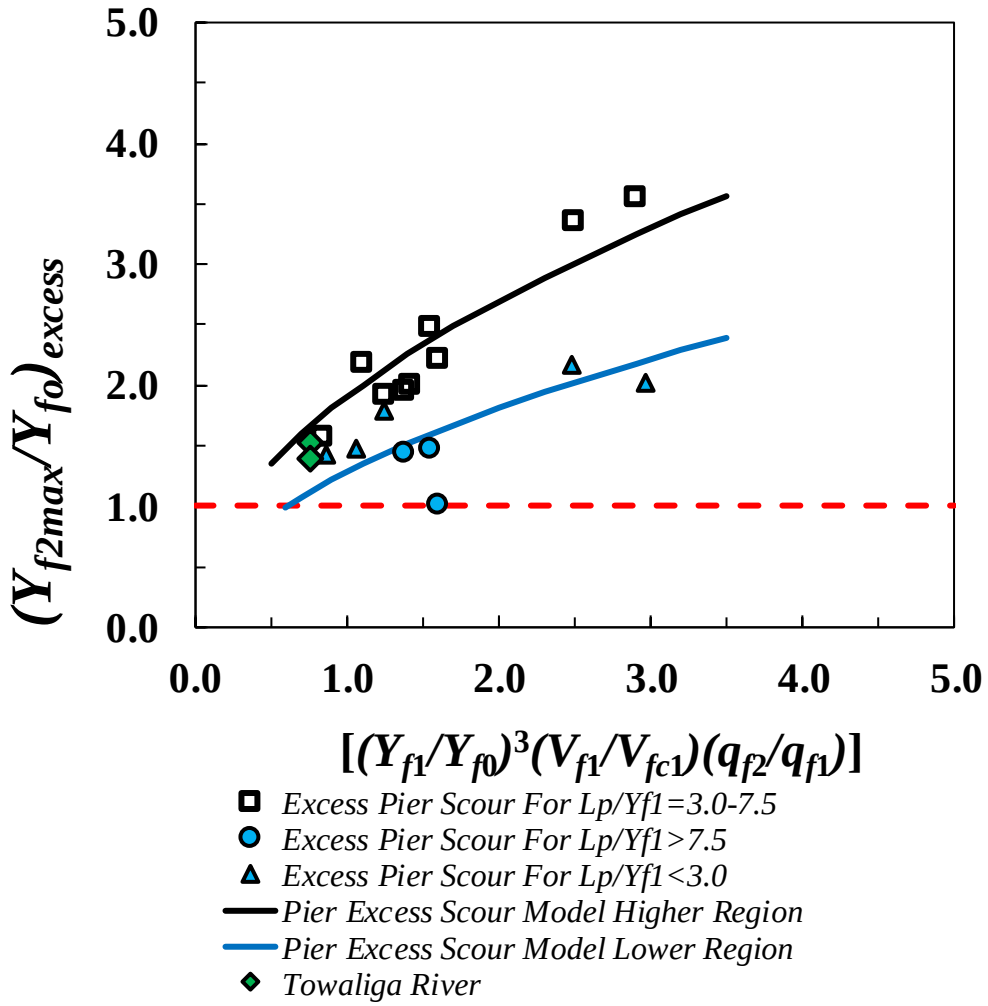

Figure 5-18 Interactive pier, abutment, and contraction scour, Towaliga river example, plotted with suggested model

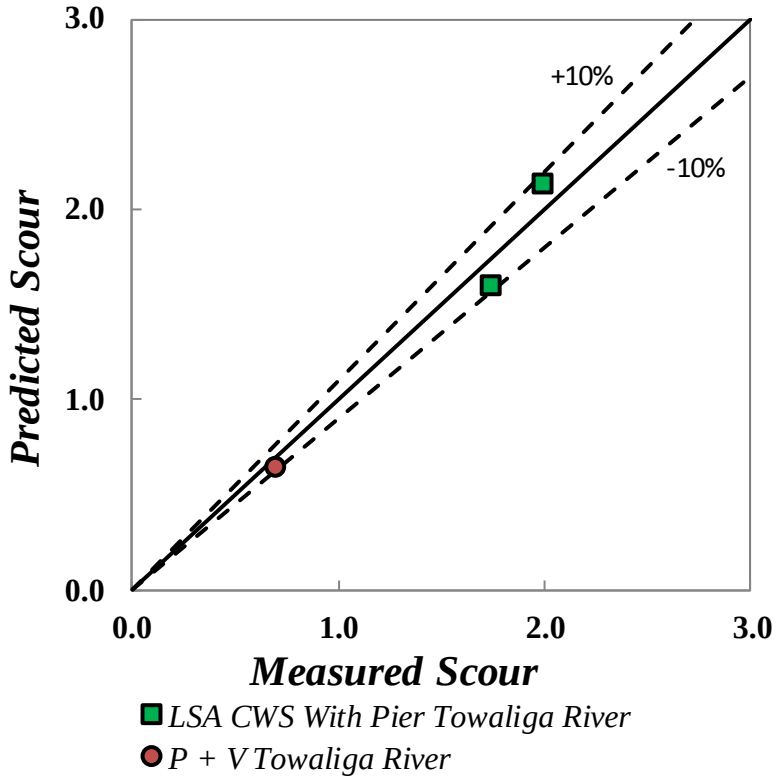

Figure 5-19 Measured vs predicted values of field examples for category III and category IV

CHAPTER VI

TIME DEVELOPMENT AND PREDICTION OF LOCATION AND MAGNITUDE OF SCOUR FOR LONG AND SHORT SETBACK ABUTMENT

6.1. General

This chapter deals with three aspects of the bridge scour which include the time development of the scour hole for all three types of flows (F, SO, and OT flows), criterion for long and short setback abutment, and prediction of the location of the deepest point of scour at equilibrium condition. Importance of the time development is more pronounced in the current scenario where the heavy intense rainfalls for shorter durations may not produce the flood duration required for equilibrium scour. Criterion for the long and short setback abutment dictates the location of the scour hole in the floodplain or in the main channel, where the scour hole largely forms part of the floodplain for an LSA. However, for SSA, the scour hole starts to develop in the floodplain but extends to the main channel with the time, and the deepest point occurs in the main channel at equilibrium. Location of the scour is also an important parameter as the deepest point of the scour hole may or may not fall under the bridge, affecting economical bridge design and downstream structures.

6.2. Time Development of Scour

Both magnitude and location of the scour hole were measured as a function of time. This helped define the equilibrium scour condition and observe the path of point of maximum scour as it moved downstream. Figure 6-1 shows the schematic diagram for definition of variables used in the time development of the location of the scour hole. In this figure, θ is the angle of the point of deepest scour from the upstream toe of the abutment, θ_e is the angle of the point of deepest scour at equilibrium, and r is the distance of point of deepest scour from upstream toe of the abutment.

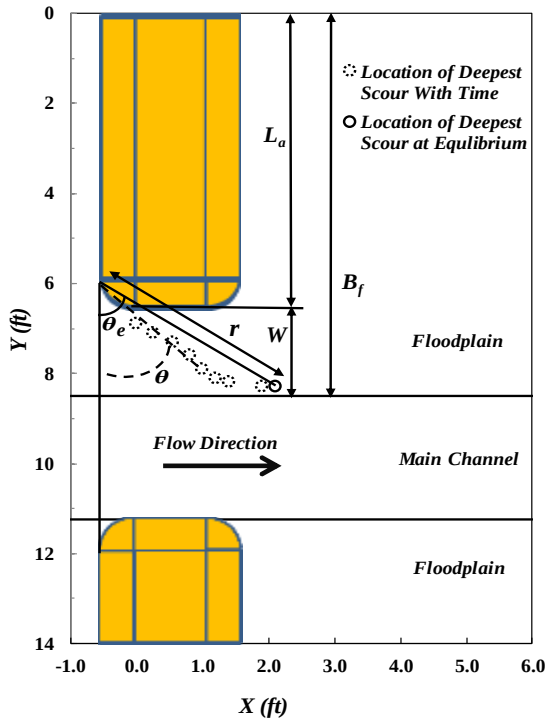

Figure 6-1 Schematic diagram for time development of location of point of deepest scour

Measuring the time development of magnitude of the scour depth assisted in identifying an accurate equilibrium scour condition, which was defined as the increase

in the scour depth to be less than 5% of the total scour in 24 hours. For different flow conditions and abutment lengths (L_a/B_f = 0.41 and 0.77), the experiments continued for up to five days, until the equilibrium criterion was achieved. The scour developed at a very fast rate in the first 4 to 6 hours and then started to slow down with an asymptotic progression towards the equilibrium scour as shown in Figure 6-2, which is consistent with other researcher's findings (Melville and Colemen 2000). Time development of the scour depth in terms of water depth at the point of maximum scour normalized by the undisturbed water level (Y_{ftmax}/Y_{fo}) shows a linear trend with dimensionless time on the logarithmic scale. An exception to this phenomenon is an SO flow case for L_a/B_f =0.77 (Run 11), where the scour hole initially developed in the floodplain near the bank of the main channel. It then merged with the main channel scour hole with time as the scour magnitude increased, resulting in expansion of the scour hole. The shifting of the point of deepest scour to the main channel gives an abrupt jump in the scour depth, contrary to the linear progression of the dimensionless scour to the dimensionless logarithmic time scale ($V_{f1}*t/Y_{fo}$) as shown in Figure 6-2.

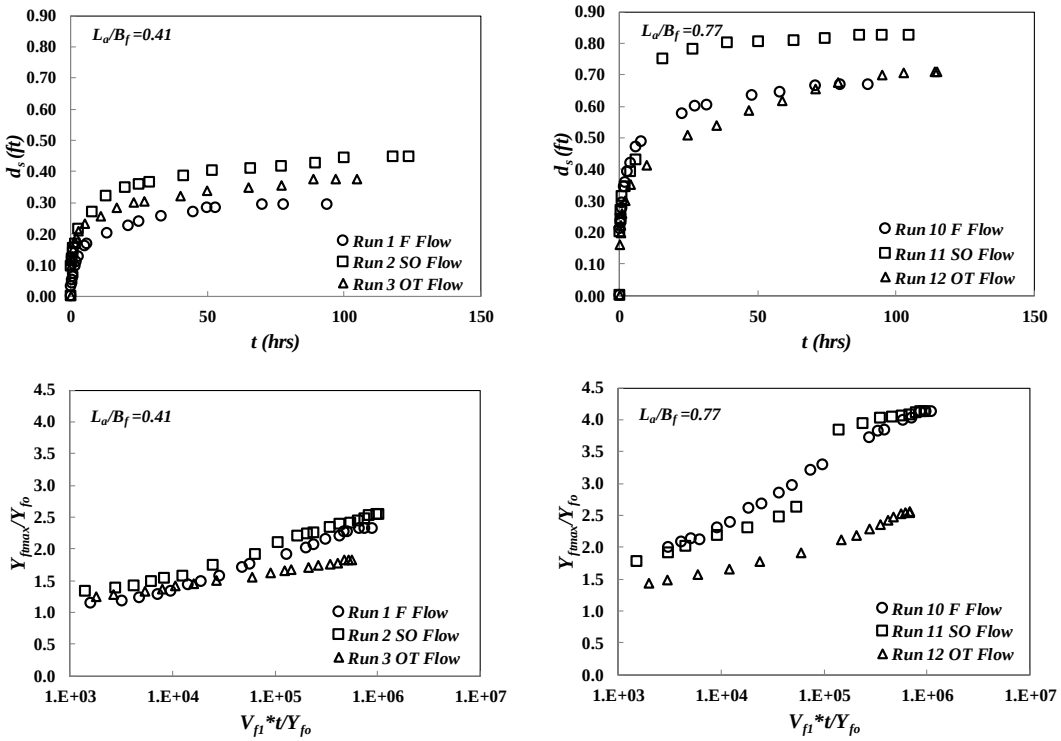

Figure 6-2 Time development of magnitude of scour in absolute and normalized terms for F, SO, and OT flows for L_a/B_f = 0.41 and 0.77

The location and time development of the point of deepest scour is a very important factor, which affects the structural stability of a bridge with respect to the location of most vulnerable bridge foundation elements for a critical design flood and its duration. The location of downstream structures is also vulnerable to scour hole development depending on the location and extent of the scour hole. Figure 6-3 shows the path of the point of maximum scour depth with respect to time for F, SO, and OT flow condition for two different abutment ratios (L_a/B_f = 0.41 and 0.77) .

For a smaller abutment size (L_a/B_f = 0.41), the time development of the points of deepest scour overlap each other for F, SO, and OT flow cases. The flow obstructed by the embankment converges around the upstream edge of the abutment and develops a flow separation angle along the abutment, which primarily governs the location and

path of the scour hole with time. For F flow, the point of maximum scour travels relatively less in the flow direction as compared to SO and OT flows. For an SO flow, the point of maximum scour travels the maximum distance having a higher velocity under the bridge. For an OT flow, the path straightens as the point of deepest scour moves out from under the bridge. This is likely because of the flow relief for the component of flow passing over the bridge accommodating the flow over the entire width.

For a longer abutment size (L_a/B_f = 0.77), the obstructed flow is much higher and the flow path experiences a larger angle of deflection from the upstream toe of the abutment making a higher angle of flow separation. This obstruction and flow convergence results in a significant transverse component of velocity in the bridge section. Thus, the point of deepest scour continues to show a significant movement with time in the transverse direction as well. For the F flow case (Run 10), the scour hole extended into the main channel, but the point of deepest scour remained in the floodplain. For the SO flow case (Run 11), the point of deepest scour entered into the main channel with time; however, the angle of flow separation remained the same. For an OT flow case, the scour hole extended in the downstream direction having a comparable scour depth under the bridge and in the downstream area which eventually resulted in a higher value at the downstream location. The cessation of the transverse movement of the point of deepest scour for an OT flow case, when it moves out of the bridge, remains consistent as in the smaller abutment length (L_a/B_f = 0.41).

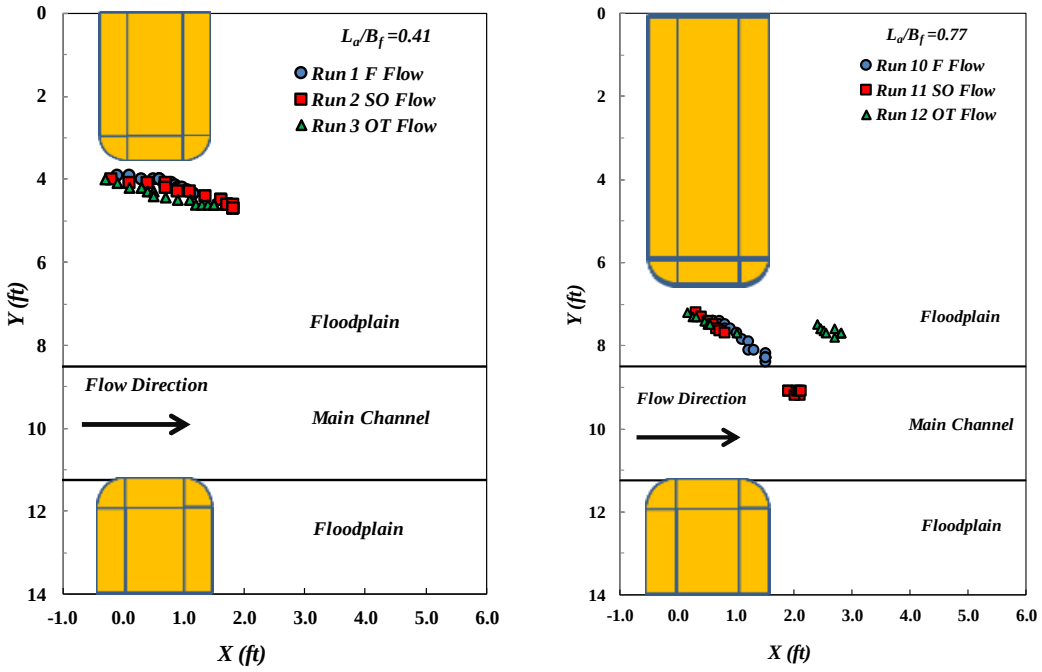

Figure 6-3 Path of point of maximum scour with time for L_a/B_f = 0.41 and 0.77 for F, SO, and OT flow cases

Figure 6-4 shows that if the time development of location of the point of deepest scour is related to the cylindrical coordinates as shown in Figure 6-1, the angle initially increases with increase in the radius normalized by the approach flow depth (r/Y_{f1}), which then becomes constant. There is a larger initial increase in the angle for the short abutment length (L_a/B_f =0.41) as compared to the longer abutment (L_a/B_f =0.77). The unit discharge contraction ratio, angle of flow separation, and transverse component of the velocity in the bridge section are much less for a shorter abutment (L_a/B_f =0.41) than for the longer abutment (L_a/B_f =0.77), which contributes a change in angle and straightening of the flow lines. For the OT flow case, in the longer abutment length (L_a/B_f =0.77), the larger spread of the scour hole, contribution of the

flow passing over the bridge, and comparable depth under the bridge and in the downstream direction justify the change in the angle with time.

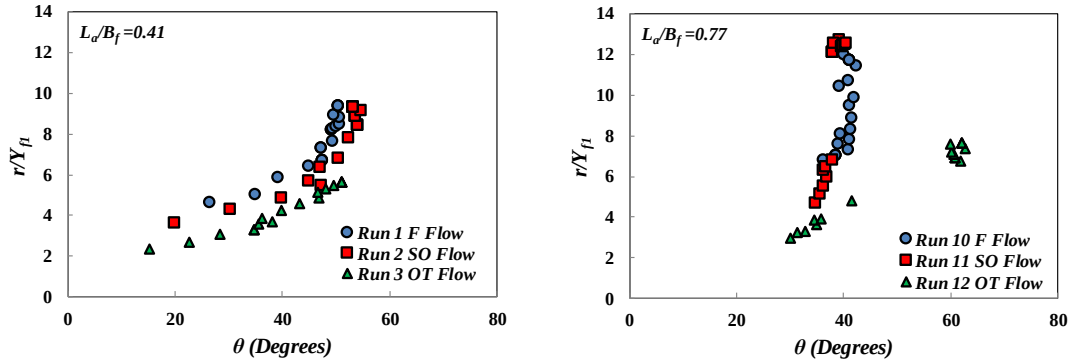

Figure 6-4 Path of point of maximum scour for dimensionless radius and angle with time, For L_a/B_f = 0.41 and 0.77 for F, SO, and OT flow cases

6.3. Criterion for Long and Short Setback Abutment

An LSA is described as the abutment for which either scour hole or major part of the scour hole remains in the floodplain such that the point of deepest scour is in the floodplain. For SSA, the scour hole starts to develop in the floodplain but extends to the main channel with time and the deepest point occurs in the main channel at equilibrium. Figure 6-5 shows the definition sketch for the location of the deepest point of scour hole in the transverse and flow directions. In this figure, L_s = distance of the point of deepest scour in the transverse direction from the left edge of the floodplain, L_m = distance of the point of the deepest scour in the transverse direction from the toe of the abutment, L_b = length of the bridge in the flow direction, L_x = distance of the point of the deepest scour from the upstream edge of the bridge in the flow direction, and W = width of floodplain in the contracted section.

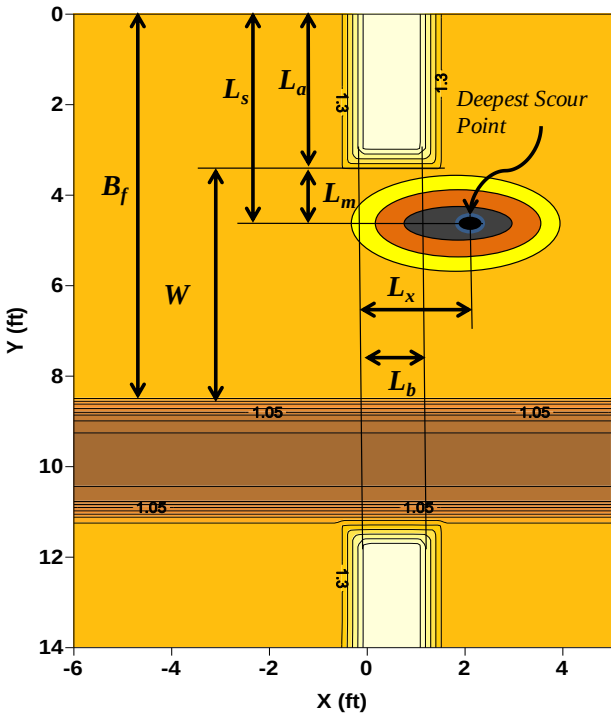

Figure 6-5 Definition sketch describing the variables of the location of the scour hole

HEC-18 defines the criterion of an LSA such that $W/Y_{f1}>5$, where width of the floodplain in the contracted section (W) is normalized by the approach flow depth in the floodplain (Y_{f1}). Hong (2013) based on his experiments further modified the criterion as $W/Y_{f1}>6$. The normalized location of the deepest point of the scour hole (L_s/B_f) corresponding to the normalized width of the floodplain in the contracted section (W/Y_{f1}, as defined by HEC-18) is shown in Figure 6-6. This includes the experiments conducted by Hong (2013), experiments for the current research at the Georgia Institute of Technology including the experiments conducted with pier, and experiments conducted at the University of Auckland (Xiong 2017). The threshold criterion defined by HEC-18 is marked as a blue dotted line and the revised criterion by Hong (2013) is marked as a green dotted line.

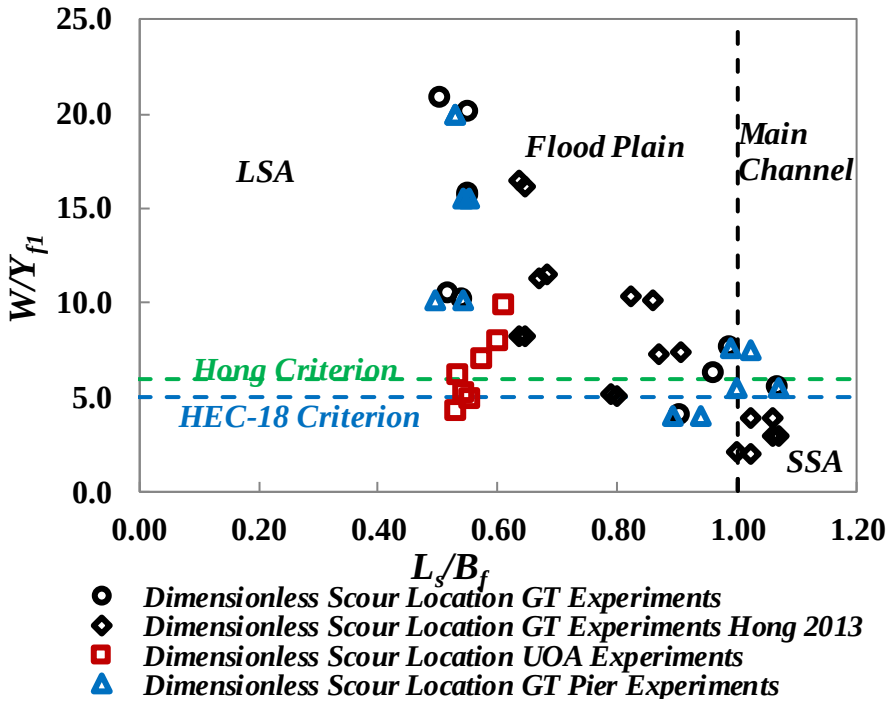

Figure 6-6 Normalized location of the deepest point of the scour hole (L_s/B_f) in the transverse direction, compared with HEC-18 criterion for classification of LSA and SSA

It can be observed that the normalized location of the deepest point of the scour hole (L_s/B_f) shows a large scatter with the normalized width of the floodplain in the contracted section (W/Y_{f1}). The normalized location of the deepest point of the scour hole (L_s/B_f) is observed to reoccur at different values of normalized width of the floodplain in the contracted section (W/Y_{f1}). The reason for this scatter and recurrence is that the width of the contracted section of the floodplain (W) does not account for the lateral contraction and a given value of contracted section floodplain width (W) may exist for different abutment lengths, which give different geometric contraction ratios.

The lateral contraction and losses incorporated in the bridge section, directly contribute to the magnitude and extents of the scour hole. Therefore, a new variable

was introduced as a product of lateral contraction ratio and backwater depth ratio in the contracted section ($L_a/B_f*Y_{f1}/Y_{fo}$) which was compared with the normalized location of the deepest point of the scour hole in the transverse direction (L_s/B_f). Figure 6-7 shows that the all the points for five different abutment ratios (L_a/B_f = 0.41, 0.53, 0.71, 0.77, and 0.88) and three types of flows (F, SO, and OT flows) for the experiments conducted by Hong (2013) and current research collapse under a single curve such that for $L_a/B_f*Y_{f1}/Y_{fo}$>0.94 the deepest point of scour hole occurs in the main channel and for $L_a/B_f*Y_{f1}/Y_{fo}$<0.94 the deepest point of the scour hole occurs in the floodplain. Depending on the experimental uncertainty and collapse mechanism of the main channel bank, the occurrence of the point of deepest scour near the junction of main channel and the floodplain may show some variability in the range of normalized variable as 0.94<$L_a/B_f*Y_{f1}/Y_{fo}$<1.0.

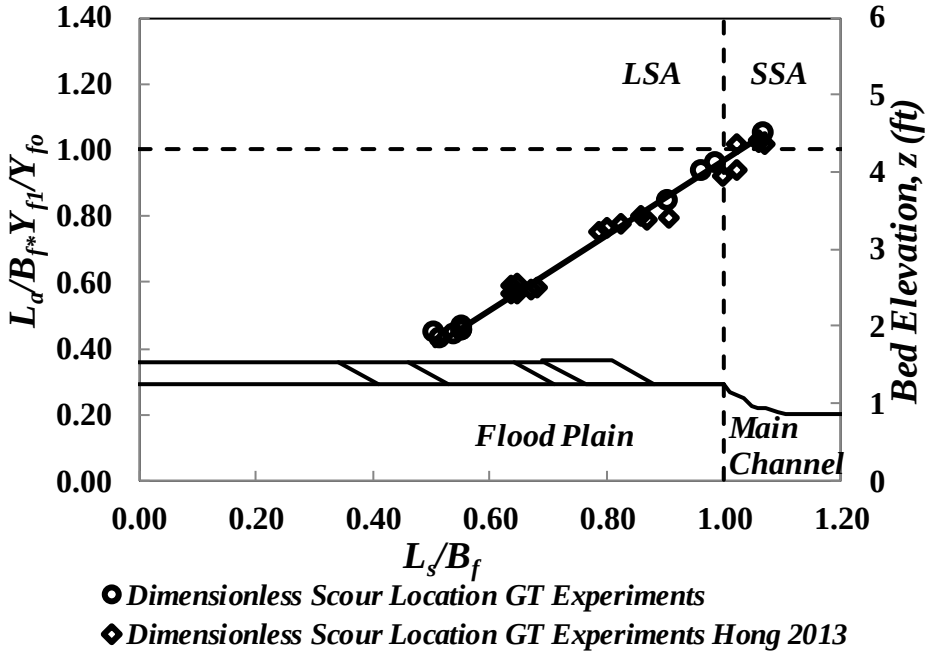

Figure 6-7 New defined criterion for LSA and SSA covering a full range of abutment lengths (For L_a/B_f = 0.41, 0.53, 0.71, 0.77, and 0.88)

As the given criterion accounts both for the geometric and flow variables, the model is capable of capturing the abutment classification where the same geometric ratio (L_a/B_f) may either fall in the category of LSA or SSA, depending on the backwater depth ratio (Y_{f1}/Y_{fo}) in the contracted section. An example of this phenomenon can be observed for the abutment ratio L_a/B_f = 0.77, for which F and OT flow cases (Run 10 and 12) fall in the category of LSA. However, SO flow (Run 11) is covered under SSA by the given criterion, and the physical measurements of the location of the deepest point correspond to the same. The criterion is thus defined as given in Equation 6.1. The model was also applied to the experiments conducted with piers at the Georgia Institute of Technology and for the experiments conducted at the University of Auckland (Xiong 2017), which show good agreement with the defined criterion as shown in Figure 6-8.

$$\left(\frac{L_a}{B_f} * \frac{Y_{f1}}{Y_{fo}}\right) < 0.94 \quad LSA$$
$$\left(\frac{L_a}{B_f} * \frac{Y_{f1}}{Y_{fo}}\right) > 0.94 \quad SSA \qquad (6\text{-}1)$$

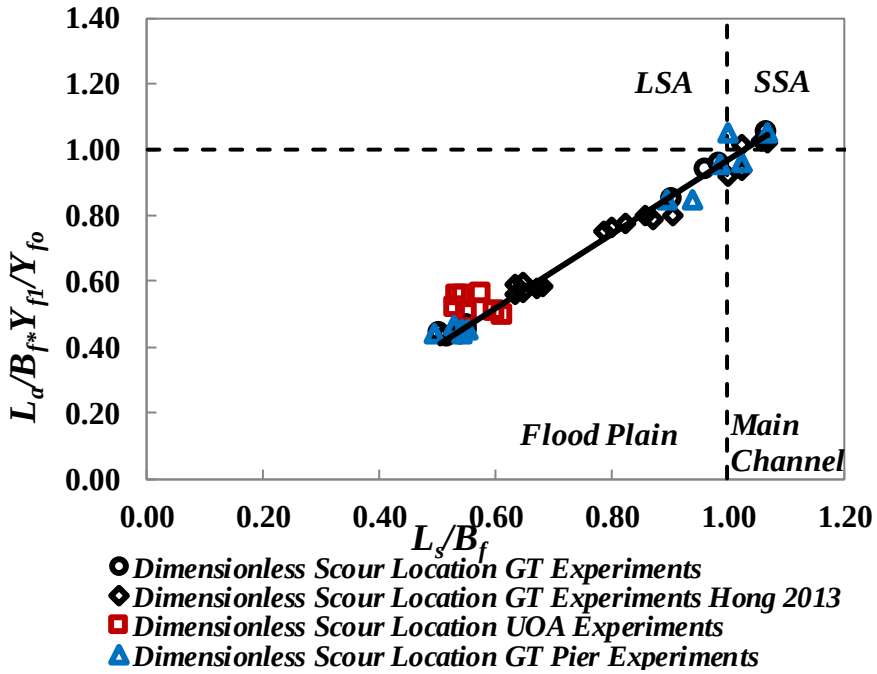

Figure 6-8 Application of the new criterion of LSA and SSA for experiments of UOA and GT experiments with pier

6.4. Prediction of Scour Location

The location and extent of the scour hole is an important parameter as the bridge design and different structures near the scour hole are affected by the scour development. The location of the deepest point of the scour hole is defined in the Cartesian coordinate system for transverse and flow directions as shown in Figure 6-5. The size or extent of the scour hole and thus the location of the deepest point in the transverse direction depend on the lateral contraction, flow contraction, roughness ratio between approach and contracted section, approach flow intensity, and head-loss in the contracted section for a given type of abutment as shown in Equation 6-2.

$$\frac{L_s}{B_f} = f\left(\frac{L_a}{B_f}, \frac{q_{f2}}{q_{f1}}, \frac{n_{f2}}{n_{f1}}, \frac{V_{f1}}{V_{fc}}, \frac{Y_{f1}}{Y_{fo}}\right) \quad (6\text{-}2)$$

The lateral and flow contraction ratios complement each other and the roughness ratio between approach and contracted section is included in flow contraction ratio. The approach flow intensity parameter contribution to the location of the scour hole is negligible in comparison to lateral contraction ratio effect. Therefore, Equation 6-2 can be rewritten as:

$$\frac{L_s}{B_f} = f\left(\frac{L_a}{B_f}, \frac{Y_{f1}}{Y_{fo}}\right) \tag{6-3}$$

Results of the experiments conducted by Hong (2013) and for the current research for F, SO, and OT flow for five different abutment ratios (L_a/B_f = 0.41, 0.53, 0.71, 0.77, and 0.88) show that normalized location of the scour hole in transverse direction (L_s/B_f) is a strong function of the normalized variable (L_a/B_f*Y_{f1}/Y_{fo}) as defined in Equation 6-3. A linear regression applied to the set of experiments gives the coefficient of determination as 0.98. Equation 6-4 shows the relationship for the prediction of the location of the deepest point of the scour hole in transverse direction. Figure 6-5 shows the graphical representation of the suggested model with physical measurements and Table 6-1 gives the summary of regression analysis. The application of the suggested model to the experiments conducted at UOA (Xiong 2017) at a model scale of 1:30 and the experiment conducted at the Georgia Institute of Technology for the current research (with rectangular pier) show a good agreement as shown in Figure 6-10. It is concluded that pier does not affect the transverse location of the deepest point of the scour hole.

$$\frac{L_s}{B_f} = 0.91*\left(\frac{L_a}{B_f} * \frac{Y_{f1}}{Y_{fo}}\right) + 0.13 \tag{6-4}$$

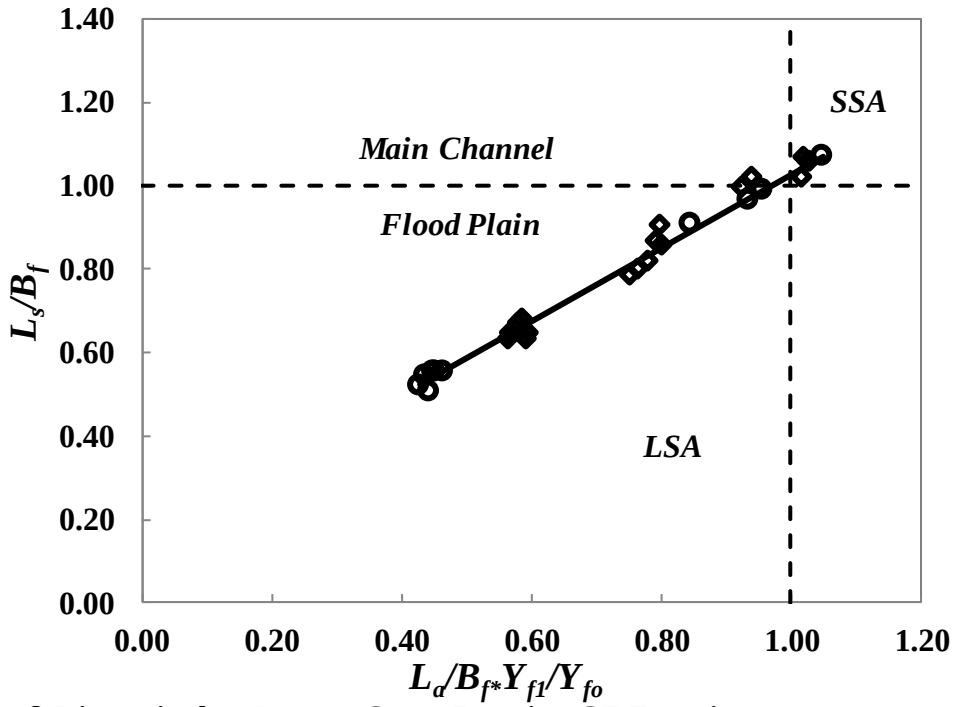

Figure 6-9 Prediction of the location of the deepest scour point in transverse direction

Table 6-1 Summary of regression for the prediction of location of the deepest point of the scour hole in transverse direction

Model	$\frac{L_s}{B_f} = 0.91*\left(\frac{L_a}{B_f} * \frac{Y_{f1}}{Y_{fo}}\right) + 0.13$ $R^2 = 0.989$			
Equation in terms of location variable from toe of the abutment	$\frac{L_m}{B_f} = \frac{L_a}{B_f}\left(0.91\frac{y_{f1}}{y_{fo}} - 1\right) + 0.13$			
Standard Error of the Parameters				
Term	Value	SE of Value	T-Value	P-Value
Constant	0.13	0.014	8.8	0.0
$L_a/B_f*Y_{f1}/Y_{fo}$	0.91	0.019	47.32	0.0

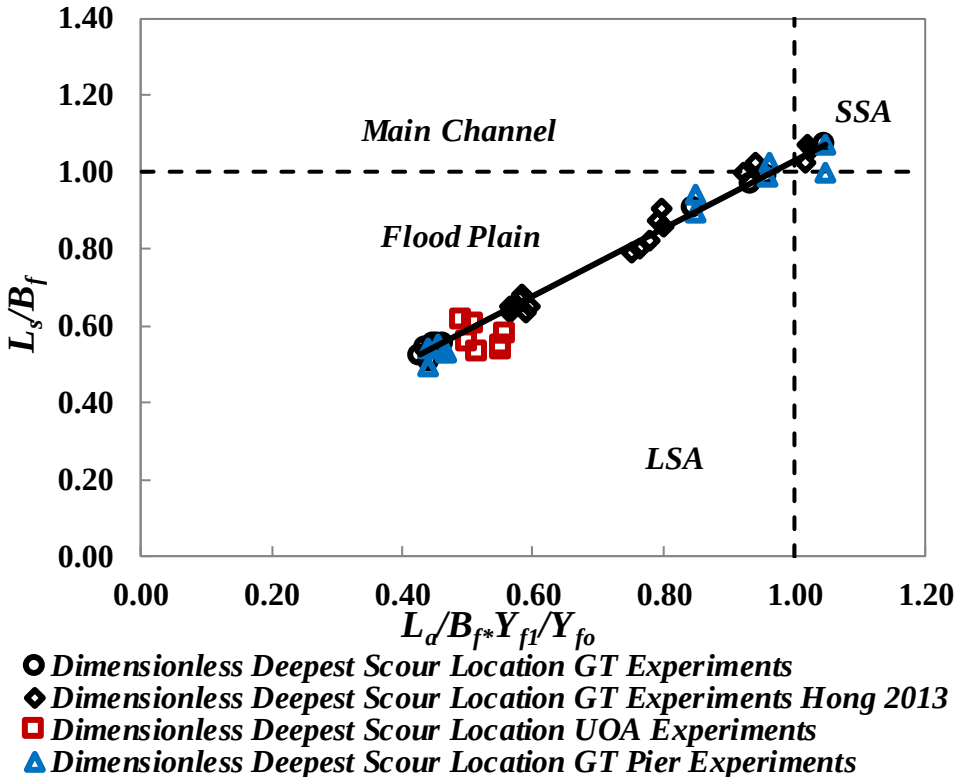

Figure 6-10 Application of the suggested model for the prediction of the deepest point of the scour hole to rectangular piers experiments and UOA experiments

The extent of the scour hole in the transvers direction is considered to be twice the distance of the point of deepest scour from the toe of the abutment (L_m). Physical measurements give a value ranging between $1.8L_m$ and $1.9L_m$, which can safely be considered as $2L_m$ as a conservative approach. If a scour hole covers the full width of the contracted section floodplain (W), the variables in Equation 6-4 can be replace as $L_s = L_a + L_m$ and $L_m = W/2$ (for the scour hole to cover the full width of the contracted section, where $W = B_f - L_a$), the resulting equation after simplification can be written as Equation 6-5. This equation gives the normalized length of the abutment in terms of normalized approach flow depth for which the scour hole covers the full width of the contracted section floodplain.

$$\frac{L_a}{B_f} = \frac{0.37}{0.91*\left(Y_{f1}/Y_{fo}\right)-0.5} \quad (6\text{-}5)$$

A scour hole generally starts in line with the upstream toe of the abutment and extends in the downstream direction. The location of the deepest point of the scour hole in the flow direction shows a larger variability and it was difficult to predict the exact location of the deepest point in the flow direction. However, it was observed that a higher shear stress, which is a function of the square of the velocity, results in a deeper and larger scour hole affecting the deepest point of the scour hole by shifting it further in the downstream direction. Figure 6-11 shows the experiments conducted for the current study, experiments conducted by Hong (2013), and experiments conducted in UOA (Xiong 2017). The location of the deepest point in the flow direction was found to be a function of an arbitrary variable given by the product of geometric contraction ratio and the square of the approach flow intensity representing the shear stress ($L_a/B_f*(V_1/V_c)^2$). The location of the point of the deepest scour is divided into three zones with their limits given in Equation 6-6.

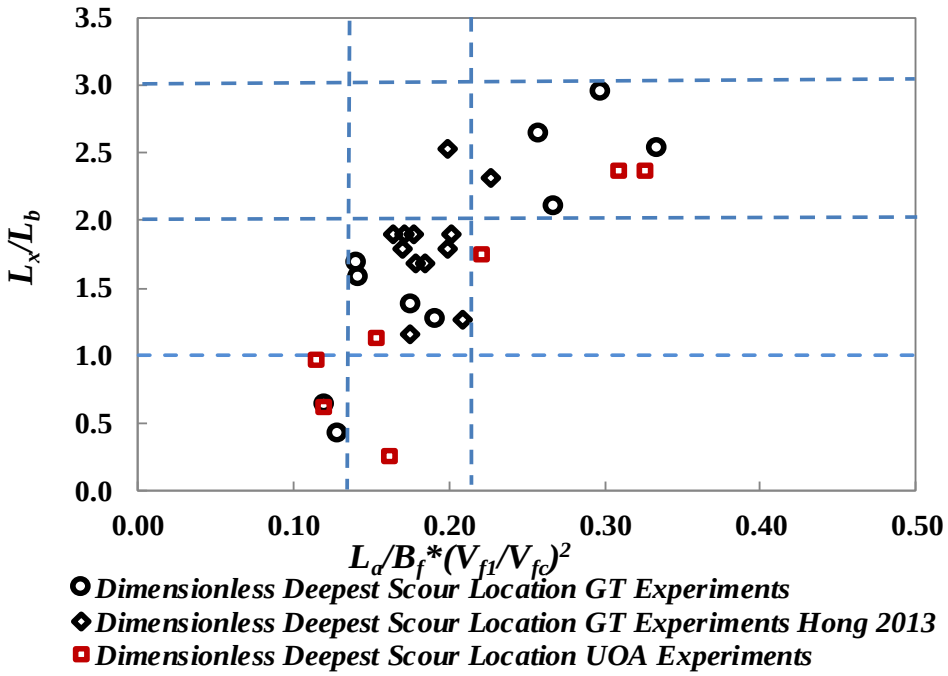

Figure 6-11 prediction of the location of point of deepest scour in the flow direction

$$\frac{L_x}{L_b} < 1 \quad For \quad \frac{L_a}{B_f} * \left(\frac{V_{f1}}{V_{fc}}\right)^2 < 0.13$$

$$1 < \frac{L_x}{L_b} < 2 \quad For \quad 0.13 < \frac{L_a}{B_f} * \left(\frac{V_{f1}}{V_{fc}}\right)^2 < 0.22 \qquad (6\text{-}6)$$

$$2 < \frac{L_x}{L_b} < 3 \quad For \quad \frac{L_a}{B_f} * \left(\frac{V_{f1}}{V_{fc}}\right)^2 > 0.22$$

The experiments conducted with a pier in the influence of the abutment and contraction scour hole show even a larger scatter for the location of the point of deepest scour in the flow direction as shown in Figure 6-12. A high velocity flow passing through the zone between abutment and pier, as explained in Para 5.4, increases the shear stress which may or may not move the point of deepest scour further in the downstream direction depending on the location of the pier. Thus, the prediction of the location of deepest point of the scour hole in the flow direction with a

pier in the influence of abutment and contraction scour hole requires further investigation to establish a relationship.

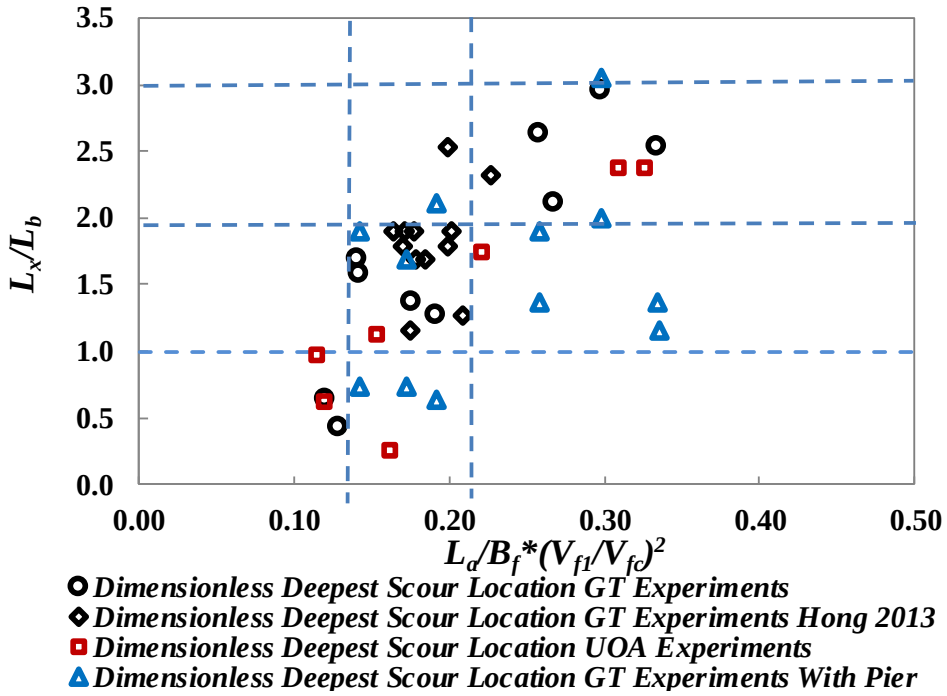

Figure 6-12 Location of point of deepest scour in flow direction including the experiments with pier in area of influence of abutment scour hole

CHAPTER VII

CONCLUSIONS

7.1. Summary

Scouring phenomena are critical to the stability of a bridge structure as the failure of more than 60% of bridges in the USA can be attributed to hydraulic parameters. Historically, the lack of knowledge concerning the complexity of scour prediction parameters resulted in rather unreliable scour prediction models. However, the focus of hydraulic engineers to investigate scour processes, especially over the past two decades, resulted in much improved scour prediction models. This advancement, however, faced another challenge of climate change phenomena in the recent past, which resulted in a great change in hydraulic parameters because of unprecedented flow conditions, in comparison to the historical free flows (F) (used for hydraulic design of bridges). This change in hydraulic parameters resulted in submerged orifice (SO) and overtopping (OT) flow conditions for existing bridges, which has threatened their structural stability requiring retrofitting to more extreme flow conditions in some cases, and replacement in others. For new bridges, modifications in design criteria have become important.

The turbulent flow structures in a bridge section are very complex as the water flow approaching a bridge section generally faces a high degree of contraction and flow acceleration. Flow around the upstream edge of the abutment encounters a sharp

bend causing a flow separation zone along the abutment face. The riprap apron along the abutment, while placed for scour control, also adds to the flow friction. Horseshoe and wake vortices at bridge piers contribute to pier scour processes. A vertical contraction in case of SO and OT flow cases, confines the flow, increases the velocity and induces a downward force. The effect of turbulence because of all these phenomena is significant to the scour process. The interaction of these phenomena for a contraction, an abutment, and a pier makes the analysis difficult, and it is more challenging due to the addition of vertical contraction interaction.

Recent laboratory studies have focused on compound channel models, rather than simple rectangular channels, which has contributed to achieving improved replication of field events. Oben and Ettema (2011) analyzed scour interactions for different components under free flow conditions. Hong (2013) investigated abutment and contraction scour (both lateral and vertical contraction) interaction for all three flow conditions (F, SO, and OT flows) both in the main channel and in the floodplain.

The current research intended to investigate the interaction between different components of scour and formulate a method to predict total interactive scour (to include all four components of scour) for all three flow conditions (F, SO, and OT flows) in a compound channel. Current design practice is to add scour depths predicted for different components as though they were acting alone without interaction. The result has been overly conservative foundation designs.

The research approach was experimental. A compound channel with floodplain on either side of the main channel was reproduced in the hydraulics laboratory of the Georgia Institute of Technology based in part on the Towaliga River site near Macon,

Georgia. The original geometry of the main channel was preserved but without meandering, and the floodplain was constructed to be horizontal in the transverse direction to remove the confounding effects on the turbulence interaction with the erodible bed. Different abutment length to floodplain width ratios (L_a/B_f) were tested with values of L_a/B_f = 0.41, 0.53, 0.77, and 1.0. Experiments were conducted for spill-through abutments and rectangular piers with a few repetitions for wing-wall abutments, wall piers, and no piers. The analysis incorporated experiments from Hong (2013), Xiong (2017), and Oben and Ettema (2011) with additional abutment ratios of L_a/B_f = 0.18, 0.24, 0.34, 0.50, 0.51, 0.60, 0.69, 0.71, 0.80, and 0.88. The results were divided into categories based on the different possible scour interactions and on the location of the scour hole, which was in the floodplain for long setback abutments (LSA), and in the main channel for short setback abutment (SSA) and bankline abutments (BLA).

7.2. Conclusions

This study has suggested a modified model for prediction of interactive abutment and contraction scour (Type I for the floodplain and Type II for the main channel) and suggested a new model for prediction of pier and vertical contraction scour (Type IV) and interactive pier, abutment, and contraction scour (Type III). The other contributions include refinement in classification criterion for LSA and SSA and a new model for prediction of the location of the point of deepest scour. The results from other researchers' experiments (Hong (2013), Hong et al. (2015), Xiong (2017), Ettema et al. (2010) and Oben and Ettema (2011)) have helped bolster the proposed

model of interactive abutment and contraction scour (Type I and Type II). The collective analysis with the experimental results of other researchers increases the reliability of the model and enhances the range of its applicability. Despite the difficulty of collecting field data during extreme floods, some limited but definitive field data were used to validate the relationships developed in the laboratory. The summary of the results and its comparison with the existing procedure is presented in Table 7-1.

Table 7-1 Summary of findings of current research for scour categories

Category	Model	Components Included	Applicability	% of data falling between ±10% of line of agreement		95% confidence interval of prediction Ratio**	
				Current method	Suggested model	Current method	Suggested model
I	$\frac{Y_{f2\max}}{Y_{fo}} = 2.363 * \left(\frac{Y_{f1}}{Y_{fo}}\right)^{3/2} * \left(\frac{q_{f2}}{q_{f1}} * \frac{V_{f1}}{V_{fc1}}\right)^{1/2}$	A, L, V	Applicable for Spill-through and WWA LSA	14.5%	75.5%	(1.16 to 1.28)	(0.97 to 1.04)
II	$\frac{Y_{m2\max}}{Y_{mo}} = 1.725 * \left(\frac{q_{m2}}{q_{m1}} * \frac{V_{m1}}{V_{mc1}}\right)^{1/2}$	A, L, V	Applicable for Spill-through and WWA BLA/SSA	0%	78%	(1.38 to 1.47)	(0.96 to 1.02)
III	Abutment and contraction scour affected by pier scour $(Yf_{2max}/Y_{fo})_{ab}$ = Same as Type-I	P, A, L, V	Applicable for Spill-through abutment LSA with rectangular and wall piers	0%	74%	(1.29 to 1.42)	(0.94 to 1.02)
	Pier scour affected by abutment and contraction scour $(Yf_{2max}/Y_{fo})_{pier}$ = $\left(\frac{Y_{f2\max}}{Y_{fo}}\right)_{excess} = 1.906 * \left(\frac{Y_{f1}}{Y_{fo}}\right)^{3/2} * \left(\frac{q_{f2}}{q_{f1}} * \frac{V_{f1}}{V_{fc1}}\right)^{1/2}$ *For* $3 < \frac{L_p}{Y_{f1}} < 7.5$ $\left(\frac{Y_{f2\max}}{Y_{fo}}\right)_{excess} = 1.283 * \left(\frac{Y_{f1}}{Y_{fo}}\right)^{3/2} * \left(\frac{q_{f2}}{q_{f1}} * \frac{V_{f1}}{V_{fc1}}\right)^{1/2}$ *For* $3 > \frac{L_p}{Y_{f1}} > 7.5$	P, A, L, V	Applicable for Spill-through abutment LSA with rectangular and wall piers	0%	79%	(1.29 to 1.51)	(0.94 to 1.06)
IV	P (CSU or S & M eq) + V (Lyn 2008)	P, V	P + V	100%*	100%*	-	-

Note: * these values are for ±20percentage from line of agreement, **prediction ratio = mean predicted value/mean observed value

A= abutment scour, L= lateral contraction scour, V= vertical contraction scour, P= pier scour, WWA = Wing-wall abutment, LSA = long setback abutment, I = interactive abutment and contraction scour in floodplain, II = interactive abutment and contraction scour in main channel, III = interactive abutment, contraction, and pier scour in floodplain, IV = interactive pier and vertical contraction scour.

An analysis of the individual scour components shows that in Type-1(LSA abutment and contraction scour) and Type-II (BLA/SSA abutment and contraction scour), abutment scour is the largest component followed by vertical contraction scour and lateral contraction scour, respectively. The dimensional analysis leads to the formulation of abutment scour parameters same as that of theoretical contraction scour. This finding supports the modification in the existing model with an amplification factor applied to a function of theoretical contraction scour parameters. An experimental approach followed by the theoretical concept of abutment and contraction scour and dimensional analysis led to the formulation of a dimensionless hydraulic parameters group governing the total interactive scour. The regression analysis led to a model which kept the theoretical contraction scour variables ($q_2/q_1 * V_1/V_c$) as a single parameter with a reduced exponent of "1/2" in comparison to "6/7" for the theoretical contraction scour (confirming the dominating contribution of abutment scour in comparison to lateral and vertical contraction scour). The results were applicable to both Type-I and Type-II interactive scour with different coefficients.

Another important finding was the difference in the effect of backwater depth ratio upstream and immediately downstream of the bridge (Y_1/Y_o) on the total interactive scour for Type-I and Type-II scour. The analysis show that a higher backwater depth ratio results in a higher scour depth. The backwater depth ratio (Y_1/Y_o) in the main channel was much lower than in the floodplain; therefore, this parameter was highly significant with an exponent of "3/2" for Type-I scour and was non-significant relative to scour processes in Type-II scour.

One of the most important contributions of this study is the interactive pier, abutment, and contraction scour model for all three types of flows (F, SO, and OT flows) for erodible spill-through abutments. The interactive pier scour experiments have been conducted for the first time in the Georgia Institute of Technology for SO and OT flow conditions. Rather than following a simpler approach of amplification factor, the investigation relied on the theoretical concept of scour contribution of each scour component for Type-III scour. Type-III scour was further divided into two types as abutment and contraction scour affected by pier scour $(Y_{f2max}/Y_{fo})_{ab}$ and pier scour affected by abutment and contraction scour $(Y_{f2max}/Y_{fo})_{pier}$. It was concluded that abutment and contraction scour affected by pier scour $(Y_{f2max}/Y_{fo})_{ab}$ remains within the experimental uncertainty of the Type-I scour model. However, the disaggregation of pier scour affected by abutment and contraction scour $(Y_{f2max}/Y_{fo})_{pier}$ into (1) pier scour and (2) excess component contributed by Type-I scour, not only validated the hypothesis that interactive scour development is less in magnitude but also quantified the reduction factor with a reduced coefficient of Type-I scour. Two scour regions were defined for Type-III scour as higher (for relative non-dimensional distance of pier from the toe of the abutment as $3<L_p/Y_{f1}<7.5$) and lower region ($3>L_p/Y_{f1}>7.5$), for which separate coefficients were determined.

For interactive pier and vertical contraction scour Type-IV, a sum of the two individual components is suggested using the Lyn (2008) modified model for calculation of the vertical contraction scour component. Lyn suggested use of the contracted section flow intensity variable (V_b/V_c) rather than the approach flow intensity variable (V_1/V_c). Use of the contracted section variable is suitable for cases

were lateral contraction is involved, as the same approach flow intensity results in different vertical contraction scour values depending on the degree of lateral contraction.

A refinement in classification criterion for LSA and SSA with a new parameter ($L_a/B_f*Y_{f1}/Y_{fo}$) has resulted in better differentiation of the two abutment types. Further application of the parameter has been shown to be useful in predicting the location of the deepest point of the scour hole in the transverse direction across the floodplain from the abutment face. A new parameter (product of relative abutment length and square of approach flow intensity, representing the shear stress effect as $L_a/B_f*(V_{f1}/V_{fc})^2$) for prediction of scour location in the flow direction has been suggested which gives a fair assessment of the scour location. However, further investigation is needed to validate this finding.

The current study suggests a model to predict the scour depth for economical design of safe bridges. In comparison to the existing practice of conservative estimate of scour depth, current model predicts about 75% of the predictions within 10% of the observed values. A comparison, as presented in Table 7-1, shows that current practice predicts only 14.5% of the predicted values within 10% of the observed values for Type-I scour and over predicts the remaining observations in comparison to suggested model, which predicts 75.5% of the predictions within 10% of the observed values. For Type-I scour 95% confidence interval of prediction ratio for the current practice ranges between 1.16 to 1.28, which shows larger variability and scatter in comparison with the suggested model with 95% confidence interval of prediction ratio reduced between 0.97 to 1.04. For Type-II and Type-III scour, current practice over predicts all

the observations with no predictions within 10% of observed values as against the suggested model which predicts about 78% of the prediction within 10% of the observed values. For Type-II and Type-III scour, 95% confidence interval of prediction ratio for the current practice ranges between 1.29 to 1.51, which shows even higher over prediction and larger scatter in comparison to suggested model for which 95% confidence interval of prediction ratio ranges from 0.94 to 1.06. The statistical analysis confirms that the variable parameters and their significance presented by the suggested model captures the scour interaction phenomenon with higher degree of accuracy.

7.3. Future Study Recommendations

This study has suggested a new model to predict interactive pier, abutment, and contraction scour for the floodplain and a modified model for prediction of interactive abutment and contraction scour both for the floodplain and the main channel. However, the improvements in the following areas of research are suggested:

1. Scour process has a larger variability depending on the type of sediment and its physical properties. In mountainous terrains, the sediment is generally a gravel material or coarser sand, or finer cohesive sediments as the river flows to its mouth in coastal areas. A study of the interactive scour for different types of sediments is suggested to broaden applicability of the interactive sediment scour relationships developed herein.
2. The degree of erodibility of an embankment affects the scour process; however, the embankment erodibility is itself a threat to structural stability.

Therefore an embankment erodibility study is suggested with a view to enhance structural stability and define embankment failure with respect to scour.

3. Although the initial investigation of wing-wall abutment and wall pier experiments showed an agreement with the spill-through abutment and rectangular pier experiments, respectively, yet there is a need to validate this observation of the effect of abutment shape through a larger set of experiments.
4. An application of the results from the current study and Hong (2013) to a three dimensional CFD numerical model is suggested. If the results from the three dimensional CFD model show an agreement with the laboratory measurements, it can greatly help to understand the dynamics of the flow structures and turbulence-scour relationship. Changing flow structures and turbulence measurements over time, in a three dimensional CFD numerical model, can give valuable input to understand the time development of the scour process.
5. In interactive pier, abutment, and contraction scour for the floodplain, reduced coefficients of pier excess scour $(Y_{f2max})_{excess}$ for higher and lower regions have been established for Type-I scour. An experimental investigation of the interactive pier, abutment, and contraction scour is suggested for main channel to investigate reduced coefficients for Type-II scour.
6. The time development study has achieved some basic conclusions in line with Hong (2013) for time development of magnitude of the scour depth. This dimension of the study has acquired more importance in the current scenario of

climate change, where high floods for short duration do not continue for the time required to reach an equilibrium scour. Therefore, more experiments with time development measurements are suggested to develop a model for time development of the interactive scour process.

7. A theoretical long contraction is different from bridge embankments, where sudden contraction and expansion result in complex flow fields in comparison to the ideal long contraction. A contraction scour study for the current bridge design practices may help in better assessment of contraction scour contribution to interactive scour conditions.

APPENDIX A

Run 1 (Free flow L_a/B_f = 0.41, Q = 3 *cfs*, TW = 1.48 *ft*)

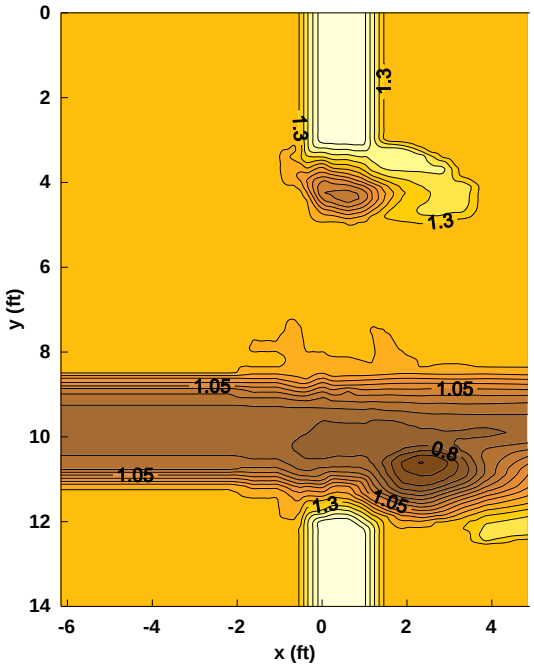

Run 2 (SO flow L_a/B_f = 0.41, Q = 4 *cfs*, TW = 1.547 *ft*)

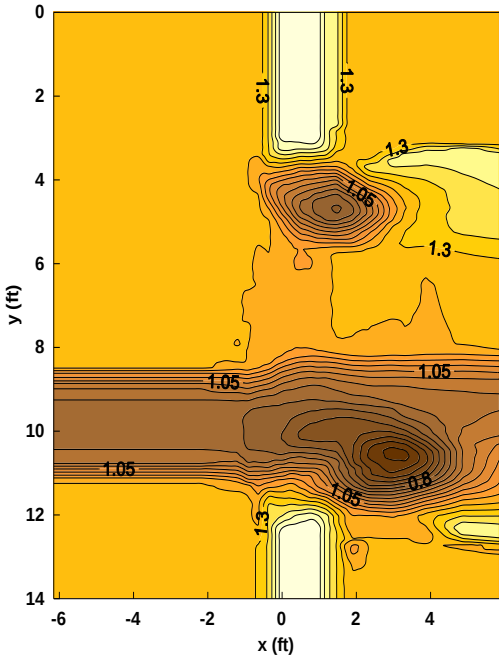

Run 3 (OT flow L_a/B_f = 0.41, Q = 5.5 *cfs*, TW = 1.714 *ft*)

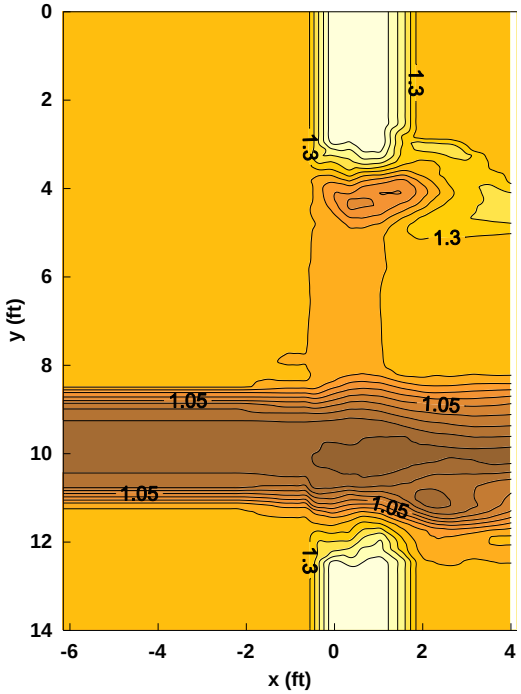

Run 4 (Free flow L_a/B_f = 0.41, Q = 3.7 *cfs*, TW = 1.477 *ft*)

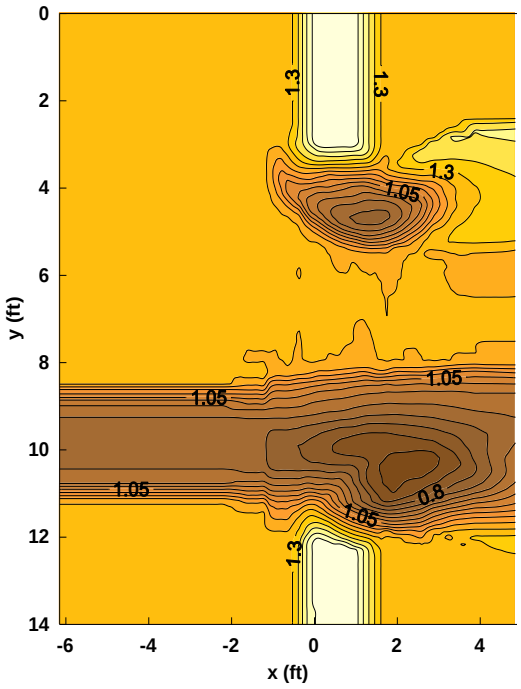

Run 5 (OT flow L_a/B_f = 0.41, Q = 7 *cfs*, TW = 1.717 *ft*)

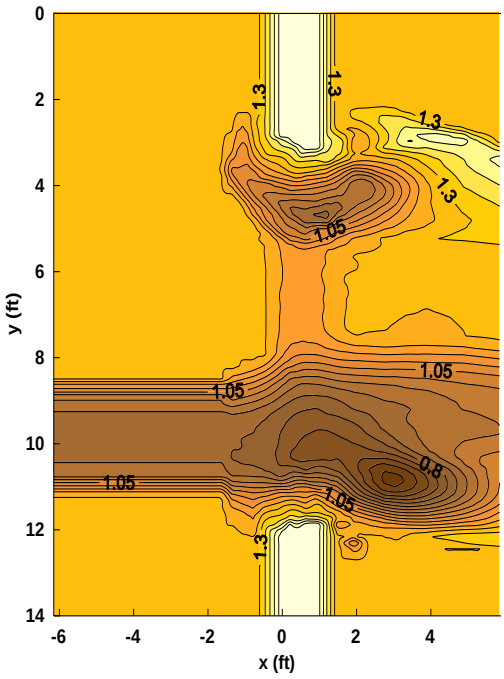

Run 6 (Free flow L_a/B_f = 0.41, Q = 3.7 *cfs*, TW = 1.477 *ft*, L_p/W = 0.18)

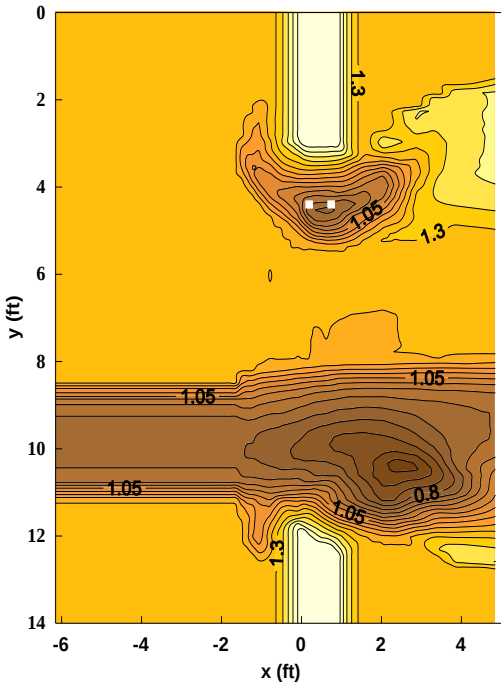

Run 7 (OT flow L_a/B_f = 0.41, Q = 7 *cfs*, TW = 1.717 *ft*, L_p/W = 0.18)

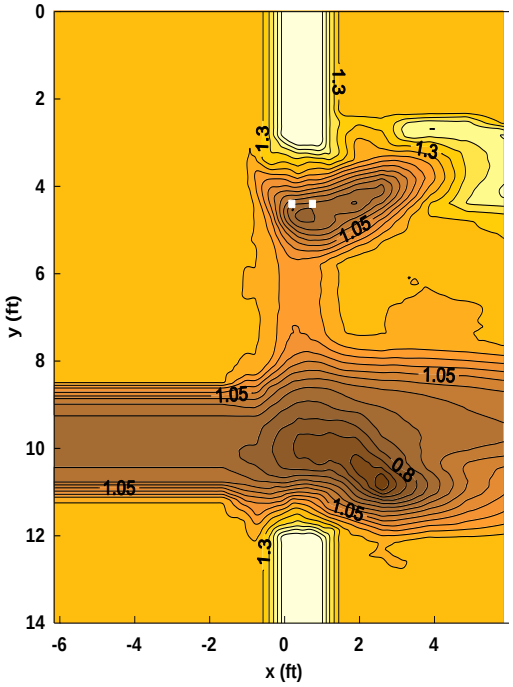

Run 8 (Free flow L_a/B_f = 0.41, Q = 3.7 *cfs*, TW = 1.477 *ft*, L_p/W = 0.35)

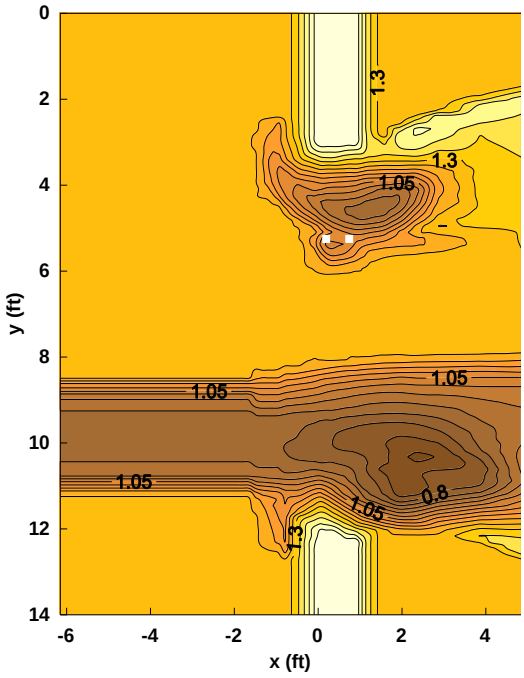

Run 9 (OT flow L_a/B_f = 0.41, Q = 7 *cfs*, TW = 1.717 *ft*, L_p/W = 0.35)

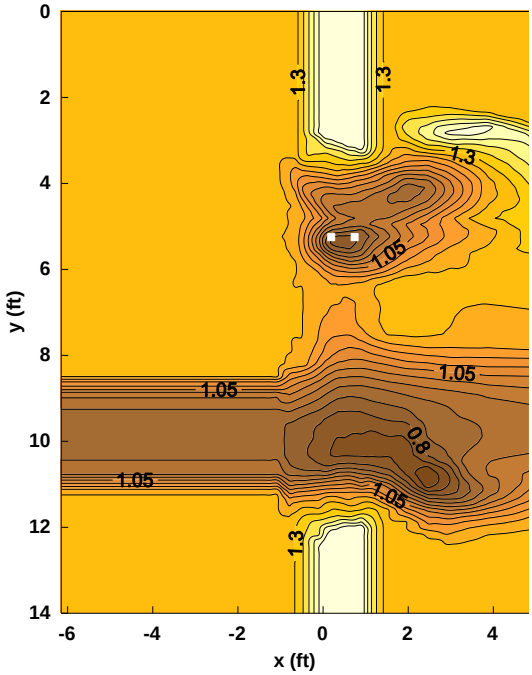

Run 10 (Free flow L_a/B_f = 0.77, Q = 3.8 *cfs*, TW = 1.47 *ft*)

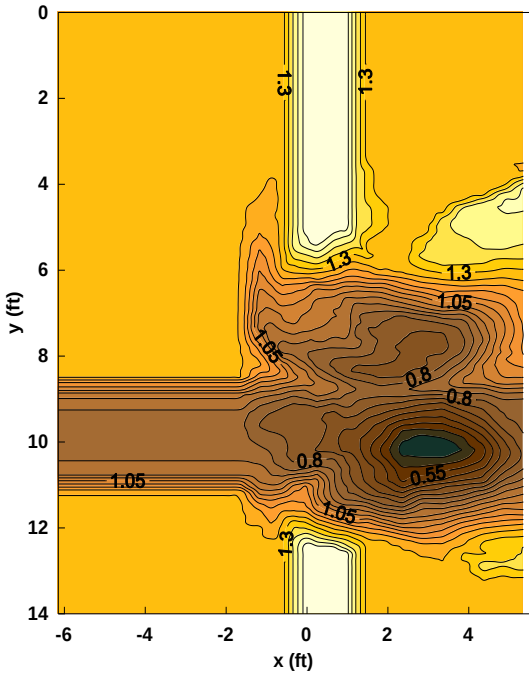

Run 11 (SO flow L_a/B_f = 0.77, Q = 4.4 *cfs*, TW = 1.522 *ft*)

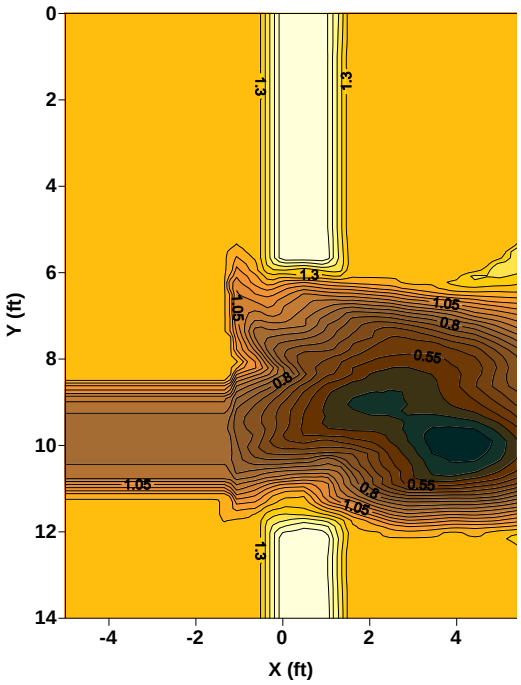

Run 12 (OT flow L_a/B_f = 0.77, Q = 6.5 *cfs*, TW = 1.714 *ft*)

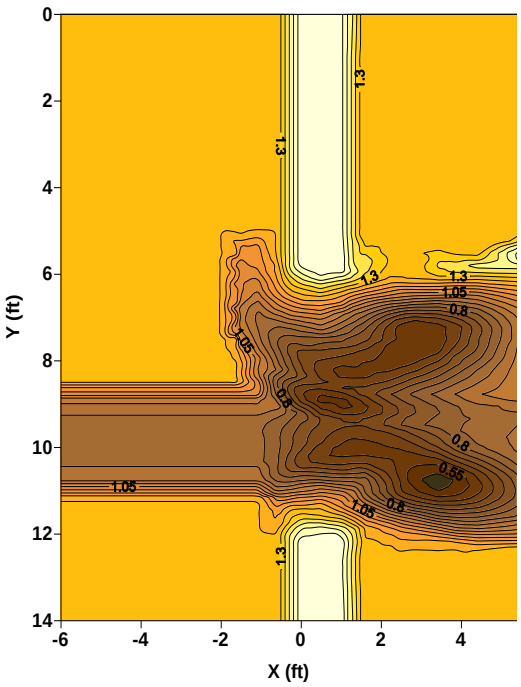

Run 14 (Free flow L_a/B_f = 0.77, Q = 3.8 *cfs*, TW = 1.47 *ft*, L_p/W = 0.4)

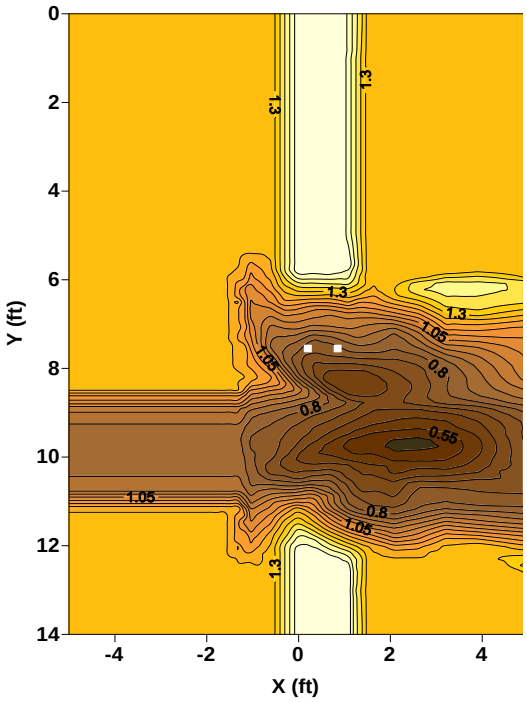

Run 15 (OT flow L_a/B_f = 0.77, Q = 6.5 *cfs*, TW = 1.714 *ft*, L_p/W = 0.4)

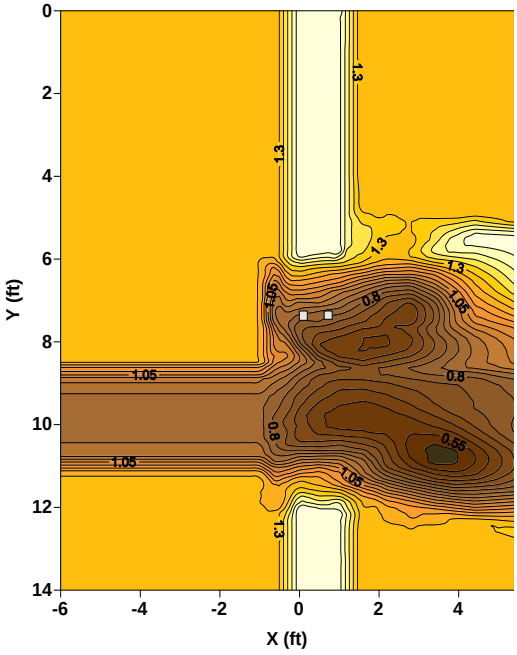

Run 16 (Free flow L_a/B_f = 0.77, Q = 3.8 *cfs*, TW = 1.47 *ft*, L_p/W = 1.0)

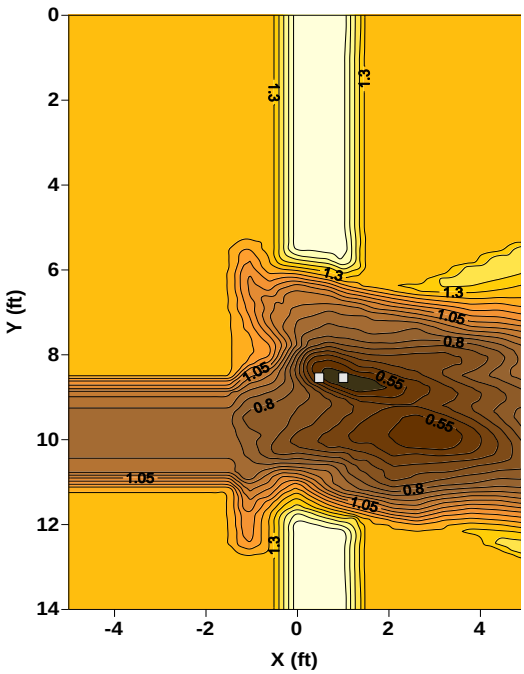

Run 17 (OT Flow L_a/B_f = 0.77, Q = 6.5 *cfs*, TW = 1.714 *ft*, L_p/W = 1.0)

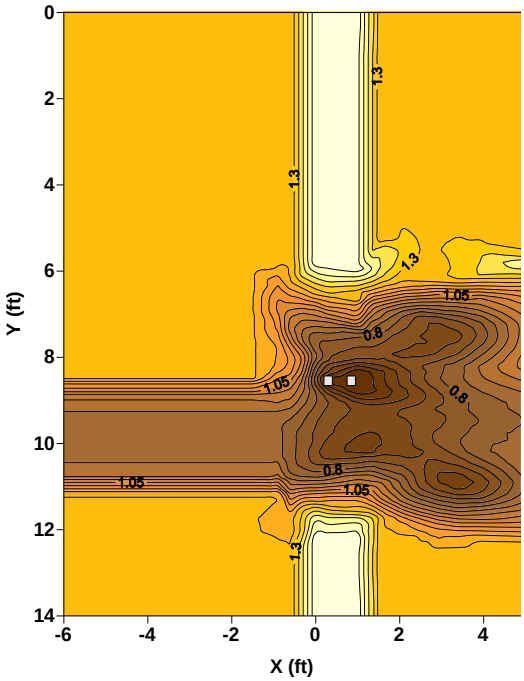

Run 18 (Free flow L_a/B_f = 0.41, Q = 4.0 *cfs*, TW = 1.547 *ft*)

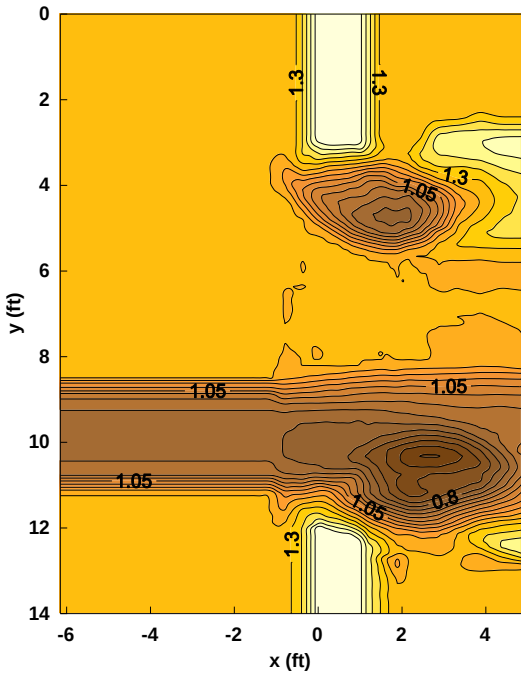

Run 19 (Free flow L_a/B_f = 0.77, Q = 4.4 *cfs*, TW = 1.522 *ft*)

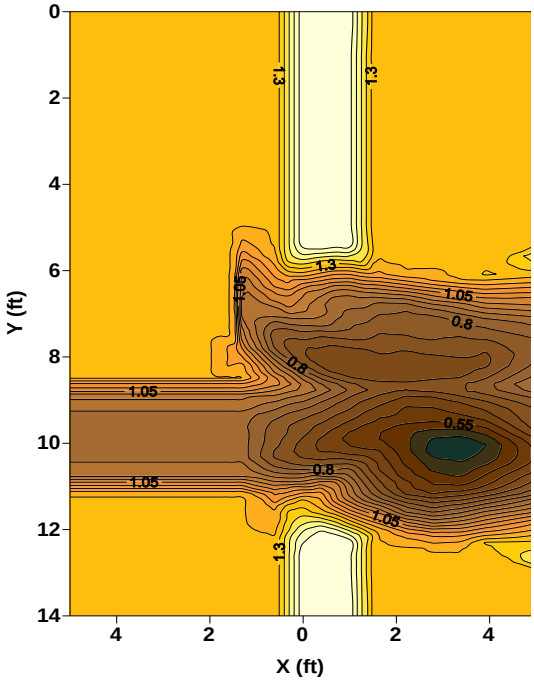

Run 20 (Free flow L_a/B_f = 0.53, Q = 4.1 *cfs*, TW = 1.572 *ft*)

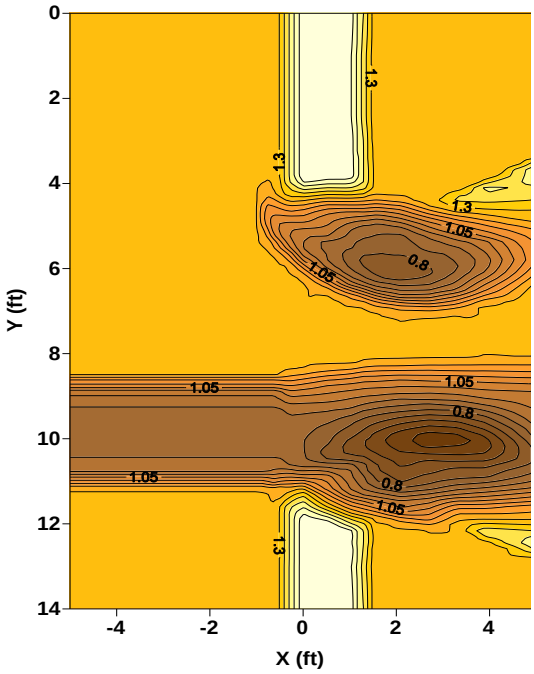

Run 22 (Free flow L_a/B_f = 0.41, Q = 3.0 *cfs*, TW = 1.48 *ft*)

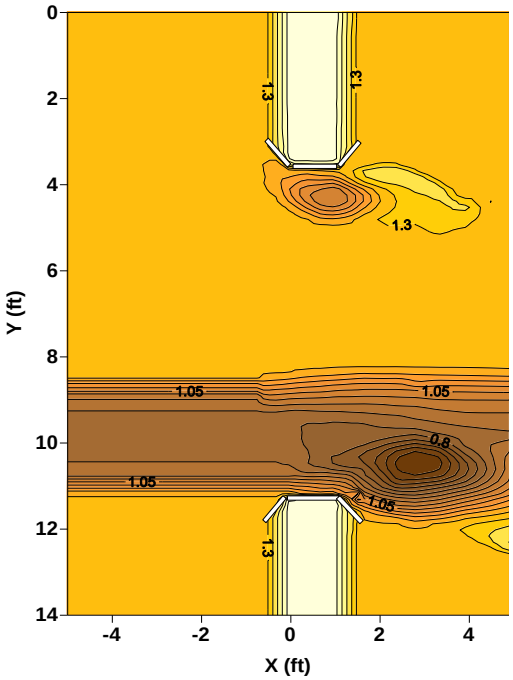

Run 23 (SO flow L_a/B_f = 0.41, Q = 4.0 *cfs*, TW = 1.547 *ft*)

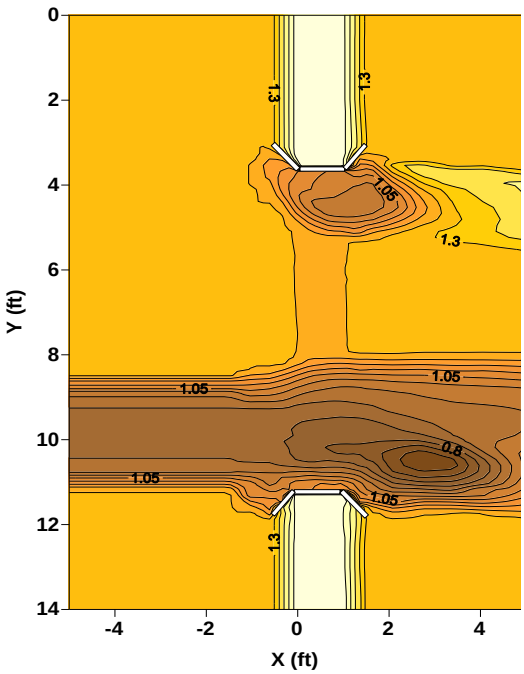

Run 24 (OT flow L_a/B_f = 0.41, Q = 5.5 *cfs*, TW = 1.714 *ft*)

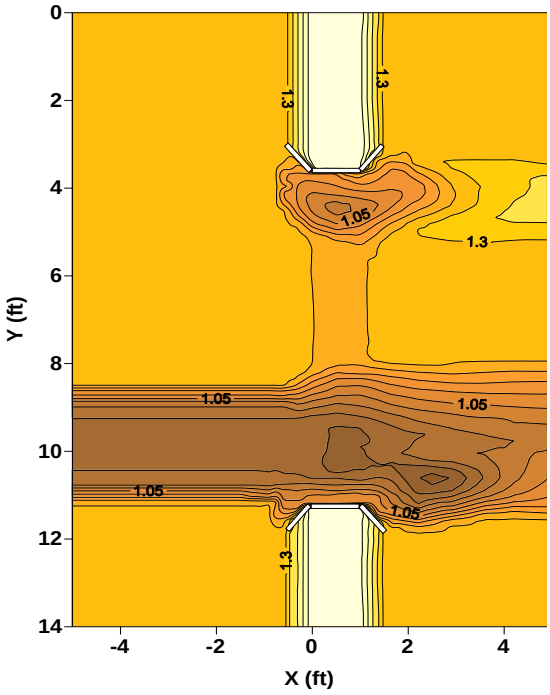

Run 25 (Free flow L_a/B_f = 0.77, Q = 3.8 *cfs*, TW = 1.47 *ft*)

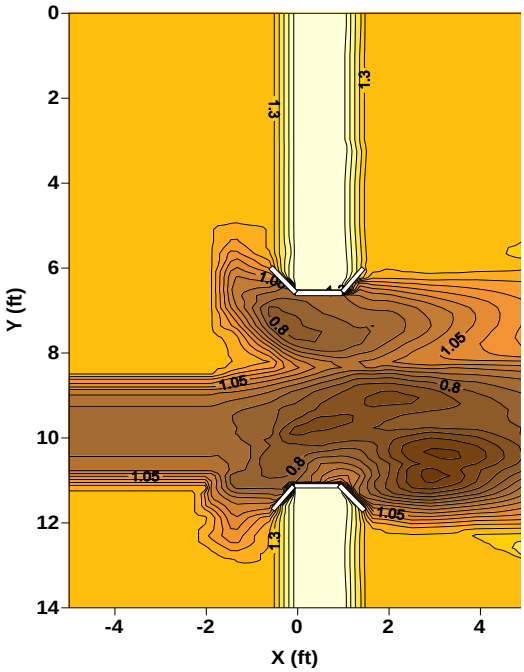

Run 26 (SO flow L_a/B_f = 0.77, Q = 4.4 *cfs*, TW = 1.522 *ft*)

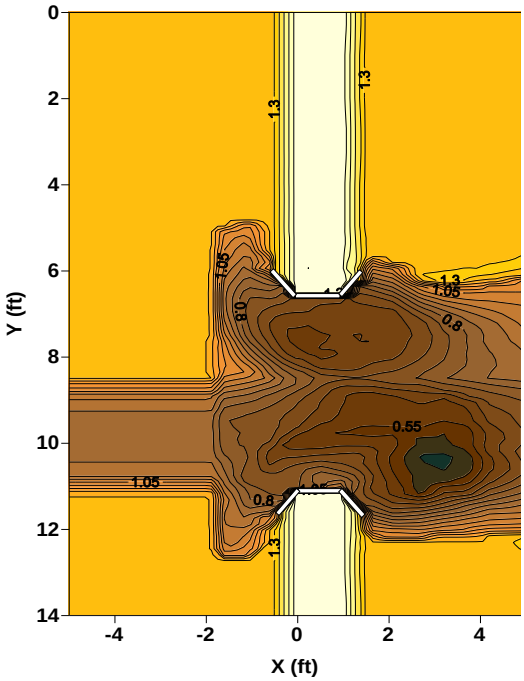

Run 27 (OT flow L_a/B_f = 0.77, Q = 6.5 *cfs*, TW = 1.714 *ft*)

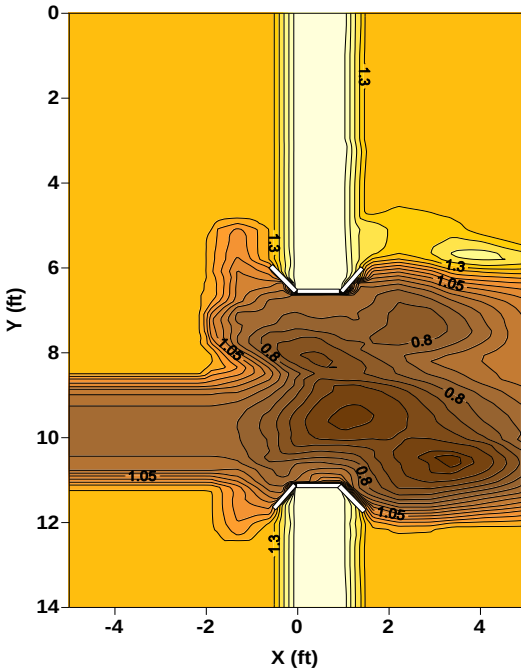

Run 28 (SO flow L_a/B_f = 0.41, Q = 4.0 *cfs*, TW = 1.547 *ft*, L_p/W = 0.18)

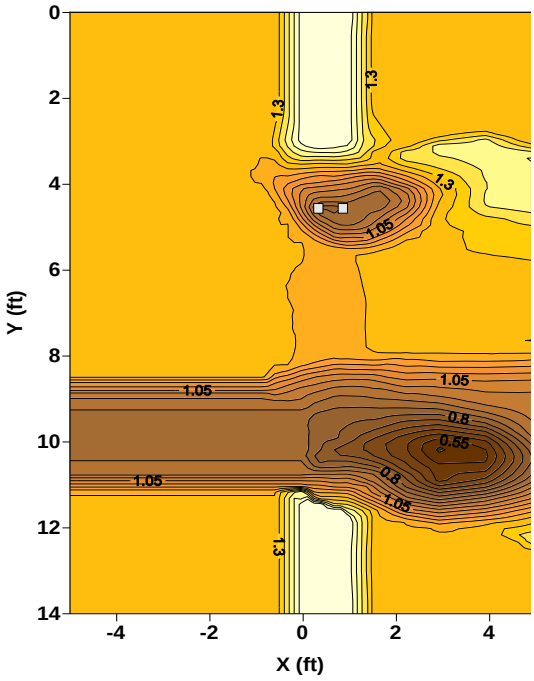

Run 29 (SO flow L_a/B_f = 0.41, Q = 4.0 *cfs*, TW = 1.547 *ft*, L_p/W = 0.35)

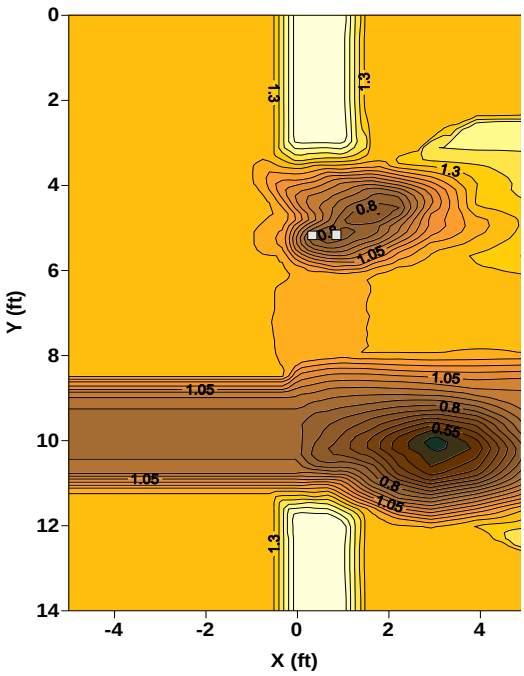

Run 30 (SO flow L_a/B_f = 0.77, Q = 4.4 *cfs*, TW = 1.522 *ft*, L_p/W = 0.4)

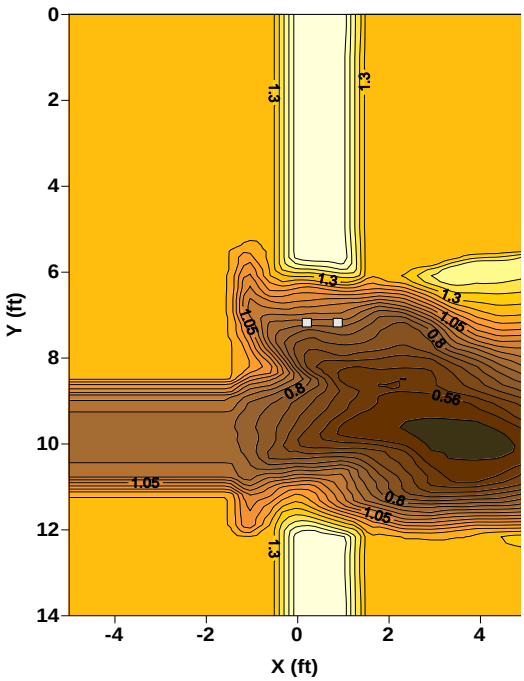

Run 31 (SO flow L_a/B_f = 0.77, Q = 4.4 *cfs*, TW = 1.522 *ft*, L_p/W = 1.0)

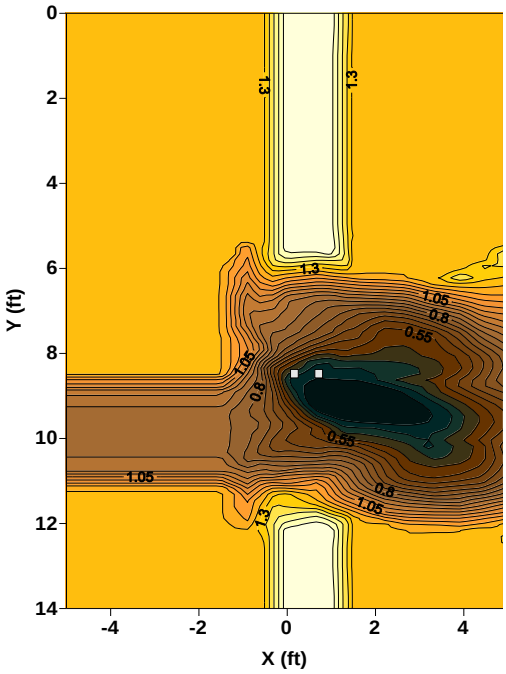

Run 32 (SO flow L_a/B_f = 0, Q = 5.0 *cfs*, TW = 1.522 *ft*)

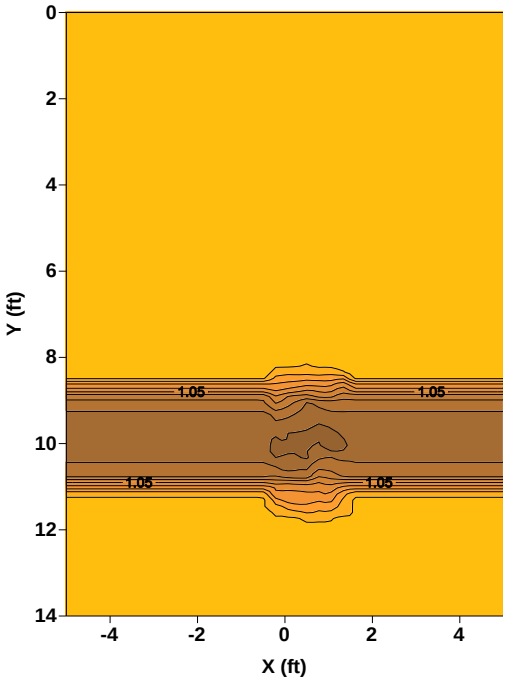

Run 33 (SO flow L_a/B_f = 0, Q = 5.5 *cfs*, TW = 1.522 *ft*)

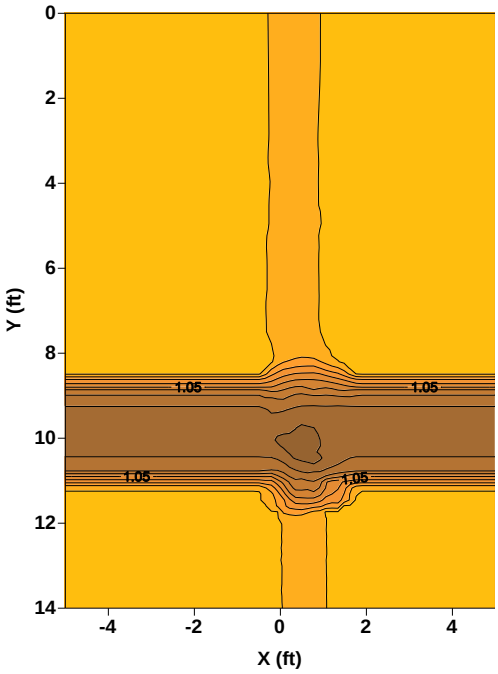

Run 35 (OT flow L_a/B_f = 0, Q = 7.0 *cfs*, TW = 1.714 *ft*)

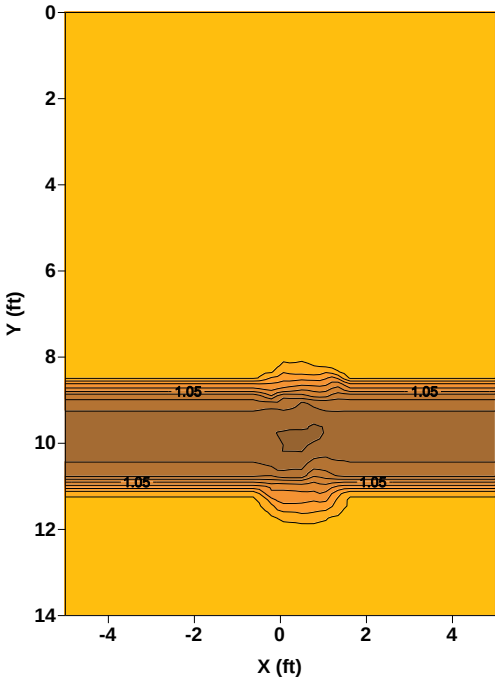

Run 36 (SO flow L_a/B_f = 0, Q = 5.0 *cfs*, TW = 1.522 *ft*, L_p/W = 0.4 & 1.0)

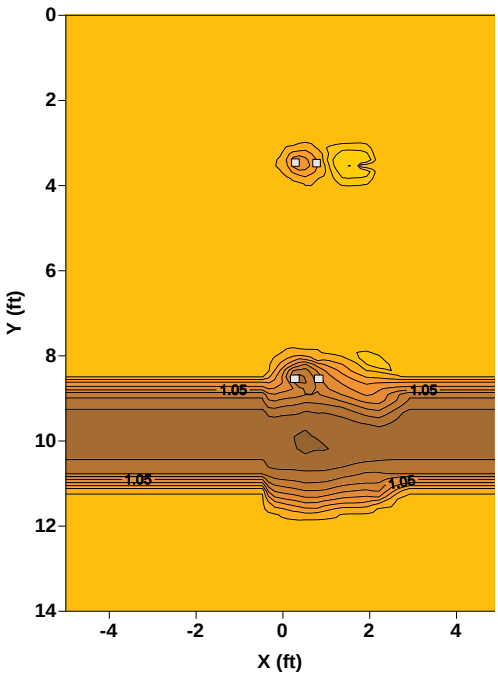

Run 37 (SO flow L_a/B_f = 0, Q = 5.5 *cfs*, TW = 1.522 *ft*, L_p/W = 0.4 & 1.0)

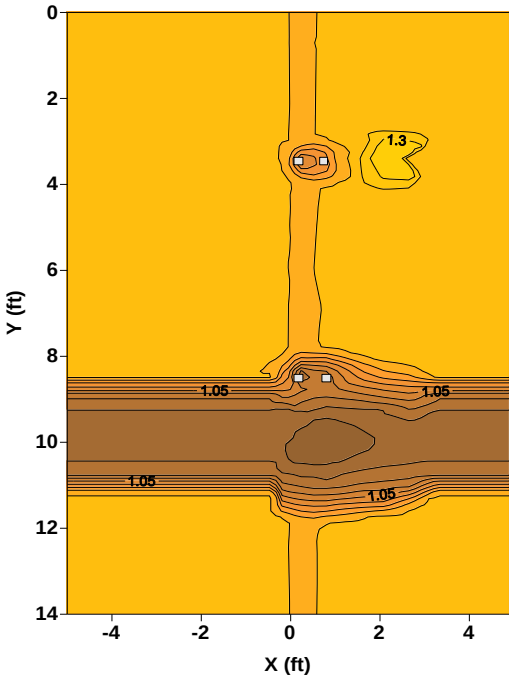

Run 38 (OT flow L_a/B_f = 0, Q = 7.0 *cfs*, TW = 1.714 *ft*, L_p/W = 0.4 & 1.0)

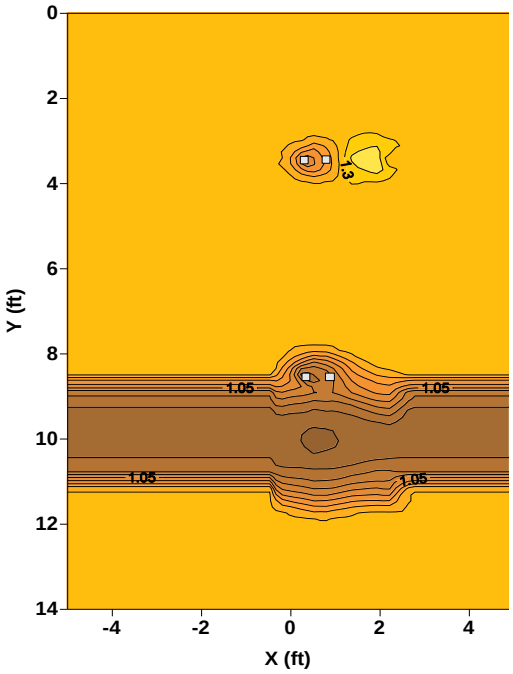

Run 39 (Free flow L_a/B_f = 0.41, Q = 3.7 *cfs*, TW = 1.477 *ft*, L_p/W = 0.18W)

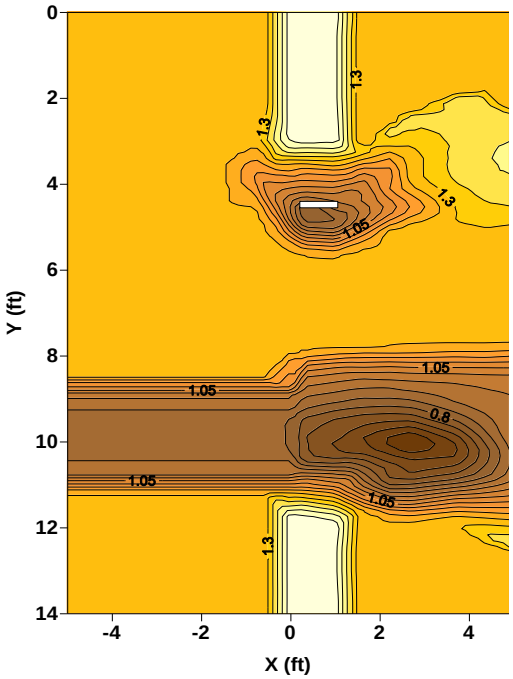

Run 40 (SO flow L_a/B_f = 0.41, Q = 4.0 *cfs*, TW = 1.547 *ft*, L_p/W = 0.18W)

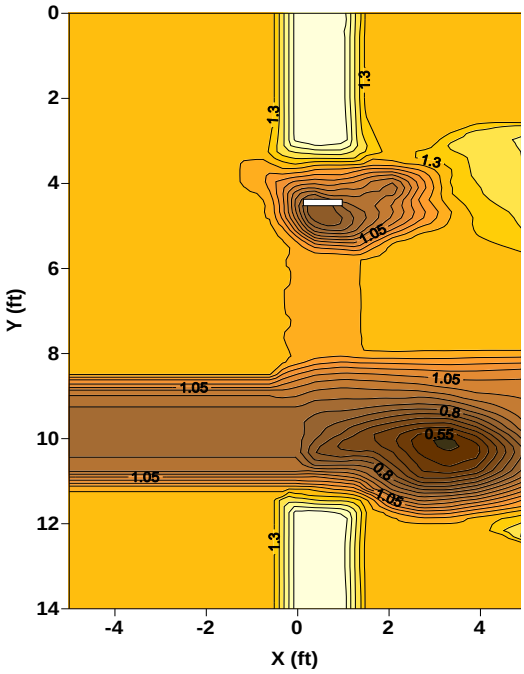

Run 41 (Free flow L_a/B_f = 0.41, Q = 3.7 *cfs*, TW = 1.477 *ft*, L_p/W = 0.35W)

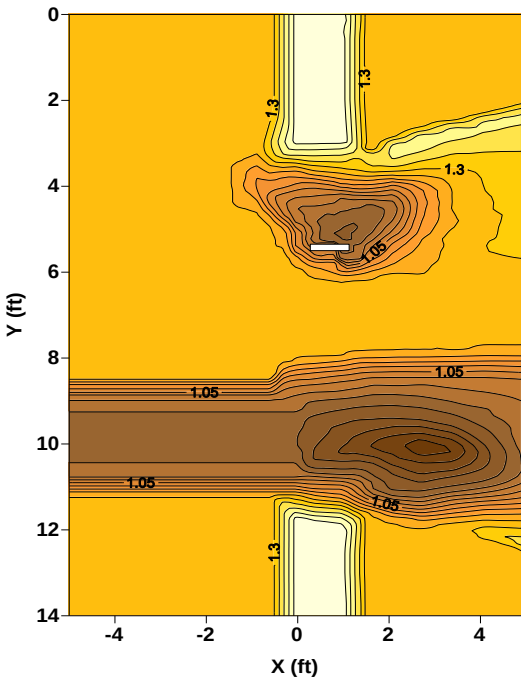

Run 42 (SO flow L_a/B_f = 0.41, Q = 4.0 *cfs*, TW = 1.547 *ft*, L_p/W = 0.35W)

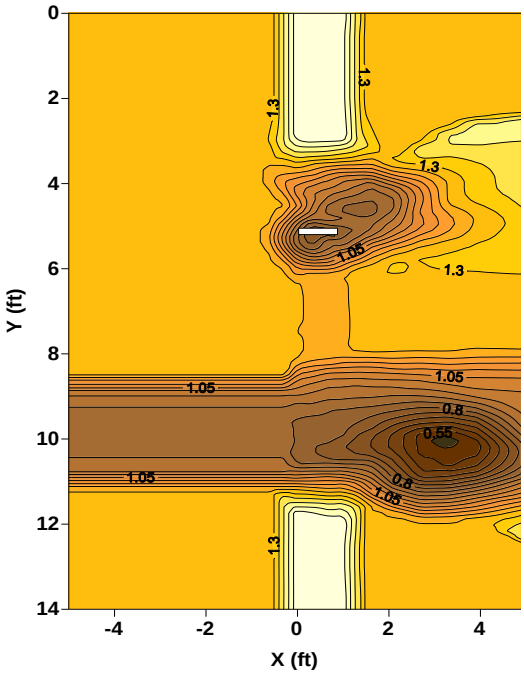

Run 43(Free flow L_a/B_f = 0.53, Q=3.3 *cfs*, TW=1.475 *ft*, L_p/W =0.23 & 0.65)

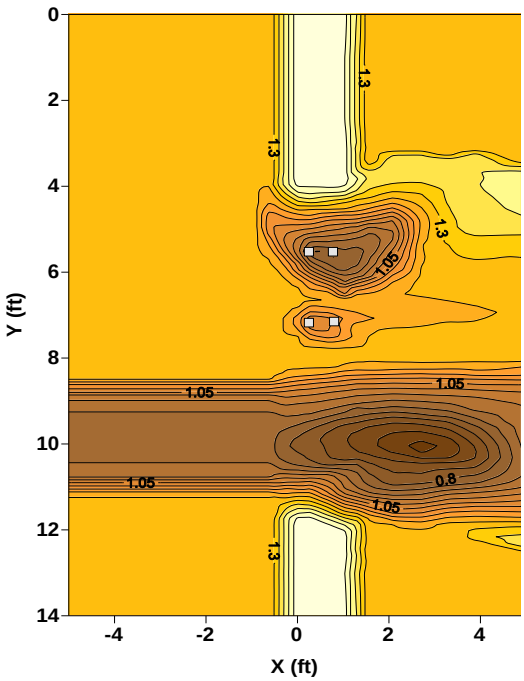

Run 44 (SO flow L_a/B_f = 0.53, Q=4.1 *cfs*, TW=1.572 *ft*, L_p/W =0.48 & 0.78)

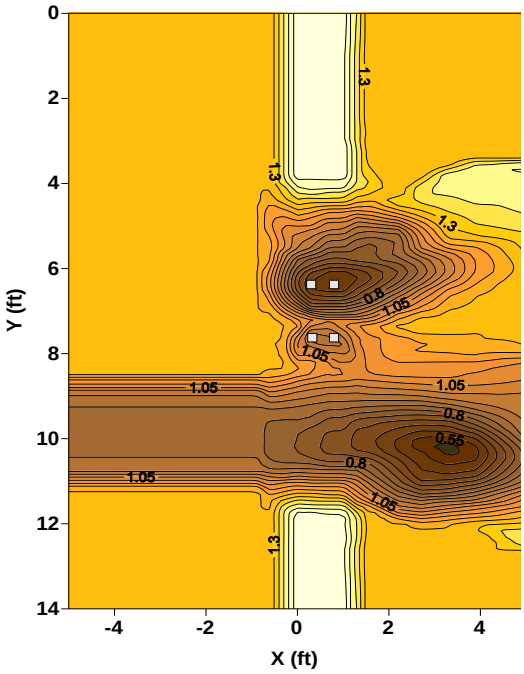

Run 45(SO flow L_a/B_f = 0.53, Q=3.9 *cfs*, TW=1.582 *ft*, L_p/W =0.43 & 0.85)

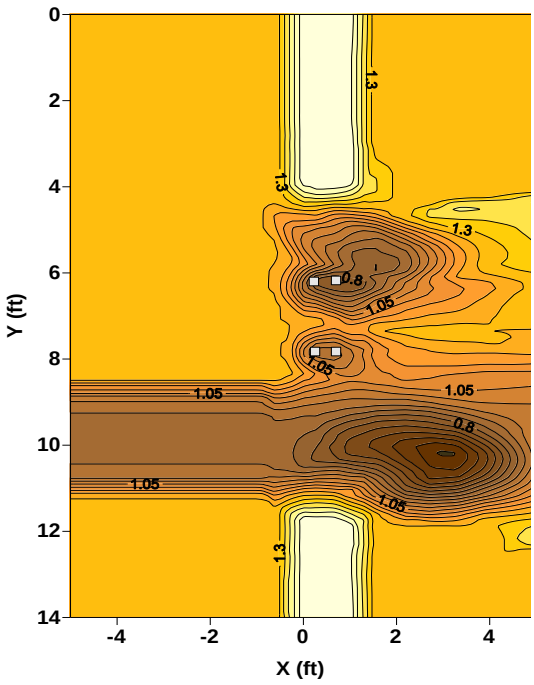

REFERENCES

Abed, L. M. (1991). Local scour around bridge piers in pressure flow.

Arneson, L. W. Zevenberge, P. F. Lagasse and P. E. Clopper (2012). Evaluating Scour at Bridges, Hydraulic Engineering Circular (HEC-18), McLean, Va. : Federal Highway Administration, 5th ed.

Arneson, L. and S. Abt (1998). "Vertical Contraction Scour at Bridges with Water Flowing Under Pressure Conditions." Transportation Research Record **1647**(1): 10.

Ataie-Ashtiani, B., Z. Baratian-Ghorghi and A. A. Beheshti (2010). "Experimental Investigation of Clear-Water Local Scour of Compound Piers." Journal of Hydraulic Engineering **136**(6): 343-351.

Benedict, S. T., N. Deshpande, N. M. Aziz and P. A. Conrads (2006). Trends of abutment-scour prediction equations applied to 144 field sites in South Carolina, Geological Survey (US).

Booij, M. J. (2005). "Impact of climate change on river flooding assessed with different spatial model resolutions." Journal of Hydrology **303**(1-4): 176-198.

Brunner, G. W. (2001). HEC-RAS river analysis system: User's manual, US Army Corps of Engineers, Institute for Water Resources, Hydrologic Engineering Center.

Chang, F. and S. Davis (1998). Maryland SHA Procedure for Estimating Scour at Bridge Abutments Part 2-Clear Water Scour. Stream Stability and Scour at Highway Bridges: Compendium of Stream Stability and Scour Papers Presented at Conferences Sponsored by the Water Resources Engineering (Hydraulics) Division of the American Society of Civil Engineers, ASCE.

Chang, F. and S. Davis (1999). Maryland SHA procedure for estimating scour at bridge abutments, part 1-live bed scour. Stream Stability and Scour at Highway Bridges: Compendium of Stream Stability and Scour Papers Presented at Conferences Sponsored by the Water Resources Engineering (Hydraulics) Division of the American Society of Civil Engineers, ASCE.

Chanson, H., M. Trevethan and C. Koch (2007). "Discussion of “turbulence measurements with acoustic doppler velocimeters” by Carlos M. García, Mariano I. Cantero, Yarko Niño, and Marcelo H. García." Journal of Hydraulic Engineering **133**(11): 1283-1286.

Chreties, C., G. Simarro and L. Teixeira (2008). "New Experimental Method to Find Equilibrium Scour at Bridge Piers." Journal of Hydraulic Engineering **134**(10): 1491-1495.

Coleman, S. E., C. S. Lauchlan and B. W. Melville (2003). "Clear-water scour development at bridge abutments." Journal of Hydraulic Research **41**(5): 521-531.

Coleman, S. E. and B. W. Melville (2001). "CASE STUDY: NEW ZEALAND BRIDGE SCOUR EXPERIENCES." Journal of Hydraulic Engineering **127**(7): 535-546.

Conaway, J. (2006). Comparison of Long-Term Streambed Scour Data with Modeled Values at the Knik River, Alaska: in. Proceedings of the Third International Conference on Scour and Erosion, Amsterdam, The Netherlands.

Conaway, J. (2007). Analysis of Real-Time Streambed Scour Data from Bridges in Alaska. World Environmental and Water Resources Congress 2007: Restoring Our Natural Habitat.

Croad (1989). Investigation of Per Excavation of the Scour Hole at Bridge Abutments, Report No-39-A9303. Central Laboratories, Walington Newzealand.

Dey, S. and R. V. Raikar (2007). "Characteristics of Horseshoe Vortex in Developing Scour Holes at Piers." Journal of Hydraulic Engineering **133**(4): 399-413.

Dongol, D. M. S. (1994). Local scour at bridge abutments. Auckland, N.Z., Auckland, N.Z. : Dept. of Civil Engineering, University of Auckland 1993.

Ettema, R. (1980). Scour at Bridge piers, Department of Civil Engineering, University of Aukland,.

Ettema, R., N. Kam, R. Chakradhar, J. Fuller and E. W. Kempema (2015). "Failure of Spill-Through Bridge Abutments during Scour: Flume and Field Observations." Journal of Hydraulic Engineering **141**(5): 1-5.

Ettema, R., G. Kirkil and M. Muste (2006). "Similitude of Large-Scale Turbulence in Experiments on Local Scour at Cylinders." Journal of Hydraulic Engineering **132**(1): 33-40.

Ettema, R., T. Nakato and M. Muste (2010). Estimation of Scour Depth at Bridge Abutments, NCHRP 24-20.

Froehlich, D. C. (1989). Local scour at bridge abutments. Proceedings of the 1989 National Conference on Hydraulic Engineering.

García, C. M., M. I. Cantero, Y. Niño and M. H. García (2005). "Turbulence measurements with acoustic Doppler velocimeters." Journal of Hydraulic Engineering **131**(12): 1062-1073.

Garde, R., K. Subramanya and K. Nambudripad (1961). "Study of scour around spur-dikes." Journal of the Hydraulics Division **87**(6): 23-37.

Ge, L., S. O. Lee, F. Sotiropoulos and T. Sturm (2005). "3D unsteady RANS modeling of complex hydraulic engineering flows. II: Model validation and flow physics." Journal of Hydraulic Engineering **131**(9): 809-820.

Gill, M. A. (1972). "Erosion of sand beds around spur dikes." Journal of the Hydraulics Division **98**(hy9).

Gill, M. A. (1981). "Bed erosion in rectangular long contraction." Journal of the Hydraulics Division **107**(3): 273-284.

Goring, D. G. and V. I. Nikora (2002). "Despiking acoustic Doppler velocimeter data." Journal of Hydraulic Engineering **128**(1): 117-126.

Gotvald, A. J. and B. E. McCallum (2010). Epic flooding in Georgia, 2009, US Geological Survey.

Grimaldi, C. (2005). Non-conventional countermeasures against local scouring at bridge piers, Dissertation for.

Guo, J., K. Kerenyi, Pagan-Ortiz and J. E. (2009). Bridge pressure flow scour for clear water conditions, United States. Federal Highway Administration. Office of Infrastructure Research and Development, Turner-Fairbank Highway Research Center.

Güven, O., J. G. Melville, J. E. Curry and J. Crim, Samuel H (2005). Observations and Evaluations of Scour at Two Bridge Sites with Cohesive Soils. Erosion of Soils and Scour of Foundations**:** 1-13.

Hager, W. H. and J. Unger (2010). "Bridge Pier Scour under Flood Waves." Journal of Hydraulic Engineering **136**(10): 842-847.

Hahn, E. M. and D. A. Lyn (2010). "Anomalous Contraction Scour? Vertical-Contraction Case." Journal of Hydraulic Engineering **136**(2): 137-141.

Hermann, S. (1979). Boundary layer theory. New York, McGarw-Hill Book Company.

Holnbeck, S. R. and C. Parrett (1997). Method for rapid estimation of scour at highway bridges based on limited site data, US Department of the Interior, US Geological Survey.

Holnbeck, S. R., C. Parrett and T. N. Tillinger (1993). Bridge scour and change in contracted section, Razor Creek. Proceedings of the National Conference on Hydraulic Engineering.

Hong, J.-H., Y.-M. Chiew, J.-Y. Lu, J.-S. Lai and Y.-B. Lin (2011). "Houfeng bridge failure in Taiwan." Journal of Hydraulic Engineering **138**(2): 186-198.

Hong, S. (2005). Interaction of bridge contraction scour and pier scour in a laboratory river model [electronic resource] / by SeungHo Hong, 2005.

Hong, S. (2013). Prediction of clear-water abutment scour depth in compound channel for extreme hydrologic events [electronic resource] / by SeungHo Hong, Atlanta, Ga. : Georgia Institute of Technology, 2013.

Hong, S. and T. Sturm (2009). Physical model study of bridge abutment and contraction scour under submerged orifice flow conditions. Proc. 33rd IAHR Congress: Water Engineering for a Sustainable Environment.

Hong, S., T. W. Sturm and T. Stoesser (2015). "Clear Water Abutment Scour in a Compound Channel for Extreme Hydrologic Events." Journal of Hydraulic Engineering **141**(6): 4015005-4015001-4015005-4015012.

Hong, S. H. and I. Abid (2015). "Physical model study of bridge contraction scour." KSCE Journal of Civil Engineering: 1-8.

Hong, S. H. and I. Abid (2016). "Physical model study of bridge contraction scour." KSCE Journal of Civil Engineering **20**(6): 2578-2585.

Hong, S. H. and T. Sturm (2010). Physical modeling of abutment scour for overtopping, submerged orifice, and free surface flows. Scour and Erosion**:** 590-598.

Hong, S. H. and T. W. Sturm (2011). Physical Modeling of Abutment Scour for Overtopping, Submerged Orifice, and Free Surface Flows, Reston Va, American Society of Civil Engineers.

Jarrett, R. D. and J. M. Boyle (1986). Pilot study for collection of bridge-scour data, Department of the Interior, US Geological Survey.

Jau-Yau, L., H. Jian-Hao, S. Chih-Chiang, W. Chuan-Yi and L. Jihn-Sung (2008). "Field Measurements and Simulation of Bridge Scour Depth Variations during Floods." Journal of Hydraulic Engineering **134**(6): 810-821.

Johnson, P. A. and E. F. Torrico (1994). "Scour around wide piers in shallow water." Transportation Research Record(1471).

Jones, J. S., D. A. Bertoldi and E. R. Umbrell (1993). Preliminary studies of pressure flow scour. Hydraulic Engineering:, ASCE.

Junke, G., K. Kornel, E. P.-O. Jorge and F. Kevin (2009). "Bridge Pressure Flow Scour at Clear Water Threshold Condition." 天津大学学报：英文版 / Transactions of Tianjin University(2): 79.

Kandasamy, J. K. (1985). Local scour at skewed abutments. Auckland, Auckland : Dept. of Civil Engineering, University of Auckland 1985.

Kandasamy, J. K. (1989). Abutment Scour. School of Engineering, The University of Auckland, Auckland, New Zealand.

Kiraga, M. and Z. Popek (2016). "Using a Modified Lane's Relation in Local Bed Scouring Studies in the Laboratory Channel." Water **8**(1): 16.

Kothyari, U. C. and A. Kumar (2012). "Temporal Variation of Scour around Circular Compound Piers." Journal of Hydraulic Engineering **138**(11): 945-957.

Kothyari, U. C., A. Kumar and R. K. Jain (2014). "Influence of cohesion on river bed scour in the wake region of piers." Journal of Hydraulic Engineering(1): 1.

Krogstadt, P.-Å. and R. A. Antonia (1999). "Surface roughness effects in turbulent boundary layers." Experiments in Fluids **27**(5): 450-460.

Kwan, T. F. (1984). "Study of abutment scour." Report No. 328, School of Engineering, The University of Auckland, Auckland, New Zealand: 225pp.

Kwan, T. F. (1984). A study of abutment scour. Auckland, Auckland : Dept. of Civil Engineering, University of Auckland 1984.

Kwan, T. F. (1988). A Study of Abutment Scour. School of Engineering, The University of Auckland, Auckland, New Zealand.

Lança, R., C. Fael, R. Maia, J. P. Pêgo and A. H. Cardoso (2013). "Clear-Water Scour at Pile Groups." Journal of Hydraulic Engineering **139**(10): 1089-1098.

Lança, R. M., C. S. Fael, R. J. Maia, J. P. Pêgo and A. H. Cardoso (2013). "Clear-Water Scour at Comparatively Large Cylindrical Piers." Journal of Hydraulic Engineering **139**(11): 1117-1125.

Landers, M. N. (1992). "Bridge scour data management." USGS Staff--Published Research: 141.

Landers, M. N. and D. S. Mueller (1993). Reference surfaces for bridge scour depths. Proceedings of the National Conference on Hydraulic Engineering.

Larsen, R. J., F. C. K. Ting and A. L. Jones (2011). "Flow Velocity and Pier Scour Prediction in a Compound Channel: Big Sioux River Bridge at Flandreau, South Dakota." Journal of Hydraulic Engineering **137**: 595-605.

Laursen, E. M. (1960). "Scour at bridge crossings." Journal of the Hydraulics Division **86**(2): 39-54.

Laursen, E. M. (1963). "An analysis of relief bridge scour." Journal of the Hydraulics Division **89**(3): 93-118.

Lee, S., T. Sturm, A. Gotvald and M. Landers (2004). Comparison of laboratory and field measurements of bridge pier scour. Proceedings of Second International Conference on SCOUR and EROSION-ICSE, Meritus Mandarin, Singapore.

Lee, S. O. and T. W. Sturm (2009). "Effect of Sediment Size Scaling on Physical Modeling of Bridge Pier Scour." Journal of Hydraulic Engineering **135**(10): 793-802.

Ligrani, P. M. and R. J. Moffat (1986). "Structure of transitionally rough and fully rough turbulent boundary layers." Journal of Fluid Mechanics **162**: 69-98.

Lim, S.-Y. and N.-S. Cheng (1998). "Scouring in long contractions." Journal of irrigation and drainage engineering **124**(5): 258-261.

Lombard, P. and G. Hodgkins (2008). Comparison of Observed and Predicted Abutment Scour at Selected Bridges in Maine, US Geological Survey.

Lopez, G., L. Teixeira, M. Ortega-Sanchez and G. Simarro (2014). "Estimating final scour depth under clear-water flood waves." Journal of Hydraulic Engineering(3): 328.

Lu, J.-Y., J.-H. Hong, C.-C. Su, C.-Y. Wang and J.-S. Lai (2008). "Field Measurements and Simulation of Bridge Scour Depth Variations during Floods." Journal of Hydraulic Engineering **134**(6): 810-821.

Lyn, D. A. (2008). "Pressure-Flow Scour: A Reexamination of the HEC-18 Equation." Journal of Hydraulic Engineering **134**(7): 1015-1020.

Melville, B. (1992). "Local Scour at Bridge Abutments." Journal of Hydraulic Engineering **118**(4): 615-631.

Melville, B. W. (1997). "Pier and abutment scour: integrated approach." Journal of Hydraulic Engineering **123**(2): 125-136.

Melville, B. W. and Y.-M. Chiew (1999). "Time Scale for Local Scour at Bridge Piers." Journal of Hydraulic Engineering **125**(1): 59.

Melville, B. W. and S. E. Coleman (2000). Bridge Scour Water Resource Pubilcations, Highland Ranch, Colorado.

Melville, B. W. and A. J. Raudkivi (1996). "Effects of foundation geometry on bridge pier scour." Journal of Hydraulic Engineering **122**(4): 203-209.

Mia, M. F. and H. Nago (2003). "Design Method of Time-Dependent Local Scour at Circular Bridge Pier." Journal of Hydraulic Engineering **129**(6): 420.

Mueller, D. S. and C. R. Wagner (2005). Field observations and evaluations of streambed scour at bridges.

Neill, C. (1968). "Note on initial movement of coarse uniform bed-material." Journal of Hydraulic Research **6**(2): 173-176.

Nezu, I. and W. Rodi (1986). "Open-channel flow measurements with a laser Doppler anemometer." Journal of Hydraulic Engineering **112**(5): 335-355.

Niehus, C. A. (1996). Scour assessments and sediment-transport simulation for selected bridge sites in South Dakota, US Department of the Interior, US Geological Survey.

Oben-Nyarko, K. and R. Ettema (2011). "Pier and Abutment Scour Interaction." Journal of Hydraulic Engineering **137**(12): 1598-1605.

Oliveto, G. and W. H. Hager (2002). "Temporal Evolution of Clear-Water Pier and Abutment Scour." Journal of Hydraulic Engineering **128**(9): 811.

Rahman, S. and D. R. Webster (2005). "The effect of bed roughness on scalar fluctuations in turbulent boundary layers." Experiments in Fluids **38**(3): 372-384.

Raudkivi, A. J. (1986). "Functional trends of scour at bridge piers." Journal of hydraulic engineering **112**(1): 1-13.

Richardson, J. and R. Trivino (2002). "Clear-water abutment scour prediction for simple and complex channels." Transportation Research Record: Journal of the Transportation Research Board(1797): 23-30.

Rossell, R. P. and F. C. K. Ting (2013). "Hydraulic and Contraction Scour Analysis of a Meandering Channel: James River Bridges near Mitchell, South Dakota." Journal of Hydraulic Engineering **139**(12): 1286-1296.

Shatanawi, K. M., N. M. Aziz and A. A. Khan (2008). "Frequency of Discharge Causing Abutment Scour in South Carolina." Journal of Hydraulic Engineering **134**(10): 1507-1512.

Shen, J., H. Shan, O. Suaznabar, Z. Xie, C. Bojanowski, S. Lottes and K. Kerenyi (2012). Submerged Flow Bridge Scour Under Clear Water Conditions. Sixth International Conference on Scour and Erosion (ICSE-6), Paris.

Sheppard, D. M., H. Demir and B. W. Melville (2011). Scour at wide piers and long skewed piers, Transportation Research Board.

Sheppard, D. M. and W. Miller Jr (2006). "Live-bed local pier scour experiments." Journal of Hydraulic Engineering **132**(7): 635-642.

Shirole, A. and R. Holt (1991). "Planning for a comprehensive bridge safety assurance program." Transportation Research Record(1290).

Simarro, G., C. M. S. Fael and A. H. Cardoso (2011). "Estimating Equilibrium Scour Depth at Cylindrical Piers in Experimental Studies." Journal of Hydraulic Engineering **137**(9): 1089-1093.

Simarro, G., L. Teixeira and A. H. Cardoso (2007). "Flow Intensity Parameter in Pier Scour Experiments." Journal of Hydraulic Engineering **133**(11): 1261-1264.

SonTek (2001). SonTek/YSI ADVField/Hydra Operation manual (firmware Version 7.9 and later). 6837 Nancy Ridge Drive, Suite A, San Diego, CA 92121-3217 USA.

Sturm, T. and N. Janjua (1994). "Clear- Water Scour around Abutments in Floodplains." Journal of Hydraulic Engineering **120**(8): 956-972.

Sturm, T. and A. Sadiq (1996). "Clear-water scour around bridge abutments under backwater conditions." Transportation Research Record: Journal of the Transportation Research Board(1523): 196-202.

Sturm, T., F. Sotiropoulos, M. Landers, T. Gotvald, S. Lee, L. Ge, R. Navarro and C. Escauriaza (2004). "Laboratory and 3D numerical modeling with field monitoring of regional bridge scour in Georgia." Atlanta, GA, Georgia Department of Transportation Final Project, Project(2002).

Sturm, T. W. (2001). Open-channel hydraulics / Terry W. Sturm, Boston : McGraw-Hill, c2001.

Sturm, T. W. (2004). Enhanced abutment scour studies for compound channels.

Sturm, T. W. (2006). "Scour around Bankline and Setback Abutments in Compound Channels." Journal of Hydraulic Engineering **132**(1): 21-32.

Sturm, T. W., R. Ettema and B. W. Melville (2011). Evaluation of bridge-scour research: abutment and contraction scour processes and prediction, NCHRP Project 24-27(02). NCHRP web-only document: 181, Washington, D.C. : National Cooperative Highway Research Program, Transportation Research Board of the National Academie.

Sturm, T. W. and N. S. Janjua (1993). Bridge abutment scour in a floodplain. Hydraulic Engineering:, ASCE.

Sturm, T. W. and N. S. Janjua (1994). "Clear-water scour around abutments in floodplains." Journal of Hydraulic Engineering **120**(8): 956-972.

Ting, F., R. Larsen and A. Jones (2011). "Hydrographs and Estimates of Scour Depth Excess for Pier Scour Prediction: Use for Ungauged Streams with Scour Rate in Cohesive Soils Method." Transportation Research Record: Journal of the Transportation Research Board(2262): 193-199.

Umbrell, E. R., G. K. Young, S. M. Stein and J. S. Jones (1998). "Clear-water contraction scour under bridges in pressure flow." Journal of Hydraulic Engineering **124**(2): 236.

Voulgaris, G. and J. H. Throwbridge (1998). "Evaluation of the Acoustic Doppler Velocimeter (ADV) for Turbulence Measurements." Journal of Atmospheric & Oceanic Technology **15**(1): 272.

Wagner, C. R., D. S. Mueller, A. C. Parola, D. Hagerty and S. T. Benedict (2006). "Scour at contracted bridges." NCHRP Web-Only Document **83**.

Wang, Y.-C. and T. W. Sturm (2013). Effects of physical properties and rheological characteristics on critical shear stress of fine sediments [electronic resource] / by Yung-Chieh (Becky) Wang, Atlanta, Ga. : Georgia Institute of Technology, 2013.

Wong, W. H. (1982). "Scour at bridge abutments." Report No. 275, School of Engineering, The University of Auckland, Auckland, New Zealand: 109pp.

Wormleaton, P. R. and P. Hadjipanos (1985). "Flow Distribution in Compound Channels." Journal of Hydraulic Engineering, ASCE 111, no. 2: pp 357-361.

Yorozuya, A. and R. Ettema (2015). "Three Abutment Scour Conditions at Bridge Waterways." Journal of Hydraulic Engineering **141**(12): 04015028.

Zhang, G., S. A. Hsu, T. Guo, X. Zhao, A. D. Augustine and L. Zhang (2013). Evaluation of Design Methods to Determine Scour Depths for Bridge Structures.